PALACKÝ UNIVERSITY OLOMOUC
FACULTY OF SCIENCE
DEPARTMENT OF BIOPHYSICS

DOCTORAL THESIS

Computer Simulations of Na^+/K^+-ATPase its Interactions with Small Molecules

Author: **Mgr. Petra Čechová**
Program: Biophysics
Supervisor: doc. RNDr. Martin Kubala, Ph.D.

DECLARATION

"I declare that, except where explicit reference is made to the contribution of others, that this dissertation is the result of my own work and has not been submitted for any other degree at the Palacký University in Olomouc or any other institution."

Olomouc 6.9.2017

Mgr. Petra Čechová

BIBLIOGRAFICKÁ IDENTIFIKACE

Jméno a příjmení autora:	Mgr. Petra Čechová
Název práce:	Počítačové simulace Na^+/K^+-ATPasy a jejích interakcí s malými molekulami
Typ práce:	Disertační
Pracoviště:	Katedra biofyziky
Vedoucí práce:	doc. RNDr. Martin Kubala, Ph.D.
Rok obhajoby práce:	2017
Abstrakt:	Výpočetní biologie využívá znalostí struktury proteinu k vytvoření počítačového modelu, který pak slouží jako základ pro zkoumání vztahu mezi jeho strukturou a funkcí. Na^+/K^+-ATPasa je membránový protein, který udržuje rovnováhu iontů v buňce a je tak nezbytný pro správnou funkci lidského těla. Tato disertační práce se věnuje popisu Na^+/K^+-ATPasy pomocí dvou výpočetních metod. Molekulární dynamika je využita k popisu iontových cest, pohybu domén a vazbě nukleotidů. Molekulární dokování bylo použito k vysvětlení mechanismu účinku flavonolignanů a quinolinonů na tento protein.
Klíčová slova:	Na^+/K^+-ATPasa, sodno-draselná pumpa, membránové proteiny, molekulární dynamika, docking, molekulární dokování, flavonolignany, quinolinony, výpočetní biologie
Počet stran:	90
Počet stran příloh:	5
Jazyk:	Anglický

BIBLIOGRAPHICAL IDENTIFICATION

Author's name and surname: Mgr. Petra Čechová

Title: Computer Simulations of Na^+/K^+-ATPase its Interactions with Small Molecules

Thesis type: Doctoral

Department: Department of Biophysics

Supervisor: doc. RNDr. Martin Kubala, Ph.D.

Year of presentation: 2017

Abstract: Computational biology utilises information of protein structure and build models that are used to study their structure-function relationship. Na^+/K^+-ATPase is a membrane protein essential to human body by maintaining ion balance in the cells. This thesis studies Na^+/K^+-ATPase by two computational methods - molecular dynamics to describe ion pathways, domain movements and nucleotide binding, and molecular docking to rationalise the interaction of flavonolignans and quinolinones with this protein.

Keywords: Na^+/K^+-ATPase, sodium-potassium pump, membrane proteins, molecular dynamics, molecular docking, flavonolignans, quinolinones, computational biology

Number of pages: 90

Pages of Appendices: 5

Language: English

TABLE OF CONTENTS

ACKNOWLEDGEMENTS

This thesis would never come to exist without the help and support of many people which I would like to show my appreciation to.

I would like to thank Martin Kubala, for his supervision and guidance, helping me with his suggestions in constructing experiments, discussing results and writing papers during my whole studies here at Palacký University; Karel Berka for the time and effort he spent teaching me how to use GROMACS and troubleshooting the dead ends I got myself into; Patrick Trouillas for allowing and overseeing my stay in France and introducing me to the field of computational chemistry.

I am immensely grateful for my classmates, with whom I shared days both good and bad. Jaroslava Šeflová, who has been my cornerstone since the day we started chatting before a chemistry lesson during our first year. Michal Biler, because even though no one knows how we ended up this close, it turned out to be great. Tibor Stolárik, who apart from enriching our vocabulary by Slovak enriched our lives by his unique point of view. Finally, our French "social coordinator" Gabin Fabre, who made me help settle down and feel welcome from the very first day.

I would not manage to overcome all the obstacles in my way without the backing of my friends. Ben Olšanský has always came up with a plan when I came to him overwhelmed and panicking, Zuzana Kocurková showed me that life can be scary, but also full of hope. Marek Eiba, who I met when we were both in a bad place and held my hand as we both got up again. Ondřej Černotík, who makes me want to be a better person than I was yesterday. Jan Provazník, whose quiet support and programming mastery improved more days than I dare to count.

I cannot name all of my co-workers, both in Czech Republic and France, whose collaboration, advice, and friendship I also deeply appreciate, as well as all members of SFK Cyrano and people from various fandoms who helped me along the way. I would also like to thank my co-workers from Camp Winnebagoe, who spent a great deal of time trying to make me believe that everything will be, eventually, fine.

Finally, I would like to express my gratitude to my family who have always given me their unconditional love and support and stood by me during all my life and studies.

This work could not happen without the financial support of the LO1024 grant from the National Program of Sustainability I and by grants 15-03037S, P208/12/G016 from the Czech Science Foundation and by Endowment Fund of Palacký University Olomouc and the computational resources provided by the CESNET LM2015042 and the CERIT Scientific Cloud LM2015085, provided under the programme "Projects of Large Research, Development, and Innovations Infrastructures".

LIST OF ABBREVIATIONS

A	Ala	Alanine
R	Arg	Arginine
N	Asn	Asparagine
D	Asp	Aspartic acid
C	Cys	Cysteine
E	Glu	Glutamic acid
Q	Gln	Glutamine
G	Gly	Glycine
H	His	Histidine
I	Ile	Isoleucine

L	Leu	Leucine
K	Lys	Lysine
M	Met	Methionine
F	Phe	Phenylalanine
P	Pro	Proline
S	Ser	Serine
T	Thr	Threonine
W	Trp	Tryptophan
Y	Tyr	Tyrosine
V	Val	Valine

6CHPQ	6-chlor-3-hydroxy-2- phenylquinolin-4(1*H*)-one
8CHPQ	8-chlor-3-hydroxy-2- phenylquinolin-4(1*H*)-one
ADP	adenosine diphosphate
ATP	adenosine triphosphate
C45	cytoplasmic loop between helices 4 and 5
CBS	cation binding site
CTS	cardiotonic steroids
DFHPQ	6,7-difluor-3-hydroxy-2- phenylquinolin-4(1*H*)-one
DHSA	dehydrosilydianin
DHSCH	dehydrosilychristin
DCHPQ	5,6-dichlor-3-hydroxy-2- phenylquinolin-4(1*H*)-one
DOPC	dioleoylphosphatidylcholine
MD	molecular dynamics
MM	molecular modelling
NKA	Na^+/K^+-ATPase
SCH	silychristin
SERCA	sarco/endoplasmic reticulum Ca^{2+}-ATPase
TFHPQ	5,6,7,8-tetrafluor-3-hydroxy-2- phenylquinolin-4(1*H*)-one
TM	transmembrane helix (number 1-10)

PUBLICATION LIST

I. **Čechová, P.**, Berka, K., and Kubala, M. (2016) *Ion Pathways in the Na^+ /K^+ -ATPase,* Journal of Chemical Information and Modeling, Volume 56, Issue 12, 27 December 2016, Pages 2434-2444

II. Šeflová J., **Čechová P.**, Biler M., Kubala M. and Hradil P. (2017) *Inhibition of Na+K+-ATPase by tetrafluoro-3-hydroxyquinolin-4(1H)-one,* Biochimie, Volume 138, July 2017, Pages 56-61

III. Kubala, M., **Čechová, P.**, Geletičová, J., Biler, M., Štenclová, T., Trouillas, P., and Biedermann, D. (2016) *Flavonolignans as a Novel Class of Sodium Pump Inhibitor,*. Frontiers in Physiology, Volume 7, Pages 1–10

IV. **Čechová, P.,** Berka, K., and Kubala, M. *Nucleotide Dynamics in the Na^+/K^+-ATPase,* submitted to Journal of Chemical Information and Modeling

Introduction

Membrane proteins play a crucial role in regulating cellular environment and cell-to-cell communication. They also serve as targets or transporters for various medically active compounds. However, due to the fact they often contain a large hydrophobic part, or require to be inserted in a lipid environment, they remain a challenge for experimental studies. Similarly, obtaining membrane protein structures faces great technical difficulties [1].

Na^+/K^+-ATPase is a membrane protein present in great amounts within all cells, where it maintains sodium ion gradient. In the brain, it takes part in the rapid repolarization of neurons between neural impulses [2], or potassium clearance [3]. In heart and muscles it facilitates ion exchange necessary for their function and in kidneys it handles sodium and fluid reabsorptions [4]. Mutations in the genes encoding this protein can result in several neurological disorders, muscle dystonia or hyperkalaemia and hypertension [5].

Computational biology uses the available information about protein sequence and structure to build a model, which can be further analysed in static or dynamic studies. Molecular dynamics simulates the time-depended evolution of the protein model. It captures large-scale movements and dynamic events that are beyond the reach of experimental methods. Moreover, it allows to observe the protein properties in a more physiological environment that the one necessary for obtaining crystal structures [6]. Molecular docking treats the protein model as a receptor for a small organic molecule and calculates binding affinities of the protein-ligand complex. It is widely used as a tool of evaluating biologically active compounds and their potential use as pharmacological drugs [7]

This thesis focuses on studies of the Na^+/K^+-ATPase by the methods of computational biology. Molecular dynamics studies of the protein in different environments were performed to depict the movements in the transmembrane part (opening and closing of ion pathways) and cytoplasmic part (with respect to the binding of ATP and ADP). Molecular docking studies were used to describe the interactions between the Na^+/K^+-ATPase with two groups of small organic compounds – flavonolignans (currently used as anti-inflammatory and liver-protection medicaments) and quinolinones (potential anti-cancer drugs).

1. Theory

1.1. P-Type ATPases and Na^+/K^+-ATPase

The Na^+/K^+-ATPase (NKA) is an essential membrane protein that is present in all animal cells. During its reaction cycle, NKA transports three intracellular Na^+ and two extracellular K^+ ions across the plasma membrane to create a sodium ion gradient, which is a part of membrane potential [8]. Moreover, sodium gradient is used as a driving force for several secondary transporters (such as glucose transporter, or Na^+/Ca^{2+} exchanger [9]).

NKA was discovered in 1957 [10] as the first member of P-type ATPases, a large family of proteins that transport a variety of ions, and lipids. The ATPases of this group utilise the energy of ATP for transport and get phosphorylated in the process. They share structural features and overall sequence similarity with several conserved sequences across the whole family. NKA is a member of PII subfamily [11], together with sarcoplasmic Ca^{2+}-ATPase (SERCA), gastric and nongastric H^+/K^+-ATPase or plasma membrane Ca^{2+}-ATPase (PMCA). SERCA and gastric H^+/K^+-ATPase are considered the closest to NKA and are used for comparative studies [12].

The smallest functional unit of NKA is a heterodimer of two subunits denoted α and β. NKA can also associate with a protein of the FXYD family, formerly denoted as subunit γ. However, several electrophoretic and kinetic measurements with NKA from tissue samples suggest the existence of higher oligomeric states, up to $(\alpha\beta)_4$ [13].

1.2. Subunits of Na^+/K^+-ATPase

1.2.1. Subunit α

Subunit α is the main catalytic subunit of the NKA. It weights approximately 110 kDa and has ten transmembrane (TM) helices. The large cytoplasmic loops between helices TM2/TM3 (C23) and TM4/TM5 (C45) form cytoplasmic (A-, P- and N-) domains that bind ATP and undergo phosphorylation [14]. Based on the structures obtained by the X-ray crystallography [15], [16], there are two main conformations of the α subunit – open, with the cytoplasmic domains standing apart and closed with the domains packed together. The structure of the α subunit is shown in *Figure 1*.

The A-domain (*actuator*) consists of the N terminal part of the subunit and C23 loop. It rotates during the reaction cycle, the movement also influencing the cytoplasmic part of TM2. It contains the conserved 217TGES motif (in human α1 numbering, unless stated otherwise), on the N-domain facing side.

The P- (*phosporylation*) and N-(*nucleotide*) domains are located on the C45 loop. The N-domain is comprised of the middle of the loop, while the P-domain consists of two parts – before and after the N-domain [17].

The P-domain contains several motifs conserved between the P-type ATPases – the phosphorylated D376 is a part of the 376DKTGTL motif. Together with the nearby 617TGD motif and the 715TGDGVND motif, it creates a binding pocket for the phosphate chain of ATP, and Mg^{2+} [17]. A binding site of a non-transported potassium is located at the P-domain and is presumed to be responsible for the activation of dephosphorylation [12] .

The N-domain contains the ATP nucleotide binding pocket, made of antiparallel β-sheets. The conserved 590-DPPR motif is located at the TM5 side of this domain [17]. This domain is connected to the P-domain by two hinge strands that allow for a wide range of movements of the domain during the reaction cycle [18].

The ATP molecule required for ion pumping is stretched between the N- and P-domains. The N-domain residues taking part in nucleotide binding are K487, Q489, K508 [19] , R430, D450, S484 [20] and F482, which binds the adenine ring by π-stacking interactions [21]. K487 and R551 of the N-domain take part in the phosphate chain binding [18], [21].

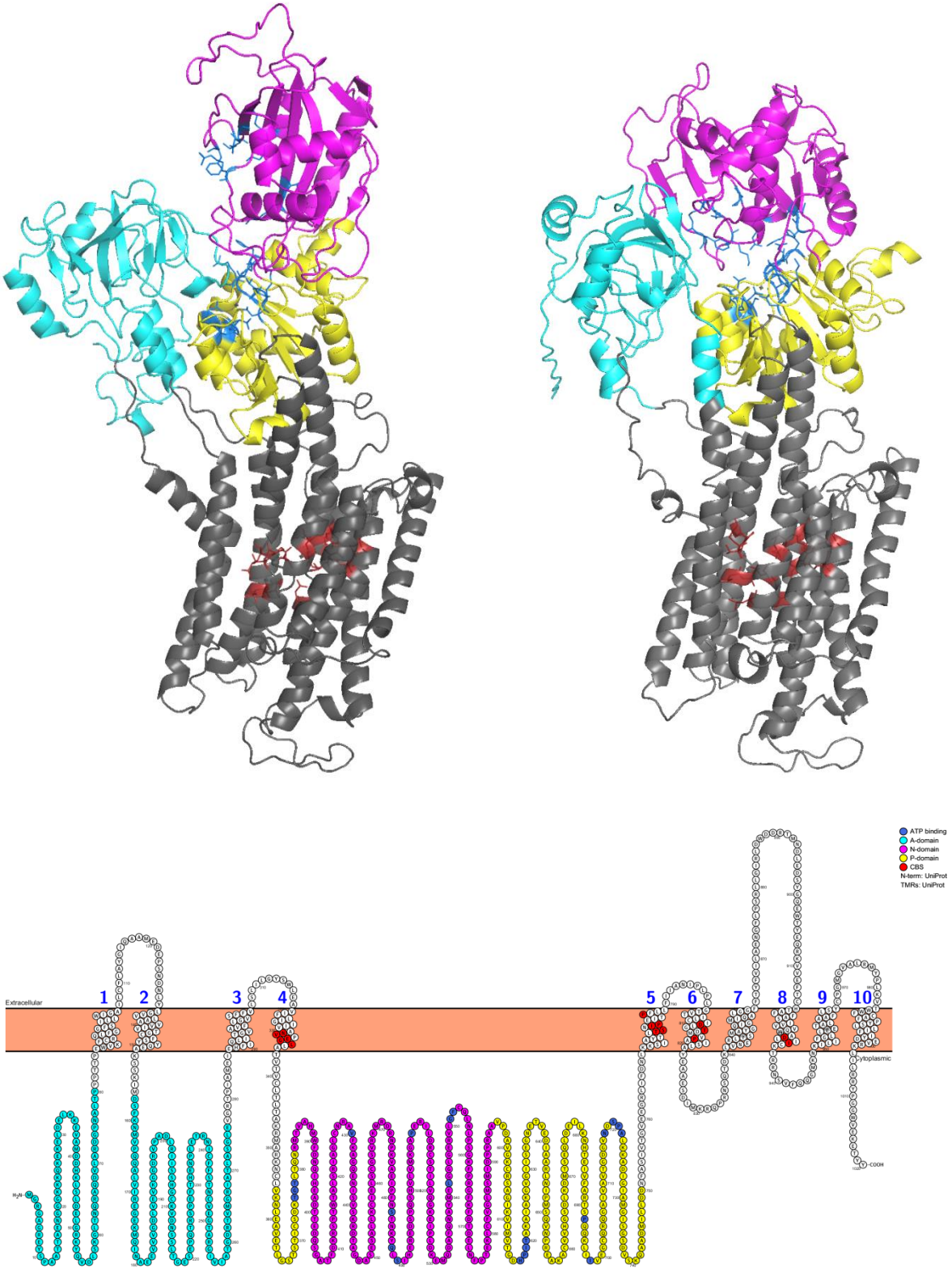

Figure 1: The α subunit in the open (left) and closed (right) conformation and schematically. The cytoplasmic domains are in cyan (A-domain), yellow (P-domain) and magenta (N-domain), ATP binding residues are in blue and cation binding residues are in red, highlighted as lines in the top image.

On the P-domain, the ATP phosphate chain ends at D376 that is later phosphorylated. To achieve the correct position, residues 377KTGT, 615MVTGD and 716GDGVND help to stabilize the phosphate chain position [22], [23].

We studied the nucleotide binding in different molecular dynamics simulation setups in publication IV.

The helices in the transmembrane part of NKA form the cation binding site (CBS) for the transported ions and several pathways for these ions (and water) to reach the CBS.

There are three cation binding sites (CBS) (*Figure 2*). Two of them can both bind sodium and potassium ions – site I between N783, S782 (TM5) and D811, D815 (TM6), site II between A330, V332, E334 (TM4), E786 (TM5) and D811 (TM6) [15]. Only sodium ions can occupy site III, between T781, Y778 (TM5) and E930 (TM8) [24], [25].

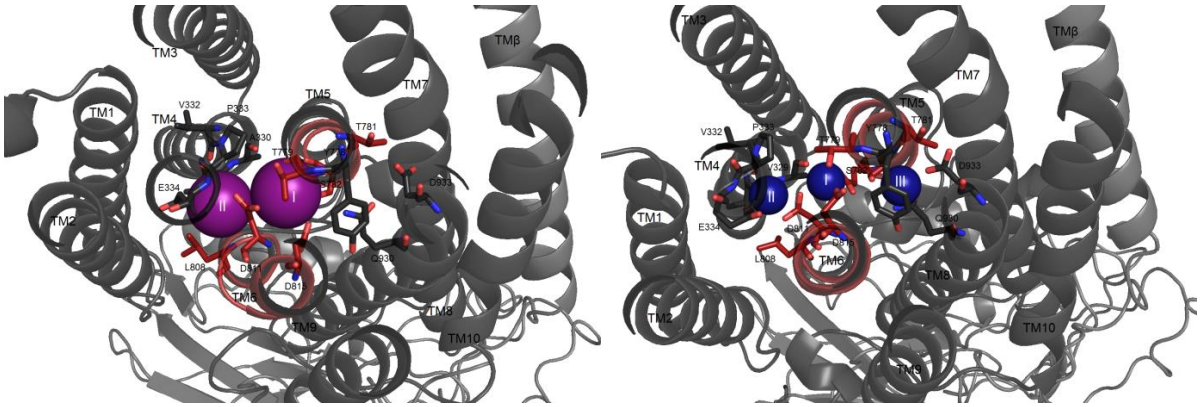

Figure 2: The transmembrane part of NKA in the the open (left) and closed (right) conformation viewed from the cytoplasmic side showing the CBS with potassium (purple) and sodium (blue) ions. Red segments depict the differences between the conformations.

Because NKA transports sodium ions against their concentration gradient, a precise gating mechanism including occluded sodium- and potassium-bound states is necessary. Subsequently, attempts to describe the extra- and intracellular pathways used by the ions to get to the CBS were published. The intracellular C-terminal pathway was described in [26] as leading between T781, Q861, Q930, D933, D1002, Y1022 and Y1023 (between TM5, TM7 and TM8). They also mentioned the existence of an N-terminal pathway analogous to the one in SERCA between TM1, TM2, TM4, and TM6 [27]. The extracellular pathway was examined by mutation experiments on palytoxin inhibited pump [28] and later confirmed as leading between TM1, TM2, TM4, TM5 and TM6 [29].

The binding and potential transport of protons through the CBS has also been discussed [30]. Based on [26], [31], it has been proposed that E334, E786, E961 with D811 and D815 in the potassium bound state are protonated. Recently it was suggested that the opening and closing of the pathways is controlled by CBS residue protonation [32], [33].

We studied the influence of different ligands and protonation on the opening and closing of ion pathways leading to CBS in publication I.

1.2.1.1. Isoforms of α-subunit

There are four isoforms of the α subunit [34], which have a great degree of sequential similarity (81% identity for isoforms α1-α3, 71% identity across all four isoforms) and are spread across the body in tissue specific manner [35].

Isoform α1 is the main housekeeping isoform. It is 1023 amino acids long and it is present in all cells. Its main role is maintaining cell homeostasis by creating sodium gradient.

Apart from this general function, the α1isoform is present in a great amount in kidneys, where it controls sodium ion reabsorption by regulating sodium excretion from blood to urine [36]. Dysfunctions in this process have been shown to play a role in hypertension [37], [38] and aldosterone-producing adenomas [39].

Isoform α2 is present in the skeletal and heart muscles, astrocytes and other glia cells [34]. It has 1020 amino acids with deletions in the N-terminal region and Q502 with respect to the α1 isoform. It is crucial for the proper function of the body, as NKA α2 knockout mice die after birth due to inability to breathe [40]. It cooperates with the α1 in the heart muscles to maintain a proper Na^+ concentration, which is necessary for the Na/Ca exchange and Ca^{2+} dependent contraction regulation [41], [42].

Mutations in the α2 subunit lead to type 2 of familiar hemiplegic migraine (FHM2) [43], a hereditary disease that leads to a weakness or paralysis of one side of the body during an attack, in addition to at least two of typical migraine with aura symptoms (flickering lights in the field of vision, feeling of pins and needles or hot and cold sensation in extremities, speech impairments, loss of balance, double vision and severe headache) combined with photophobia and nausea [44], resulting in some cases in decreased consciousness or even coma[45]. FHM2 associated mutations can also occur *de novo*, leading to sporadic hemiplegic migraine [46] with similar symptoms.

The mutations linked to FHM2 are L764P (near TM5 and the P-domain), W887R (L78) [47] and G301R and others [48]. Sporadic, *de novo* hemiplegic migraine was also connected to α2 subunit mutations, namely E120A, E492K, P786L, R834X and R908Q [46].

The α2 mutations in mouse models were reviewed in [49].

Isoform α3 is present in neurons and central nervous system, taking care of rapid ion exchange required for their function. It has 1013 amino acids, with a deletion in the N-terminal region with respect to the α1 isoform. There are several diseases caused by mutations of the α3 isoform of the NKA.

The typical symptoms of alternating hemiplegia of childhood (AHC) consist of episodes hemiplegia (paralysis of a half of the body) that may spread through the rest of the body, which disappear during sleep (but can reappear 10-20 minutes after reawakening). The first episode appears before 18 months of age [50]. Additionally, episodes of abnormal eye movement, dystonia (uncontrolled muscle contractions) and developmental delay accompany this disorder [51]. The α3 isoform mutations connected to AHC occur mostly *de novo* [52] and have been identified in two different studies [52], [53] with the most frequent mutations being D801N (corresponding to D811 in α1, a part of the CBS) and E815K (corresponding to E825 in α1, at the C-terminal pathway).

The onset of rapid-onset dystonia parkinsonism (RDP) is typically caused by stress caused by fever, heat, childbirth or emotional factors [54]. Its main symptoms are dystonia combined with the features of the Parkinson's disease – tremors, akinesia (decreased bodily movement), slowness of movement and instability [55]. Unlike the Parkinson's disease, whose symptoms start to show at about 50 years of age in the majority of patients, RDP is typical by onset in late adolescence or early adulthood [56]. The mutations connected to this disease are I284T [54], E287K [54] on TM3, T623M the P-domain [57], [58], I768S [59], F790L on TM5 [54] and D811Y in the CBS [56].

The CAPOS syndrome [60] is a rare disease that was discovered within a family in 1996, and observed in two more cases since then. Its symptoms are cerebellar ataxia (the lack of voluntary muscle coordination originating in the brain), areflexia (the lack of reflexes), *pes cavus* (high foot arch), optic atrophy (wasting away of the optic nerve), and sensorineural hearing loss (hearing loss originated in the inner ear or in the neural part). It is caused by a

mutation of E818 (E828 in α1) to a lysine on the cytoplasmic TM6/TM7 loop in the vicinity of both TM5 and the C-terminal pathway [61].

The α3 mutations in animal models were reviewed in [62].

Additionally, mutations of the α3 isoform were connected to even rarer disorders, such as fever-induced paroxysmal weakness and encephalopathy (R756H, R756L mutations [63]) or multi-symptom borderline disorder with features of both AHC and RDP (G867D mutation [64]) or take part in early infantile epileptic encephalopathy (G358V mutation [65]) or relapsing encephalopathy with cerebellar ataxia (R756C [66]).

Isoform α4 is present in the male germ cells [67]. Electrophysiology experiments suggest that this isoform is tuned to maintain a stable turnover rate in varying extracellular environments the sperm cell encounters before and during capacitation [68]. It has 1029 amino acids, with the additional ones present in the N-terminal region with respect to the α1 isoform.

1.2.2. Subunit β

The β subunit is located mostly in the extracellular environment, with one transmembrane helix (TMβ) at the N-terminus. The cytoplasmic part of β subunit forms an α-helix that interacts with the C-terminal end of the α subunit. The extracellular part of β subunit covers the extracellular ends of α subunit transmembrane helices which protects them from degradation during protein folding [69].

The extracellular part of β subunit can be heavily glycosylated, with three to nine glycosylation sites, present in an isoform and species specific manner. NKA can function without the core glycosylation, it is, however, more susceptible to trypsine proteolysis. Glycosylation also influences the adhesive properties of the protein [70].

The presence of β subunit in H^+/K^+-ATPase, but not in the sarcoplasmic Ca^+-ATPase (SERCA), suggests that β subunit is also necessary for potassium transport. Different β subunit isoforms combined with the same α subunit isoform lead to a protein with different potassium affinities [71]. The conformation of β subunit follows the conformational changes of the α subunit during the reaction cycle [72].

Apart from its role in the NKA function, β subunit also serves as a molecular chaperone, which allows the protein to fold properly and plays a crucial role in the protein maturation. Moreover, β1-β1 intercellular interaction can occur between cells expressing identical β1

subunits, anchoring NKA at lateral borders of epithelial cells. Differential expression of β subunit isoforms also influences spatial localisation of NKA in the cells [71], [73].

There are three isoforms of the β subunit forming a functional protein with the α subunit and they are distributed in tissue specific manner [71] and a regulatory β subunit-like protein [74] present in muscles, which does not assemble with NKA, but serves as a transcription coregulatory [75].

The α and β subunits bind together in an isoform specific manner, which in turn influence properties of the whole enzyme. Isoform β1 preferentially binds to α1, while β2 preferentially binds to α2 [76]. In the brain cells, β3 transcript is prevalent in oligodendrocytes but negligible in astrocytes and neurons [77], while α1 and β1 are detected in neurons and astrocytes, α2 and β2 predominantly in astrocytes and α3 in neurons [78].

The α2β2 combination with a lower K^+ affinity and higher voltage sensitivity than other αβ isoform combinations seems to be tuned to work in an environment with a high potassium concentration. It is found in astrocytes [78] and muscles [79], maintaining the extracellular potassium concentration. Similarly, the activity of the α3β1 isoform combination present in neurons with a low apparent Na^+ affinity is enhanced by a high intracellular sodium concentration which occurs during membrane depolarisation [78].

1.2.3. The FXYD Family Proteins

The FXYD family proteins are a group of tissue specific NKA regulators, which consist mostly of one transmembrane helix. The FXYD helix is located next to α subunit TM9 and TMβ and connects with them on the extracellular side by the specific FXYD sequence. There are seven members of this family present in the human body with a great variability – only six amino acids of approximately 60 are identical among all of them [80].

The FXYD1 protein is present mostly in the heart, liver and skeletal muscle. It is presumed to have a role in muscle contractility and cell volume regulation. It decreases Na^+ affinity of NKA and its dissociation is controlled by protein kinase A phosphorylation.

The FXYD2 protein is predominantly expressed in kidneys and it is present in all crystal NKA structures. It can either increase or decrease K^+ affinity of the pump, depending on the membrane potential, and it increases Na^+ affinity.

The FXYD3 protein had been found in stomach, skin, colon and uterus tissues. Moreover, it is present in breast tumours, prostate tumour and breast tumour and colorectal cancer cell lines. When associated with NKA, it causes a decrease in both K^+ and Na^+ affinity.

The FXYD4 protein is expressed in basolateral membranes of kidney medulla and distal colon. It leads to increased Na^+ affinity, which allows the pump to transport ions even at low intracellular Na^+ concentrations.

The FXYD5 protein is characteristic by longer N-terminal (extracellular) tail sequence than other proteins of this family. It has been found in kidneys, lungs, heart and spleen. It has not been found to associate with NKA.

The FXYD6 protein is expressed in the central nervous system. It influences potassium affinity and its role in neuronal excitability has been suggested [81].

The FXYD7 protein is present only in brain – in neurons and to lesser degree in glial cells. It associates with the combination of α1, β1, and β3 NKA isoforms, but not with β2. It increases K^+ affinity of NKA, enhancing extracellular K^+ clearance at low concentrations [80].

1.3. Available Structures

1.3.1. N-domain Structures

Taking advantage of its small size and solubility, N-domain structures appeared in the Protein Data Bank (PDB) archive [82] several years before the structures of the whole NKA.

There are currently two NMR based structures of the NKA, both describing an isolated N-domain of α subunit. They are submitted as a series of 20 snapshots sorted according to energy. The structure with PDB ID 1MO7 is captured in the absence, while 1MO8 [18] in the presence of an ATP molecule. In 1MO7, the loops between sheets β2/β3 and β5/β6 are flexible, in 1MO8, the β2/β3 loop is stabilised by the ATP molecule and only the loop between sheets β5/β6 fluctuates.

The main difference between these two structures is in the hinge region between the N- and P-domains, which influences the tilt angle of N-domain with respect to P-domain. The ATP-binding residues were described as F482, K487, K508-E513 and Q489 [18].

A crystal structure of the N-domain at 2.6 Å resolution was obtained in the same year as the NMR structures, and it is deposited under the PDB ID 1Q3I [83]. In contrast to the NMR structures, they define seven β-sheets instead of six, but they agree on five α- helixes (*Figure 3*). This discrepancy is probably caused by differing experimental conditions – NMR measurements are performed in solution and allow for a wider range of small-scale structure fluctuations than conditions necessary for crystallisation. The structure does not include any nucleotide, but there are three nickel ions, serving as a crystallisation agents.

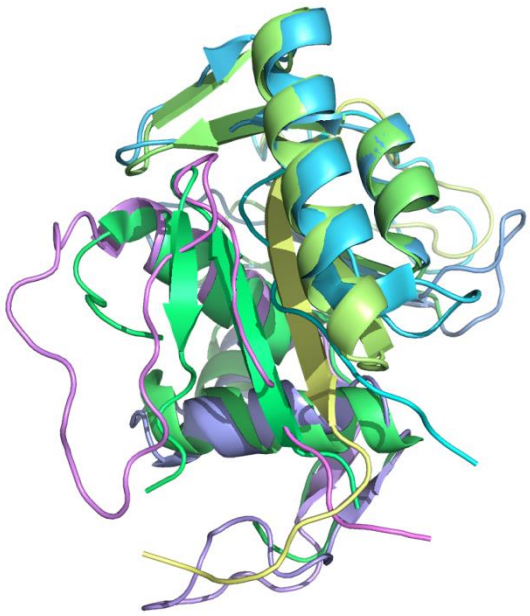

Figure 3: Comparison of the NMR-solved N-domain structures 1MO7 (cyan to pink) and crystal 1Q3I (green to yellow) structures. The extra β sheet of 1Q3I is visible on the left side of the picture.

1.3.2. Whole Protein Structures

All structures of the whole NKA were obtained by the X-ray crystallography with different resolutions. They can be divided into two groups according to the conformational state of the protein (*Figure 4*).

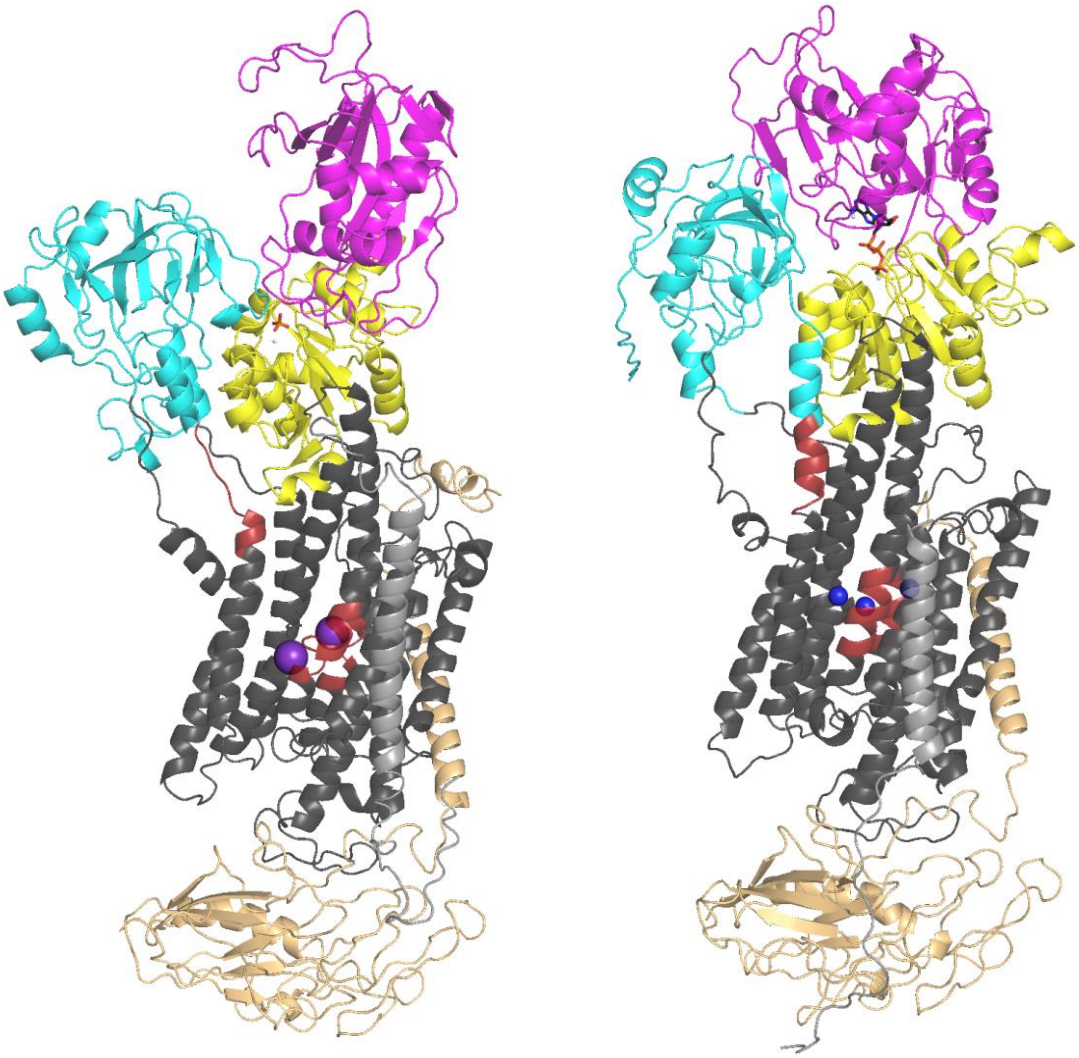

Figure 4: Open (left) and closed (right) crystal conformations. The transmembrane part of α subunit is in dark grey with cytoplasmic domains in cyan (A-domain), magenta (N-domain) and yellow (P-domain). The β subunit is in pale yellow, the FXYD family protein in light grey. CBS ions are in purple (potassium) or blue (sodium; between the domains there is phosphate in orange, ATP in black with orange phosphate chain. Red colour highlights the main structural differences of TM helixes between the open and closed conformation.

1.3.2.1. Open Conformations

The most prominent feature of the open conformation of the NKA is the position of the A- and N- domains wide apart (about 3.5 nm). The intracellular part of TM2 unwinds to allow the A-domain to rotate away from it, and at least one of TM4, TM5 and TM6 unwind at the CBS.

There are two main groups of the open crystal structures based on the phosphorylation state of the protein: structures with bound MgF_4^{2-} as a free phosphate analogue (mimicking the E2·Pi state) and structures with phosphorylated D376 (or corresponding residue in porcine or bovine form, mimicking the E2-P state). However, the structures are very similar.

The MgF_4^{2-} bound open structures were published earlier, but they have better resolution than the phosphorylated ones. Structures with PDB IDs 3B8E [84] and 3KDP [84] are both with bound rubidium ions (as potassium ion analogues) in the CBS and another one below the P-domain, and a lipid molecule between TM7 and TMβ (phosphatidylcholine and cholesterol, respectively). Due to its low resolution, 3B8E is missing the extracellular part of the β subunit. 2ZXE [85], isolated from the spiny dogfish shark, includes two potassium ions in the CBS, one under the P-domain and a cholesterol molecule between TM7 and TMβ. It is the structure with the best resolution available; therefore it is often used as template for molecular models. 3A3Y [86] includes two potassium ions in the CBS, one under the P-domain and a cholesterol molecule between TM7 and TMβ, and an ouabain molecule in the low-affinity position in the extracellular pathway.

All the structures differ only slightly by the position of TM1 and mobile N-domain loops. The ouabain molecule bound in 3A3Y causes also a movement of the extracellular ends of TM3 and TM4.

A series of snapshots of CBS ion exchange was recently published [87] under the IDs 5AVQ-5AVZ and 5AW0-5AW9. They contain a potassium ion under the P-domain, cholesterol between TM7 and TMβ, and either two potassium; or one potassium and one tellurium/rubidium; or two tellurium/rubidium ions in the CBS, depending on the buffer and the length of incubation.

The phosphorylated open structures are usually captured in the presence of ouabain or other cardiotonic steroids (CTS). 3N2F [88], the only structure without a CTS molecule, was superseded by 4RES [89] and removed from the PDB database. 3N23 [88] captures the high-affinity ouabain binding in the absence of ions in the CBS, while 4HYT[90] contains a magnesium ion in the CBS. Similarly, digoxin-bound 4RET [89] contains a magnesium ion in the CBS and bufalin-bound 4RES [89] contains potassium in the CBS. These two structures also differ by the position of the N-domain. Finally, 4XE5 [91] is a bovine structure with a magnesium ion in the CBS and high-affinity bound ouabain, which differs from 4HYT by a 10° displacement of the N-domain.

1.3.2.2. Closed Conformations

The cytoplasmic domains of the closed structures are closely packed together, with an ADP molecule in the binding pocket between the N- and P-domains. A helix at the start of C23 loop of the A-domain leads continuously from the cytoplasmic end of TM2 and both TM4 and TM6 remain unbroken at the CBS (*Figure 4*).

To date there are three crystal structures of NKA in the closed conformation. 4HQJ [16] was the first closed conformation published and even though it has the lowest resolution of all currently available crystal structures, it illustrated the different position of the cytoplasmic domains with bound ADP and AlF_4^-, and confirmed, which of two putative sites is the sodium specific CBS site III. 3WGU and 3WGV [24] bring better resolution of the closed NKA conformation and 3WGV also contains a bound molecule of oligomycin A, an inhibitor impairing the E1-P→E2-P state transition of the protein [92].

The crystal structures, CBS-bound ions, other ligands, protein states, resolutions and years of publication are summarized in Table 1.

Table 1. Available high-resolution structures of NKA

[a] Rb^+ and Tl^+ are K^+-analogs. [b] MgF_4^{2-} and AlF_4^- are phosphate analogues; ouabain, bufalin, digoxin and oligomycin A are NKA inhibitors; cholesterol (CHOL), 1,2-dioleoyl-sn-glycero-3-phospho-L-serine (DOPC) and 3-sn-phosphatidylcholine (PC) are the membrane lipids; N-acetyl-D-glucosamine (NAG), 2-(acetylamino)-2-deoxy-α-D-glucopyranose (NDG), o-dodecanyl octaethylene glycol ($C_{12}E_8$), 1-O-decanoyl-β-D-tagatofuranosyl β-D-allopyranoside (DTFA), β-D-fructofuranosyl 6-O-decanoyl-α-D-glucopyranoside (FFDG) and sucrose are compounds of the crystallization buffers. [c] E2P denotes the phosphorylated enzyme, while E2·Pi and E1·Pi denote the enzyme with non-covalently bound phosphate.

PDB ID (ref.)	Ions in CBS [a]	Other ligands [b]	Position of domains	Assigned state [c]	Resolution	Year
3B8E [84]	2 Rb^+	Mg^{2+}, MgF_4^{2-}, PC	open	E2·Pi	3,5 Å	2007
3KDP [84]	2 Rb^+	Mg^{2+}, MgF_4^{2-}, CHOL,	open	E2·Pi	3,5 Å	2007
2ZXE [85]	2 K^+	Mg^{2+}, MgF_4^{2-}, CHOL, NAG, NDG	open	E2·Pi	2,4 Å	2008
3A3Y [86]	2 K^+	Mg^{2+}, MgF_4^{2-}, CHOL, ouabain, NAG	open	E2·Pi	2,8 Å	2009
5AVQ-5AW9 [87]	K^+/Rb^+ /Tl^+	Mg^{2+}, MgF_4^{2-}, NAG	open	E2·Pi	2,6-3,5 Å	2015
3N23 [88]	---	Mg^{2+}, ouabain	open	E2P	4,6 Å	2010
3N2F [88]	2 K^+	---	open	E2P	4,1 Å	2011
4HYT [90]	1 Mg^{2+}	Mg^{2+}, ouabain, CHOL, DOPS, $C_{12}E_8$, DTFA, FFDG	open	E2P	3,4 Å	2013
4RES [89]	2 K^+	Mg^{2+}, bufalin, CHOL, DOPS, NAG, sucrose	open	E2P	3,4 Å	2015
4RET [89]	1 Mg^{2+}	Mg^{2+}, digoxin, CHOL, DOPS, NAG, sucrose	open	E2P	4,0 Å	2015
4XE5 [91]	1 Mg^{2+}	Mg^{2+}, ouabain, CHOL	open	E2P	3,9 Å	2016
4HQJ [16]	3 Na^+	Mg^{2+}, AlF_4^-, ADP, CHOL	closed	E1·Pi–ADP	4,3 Å	2013
3WGU [24]	3 Na^+	$2Mg^{2+}$, AlF_4^-, ADP, CHOL, PC, NAG	closed	E1·Pi–ADP	2,8 Å	2013
3WGV [24]	3 Na^+	$2Mg^{2+}$, AlF_4^-, ADP oligomycin A, CHOL, PC, NAG	closed	E1·Pi–ADP	2,8 Å	2013

1.4. The Reaction Cycle

The basics of the NKA reaction cycle were already outlined in the 1960's by Post [93] and Albers [94] and later refined by other authors. The reaction cycle can be described as the sequence of following steps: ATP binding → intracellular sodium binding → protein phosphorylation → ADP release → extracellular sodium release → extracellular potassium binding → protein dephosphorylation → intracellular potassium release → ATP binding.

The main feature of the Post-Albers diagram is dividing the protein conformations into E1 and E2 states. However, the exact definition of the E1 and E2 state properties vary, as well as the exact sequence of steps (*Figure 5*). Originally, Post [93] postulated the protein adopts states either open to the extracellular side (E_o), open to the intracellular side (E_i), both of which are at some point of the reaction cycle phosphorylated and ion bound. Albers [94] didn't take the transported ions into account and described the enzyme states as E1 and E2, stating "the various forms of E1 are enzyme molecules with inwardly oriented cation sites of high Na^+ affinity, the E2 forms have outwardly oriented cation sites of high K^+ affinity". These two approaches were summarised by Post and Hegyvary in ref [95]. They also observed that K^+ binding reduces the enzyme affinity to ATP, which might be an indication of the E1 (high ATP affinity) to E2 (low ATP affinity) conformational change. Currently, both the ion affinity and ATP affinity definitions of the states are in use.

Different versions of the Post-Albers diagram are compared in *Figure 5* and presented separately in Appendix A. The most agreed-upon step is the E2-P → 2K-E2-P, which presumes all Na^+ ions leave the CBS before potassium binding starts, while the protein is in the phosphorylated E2 state. Then either dephosphorylation combined with the occlusion of the potassium ions in the CBS occurs, or the dephosphorylation of the protein is a separate step in the reaction cycle. The E2 → E1 transition and ions/ligands bound during this step is still unclear, though the majority of authors presume it happens to the potassium- and ATP-bound protein. Some authors then consider the protein to be yet again in a state without the CBS bound ions (either as E1 or as E1-ATP), after which there is the widely agreed-upon 3Na-E1-ATP step. There is variability in the phosphorylation and sodium occlusion and subsequent release steps; however, most authors agree that the E1 → E2 transition occurs with the sodium ions still bound to the CBS.

The CBS ion binding sequence is better understood than whole protein moments, thanks to both crystallography and other binding experiments. It has been shown that potassium ions

bind sequentially first in site I and then in site II [87]. The studies of sodium ions binding discovered that both sodium intracellular binding [96]and extracellular release [97] are sequential as well, first the ions occupying the binding sites I and II, then III [98], [99].

Magnesium is necessary to NKA function and it is present in all the crystal structures. It probably binds in a separate step from the ATP [100], and it helps with the NKA phosphorylation [101]. The ion stays in the vicinity of D376, even after the phosphorylation of the residue [102], but it is still unclear, in which part of the reaction cycle it is released. Moreover, most studies don't take the role of magnesium into account and don't even mention it in their Post-Albers diagrams.

Even though the authors usually assign a reaction cycle state to the crystal structures (2K-E2 to the open structures and 3Na-E1 for the closed structures, see Table 1), the relationship between different states and conformations is still unclear. Moreover, in SERCA, the closest similar ATPase to NKA, the open conformation corresponds to the E1 state, while the closed conformation corresponds to the E2 state, opposite from the NKA, which caused especially older publications to describe the domain movements incorrectly [103] . Given that the E1/E2 states can be defined both by the ATP and ion affinity, which correspond to different regions of the structure, it is difficult to say, which conformational change leads to the E1↔E2 state transition.

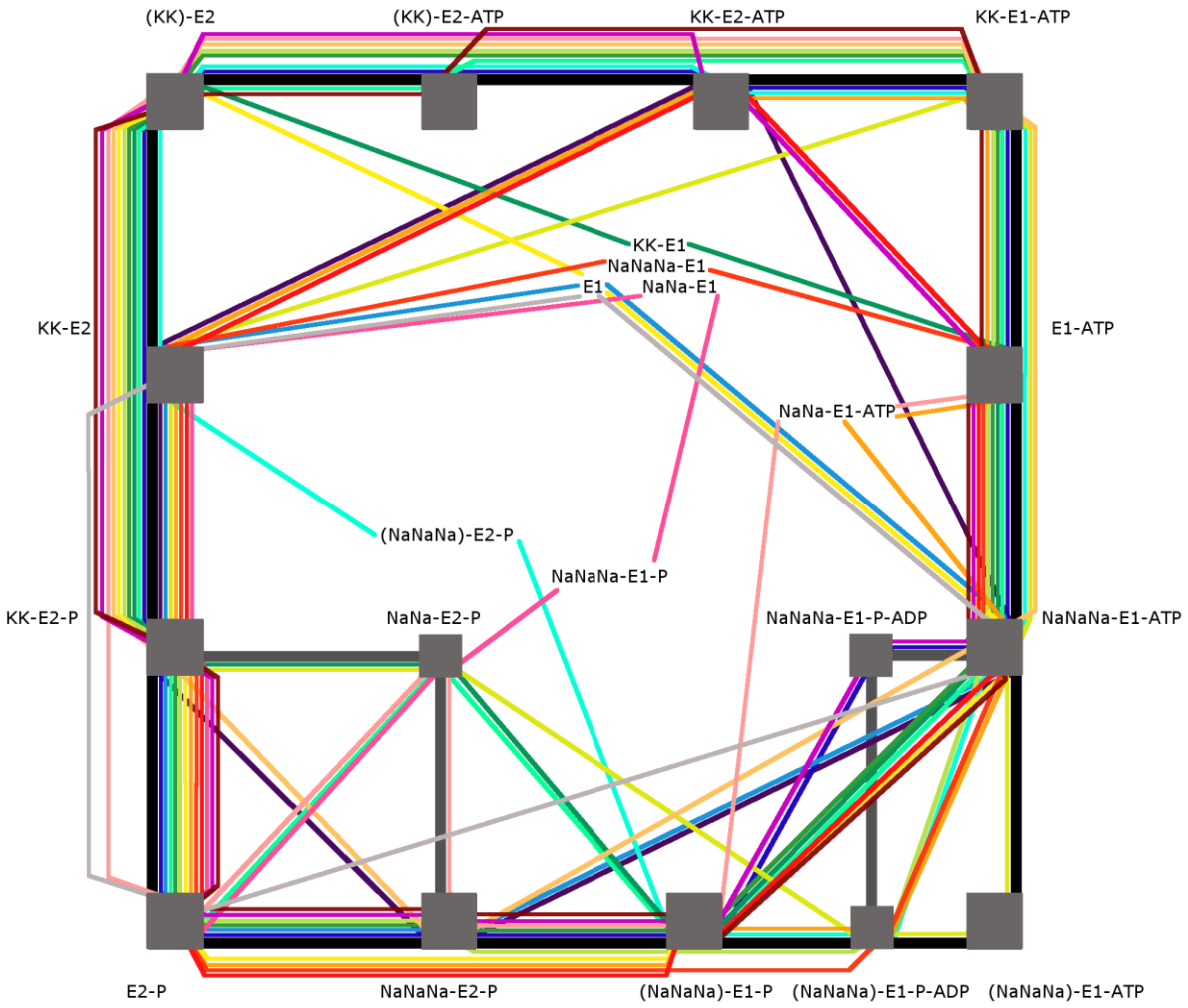

Figure 5: The different versions of the Post-Albers diagram. The colours depict the diagram as used by Post [95] (purple), Vasilets [104] (dark blue), Rose [5] (light blue), Wagg [105] (cyan), Kaplan [8] (light green), Jorgensen [17] (forest green), Martin [14] (dark green), Dempski [72] (yellow-green), Morth [84] (green-yellow), Schack [106] (yellow), Grycová [100] (orange), Bublitz [11] (orange-red), Gadsby [107] (light orange), Vedovato [108] (salmon), Toyoshima [15] (red), Grichanin [109] (pink), Ogawa [87] (fuchsia) and Appel [110] (dark red). The lines go inside of the rectangle in cases where the states go through all depicted step and outside when skipping a step.

1.5. Compounds Interacting with Na^+/K^+-ATPase

Compounds influencing the NKA function have been long used in the treatment of heart problems [111], to promote blood circulation [112] or, more recently, are in the clinical trials for cancer therapy [113]. On the other hand, in higher doses, they can induce acute organ failure [114] and were used in poison arrows [115].

Compound interacting with NKA have also been studied with respect to side effects of medicaments used for treating other diseases, such as cancerostatic cisplatin [116] or mood stabilising lithium [117].

1.5.1. Cardiotonic Steroids

The largest group widely used group of NKA active compounds currently used in medicine are cardiotonic steroids (CTS). They can be plant (digitalis, digoxin, ouabain) or animal (bufalin, marinobufagenin) based [118], [119] and they inhibit NKA function by binding into the open extracellular pathway (*Figure 6*) in E2P state of the protein and obstructing K^+ ion movement [120].

There are several CTS present in nanomolar concentration the body, such as ouabain, marinobufagenin, telocinobufagin or bufalin, serving as endogenous hormones [42].

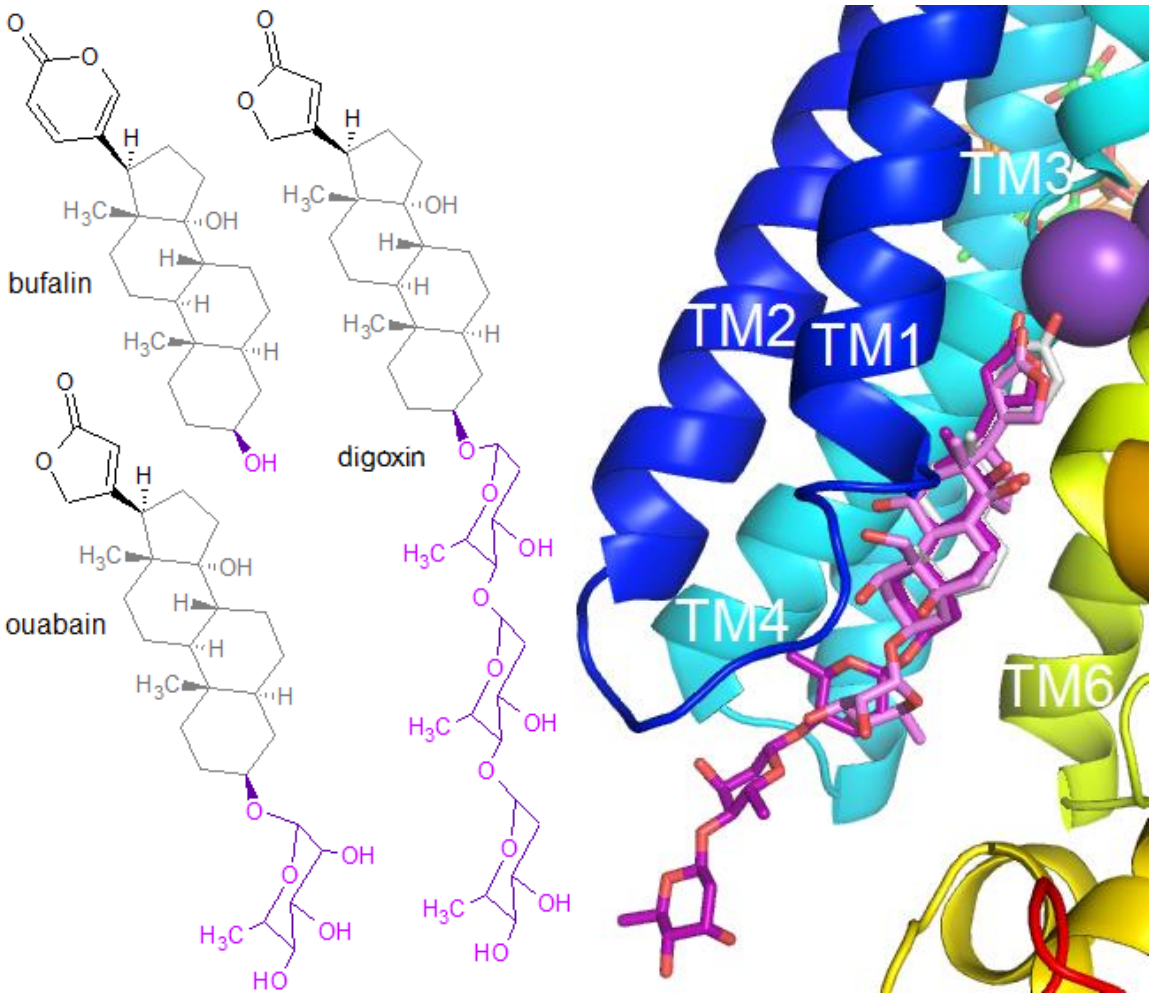

Figure 6: The structures of CTS available in crystal structures (left), with the steroid core depicted in grey, lactone ring in black and glycones in purple. Overlay of the CTS bound in the extracellular pathway – bufalin is in white, ouabain in light violet, digoxin in purple, CBS potassium as a dark purple ball.

The mechanism of CTS function in heart failure treatment is by indirectly stimulating the heart muscle. CTS inhibition of NKA stops efflux of sodium ions, leading to disruption of the ideal Na^+ concentration. To counter this, the Na^+/Ca^{2+} exchanger reverses its ion transport, which raises the concentration of intracellular calcium. Increased calcium concentration induces a muscle contraction [121].

Even though ouabain and digoxin are used in the treatment of congestive heart failure and atrial arrhythmias; however, their toxicity requires only low doses to be administered [122], [123]. As they also function as endogenous hormones, heightened levels used in heart therapy lead to long term effects such as hypertension, reduced heart contractibility [124] or hyperthorpy, fibrosis or arrhythmia [42] .

Therefore, the search for novel compounds acting on NKA from plants [125], animals [126] or in databases of small molecules [119], [127] continues.

1.5.2. Flavonolignans

Flavonoids are a group of compounds present in extracts from medical plants such as *Silybum marianum* or *Ginkgo biloba*. They have been shown to possess antioxidant, anti-cancer antibacterial and anti-ageing properties. Together with lignans they are present in whole grains, fruits and vegetables [128].

Flavonolignans are a subclass of flavonoids where the flavonoid is connected to a lignan. They can be extracted from plants, such as *Silybum marianum* (milk thistle [129]), *Verbascum sinaiticum* (mullein [130]) or *Hyparrhenia hirta* (Coolatai grass [131]) or they can be synthetized chemically.

A standardised extract from the milk thistle seeds (its name is derived from the droplets of milk used to feed infant Jesus that supposedly fell on the plant) is called silymarin. It contains approximately 70% of flavonolignans and exhibits hepatoprotective properties. It is used in liver disease therapy and it is in clinical trials as a supplement to reduce chemotherapy toxicity [132]. Apart from already medically utilised effects of silymarin, the extract also exhibited neuroprotective activity, intestinal anti-inflammatory effect, inhibited pancreatic cell damage and photochemical cell damage, reduced efflux of drugs mediated by membrane efflux proteins and exhibited anti-cancer and anti-atherosclerotic activity [133].

Among frequently studied compounds present in silymarin (*Figure 7*) are flavonolignans silybin, isosylibin, silychristin and silydianin (differing by the position of the lignan group and its substituents); and flavonoids quercetin and taxifolin [134] .

Silybin, the most frequent and the most studied of these compounds is naturally present as a nearly equimolar mixture of two diastereomers, differing by the stereometry of the 9’ bound OH group. Silybin contains five hydroxyl groups that can be chemically modified or substituted. The C3-OH group can be easily oxidised leading to 2,3-dehydrosylibin. Regardless of these hydroxyl groups, the overall character of the molecule is hydrophobic which leads to silybin’s poor water solubility. The 2,3-dehydrosylibin is even less water-soluble than sylibin, but the extra double bond enhances its antioxidant properties – it has better performance as both radical scavenger and inhibitor of lipid peroxidation [129].

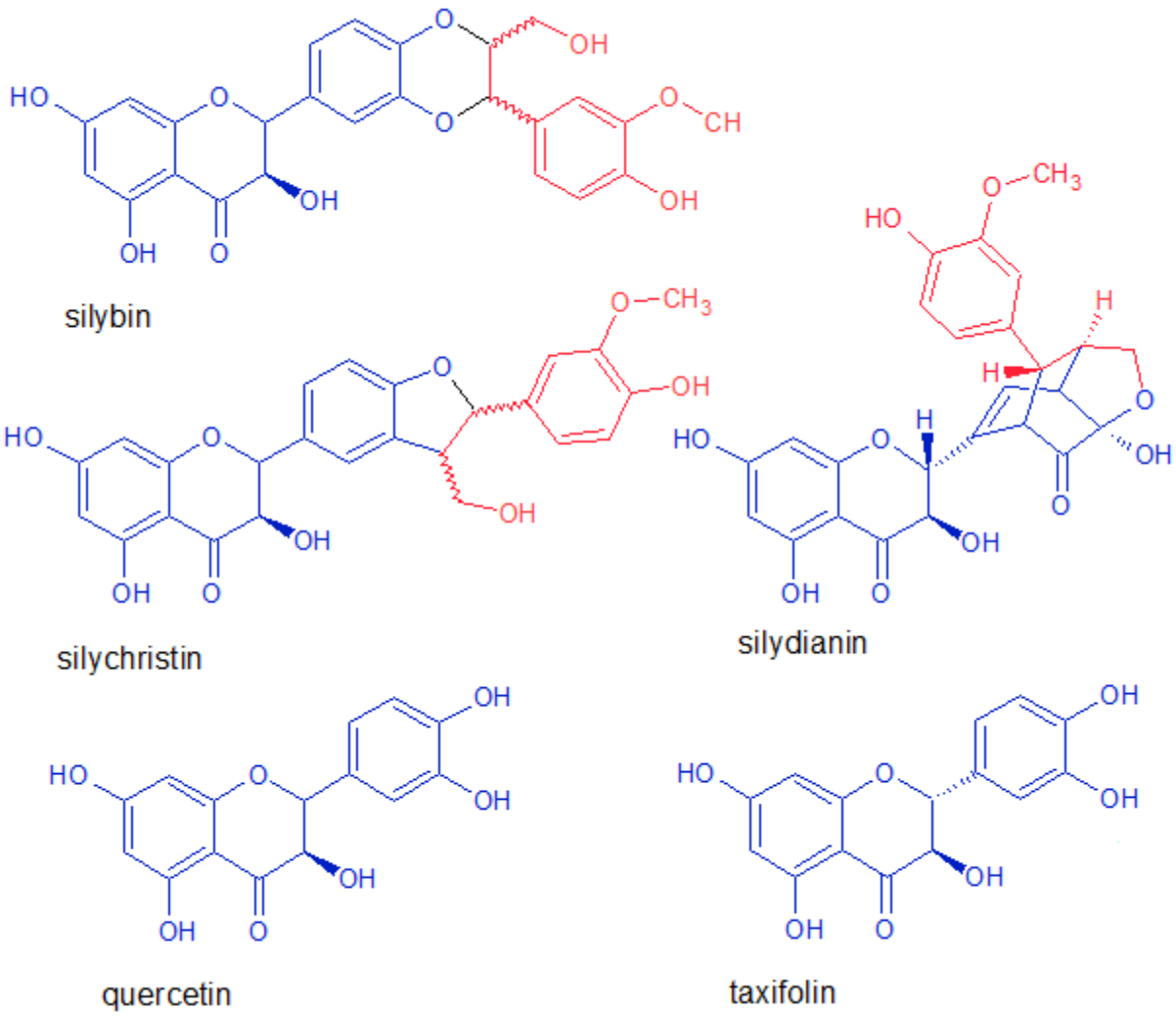

Figure 7: Compounds present in silymarin. Flavonoid part is in blue, lignan part in red.

The effect of silymarin was also studied with the respect to NKA and neurodegenerative diseases. In vitro study of mouse brain NKA showed that the activity of the pump increased with the increasing concentration of silymarin, possibly due to membrane stabilisation by reducing lipid peroxidation [135].

In publication III, we examined the inhibitory effect of different flavonolignans on NKA using both experimental and computational approach.

1.5.3. Quinolines

Quinoline and its derivatives are a diverse group of pharmacologically active compounds, exhibiting antibiotic, antitumor or anti-inflammatory activities. A medically important quinoline derivative is quinine ((R)-[(2S,4S,5R)-5-ethenyl-1-azabicyclo[2.2.2]octan-2-yl]-(6-

methoxyquinolin-4-yl)methanol), which, with its derivatives, is used in the treatment of malaria [136].

8-hydroxyquinoline derivatives show cytotoxic activity on myeloma cell lines [137], 3-hydroxyquinoline derivatives exhibit cytotoxic activity on different leukaemia cell lines and lung adenocarcinoma lines. 3-hydroxyquinoline also exhibit fluorescent properties [138] and cause DNA cleavage [139]. 4-hydroxyquinoline is a tautomer of 4-quinolone, a skeletal structure of a wide range of antibiotics [140].

Phenylquinolone (or 3-hydroxy-2-phenylquinolin-4(*1H*)-one) derivatives (*Figure 8*) are isosteric to natural flavonoids. They also exhibit cytostatic properties [141] and can possibly cause disruption in cell-to-cell signalling [142].

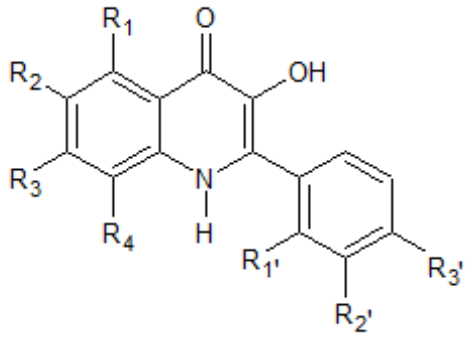

Figure 8: The structure of phenylquinolone and sites of chemical modifications.

Different isomers of chloro-derivatives of phenylquinolone can be distinguished using mass spectrometry [143] and they are active against breast, lung and colon cancer lines [141].

In publication II, we studied the interactions of chloro- and floro-derivatives of 3-hydroxy-2-phenylquinolin-4(*1H*)-one with NKA using activity measurements and the methods of computational chemistry and biology.

1.6. Computational Methods in Biology

1.6.1. Homology Modelling

There are several experimental methods for obtaining the structure of a protein, such as X-ray crystallography, NMR spectroscopy or cryo-electron microscopy. However, the great numbers of proteins present in organisms and technical requirements of these methods are still limiting factors of the amount of available structures [144]. On the other hand, DNA and protein sequences are easier to obtain and they can be used as a template for structure determination. While *de novo* modelling is useful for short sequences and necessary for exotic proteins, homology modelling is the leading method of calculating unknown protein structures [145].

To build a reliable model, a homologous protein of a known structure is necessary, ideally with a high similarity of the sequence. Then the sequences are aligned and a template structure is selected, either manually or as a part of the modelling software. The homology model sequence is then built as close to the template structure as possible, while taking into the account amino acid differences, insertions and deletions. The new structure is optimised to avoid steric clashes and energetically unfavourable conformations [146], [147].

1.6.2. Molecular Mechanics

Molecular mechanics (MM) describes molecular systems using classical mechanics to evaluate the energy of the system. Therefore it can be used for much larger systems than quantum mechanics.

1.6.2.1. Force Fields

To simulate the properties of different atoms and interactions force fields are implemented [148]. They consist of a series of equations describing bonded and non-bonded interactions and constants describing atoms which can be parametrised empirically (eg CHARMM or GROMOS [149]) or based on quantum mechanics (AMBER [150] or OPLS-AA [151].

The total potential can then be described as:

$$V_{total}(r,s) = V_{bonded}(r,s) + V_{non-bonded}(r,s),$$

where *r* is the position of the atoms and *s* force field parameters.

Bonded Interactions

Bonded interactions can occur across one bond, two bonds (angle) or three bonds (dihedrals), see *Figure 9*.

$$V_{bonded} = V_{bond} + V_{angle} + V_{dihedral}$$

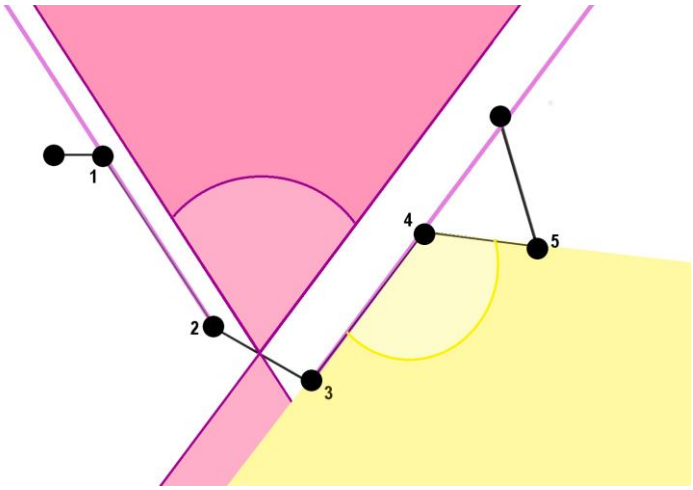

Figure 9: Illustration of angle between the atoms 3, 4 and 5 (yellow) and dihedral angle between atoms 1, 2, 3 and 4 (red).

The stretching of a bond can be described by the bond term of the bonded potential:

$$V_{bond} = \frac{1}{2} K_{bond} (r_{ij} - r_0)^2$$

where K_{bond} and r_0 are force field parameters force constant and equilibrium bond length, and r_{ij} the current distance between atoms, respectively.

The bending along an angle can be described by the angle term:

$$V_{angle} = \frac{1}{2} K_{angle} (\theta_{ijk} - \theta_0)^2$$

where K_{angle} is the force constant θ_{ijk} the current angle and θ_0 the equilibrium angle.

The torsion of atoms around a bond can be described by the dihedral term:

$$V_{dihedral} = \frac{1}{2} K_{dihedral} \left(1 + \cos(m\varphi_{ijkl} - \varphi_0)\right)$$

where $K_{dihedral}$ is a force constant, m the order of the expansion of the periodic function, φ_{ijkl} the current and φ_0 the equilibrium dihedral angle.

In some applications an improper dihedral term can be used to help describe e.g. chains of carbon atoms or organic rings.

Non-bonded Interactions

To avoid the high computational cost of calculating large number of non-bonded interactions between all the atoms in the system, only the interaction between pairs of atoms are considered.

The non-bonded interactions are usually described by two main contributions – electrostatic (described by the Coulomb potential) and van der Waals (described by the Lennard-Jones potential):

$$V_{non-bonded} = V_{Coulomb} + V_{LJ}$$

The Coulomb potential can be described as:

$$V_{Coulomb} = \frac{q_i q_j}{4\pi\varepsilon_0\varepsilon_r}\frac{1}{r_{ij}}$$

where q_i, q_j are the partial charges of the atoms, ε_0 is the dielectric permittivity of vacuum, ε_r is the relative permittivity and r_{ij} the current distance between atoms.

The Lennard-Jones potential can be described as

$$V_{LJ} = \frac{C12_{ij}}{r_{ij}^{12}} - \frac{C6_{ij}}{r_{ij}^{6}}$$

where $C12_{ij}$ and $C6_{ij}$ are parameters describing the type of the atom and r_{ij} the current distance between atoms. The r_{ij}^{-12} term corresponds to the repulsive and the r_{ij}^{-6} to the attractive dispersion interaction.

The non-bonded potential can also include terms describing polarizability of the atoms or better characterising hydrogen bonds or halogen interactions. As the non-bonded interaction weaken considerably with distance, a cut-off distance is introduced, after which the non-bonded interactions are approximated as a long-range correction.

1.6.2.2. Force Field Resolution

Ideally, a force field would describe all atoms explicitly (all-atom force field), however, the large numbers of hydrogen atoms in organic molecules requires a considerable computational capacity. Therefore, approaches describing the molecules in less detail are introduced.

A united atom force field omits nonpolar hydrogens and includes their contribution to the overall potential by creating hydrogen included atom parameters (e.g. CH_2, CH_3), which decreases the number of atoms in the system. This approach is especially useful while simulating membranes, as phospholipids consist of long aliphatic chains.

A coarse grained force field groups several non-hydrogen atoms into one bead (e.g. polar, non-polar with the ability to form hydrogen bonds, charged positive) described by empirical parameters. Coarse grain force fields are widely used for long-time simulations of large systems such as membrane protein complexes [152] or DNA nanopores [153] .

Molecular dynamics with an added guiding potential obtained by cryo-electron microscopy [154] can be used to describe systems containing up to several million atoms [155] by fitting smaller parts into an experimentally gained structure.

Force fields with different resolutions can be used as two different simulation setups to describe both precise binding mechanisms and large scale conformational changes (e.g. membrane sculpting via the scaffolding mechanism [156]), or in one system [157], [158], which, however, requires deep understanding of the force fields used and the compatibility of their features [159].

1.6.3. Molecular Dynamics

Molecular dynamics (MD) is a computational method that allows the simulation of biological systems in an environment closer to physiological that is necessary for obtaining the crystal structures and on a timescale of the biological processes. It is based on periodic calculations of potentials and velocities of the atoms in the system.

1.6.3.1. Molecular Dynamics Algorithm

The potential energies of the system are in a given steps are calculated using a MM force field. Then, in a certain time step (usually 2 fs for biological systems), the atomic forces in the system are computed using the second Newton's law in the direction of coordinate *x* as:

$$\mathrm{F} = -\frac{\partial}{\partial x} V(\mathrm{x})$$

where F is force acting on the particle, and V(x) potential at the particle.

Moreover, we can use:

$$m\frac{d^2\mathrm{x}}{dt^2} = \mathrm{F}$$

to describe the change of the coordinates caused by this force, where x is the position of the particle and m) its mass.

In practice, the MD algorithm can calculate both the velocities (v) and coordinate change (x) in the same time step (e.g. the velocity Verlet algorithm):

$$x(t + \Delta t) = x(t) + \Delta t v(t) + \frac{\Delta t^2}{2m} F(t)$$

$$v(t + \Delta t) = v(t) + \frac{\Delta t}{2m} [F(t) + F(t + \Delta t)]$$

Or the velocities and coordinate change can be calculated in alternating half-steps as in the leap-frog algorithm:

$$v\left(t + \frac{1}{2}\Delta t\right) = v\left(t - \frac{1}{2}\Delta t\right) + \frac{\Delta t}{m} F(t)$$

$$x(t + \Delta t) = x(t) + \Delta t v(t + \frac{1}{2}\Delta t)$$

where Δt is the size of a time step.

1.6.3.2. Periodic Boundary Conditions

To ensure the proper behaviour of an MD simulated system, it is necessary to pay attention to several more factors. Traditionally, the simulated molecule is placed into a MD box, which is then filled with solvent (usually water) molecules (*Figure 10*).

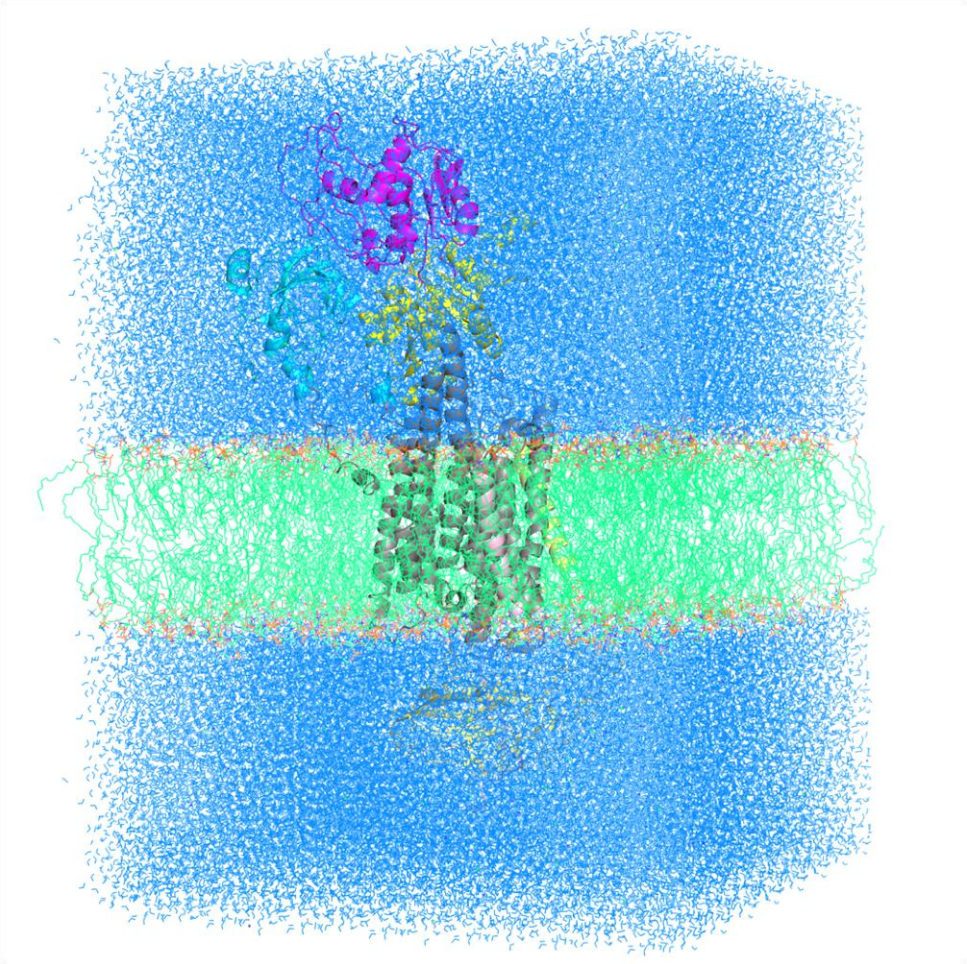

Figure 10: The simulation box of NKA in membrane. The transmembrane part of α subunit is in grey with the A-, P- and N- domains in cyan, yellow and magenta, respectively; the β subunit is in pale yellow, the FXYD protein in light pink. The membrane lipids are in green with coloured heads, water molecules are in blue.

Periodic boundary conditions are applied to mimic systems larger than it is computationally possible and to avoid molecules leaving the simulation box. This approach creates virtual copies of the system surrounding the box and the interactions of the molecules near box edges are calculated with respect to these copies. Moreover, when a molecule coordinate exceeds the boundaries of the box, it is translated to a corresponding position on the opposite side of the box as shown in *Figure 11*.

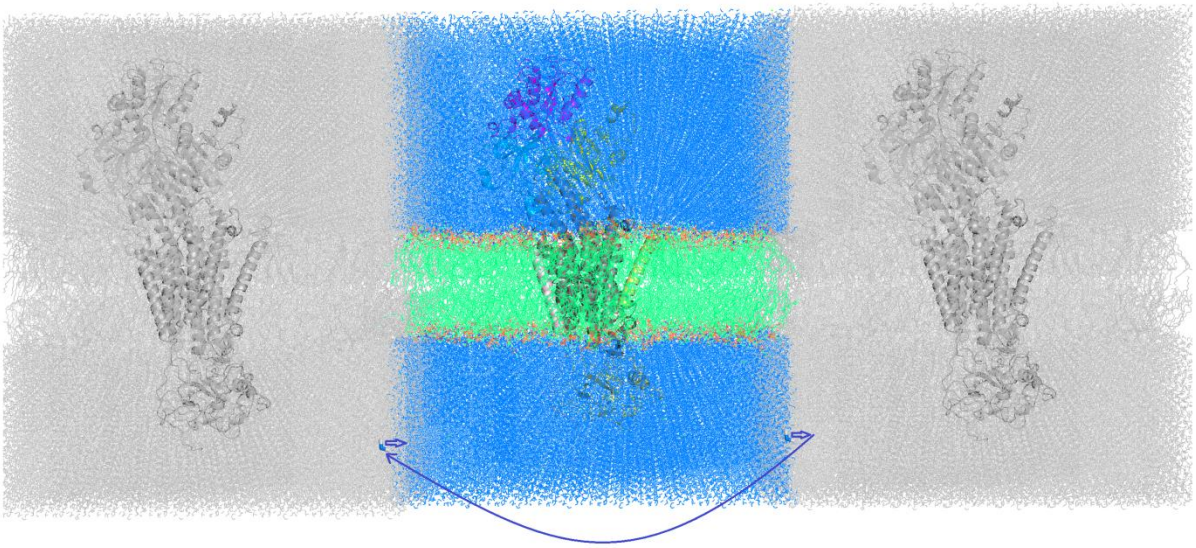

Figure 11: The simulation box (in colour) and its virtual version on the x axis (grey). The periodic boundary conditions applied to a water molecule leaving the box highlighted in blue arrows.

1.6.3.3. Regulation of Box Properties

The temperature of the system is a macroscopic property which on atomic level corresponds to the velocity of atom movement:

$$E_{kin} = \frac{1}{2}\sum_{i}^{n} m_i {v_i}^2 = \frac{1}{2} N_f kT$$

where m_i is the mass of the particle, v_i its velocity, N_f is the number of degrees of freedom, T thermodynamic temperature and k the Bolzmann's constant. While the direct use of MD creates a NVE ensemble, with constant number of particles, volume and energy, it is in practice more useful to work with the NVT ensemble (with constant number of particles, volume and pressure) and a constant temperature. To achieve that, thermostat algorithms regulating the temperature of the system by scaling velocities of the atoms are introduced.

The Berendsen thermostat [160] maintains stable thermal environment by correcting deviations of the current temperature (T) from the desired temperature (T_0) according to:

$$\frac{dT}{dt} = \frac{T_0 - T}{\tau}$$

so that the temperature deviations decrease exponentially with a time constant τ. The time constant can be changed depending on the equilibrium of the system.

To achieve a correct distribution of kinetic energies, a velocity rescaled thermostat is used, which adds a term modifying the kinetic energy according to:

$$dK = \frac{K_0 - K}{\tau_T} dt + 2\sqrt{\frac{KK_0}{N_f}} \frac{dW}{\tau_T}$$

where K_0 is the desired and K is the current kinetic energy, N_f the number of degrees of freedom and τ_T a time constant similar in size to τ. dW is a Wiener noise, a stochastic process similar to Brownian motion.

In contrast, Nosé-Hoover thermostat introduces the thermal factor directly into the equations of motion in the form of a friction coefficient ξ with its momentum p_ξ:

$$\frac{dp_\xi}{dt} = T - T_0$$

And the equation of motion then becomes

$$\frac{d^2x_i}{dt^2} = \frac{F_i}{m_i} - \frac{p_\xi}{Q}\frac{dx_i}{dt}$$

with

$$Q = \frac{\tau_T^2 T_0}{4\pi^2}$$

The Nosé-Hoover thermostat causes the temperatures to oscillate while slowly converging to T_0, the Berendsen thermostat induces a quick convergence and the velocity rescaled thermostat maintains a correct distribution of kinetic energies. Therefore, each of these thermostats can be used for a different application – Berendsen for equilibrating a system, velocity rescaled for applications where the kinetic energy is evaluated and Nosé-Hoover for examining an equilibrated system.

Additionally, to generate velocities at the first step of the simulation when starting only with a set of coordinates, the Maxwell-Bolzmann distribution can be used:

$$p(v_i) = \sqrt{\frac{m_i}{2\pi kT}} e^{-\frac{m_i v_i}{2kT}}$$

Similarly to temperature, pressure of the system is maintained by barostat algorithms to achieve a NPT ensemble with constant number of particles, temperature and a variable size of the simulation box.

The Berendsen barostat works similarly to the Berendsen thermostat, as

$$\frac{dP}{dt} = \frac{P_0 - P}{\tau_P}$$

and scales the box coordinates as

$$\mu_{ij} = \delta_{ij} - \frac{n_P \Delta t}{3\tau_P} \beta_{ij} \{P_{0ij} - P_{ij}(t)\}$$

where n_P is the size of the pressure correcting step and β_{ij} the isothermal compressibility of the box.

The Parrinello-Rahman barostat works similarly to the Nosé-Hoover thermostat as

$$\frac{d^2 x_i}{dt^2} = \frac{F_i}{m_i} - \mathrm{M} \frac{dx_i}{dt}$$

and

$$M = b^{-1} \left[b \frac{\mathrm{d}b'}{\mathrm{d}t} + \frac{\mathrm{d}b}{\mathrm{d}t} b' \right] b'^{-1}$$

where b is the matrix of the box vectors b^{-1} its inverse and b' its transposed form.

1.6.4. Molecular Docking

Molecular docking is a method used in computational drug design to describe and evaluate the binding of small molecules to proteins. It consists of two main steps – a binding conformation search and the binding energy evaluation. In some cases, a structure of a drug within the target protein is known beforehand and can be used as a reference for the docking evaluation.

1.6.4.1. Conformation Search

Usually, the whole target protein (with the possible exception of a known binding site) is considered to be a rigid structure and does not move in the course of docking. Therefore, the main objective of this step is to generate different conformations of the ligand (based on the number of rotable bonds) and to fit them into the target protein structure.

There are many ways of generating the conformations of the small molecules and generally, each docking program uses a different one. The most general method is to use the Monte Carlo algorithm, which require a large computational capacity [161]. To decrease the computational cost while generating sufficient amount of possible conformations, other methods of the conformational space search and optimisation have been developed.

Genetic algorithms are based on the principles of evolutional biology. Ligand conformation, position and orientation with respect to the target protein then create different "genes". These "genes" are mutated and subsequently their fitness (defined as lowest total interaction energy) in comparison to the rest of the population is evaluated in each docking cycle. Random individuals are then combined ("mated") to create an offspring with a combination of parent genes, and some offspring genes are also mutated. Only individuals with the fitness above a selected threshold are selected to "survive" into the next generation and round of evaluation [162].

Simulated annealing [163] generates new conformations of the system by a random temperature-dependent atom displacement and subsequent optimisation. By lowering the temperature during the course of the docking, the process at first samples larger and then smaller conformation changes until it reaches an energy minimum of the system.

A gradient of the energy scoring function with respect to position and torsions can also be used to speed up the optimisation by guiding the search algorithm in the direction of the steepest descend of energy [164].

1.6.4.2. Energy Evaluation

To evaluate the binding energy of the ligand a free binding energy between the target protein and ligands can be used. It features similar contributions to molecular modelling potentials, but with more focus on evaluating different non-bonded interactions and ligand properties [165]:

$$\Delta G_{binding} = \Delta G_{polar} + \Delta G_{vdW} + \Delta G_{H-bond} + \Delta G_{trans+rot} + \Delta G_{conform} + \Delta G_{solvent}$$

where the terms correspond to polar (ΔG_{polar}), van der Waals (ΔG_{vdW}), and hydrogen bond ($\Delta G_{H\text{-}bond}$) interactions, the ligand internal translation and rotation ($\Delta G_{trans+rot}$), influence of the binding on ligand geometry ($\Delta G_{conform}$), and solvent-related effects (e.g. desolvatation, hydrophobic interactions, $\Delta G_{solvent}$), respectively.

As in the case of the optimisation algorithms, the exact method of binding energy evaluation differs widely among docking programs, which can also use a combination of different approaches [7].

1.6.5. Relationship between Computation and Experiment

In silico studies of molecular systems date back to the half of the 20th century [166] but the rise of protein simulations came in the 80's with increasingly available computational capacity [167].

Even the first force fields used both parameters derived from quantum chemistry calculation (partial charges) and experimental values such as bond length or bond angles, derived from crystallography [168]. Experimental results therefore play an important role as a base for simulation setup and a tool for validating simulation results.

To evaluate the quality of simulation software, standardised datasets and challenges can be used. CASP (The Critical Assessment of protein Structure Prediction) provides tools to test the accuracy of protein structure prediction and refinement [169] tools for both offline programs and online servers.

Similarly, there are various test compound sets for molecular docking based on ligand-protein complexes [170] or a directory of useful decoys, which also features non-active compounds [171]. When operating within one system it is useful to check the accuracy of docking by redocking a compound originally present in a crystal back to the same binding site if such a crystal is available.

Computer simulations can also confirm or help to interpret experimental results. An apparent disparity between different experimental results can be explained by a simulation as in the case of $(Aib)_6$-Leu-Aib peptide where experimentally measured NMR ^3J values and the ^3J values obtained from a crystal structure differed by about 2Hz. Molecular dynamics reproduced the experimental data and showed that in the solution, there are several

conformations that contribute to the NMR ^{3}J signal and therefore the average value measured is higher than the average value of the peptide in crystal, where the peptide movement is restricted.

Computer simulations can also gain results that can set in doubt the interpretation of experimental results. For example, molecular dynamics simulation and subsequent spectra calculation used to explain why a peptide circular dichroism spectrum show that there are several different non-helical conformational states, which however have a similar spectra to a helical conformation [172].

1.7. Previous Simulations of Na^+/K^+-ATPase

Due to lower technical requirements, the crystal structures of SERCA (sarcoendoplasmic reticulum Ca^{2+} ATPase) were available several years earlier than the crystal structure of Na^+/K^+-ATPase [173], lead to a rise of SERCA-based NKA homology models. After the crystal structures of NKA were obtained, the first NKA-crystal based NKA models as well as molecular dynamics studies appeared at around 2010.

The early SERCA-based studies results can be a little confusing with today's knowledge, because based on the crystal structures and cytoplasmic domain positions, Na-ADP-Pi-E1 state of NKA is the closest to Ca-ADP-Pi-E1 of SERCA. The open conformation however is the K-E2 state of NKA but the Ca-E1 state of SERCA. The E2 conformation of SERCA corresponds to conformations without calcium in CBS and with the cytoplasmic domains in different degree of closing and rotation depending on other ligands present [174].

1.7.1. Partial Models

Homology models NKA were used to support and explain experimental data in numerous cases. The early models were based on the on the first SERCA crystal structure available, in the open conformation with two bound calcium ions [175].

To explain previous iron-catalysed oxidative cleavage experiments, an α subunit model was built based on a SERCA crystal in the open conformation, a hexokinase and by severing and manually rotating the N-domain+ATP complex [22]. The system was then a subject of energy minimisation to discover the most favourable conformation of the domains and nucleotide. This approach is very approximate, but it illustrates the difficulties of creating a closed conformation model before the crystal structure was available.

The C45 loop, between the transmembrane helixes TM4 and TM5, contains the P- and N-domains, constituting the phosphorylation and nucleotide binding sites. It retains catalytic activity and it is well soluble, therefore it has been a target of a number of studies, both experimental and theoretical.

The first C45 loop model [176] was built on SERCA structure in an open conformation, and replacing the original rabbit SERCA sequence with a porcine one. It was used as a template for MgATP docking to describe the structural features of the N- and P-domains and an ATP binding site. A model of the N-domain with mouse sequence based on the same template was

used in combination with circular dichroism and Raman spectroscopy [177] to describe the changes in the secondary structure of the N-domain upon ATP binding.

In accord with experimental setup, models of the C45 loop mutant sequences were then prepared [178] to further evaluate the roles of Phe482 and Phe555 in ATP binding.

The SERCA-based model of the C45 loop (in the open conformation, with mouse sequence) was later refined using the first NKA crystals [20] and served as a template for ATP and TNP-ATP docking to support fluorescence measurements on a series of point-mutation constructs, which together described the roles of R430 and D450 in nucleotide binding.

A molecular dynamics simulation of the C45 loop in the presence and absence of ATP and cations was performed to support fluorescence quenching and anisotropy measurements [100]. The article focused on the difference between binding ATP together with Mg^{2+} and free ATP and its influence on the opening of the N- and P- domains from their originally closed state. It was shown that in the presence of MgATP, the system stayed in the closed conformation, while when ATP was bound separately, the domains opened, and after the addition of Mg^{2+} ion started closing again. The same model was then used for surface potential calculations that for the N-domain correlated with the fluorescence quenching results probing the local charge on the surface of the C45 loop [179].

1.7.2. Whole Protein Models

The main goal of static homology models of the whole α subunit of NKA was to discover and describe the cation binding sites, especially the location of sodium binding sites, because calcium ions in SERCA provided binding positions of two cations in the CBS, analogous to potassium.

Both sodium and potassium binding sites were described in [180], who used crystals of SERCA in E1 and E2 states and created models including possible water molecules and discovered a position difference in the Na^+ and K^+ binding to the CBS sites I and II and a possible location of the sodium-only binding site either between TM5, TM6, and TM9 helices, with Y788 and E961 binding the ion.

A homology model based on SERCA in the open conformation [175] places the sodium CBS binding sites I and II to a similar positions, but due to a lack of water molecules in this model, different residues take part in cation binding, the sodium-only binding site was not described.

Based on this model, putative extracellular and C-terminal ion pathways were suggested [181].

A homology model based on the same open structure [175] was used together with site-directed mutagenesis and ATPase activity measurement to explain the measured differences in NKA activity in different mutants with respect to sodium binding. The CBS sites I and II were placed similarly to [180], while the sodium-only binding site was placed between TM5 and TM8, bound by T781, Y778 and Q930, close to the intracellular side of the membrane.

A different model of sodium binding (using again [175] as the template) was made [182] to explain previous electrophysiology measurement placed the sodium-only binding site between TM4, TM5 and TM6, halfway between the CBS sites I and II and the intracellular membrane layer.

Ultimately, the sodium-only binding site was placed in all sodium bound crystals [16], [24] between TM5, TM7 and TM8 and residues T781, Y778 and E930.

To examine and visualise the way ions move to the CBS from the extracellular side of the protein, a SERCA-based homology model of NKA in the closed conformation with the *Xenopus laevis* sequence was created [183]. The model served as a support for experimental data obtained using MTSET as a probe and in a subsequent study as a subject of tunnel analysis. The extracellular pathway was described as leading between TM1, TM2 and TM4, with D811 and E334 serving as selectivity filters[29].

NKA has also been a target of molecular docking studies – a crystal structure in the open conformation was used as a template for docking of steroid-like compounds found in Chinese medicines, together with protein activity measurements. All studied compounds bound the extracellular pathway, similarly to ouabain, but differed by the depth of insertion [112]. Fluorone dyes were docked into a human-sequence homology model of the protein in the open conformation and into the closed C45 loop [184]. The dyes occupied the nucleotide binding site, another site at the P-domain and two sites on the extracellular side of the protein, between the α and β subunits and between the β subunit and the FXYD family protein, respectively.

1.7.3. Molecular Dynamics

Molecular dynamic studies of the whole NKA started to appear as the first NKA crystal structures were available, which together with the lowering cost of high-performance computational systems led to better achievability of whole protein computational studies.

A set of structures, with porcine sequence in open conformation with phosphorylated D376, was created to examine the role of a mutation in the C-terminal region of the α subunit present in patient suffering from FHM2 [26]. The simulations explained the results of electrophysiology measurements of mutant protein by showing a C-terminal water pathway leading between TM5, TM7 and TM8 leading to a presumptive sodium-only binding site. The pathway was suggested to serve as a way for proton movement form the cytoplasmic side to CBS as a possible explanation of previous studies. The role of protonation of an aspartate (corresponding to D933 in human α1 numbering) on the reaction cycle was also highlighted.

This water pathway was subsequently studied with respect to a protein kinase A NKA phosphorylation in systems comparing the models of S941E mutation simulating the phosphorylation in electrophysiological measurements and in-silico phosphorylated protein, still with porcine sequence in open conformation with phosphorylated D376. The C-terminal water pathway opened in the simulation with phosphorylated protein, but stayed closed in the S941E mutated one, providing an explanation for the lack of leak current in the experimental data. Therefore, a phosphorylation-induced opening of the C-terminal pathway was proposed to be the cause of lowered sodium affinity causing the experimentally observed NKA inhibition [185].

A series of mutants of phosphorylated NKA in the open conformation with empty CBS was created to study mutations connected to adrenal hypertension. Mutated or deleted amino acids were located on TM1 and TM4, near the N-terminal pathway, and on TM9, in the vicinity of the CBS binding site III. Sodium ions from the bulk solution move spontaneously into CBS in the wild type simulation, this binding is however, disrupted in the mutants. An intracellular water pathway was observed between TM1, TM4 and TM5 in one of the mutated systems, with a deletion in the M1 region. Similarly, a deletion on TM9 led to opening of a water pathway from the intracellular side [186].

With the availability of the crystal structures of NKA in the closed conformation, the binding of small molecules to the phosphorylated, ADP-bound closed conformation NKA model was

examined, together with protein activity measurements. Sizes of the channels leading to CBS as well as rotation of T779 were identified as the main factors of ion selectivity [187].

The interaction between α subunit and different isoforms and isoform hybrids of β subunit was studied on a series of models in the closed conformation. The tilt of the transmembrane helix TMβ was found to be the determining factor influencing the E1-E2 protein equilibrium and ion affinity [188].

Molecular dynamics studies of NKA were also used in determining the protonation states of residues in CBS. A pKa analysis followed by simulations of simplified models based on the NKA in the open conformation, lead to the conclusion that the protonation of E334, E786 and D815, but not D811 lead to CBS selectivity for potassium and ensure the stability of CBS in the E2-P state [31]. A large series of models in both open and closed conformation with differing protonation states of selected residues was created and pKa and Na/K binding free energy difference was calculated. According to them, E334, E786 and E961 are protonated in both open protein conformation with bound potassium and closed protein conformation with sodium, protonated D811 assures the Na^+ selectivity of all three CBS sites, while D815 and D933 are deprotonated in the Na^+-bound state. On the other hand, in the K^+-bound state, D811 is deprotonated and D815 with D933 are protonated D815 and D933 [32]. Finally, a series of NKA models in the closed conformation with different protonation states of CBS aspartates and glutamates and showed that the different protonation stated of E334, E786 and E961 can serve as a gating mechanism for opening and closing of the CBS end of ion pathways [33].

2. Simulation Setup

2.1. Molecular Dynamics

The protein structure was based on the crystal structures with PDB IDs 2ZXE [85] for the open conformation, and 4HQJ [25] for the closed conformation. Homology models with the human $\alpha_1\beta_1$FXYD2 sequence were created using MODELLER 9.9 package [189] and Uniprot [190] IDs P05023, P05026 and P54710 respectively. The simulations were performed and processed with GROMACS 4.5.4 [191] for earlier simulations and GROMACS versions 5.1.1 and 5.1.2. [192] were used for later simulations. The results were visualised by PyMol 1.6.0.0 [193] and VMD 1.9.1 [194]. Tunnel analysis was performed by MOLE 2.0 [195] and ligand binding analysis was performed by Maestro ligand interaction tool [196] and by PLIP 1.2.0 [197].

Several different combinations of protein conformation, CBS ions, CBS residue protonation, cytoplasmic domain ligands and bulk ions were created to simulate NKA in different points of the reaction cycle (full list in tables 2 and 3).

The protein was inserted into a dioleoylphosphatidylcholine (DOPC) bilayer using g_membed [198] in a 15×15×20 nm hydrated box. To simulate conditions closer to physiological, ions corresponding to 154 mM of NaCl or KCl were added to the system. Periodic boundary conditions were applied in all directions. The force field used for protein, ion and ATP was Gromos53a6 [199]. The ATP molecule was placed either next to F482 in the open structures as argued in [19] or replacing the ADP+AlF_4^- in the closed structures. A magnesium ion was either retained at D376 as in the crystal structures, or deleted. The CBS ions were either retained at their positions in the crystal structures, replaced at the same positions, or in the case of the sodium only CBS site III either deleted or placed between D933 and T781 in the open structures. Berger parameters [200] were used for phospholipids. A phosphate ion ($H_2PO_4^-$) was inserted in the place of MgF_4^{2-} or AlF_4^- in the crystal structures or instead of the γ-phosphate of ATP, respectively and parametrised according to [201]. ADP molecule parameters were obtained in the ATB repository [202] and it was either retained at its location in the closed crystal structures or it was placed instead of the corresponding part of ATP. In several simulations, E344, E786 and E961 were protonated as argued in [31] and [26].

The system was minimised using the steepest descend method, with maximum 1500 steps and the maximum force to converge 1000 $kJ.mol^{-1}nm^{-1}$. A 10 ns prerun with fixed protein

backbone was performed before each simulation, with the temperature set to 310K with V-rescaled thermostat [203], and pressure set to 1 bar using anisotropic Berendsen barostat [160], the leap-frog Verlet integrator [166] was used with time step 2 fs.

The main run was performed with leap-frog Verlet integrator [166] and time step 2 fs, for 100 ns in the majority of the simulations, with some simulations running for 50 or 70 ns of the due to technical reasons. The thermal coupling was performed by V-rescaled thermostat set to 310 K [203] and the pressure coupling by Parrinello-Rahman barostat [205] set to 1 bar.

Table 2: Simulation setups – closed conformation of the protein

simulation name	protonated	conf.	CBS ions	ligandss	solvent
hC_2K_Mg_ATP	yes	closed	2 K	Mg, ATP	NaCl
C_2K_Mg_ATP	no	closed	2 K	Mg, ATP	NaCl
C_2K_Mg_ATP_KSOL	no	closed	2 K	Mg, ATP	KCl
C_2K_Mg_ATP2D	no	closed	2 K	Mg, ADP, Pi	NaCl
C_2K_Mg_ADP_Pi	no	closed	2 K	Mg, ADP, Pi	NaCl
C_2K_Mg_ADP_Pi_KSOL	no	closed	2 K	Mg, ADP, Pi	KCl
hC_2K_ATP	yes	closed	2 K	ATP	NaCl
C_2K_ATP	no	closed	2 K	ATP	NaCl
hC_2K_Mg	yes	closed	2 K	Mg	NaCl
C_2K_Mg	no	closed	2 K	Mg	NaCl
hC_3Na_Mg_ATP	yes	closed	3 Na	Mg, ATP	NaCl
C_3Na_Mg_ATP	no	closed	3 Na	Mg, ATP	NaCl
C_3Na_Mg_ATP_KSOL	no	closed	3 Na	Mg, ATP	KCl
C_3Na_Mg_ATP2D	no	closed	3 Na	Mg, ADP, Pi	NaCl
C_3Na_Mg_ADP_Pi	no	closed	3 Na	Mg, ADP, Pi	NaCl
C_3Na_Mg_ADP_Pi_KSOL	no	closed	3 Na	Mg, ADP, Pi	KCl
hC_3Na_ATP	yes	closed	3 Na	ATP	NaCl
C_3Na_ATP	no	closed	3 Na	ATP	NaCl
C_3Na_ATP_KSOL	no	closed	3 Na	ATP	KCl
hC_3Na_Mg	yes	closed	3 Na	Mg	NaCl
C_3Na_Mg	no	closed	3 Na	Mg	NaCl
C_K_Na_ATP	no	closed	1 Na 1K	ATP	NaCl
C_K_Na_Mg	no	closed	1 Na 1K	Mg	NaCl
C_Na_K_ATP	no	closed	1 Na 1K	ATP	NaCl
C_Na_K_Mg	no	closed	1 Na 1K	Mg	NaCl
C_2Na_ATP	no	closed	2 Na	ATP	NaCl
C_2Na_Mg	no	closed	2 Na	Mg	NaCl

Table 3: Simulation setups – open conformation of the protein

simulation name	protonated	conf.	CBS ions	ligands	solvent
hO_2K_Mg	yes	open	2 K	Mg	NaCl
O_2K_Mg	no	open	2 K	Mg	NaCl
hO_2K_Mg_Pi	yes	open	2 K	Mg, Pi	NaCl
O_2K_Mg_Pi	no	open	2 K	Mg, Pi	NaCl
hO_2K_Mg_ATP	yes	open	2 K	Mg, ATP	NaCl
O_2K_Mg_ATP	no	open	2 K	Mg, ATP	NaCl
O_2K_Mg_Pi_ATP	no	open	2 K	Mg, Pi, ATP	NaCl
hO_2K_Pi	yes	open	2 K	Pi	NaCl
O_2K_Pi	no	open	2 K	Pi	NaCl
hO_2K_ATP	yes	open	2 K	ATP	NaCl
O_2K_ATP	no	open	2 K	ATP	NaCl
O_2K_Pi_ATP	no	open	2 K	Pi, ATP	NaCl
hO_2K	yes	open	2 K	-	NaCl
O_2K	no	open	2 K	-	NaCl
hO_3Na_Mg_ATP	yes	open	3 Na	Mg, ATP	NaCl
O_3Na_Mg_ATP	no	open	3 Na	Mg, ATP	NaCl
hO_3Na_ATP	yes	open	3 Na	ATP	NaCl
O_3Na_ATP	no	open	3 Na	ATP	NaCl

2.2. Molecular Docking

The protein models for molecular docking were crystal structures with PDB IDs 3KDP (open conformation) and 4HQJ [16] (closed conformation) or human sequence homology model – the starting point of simulation C_3Na_Mg_ATP. The structures of organic compounds for docking were obtained by DFT calculations by M. Biler.

The structures were prepared for docking by Autodock Tools 1.5.6 [206], with all single bonds remaining rotable.

The docking was performed by Autodock Vina 1.1.2 [164] with the grid covering the whole protein (exhaustiveness set to 400 and num_modes to 9999). In the case of quinolinones, an extension of Vina [207] was used to better describe halogen binding.

3. Results and Discussion

3.1. Simulation Properties

All molecular dynamics simulations shared the same basic structure. Homology models of NKA were created using crystal structures from the Protein Data Bank archive. The animal amino acid sequence (shark in 2ZXE with the open conformation, porcine in 4HQJ with the closed conformation) was replaced by human sequence with isoforms α1β1FXYD2. The protein was then placed into a membrane consisting of DOPC (dioleoylphosphatidylcholine), a phospholipid present in large amount in eukaryotic plasma membranes [208] or experimental lipid mixtures [209]. The simulation box was filled with water molecules, and ions mimicking the physiological concentration (154 mmol/L, corresponding to about 350 atoms) were added (*Figure 12*). Different simulations were then obtained by varying ions in the bulk solution (NaCl or KCl), ions in the CBS (Na^+ or K^+), protonation of CBS (E344, E786 and E961) and ligands at the cytoplasmic domains (Mg^{2+}, Pi, ATP, ADP).

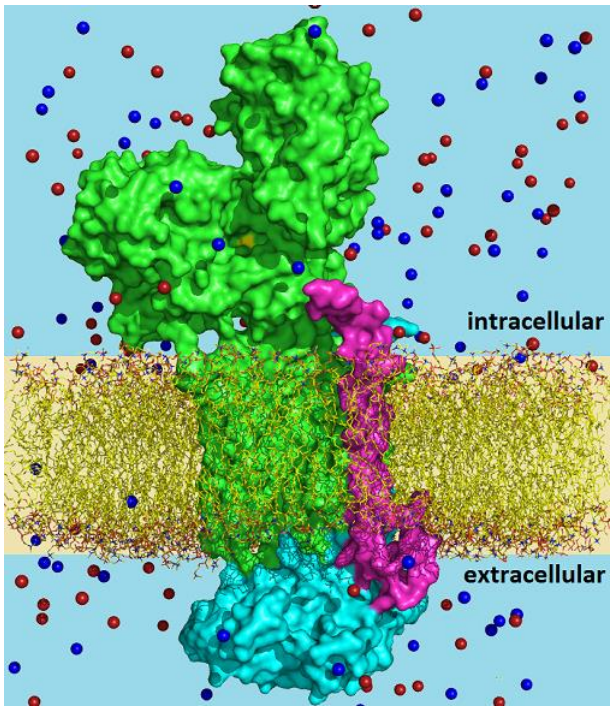

Figure 12: A schematic view of the simulation box [210]. The α subunit is in green, β subunit in cyan, the FXYD protein in magenta, magnesium ion in yellow, the membrane in yellow-orange, bulk ions in blue (cations) and red (Cl^-).

After the initial relaxation from the crystal structure (cca 10 ns), all simulations remained stable for the rest of the simulation with only gradual conformational changes. The overall

movements were less prominent in the simulations with the protein in the closed conformation. The cytoplasmic domains did not move significantly from their original positions, remaining closed. The domains were more mobile in the simulations with the protein in the open conformation, and generally moved closer together. However, no originally open structure reached a properly closed conformation. To achieve that, the A-domain must not only move towards the N-domain, but also rotate considerably, which probably requires much longer time scale. To describe the domain movements, several amino acids were selected – L203, F555 and M615, to measure the distances between the centres of mass of the A-, N- and P-domain, respectively (*Figure 13*). The distances between E223 and R551 or G196 and D740 were used to describe the rotation of the A-domain. Interestingly, the distances between domains differed in several cases depending on the protonation state of the CBS ions, suggesting a sensitive long-distance communication system.

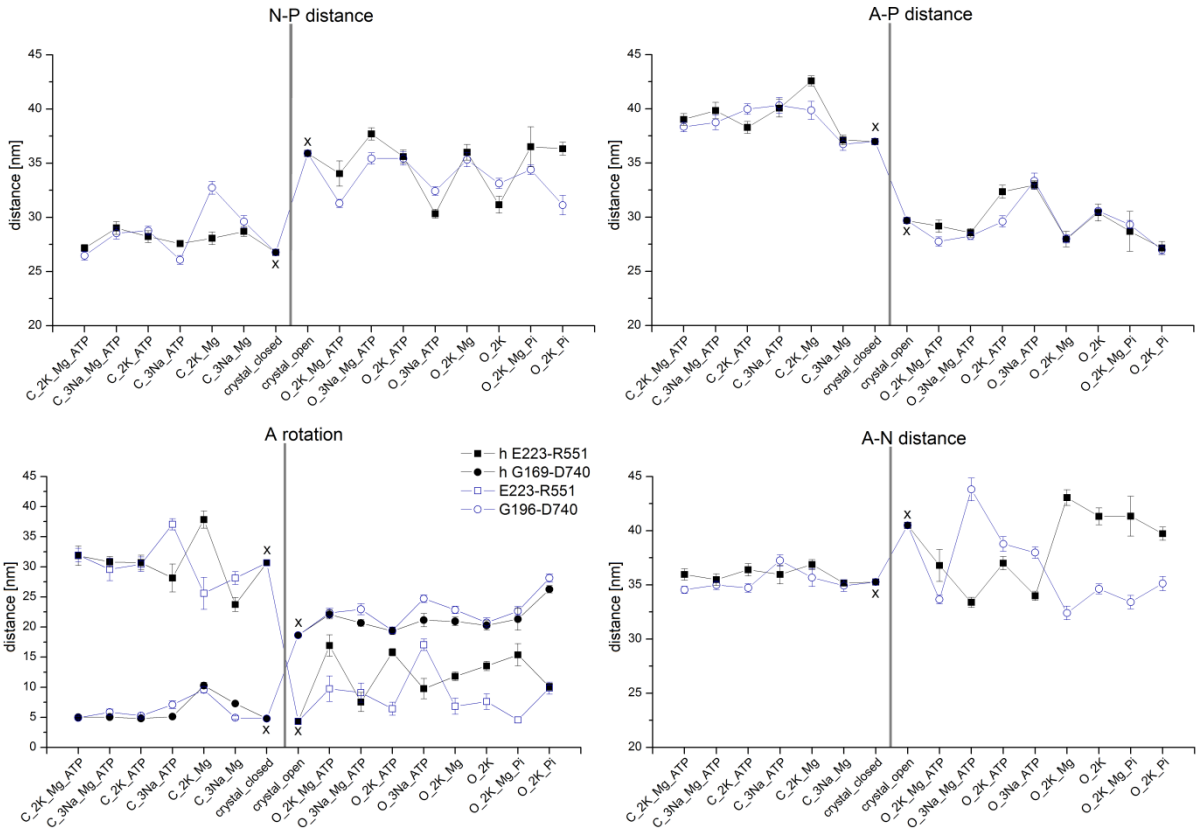

Figure 13: Distances between the cytoplasmic domains. Full symbols denote simulations with protonated CBS amino acids, empty the deprotonated ones, "x" the crystal structures[210].

3.2. Ion Pathways

The main function of NKA is to transport sodium ions against concentration gradient out from the cell and potassium ions inside. To achieve that, ions must move into the CBS, where they are occluded, before they are released on the opposite side of the membrane. Therefore, the knowledge of molecular pathways and when in the reaction cycle they open and close, is an large important step towards better understanding the details of protein function and the way how a mutation impacts its function leading to a disease.

We identified five different ion and water pathways leading to the cation binding site from both intracellular and extracellular side of the membrane (*Figure 14*). Three of them – the N-terminal, the C-terminal and the extracellular pathway had been described before. The TM3/TM7 and TM6/TM9 pathways are novel.

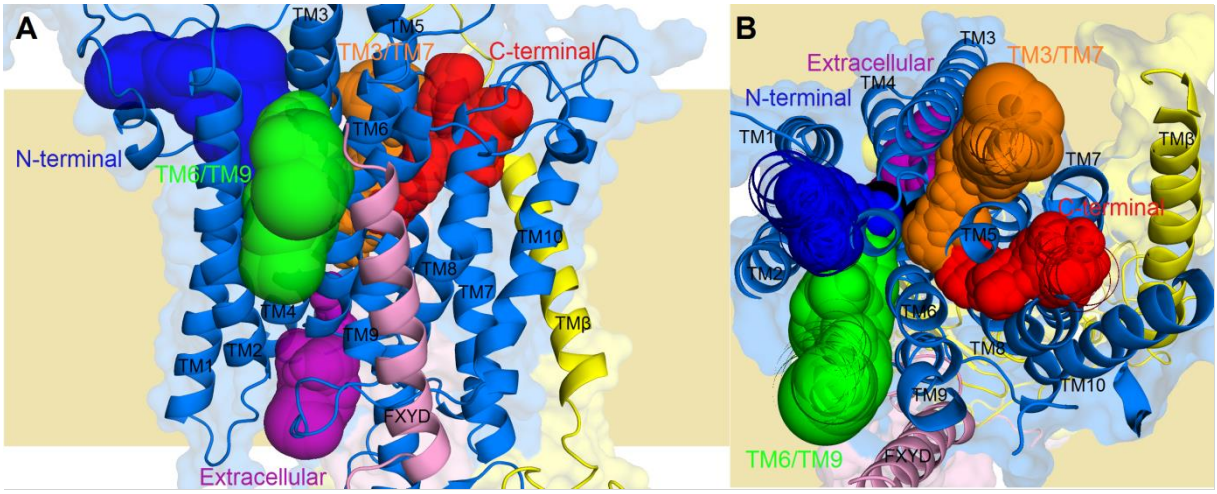

Figure 14: The pathways from the view parallel to the membrane (A) and from the intracellular side (B) [210].

Moreover, we observed various dynamic properties of the pathways, such as their opening, closing, or movement of water molecules and ions from the bulk solution to the CBS.

3.2.1. N-terminal Pathway

The intracellular N-terminal pathway *(Figure 15)* starts under the A-domain and leads to CBS site II. It is situated between helixes TM1 (R94, Q95, G99, F100, S101, L104), TM2 (V39, T143, S147, Q150, E151), TM3 (A285, E289), TM4 (V332, E334, L337, V340, T341) and TM6 (M816). Ion movement through this pathway was observed during a simulation.

The mutations of amino acids in the outer region of this pathway (R94, Q95, and G99), decreased the sodium affinity. On the other hand, mutations of F100, L104, or L337 that lie closer to the CBS end of the pathway influenced the affinity of potassium and increased its deocclusion [211]–[214] .

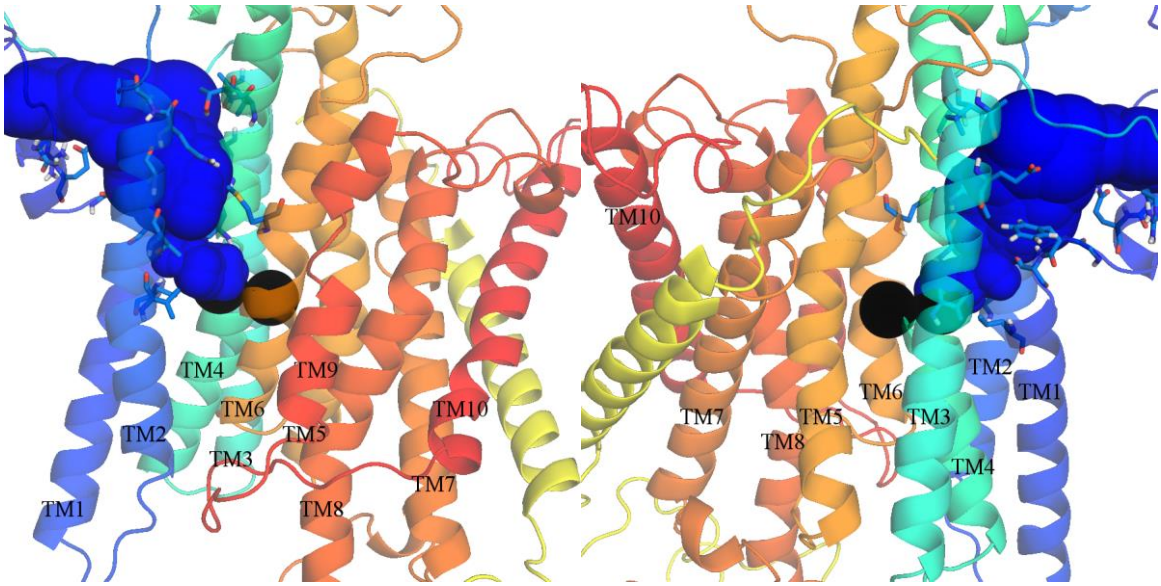

Figure 15: The intracellular N-terminal pathway (blue), from the "front" and "back" of the protein. The α subunit is coloured in a rainbow scale blue to red (N-terminus to C-terminus), the β subunit is in yellow, CBS ions in black, the FXYD protein is hidden for clarity.

3.2.2. C-terminal Pathway

The intracellular C-terminal pathway *(Figure 16)* starts at the C-terminal end of α subunit and continues through the CBS III to the CBS I. It leads between TM5 (K774, A777, Y778, T781, N783), TM6 (D815), TM7 (E847, M852, A853, Q856, I857, Q861), TM9 (Q930, W931, D933, V935, I936, C937, K938, R940), and TM10 (I998, Y1001, D1002, R1005, I1009, Y1022, Y1023). No ion movement was observed through this pathway. It is usually narrower than the other pathways, with water molecules forming only a one-by-one chain of molecules instead of moving freely. It has been proposed that this pathway serves as a channel for CBS protonation from the intracellular site [26].

Experimental studies reported greatly reduced enzyme activity after mutation of C937 [215] or N783 [216].

The entrance to this pathway was blocked by binding of flavonolignans (publication III) and quinolinones (publication II) in our docking studies.

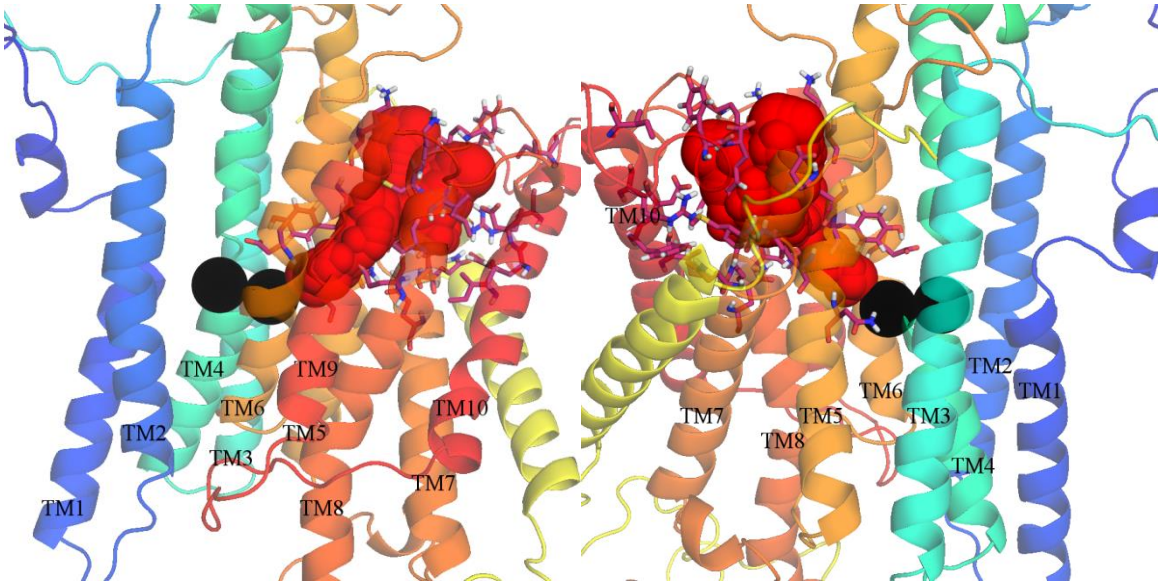

Figure 16: The intracellular C-terminal pathway (red), from the "front" and "back" of the protein. The α subunit is coloured in a rainbow scale blue to red (N-terminus to C-terminus), the β subunit is in yellow, CBS ions in black, the FXYD protein is hidden for clarity.

3.2.3. Extracellular Pathway

The extracellular pathway (*Figure 17*) is the only one leading towards the extracellular side of the membrane. It is situated between TM2 (N129, Y131), TM6 (T804, T806, I807, L808, C809), TM8 (F916) and A977 with R979 on the loop between TM9 and TM10. It is only present in a few of our simulations, because our combinations of ligands and bulk ions promoted opening of other pathways.

This pathway has been examined using an palytoxin-inhibited pump, cysteine point mutations and methanethiosulfate probes [28], [29]. This pathway is also the binding site for ouabain and other cardiotonic steroids in the crystal structures [86], [89], [90], as well as several flavonolignans in our docking study (publication III) .

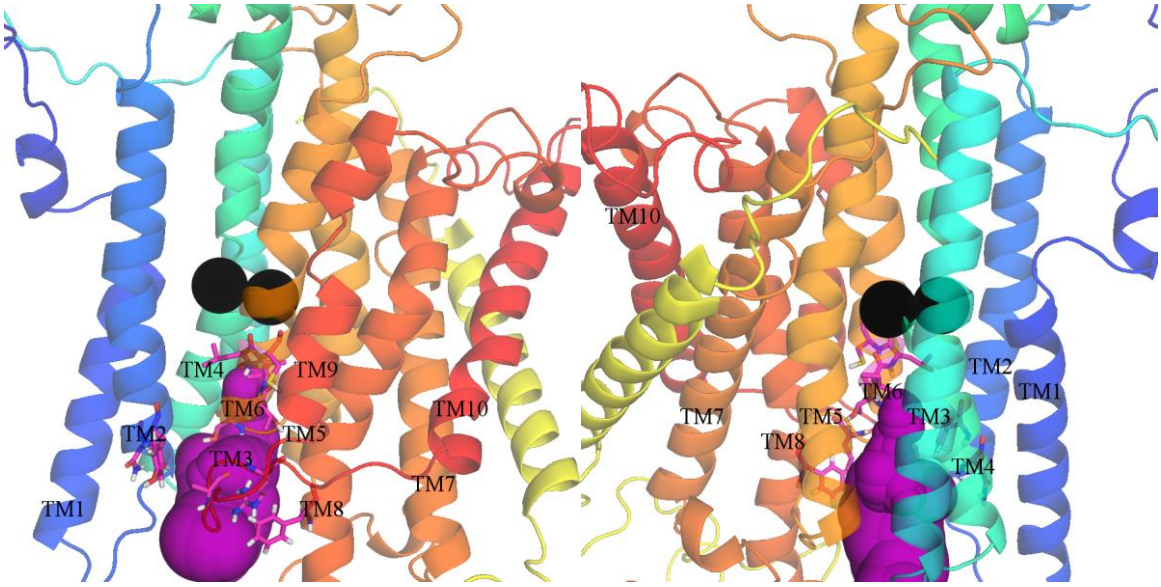

Figure 17: The extracellular pathway (purple), from the "front" and "back" of the protein. The α subunit is coloured in a rainbow scale blue to red (N-terminus to C-terminus), the β subunit is in yellow, CBS ions in black, the FXYD protein is hidden for clarity.

3.2.4. TM3/TM7 Pathway

The intracellular TM3/TM7 pathway (*Figure 18*) leads between TM3 (H290, F291, I294, I295, V298) and TM7 (N783, E786, I787, V845, E847, I850, S851, Y854, G855) towards the CBS I. Residues of TM4 (A330, N331, P333) and the β subunit (K21, E24, F27, R28, W32) also take part in this pathway. It allows water molecules, and in one case Na^+ ion, to enter CBS. This pathway often closes in the course of a simulation.

In mutagenesis studies, it was discovered that modifying H290 or F291 increased the enzyme affinity to potassium and decreased the affinity to ATP and that the H290A mutation produces non-viable cells [218]. These residues are located at the membrane level of the TM3/TM7 pathway. On the other hand, the mutation of E786A, at the CBS end of this pathway, decreased affinity to both sodium and potassium ions and increased the affinity to ATP [219].

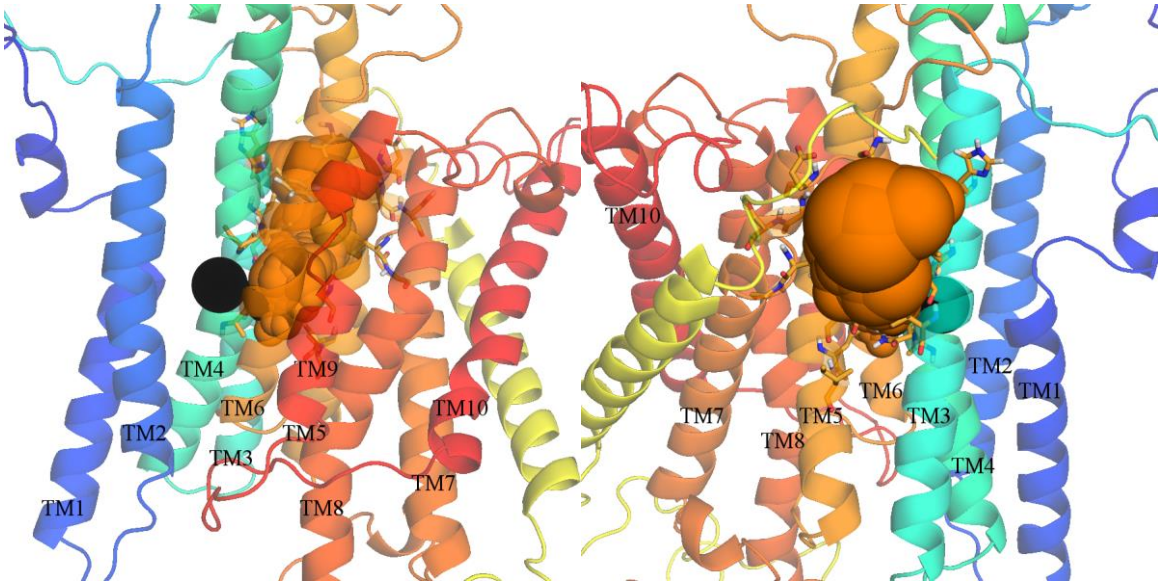

Figure 18: The intracellular TM3/TM7 pathway (orange), from the "front" and "back" of the protein. The α subunit is coloured in a rainbow scale blue to red (N-terminus to C-terminus), the β subunit is in yellow, CBS ions in black, the FXYD protein is hidden for clarity.

3.2.5. TM6/TM9 Pathway

The intracellular TM6/TM9 pathway (*Figure 19*) leads along the helices TM6 (L812, T814, D815, M816, V817, S821, Y824) and TM9 (L934, I953, F956, E960, E961), but it can also reach to TM2 (F146), TM5 (Y778) or past TM9 towards the intracellular end of the FXYD family protein (R48, R51). Ions used this pathway to move to CBS in two simulations with bound potassium and ATP.

In experimental studies, mutations of E960 and E961 to alanine did not produce a significant change in affinities, however, the mutations to lysine result in non-viable cells [220]. E961 can turn inwards and reach to the CBS III, which can be disrupted by the charge switch from glutamate to lysine. E960 is a stable point for ions moving through the TM6/TM9 pathway towards the CBS.

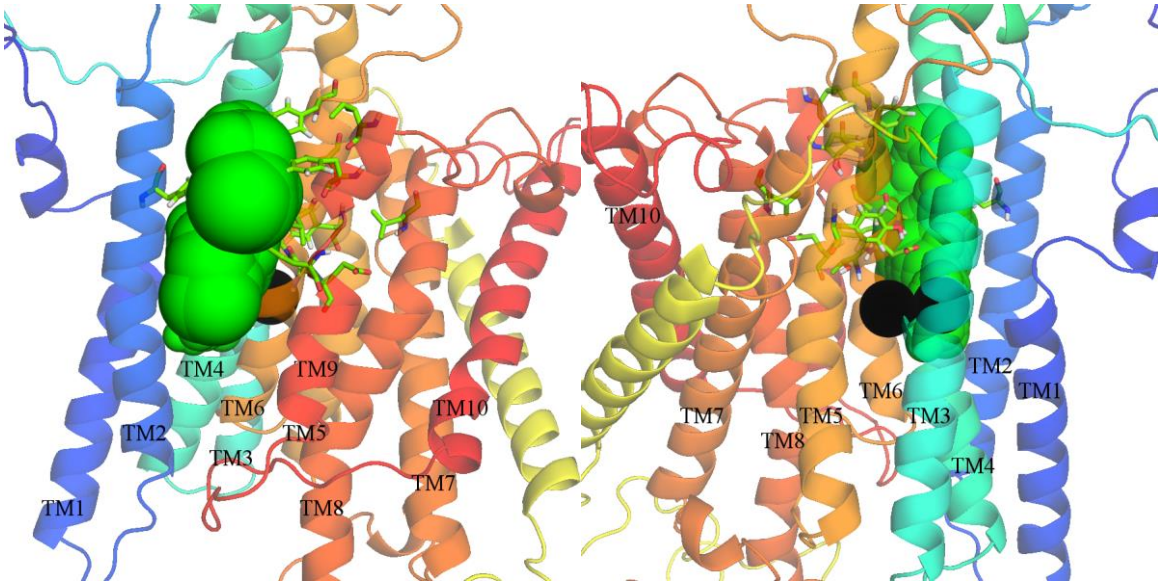

Figure 19: The intracellular TM6/TM9 pathway (green), from the "front" and "back" of the protein. The α subunit is coloured in a rainbow scale blue to red (N-terminus to C-terminus), the β subunit is in yellow, CBS ions in black, the FXYD protein is hidden for clarity.

3.3. Nucleotide Binding

3.3.1. The Nucleotide Binding Modes

To describe the nucleotide binding, several simulations with bound ATP and ADP+Pi and different combinations of ions in CBS and the bulk solution were analysed. We used three different methods (PLIP, ligand interaction diagram, both for the last frame of the simulation, and analysis of residues closer than 3.5 Å from the nucleotide in the last 10 ns of the simulation) to depict the nucleotide binding. We identified five different residue clusters on the P- and N-domain (*Figure 20*) interacting with the nucleotide.

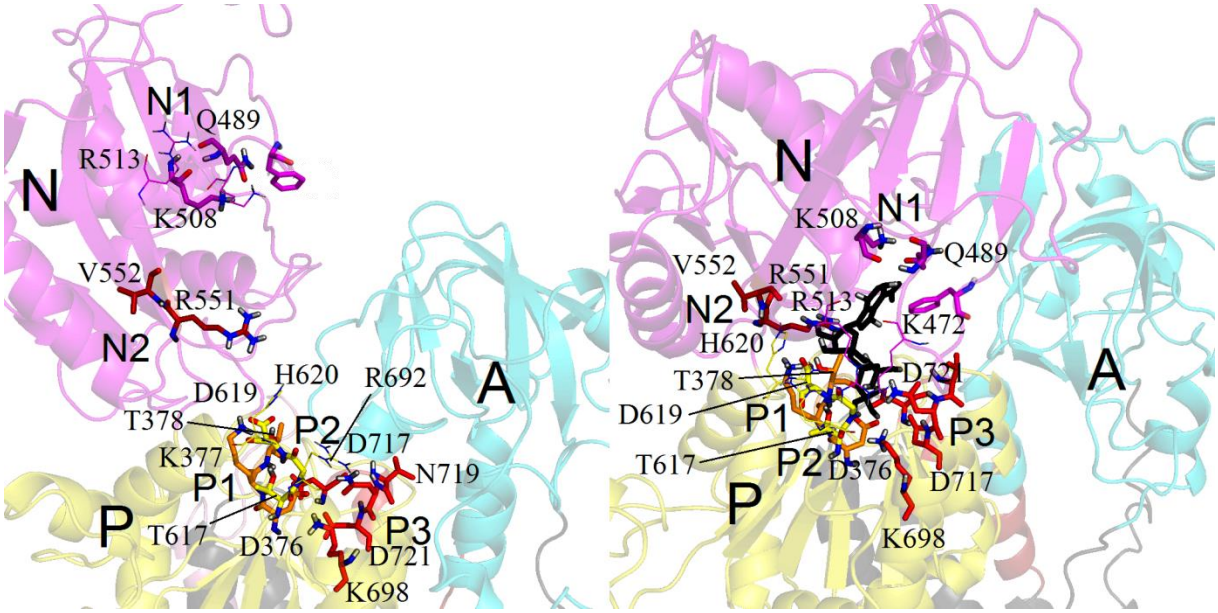

Figure 20: The nucleotide binding sites in the open (left) and closed (right) conformation of the protein. A-domain is in cyan, P-domain in yellow, N-domain in magenta, ATP in black. The residues taking part in nucleotide binding are in stick representation. Site P1 in orange, P2 yellow, P3 and N2 different shades of red, N1 in purple. K487, R513, H620, and R692 are displayed in lines.

There are three clusters located on the P-domain, and they bind the phosphate chain of a nucleotide, occasionally reaching towards the ribose. **Site P1** consists of D376, K377 and T378. It binds the terminal phosphate of ADP or ATP, and D376 is phosphorylated during the reaction cycle. A magnesium ion, or in the simulations without it, a cation from the bulk solution, binds into this site as well. **Site P2** contains T617, G618 and D619 and binds the phosphate chain and, in some cases, the ribose. The free phosphate in simulations with the closed protein conformation binds in this site. **Site P3** completes the third part of the binding

pocket and it contains the residues K698, D717, V719, N720 and D721. This site takes part in the catalytic magnesium and nucleotide phosphate chain binding. Experimentally, the 716GDGVND sequence was shown to stabilize the NKA state before phosphorylation [23]. Cleavage experiments with Fe^{2+} as a Mg^{2+} substitute have produced fragments with sequences corresponding to 376DKTGT, 615MVTGD, and 715TGDGVNDS are located near the Mg^{2+} binding site [22].

On the N-domain, there are only two binding sites. However, it contains a great amount of charged residues with long side chains such as arginine or lysine, which can move considerably and reach relatively far from their backbone. **Site N1** consists of Q489 and K508, which can both bind the nucleotide with their backbone, sidechain or both, as confirmed by the last 10 ns analysis which shows G509 and A510 in the vicinity of the nucleotide as well. Residues of this site have been experimentally shown to bind nucleotide [19]. **Site N2** consists of the backbones of R551 and V552, together with L553 in the last 10 ns analysis. This residues can bind the nucleotide adenine, ribose or α phosphate of the phosphate chain, depending on the orientation of the nucleotide. As mentioned above, R551 can also reach quite far into the binding pocket, or into the space between domains, and take part in the nucleotide binding with the sidechain as well. The role of R551 in nucleotide binding has also been observed experimentally [221].

Apart from these sites, there are several other significant residues taking part in the nucleotide binding. **F482** is spatially located near the N1 site and in the simulations with the open conformation of the protein; the ATP was placed at this residue as argued in [179]. The PLIP analysis and ligand interaction diagram did not show this residue very often, probably due to their strict π-stacking position requirements; however, the last 10 ns analysis confirmed that F482 is present in the vicinity of the nucleotide. **K487** was not included in any of the binding sites, although it binds the nucleotide in more than 80% of simulations. It can bind either adenine or the phosphate chain of the nucleotide. This residue has also been experimentally shown to take part in the nucleotide binding [222].

Given the large distance between the domains in the open conformation of the protein, it is not surprising that the P-domain sites take part in the nucleotide binding only in the simulations with the closed conformation. However, **H620** and **R692** can extend their sidechains to the space between the domains and bind the phosphate chain even in the open conformation. **R513** is located on the surface of the N-domain and it takes part in the

nucleotide binding in the simulations where the nucleotide leaves the above defined binding sites.

The residues of the above mentioned nucleotide binding sites also take part in ADP binding in the available crystal structures [24], [25] . Our simulation results are also in good agreement with the fact that the N- and P-domain sequences 376DKTGTLT (site P1), 508KGAPE (site N1), 615MVTGD (site P2) and 712VAVTGDGVNDS (site P3) are conserved among the P-type ATPases [223].

3.3.2. The Nucleotide Binding Conformations

Apart from the position of the nucleotide on NKA, we also studied the different conformations of the nucleotide itself. To describe them, we defined two dihedral angles. The angle describing the conformation of ribose (because compounds with immobile ribose have been shown to be NKA inhibitors [224]) as the ribose carbons dihedral angle C1'-C2'-C3'-C4' and the dihedral angle between ribose and adenine as O4'-C1'-N9-C4 (*Figure 21*). The C1'-C2'-C3'-C4' angle larger than 180° corresponds to the C2'-endo conformation while the angle smaller than 180° corresponds to the C3'-endo conformation of the ribose.

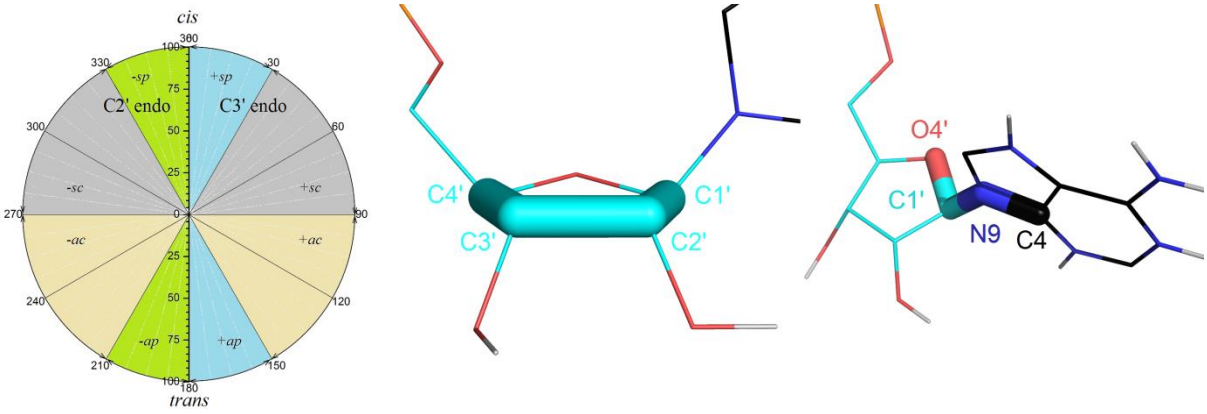

Figure 21: The circle of possible angles and depiction of the the dihedral angle between the ribose carbons and between the ribose and the adenine. The positive values are in the clockwise direction viewed from the first bond, letters correspond to the sp, synperiplanar; sc, synclinal, ap, antiperiplanar; ac, anticlinal positions respectively.

The prevalent ribose conformation is the C2'-endo; the C3'-endo is present only in three simulations. The ribose angles in the C2'-endo conformation are spread around 330° in the closed conformations and at 340° in the open ones. In the simulations with bound ADP, the

angle spread is narrower than in the ATP-bound ones – at about 325°. The ribose dihedral angles are at about 35° in the C3'-endo conformation (*Figure 22*A).

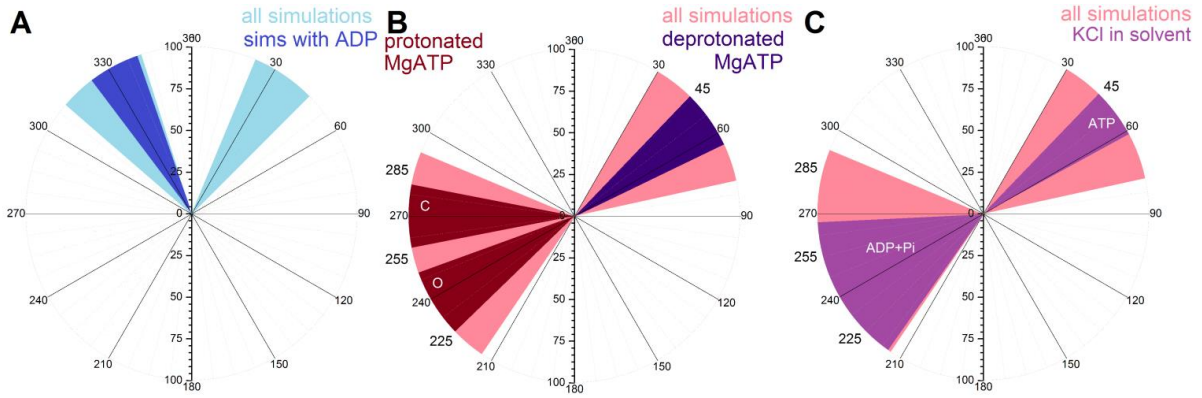

Figure 22: The area where most of the dihedral angle values are located for ribose (A) - light blue depicts the angle range where most of the values lie in all the simulations, and dark blue depicts the most frequent angle range for the simulations with bound ADP. B and C show the angle between ribose and adenine, with the pink area depicting the angle range where most of the values lie in all the simulation. In B) the purple highlighted area shows the angle range for simulations with MgATP and deprotonated CBS, while crimson shows the angle range for simulations with MgATP and protonated CBS in open and closed conformations. In C) the violet highlighted area shows the ribose-adenine dihedral angle range for simulations with KCl in the bulk solutions for simulations with bound ATP or ADP+Pi, respectively.

There are two main positions of the adenine moiety – corresponding to about 50±20° (+sc), and about 250±35° (-ac) (light pink in *Figure 22B* and *C*). There are distinct trends in between angles in two groups of simulations. In the simulations with bound MgATP in the cytoplasmic domain region, the protonation of the CBS residues plays a role in the nucleotide conformation. In the simulations with deprotonated CBS residues, the angles are spread around 55°±10° (+sc conformation). When the CBS residues are protonated, the adenine position flips to the –ac conformation (240°) for the ATP in the simulations with the open conformation of the protein and to 270° in the case of the protein in the closed conformation (*Figure 22B*). In the simulations with KCl in the bulk solution, there are also two distinct substates of the nucleotide angles – at 50° for the ATP-bound simulations and at 240° for the ADP-bound ones (*Figure 22C*).

Collectively, the angles between different parts of the nucleotides show that there are several possible conformations of the nucleotide in the binding pocket on the protein, documenting the flexibility of the nucleotide necessary for NKA substrates [224]. Interestingly, the ions in

the bulk solution also influence the nucleotide binding, suggesting a possible feedback loop for NKA regulation.

3.4. Molecular Docking of Potentially Therapeutic Compounds

3.4.1. Flavonolignans

A series of flavonolignans was obtained in the collaboration with laboratory of V.Křen from the Institute of Microbiology of the Czech Academy of Sciences. Based on the results of the initial screening of the effect of the compounds on NKA activity, silychristin (SCH), dehydrosilychristin (DHSCH), and dehydrosilydianin (DHSD) were selected for molecular docking (*Figure 23*). As docking targets, the NKA crystal structures 3KDP (open conformation, [84]) and 4HQJ (closed conformation, [25]) were selected.

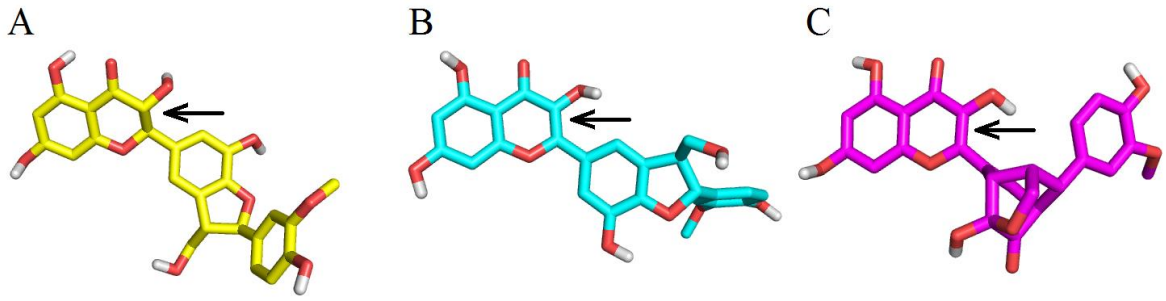

Figure 23: The structures of flavonolignans used in molecular docking. The carbons of silychristin (A) are in yellow, dehydrosilychristin (B) in cyan and dehydrosilydianin (C) in magenta, oxygens in red, hydrogens in white. The arrow denotes the dehydrated bond.

The flavonolignans bind to the pump in five different positions (*Figure 24*) – three at the entrances to different pathways and two at the cytoplasmic domains. However, the sites partly differ between the NKA conformations and their binding also depends on the conformer of the flavonolignans, differing by the rotation of bonds between their aromatic cycles.

There are four sites on each conformation of the protein. The C-terminal and extracellular positions, corresponding to the entrance of the C-terminal and extracellular pathways, are present on both open and closed conformation. Both conformations also exhibited flavonolignans binding at the phosphorylation site (P-site), albeit in different positions. The pose specific for the open conformation is under the A-domain, near N353 (porcine numbering), while the closed-conformation specific one is near R248.

The binding sites have all similar binding affinities for studied flavonolignans. However, different flavonolignans bind to different binding sites. On the open conformation, only dehydrosilychristin and dehydrosilydianin bind to the C-terminal site. All conformers of silychristin bind the most frequently at the phosphorylation site, while DHSCH and DHSD are spread across the other binding sites and only one conformer each binds most frequently to the P-site. Two conformers of DHSCH and one of DHSD bind preferentially near N353. Only one conformer of DHSD binds the most frequently to the extracellular site.

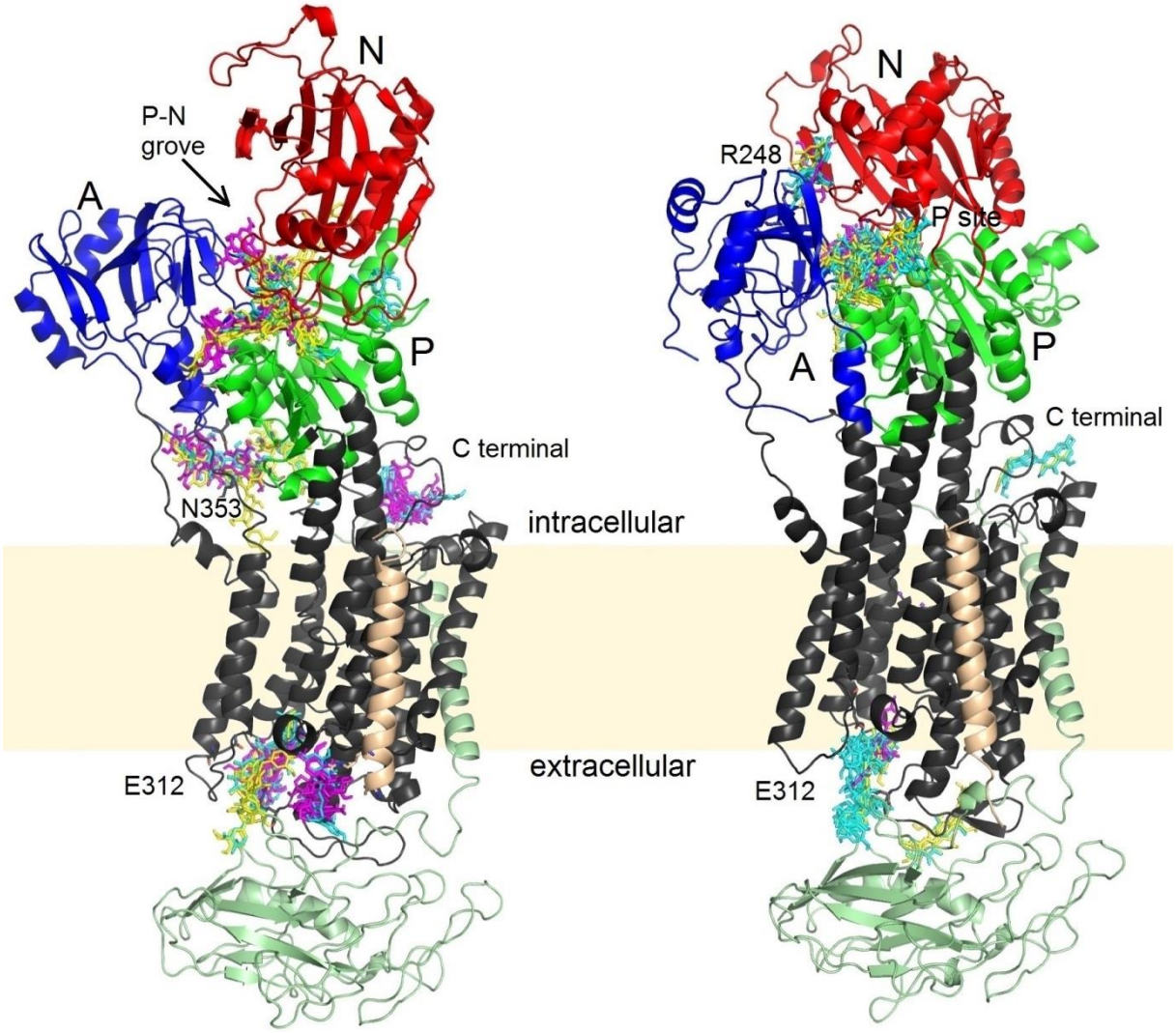

Figure 24: The open (left) and closed (right) conformations of NKA with the binding sites for flavonolignans. Silychristin is in yellow, dehydrosilychristin in cyan and dehydrosilydianin in magenta. Beta subunit is in light green, the FXYD protein light orange, A-domain blue, N-domain red and P-domain green [217].

On the closed conformation, all flavonolignans bind in the vicinity of phosphorylation site, and in the proximity of R248. All flavonolignans also to a degree bind to the extracellular site, but only SCH and DHSCH bind to the C-terminal site. One DHSCH conformer binds the most frequently to the extracellular binding site, while other DHSCH conformers and all SCH and DHSD conformers prefer the P-site.

Given that all compounds bind frequently to the cytoplasmic domains, this area was further analysed (*Figure 25*).

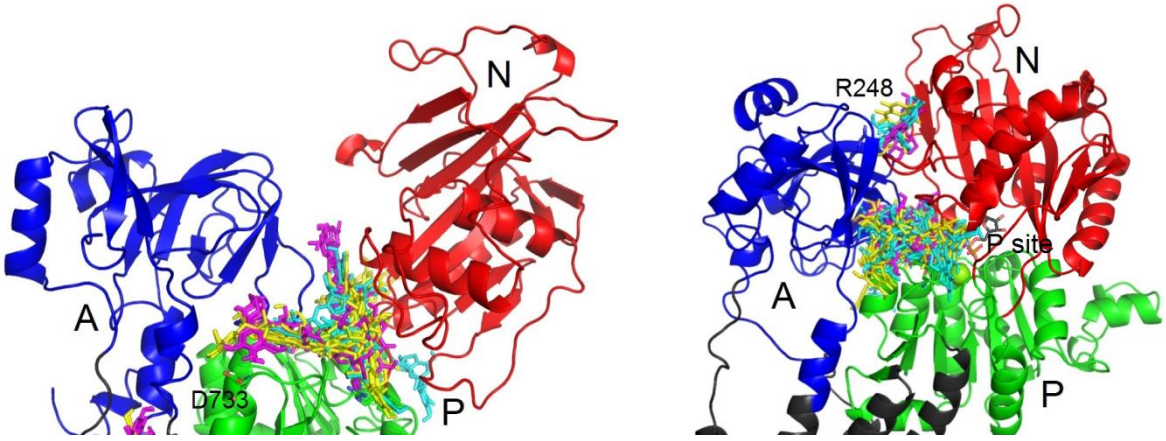

Figure 25: The open (left) and closed (right) conformations of the cytoplasmic domains (A-domain blue, N-domain red and P-domain green). Silychristin is in yellow, dehydrosilychristin in cyan and dehydrosilydianin in magenta [217].

In the open conformation, the compounds bind either between the A- and P-domains, or, more frequently, in the groove between P- and N-domains. In the closed conformation, this groove is not present due to the movement of the domains and the compounds bind in the pocket between domains in different orientations.

Flavonolignan binding at the pathway exits can hinder the ion movement through the pathways or interfere with the opening and closing of these pathways. On the other hand, binding in the cytoplasmic domain region, such as in the P-N groove, can obstruct the domain movement and lead to allosteric inhibition.

3.4.2. Quinolinones

In contrast to flavonolignans, the protein targets for quinolinones were human-sequence homology models of NKA in the open and closed conformation. The main focus was aimed on 5,6,7,8-tetrafluor-3-hydroxy-2- phenylquinolin-4(1*H*)-one (TFHPQ), which exhibited the

biggest NKA activity change in experimental measurements, while the other compounds were 6,7-difluor-3-hydroxy-2- phenylquinolin-4(1*H*)-one (DFHPQ), 5,6-dichlor-3-hydroxy-2-phenylquinolin-4(1*H*)-one (DCHPQ), 6-chlor-3-hydroxy-2- phenylquinolin-4(1*H*)-one (6CHPQ) and 8-chlor-3-hydroxy-2- phenylquinolin-4(1*H*)-one (8CHPQ), see *Figure 26*.

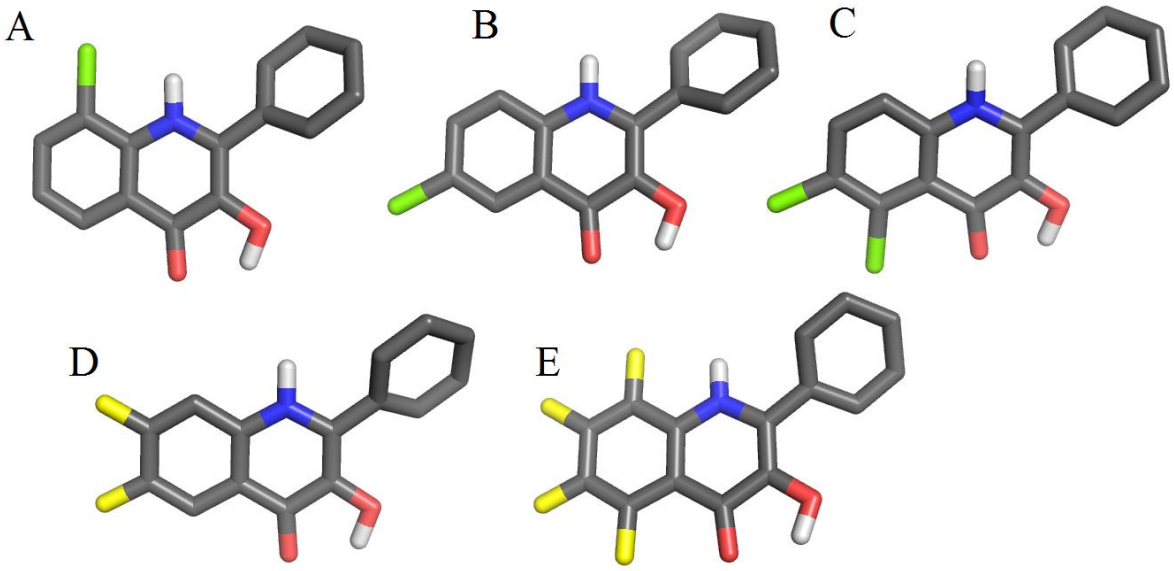

Figure 26: The quinolinones used for docking - 6CHPQ (A), 8CHPQ (B), DCHPQ (C), DFHPQ (D) and TFHPQ (E). The carbon atoms are in grey, oxygen in red, nitrogen in blue, chlorine in green, fluorine in yellow and hydrogen in white.

Molecular docking of quinolines was performed to both open and closed conformations of NKA. However, the binding sites on the closed structure are scattered across the whole structure, with lower binding affinities than for the open structure. The most frequently occupied binding site on the protein in the closed conformation is in the transmembrane part, in the vicinity of Y970, W988 of α subunit and F33 of the FXYD protein (*Figure 27*). The binding affinities of different poses in this binding site are -8.7 to -7.6 kcal/mol for TFHPQ and -8.0 to -6.6 kcal/mol for other compounds. In the NKA crystal structures, a cholesterol molecule is located in this binding site. It is, however, not accessible from the bulk solution in the native environment, therefore we focused further studies on the open conformation.

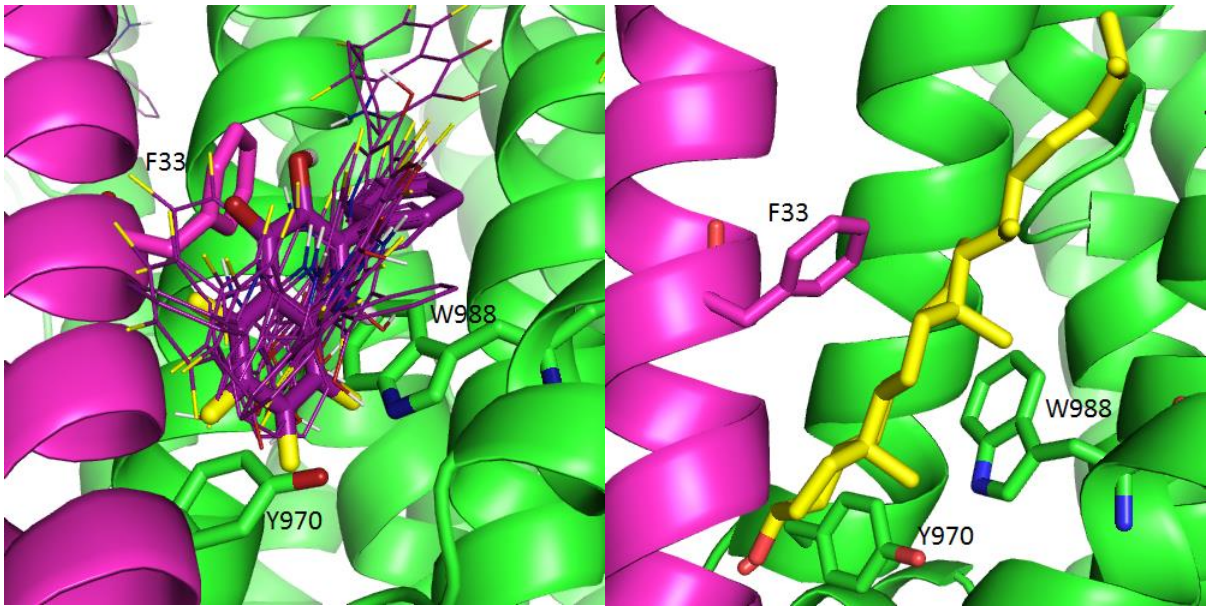

Figure 27: The most frequent TFHPQ binding site on the closed structure (left) and a cholesterol molecule bound in the 4HQJ crystal structure (right). TFHPQ is in purple, cholesterol in yellow, α subunit in green and the FXYD protein in pink.

On the open conformation, TFHPQ binds exclusively to the C-terminal area of NKA, in the vicinity of Y1022 of α subunit and W12 of β subunit (*Figure 28*). The binding affinity of this site is -10.4 to -8.9 kcal/mol for TFHPQ and with affinities -10.0 to -7.6 kcal/mol for other compounds. In contrast to TFHPQ, the other compounds bind not only to the C-terminal site, but also in different positions on the protein.

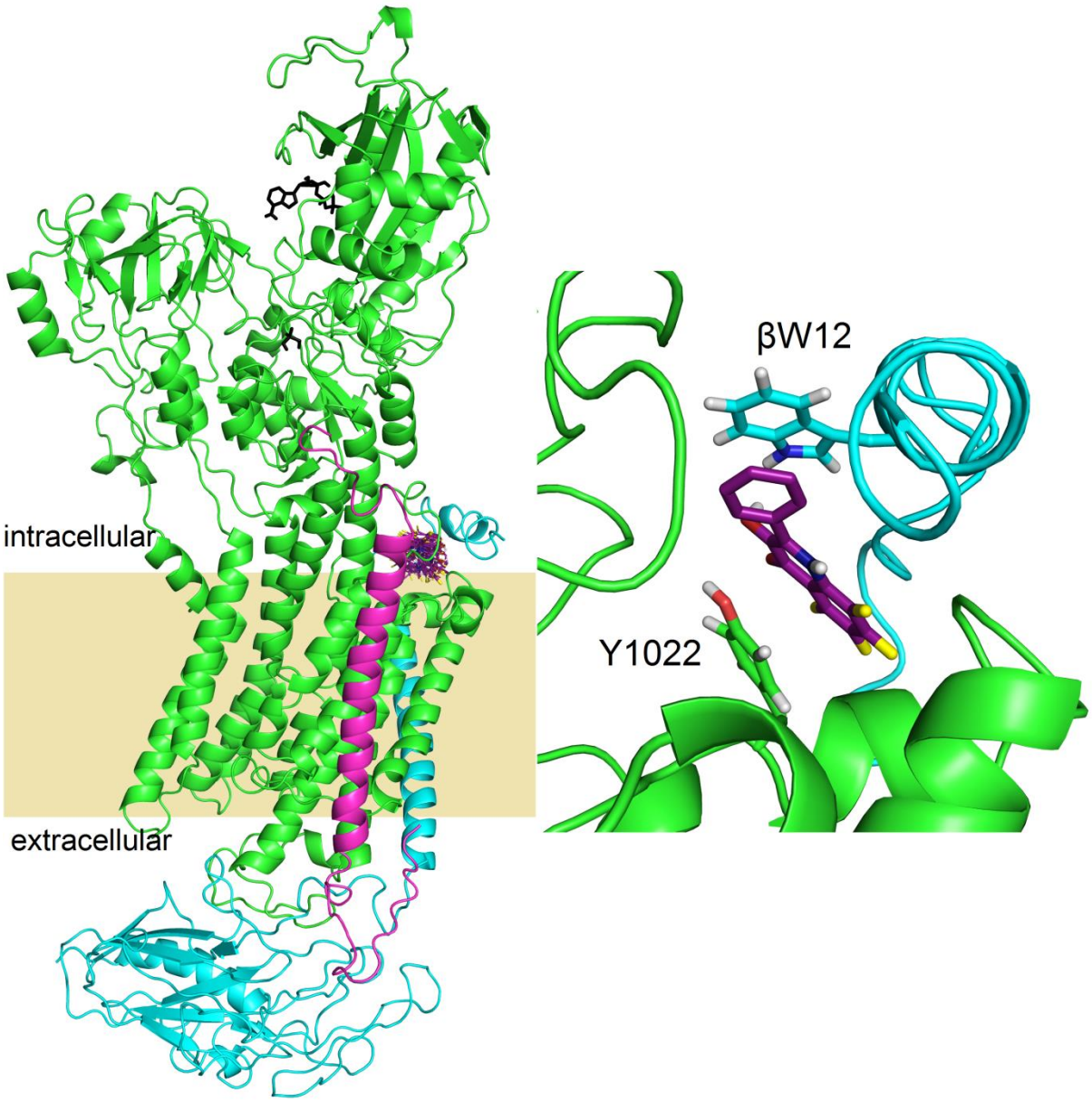

Figure 28: The binding site of TFHPQ on the open structure of NKA. TFHPQ is in purple,α subunit in green, β subunit in cyan, the FXYD protein in pink [225].

When compared to the other quinolinones studied by molecular docking, TFHPQ binds with higher affinity on both open and closed conformation of NKA. Moreover, on the open conformation, it binds exclusively to the C-terminal area, while the other compounds also occupy other sites on the protein. Therefore, the higher inhibitory effect of TFHPQ over the other compounds seems to be a combination of higher affinity and higher specificity to the binding site.

4. Conclusions

Na^+/K^+-ATPase is a membrane protein essential for its role in maintaining cell homeostasis and ion clearance. Its malfunction can lead to hyperkalaemia, hypertension or several disorders of the neural and muscular system. Recently available crystal structure of NKA in two different conformations can be a starting point for examining the structure – function relationship of the protein on a molecular level.

Computational biology serves as a powerful tool to corroborate and explain experimental findings by creating a model of a selected protein in a selected environment. Molecular dynamic simulates biomolecule movements with atomic resolution on the nanosecond timescale, while molecular docking describes the binding of small molecules to a selected protein target.

In two studies, we examined NKA using molecular dynamics – the transmembrane part, with focus on ion movements and the cytoplasmic part with respect to nucleotide binding. In the transmembrane part, we revealed that water molecules and ions from the solution can move to the cation binding site through five different pathways, two of which had not been described before. Amino acids lining these pathways had been previously connected to diseases- or protein activity affecting mutations. The nucleotide binding to the cytoplasmic domain is a dynamic process with several possible substates of the binding pocket. Interestingly, the nucleotide binding is also influenced by the protonation of CBS residues and ions present in the bulk solution, suggesting a possible feedback loop for protein activity.

Using molecular docking, we studied two groups of potentially pharmacological compounds – flavonolignans and quinolinones. Flavonolignans can bind to the transmembrane part of the protein, obstructing the entry to the C-terminal and extracellular ion pathways and consequently hampering the protein function. In addition to that, they bound with great frequency on the cytoplasmic domains. Due to significant structural rearrangements of these domains during the reaction cycle, flavonolignan binding here can obstruct the proper domain movement and inhibit the protein allosterically. Quinolinones bind with the greatest frequency at the entrance to the C-terminal pathway. Experimentally the most active quinolinone, TFHPQ, binds with higher specificity and affinity than the other quinolinones. Therefore it can inhibit NKA more efficiently than the other compounds.

The findings of ion pathways and the nucleotide binding dynamics suggests that the NKA reaction cycle is on the molecular level more complex than what can be efficiently described by the currently used E1-E2 state notation. They also indicate a complex long-distance communication system between the transmembrane cation binding site and the cytoplasmic domains. Molecular docking helped to describe two groups of active compounds that have different mechanism of effect from currently medically used cardiotonic steroids, and can therefore serve as potential new drugs affecting the Na^+/K^+-ATPase.

References

[1] E. Lindahl and M. S. P. Sansom, “Membrane proteins: molecular dynamics simulations.,” *Curr. Opin. Struct. Biol.*, vol. 18, no. 4, pp. 425–431, Aug. 2008.

[2] M. D. Forrest, “The sodium-potassium pump is an information processing element in brain computation,” *Front. Physiol.*, vol. 5, no. Nov, pp. 1–4, 2014.

[3] M. Dobretsov and J. R. Stimers, “Neuronal Function and Alpha3 Isoform of the Na/K-ATPase,” *Front. Biosci.*, no. 10, pp. 2373–2396, 2005.

[4] E. Féraille and a Doucet, “Sodium-potassium-adenosinetriphosphatase-dependent sodium transport in the kidney: hormonal control.,” *Physiol. Rev.*, vol. 81, no. 1, pp. 345–418, 2001.

[5] a M. Rose and R. Valdes, “Understanding the sodium pump and its relevance to disease.,” *Clin. Chem.*, vol. 40, no. 9, pp. 1674–85, Sep. 1994.

[6] F. Khalili-Araghi, J. Gumbart, P.-C. Wen, M. Sotomayor, E. Tajkhorshid, and K. Schulten, “Molecular dynamics simulations of membrane channels and transporters.,” *Curr. Opin. Struct. Biol.*, vol. 19, no. 2, pp. 128–137, Apr. 2009.

[7] K. K. Chaudhary and N. Mishra, “A Review on Molecular Docking : Novel Tool for Drug Discovery,” *JSM Chem.*, vol. 4, no. 3, pp. 1–4, 2016.

[8] J. H. Kaplan, “Biochemistry of Na,K-ATPase.,” *Annu. Rev. Biochem.*, vol. 71, pp. 511–535, Jan. 2002.

[9] Z. Zhou, J. Zhen, N. K. Karpowich, R. M. Goetz, C. J. Law, M. E. Reith, D. N. Wang, J. A. Javitch, L. Kale, and K. Schulten, “LeuT-desipramine structure reveals how antidepressants block neurotransmitter reuptake,” *Science (80-.).*, vol. 317, no. 6, pp. 1390–1393, Jun. 2007.

[10] J. C. H. R. Skou, “The Influence of Some Cations on an Adenosine Triphosphatase from Pheripheral Nerves,” vol. 23, pp. 394–401, 1957.

[11] M. Bublitz, H. Poulsen, J. P. Morth, and P. Nissen, “In and out of the cation pumps: P-type ATPase structure revisited.,” *Curr. Opin. Struct. Biol.*, vol. 20, no. 4, pp. 431–439, Aug. 2010.

[12] M. Chourasia and G. N. Sastry, “The nucleotide, inhibitor, and cation binding sites of P-type II ATPases.,” *Chem. Biol. Drug Des.*, vol. 79, no. 5, pp. 617–627, May 2012.

[13] K. Taniguchi, S. Kaya, K. Abe, and S. Mårdh, “The oligomeric nature of Na/K-transport ATPase.,” *J. Biochem.*, vol. 129, no. 3, pp. 335–342, Mar. 2001.

[14] D. W. Martin, “Structure-function relationships in the NA+,K+-pump.,” *Semin. Nephrol.*, vol. 25, no. 5, pp. 282–291, Sep. 2005.

[15] C. Toyoshima, R. Kanai, and F. Cornelius, “First crystal structures of Na+,K+-ATPase: new light on the oldest ion pump.,” *Structure*, vol. 19, no. 12, pp. 1732–1738, Dec. 2011.

[16] M. Nyblom, H. Poulsen, P. Gourdon, L. Reinhard, M. Andersson, E. Lindahl, N. U. Fedosova, and P. Nissen, “Crystal Structure of Na+, K+-ATPase in the Na+-Bound State.,” *Science*, vol. 342, no. 6154, pp. 123–127, Oct. 2013.

[17] P. L. Jorgensen, K. O. Hakansson, and S. J. D. Karlish, “Structure and mechanism of Na,K-ATPase: functional sites and their interactions.,” *Annu. Rev. Physiol.*, vol. 65, pp. 817–849, Jan. 2003.

[18] M. Hilge, G. Siegal, G. W. Vuister, P. Güntert, S. M. Gloor, and J. P. Abrahams, “ATP-induced conformational changes of the nucleotide-binding domain of Na,K-ATPase.,” *Nat. Struct. Biol.*, vol. 10, no. 6, pp. 468–474, Jun. 2003.

[19] M. Kubala, R. Krumscheid, and W. Schoner, “Phe 475 and Glu 446 but not Ser 445 participate in ATP-binding to the a -subunit of Na+/K+-ATPase,” *Biochem. Biophys. Res. Commun.*, vol. 297, pp. 154–159, 2002.

[20] Z. Lánský, M. Kubala, R. Ettrich, M. Kutý, J. Plášek, J. Teisinger, W. Schoner, and E. Amler, “The Hydrogen Bonds between Arg 423 and Glu 472 and Other Key Residues , Asp 443 , Ser 477 , and Pro 489 , Are Responsible for the Formation and a Different Positioning of TNP-ATP and ATP within the Nucleotide-Binding Site of Na + / K + -ATPase,” *Biochemistry*, vol. 43, pp. 8303–8311, 2004.

[21] M. Kubala, “ATP-Binding to P-Type ATPases as Revealed by Biochemical , Spectroscopic , and Crystallographic,” *Proteins Struct. Funct. Bioinforma.*, vol. 12, no. April, pp. 1–12, 2006.

[22] G. Patchornik, K. Munson, R. Goldshleger, A. Shainskaya, G. Sachs, and S. J. D. Karlish, “The ATP-Mg2+ binding site and cytoplasmic domain interactions of sodium, potassum-ATPase investigated with Fe2+-catalyzed oxidative cleavage and molecular modeling,” *Biochemistry*, vol. 41, no. 39, pp. 11740–11749, 2002.

[23] P. A. Pedersen, “Importance of Conserved alpha -Subunit Segment 709GDGVND for Mg2+ Binding, Phosphorylation, and Energy Transduction in Na,K-ATPase,” *J. Biol. Chem.*, vol. 275, no. 48, pp. 37588–37595, Sep. 2000.

[24] R. Kanai, H. Ogawa, B. Vilsen, F. Cornelius, and C. Toyoshima, “Crystal structure of a Na + -bound Na +,K + -ATPase preceding the E1P state,” *Nature*, vol. 502, no. 7470, pp. 201–206, 2013.

[25] M. Nyblom, L. Reinhard, M. Andersson, E. Lindahl, N. Fedosova, and P. Nissen, “Crystal Structure of Na+,K+-ATPase in the Na+-bound state,” *Science (80-.).*, vol. 342, no. 2013, pp. 123–127, 2013.

[26] H. Poulsen, H. Khandelia, J. P. Morth, M. Bublitz, O. G. Mouritsen, J. Egebjerg, and P. Nissen, “Neurological disease mutations compromise a C-terminal ion pathway in the Na(+)/K(+)-ATPase.,” *Nature*, vol. 467, no. 7311, pp. 99–102, Sep. 2010.

[27] M. Bublitz, M. Musgaard, H. Poulsen, L. Thøgersen, C. Olesen, B. Schiøtt, J. P. Morth, J. V. Møller, and P. Nissen, “Ion pathways in the sarcoplasmic reticulum Ca2+-ATPase.,” *J. Biol. Chem.*, vol. 288, no. 15, pp. 10759–65, Apr. 2013.

[28] S. Guennoun and J.-D. Horisberger, “Structure of the 5th transmembrane segment of the Na,K-ATPase alpha subunit: a cysteine-scanning mutagenesis study.,” *FEBS Lett.*, vol. 482, no. 1–2, pp. 144–148, 2000.

[29] A. Takeuchi, N. Reyes, P. Artigas, and D. C. Gadsby, “Visualizing the mapped ion pathway through the Na , K-ATPase pump,” *Channels*, vol. 3, no. 6, pp. 383–386, 2009.

[30] N. Vedovato and D. C. Gadsby, “Route, mechanism, and implications of proton import during Na+/K+ exchange by native Na+/K+-ATPase pumps.,” *J. Gen. Physiol.*, vol. 143, no. 4, pp. 449–64, Apr. 2014.

[31] H. Yu, I. M. Ratheal, P. Artigas, and B. Roux, “Protonation of key acidic residues is

critical for the K+ -selectivity of the Na/K pump," *Nat Struct Mol Biol*, vol. 2, no. 2, pp. 1159–1163, 2011.

[32] H. Rui, P. Artigas, and B. Roux, "The selectivity of the Na(+)/K(+)-pump is controlled by binding site protonation and self-correcting occlusion.," *Elife*, vol. 5, pp. 1–24, Aug. 2016.

[33] M. Han, W. Kopec, I. A. Solov'yov, and H. Khandelia, "Glutamate Water Gates in the Ion Binding Pocket of Na+ Bound Na+, K+-ATPase," *Sci. Rep.*, vol. 7, no. January, p. 39829, 2017.

[34] G. Blanco and R. W. Mercer, "Isozymes of the Na-K-ATPase: heterogeneity in structure, diversity in function.," *Am. J. Physiol. Ren. Physiol.*, vol. 275, no. 5 Pt 2, pp. F633–F650, 1998.

[35] K. J. Sweadner, "Isozymes of the Na+/K+-ATPase," *Biochim. Biophys. Acta - Rev. Biomembr.*, vol. 988, no. 2, pp. 185–220, May 1989.

[36] A. Jaitovich and A. M. Bertorello, "Salt, Na+,K+-ATPase and hypertension," *Life Sci.*, vol. 86, no. 3–4, pp. 73–78, 2010.

[37] N. Glorioso, F. Filigheddu, C. Troffa, a Soro, P. P. Parpaglia, a Tsikoudakis, R. H. Myers, V. L. Herrera, and N. Ruiz-Opazo, "Interaction of alpha(1)-Na,K-ATPase and Na,K,2Cl-cotransporter genes in human essential hypertension.," *Hypertension*, vol. 38, no. 2, pp. 204–9, 2001.

[38] E. A. Azizan, H. Poulsen, P. Tuluc, J. Zhou, M. J. V. Clausen, A. Lieb, C. Maniero, S. Garg, E. G. Bochukova, W. Zhao, L. H. Shaikh, C. A. Brighton, A. E. Teo, A. P. Davenport, T. Dekkers, B. Tops, B. Küsters, J. Ceral, G. S. Yeo, S. G. Neogi, I. McFarlane, N. Rosenfeld, F. Marass, J. Hadfield, W. Margas, K. Chaggar, M. Solar, J. Deinum, A. C. Dolphin, I. S. Farooqi, J. Striessnig, P. Nissen, and M. J. Brown, "Somatic mutations in ATP1A1 and CACNA1D underlie a common subtype of adrenal hypertension," *Nat Genet*, vol. 45, no. 9, pp. 1055–1060, 2013.

[39] F. Beuschlein, S. Boulkroun, A. Osswald, T. Wieland, H. N. Nielsen, U. D. Lichtenauer, D. Penton, V. R. Schack, L. Amar, E. Fischer, A. Walther, P. Tauber, T. Schwarzmayr, S. Diener, E. Graf, B. Allolio, B. Samson-Couterie, A. Benecke, M. Quinkler, F. Fallo, P.-F. Plouin, F. Mantero, T. Meitinger, P. Mulatero, X. Jeunemaitre,

R. Warth, B. Vilsen, M.-C. Zennaro, T. M. Strom, and M. Reincke, “Somatic mutations in ATP1A1 and ATP2B3 lead to aldosterone-producing adenomas and secondary hypertension.,” *Nat. Genet.*, vol. 45, no. 4, 2013.

[40] A. E. Moseley, S. P. Lieske, R. K. Wetzel, P. F. James, S. He, D. A. Shelly, R. J. Paul, G. P. Boivin, D. P. Witte, J. M. Ramirez, K. J. Sweadner, and J. B. Lingrel, “The Na,K-ATPase alpha2 isoform is expressed in neurons, and its absence disrupts neuronal activity in newborn mice,” *J. Biol. Chem.*, vol. 278, no. 7, pp. 5317–5324, 2003.

[41] I. Dostanic, J. E. J. Schultz, J. N. Lorenz, and J. B. Lingrel, “The α1 isoform of Na,K-ATPase regulates cardiac contractility and functionally interacts and co-localizes with the Na/Ca exchanger in heart,” *J. Biol. Chem.*, vol. 279, no. 52, pp. 54053–54061, 2004.

[42] M. J. Shattock, M. Ottolia, D. M. Bers, M. P. Blaustein, A. Boguslavskyi, J. Bossuyt, J. H. B. Bridge, Y. Chen-Izu, C. E. Clancy, A. Edwards, J. Goldhaber, J. Kaplan, J. B. Lingrel, D. Pavlovic, K. Philipson, K. R. Sipido, and Z.-J. Xie, “Na(+) /Ca(2+) exchange and Na(+) /K(+) -ATPase in the heart.,” *J. Physiol.*, vol. 593, no. 6, pp. 1361–1382, 2015.

[43] M. D. Ferrari, R. R. Klever, G. M. Terwindt, C. Ayata, and A. M. J. M. van den Maagdenberg, “Migraine pathophysiology: Lessons from mouse models and human genetics,” *Lancet Neurol.*, vol. 14, no. 1, pp. 65–80, 2015.

[44] M. A. Moskowitz, H. Bolay, and T. Dalkara, “Deciphering Migraine Mechanisms: Clues from Familial Hemiplegic Migraine Genotypes,” *Ann. Neurol.*, vol. 55, no. 2, pp. 276–280, 2004.

[45] M. B. Russell, A. Ducros, H. Diener, and V. Limmroth, “Sporadic and familial hemiplegic migraine: pathophysiological mechanisms, clinical characteristics, diagnosis, and management.,” *Lancet. Neurol.*, vol. 10, no. 5, pp. 457–70, May 2011.

[46] B. De Vries, T. Freilinger, K. R. J. Vanmolkot, J. B. Koenderink, A. H. Stam, G. M. Terwindt, E. Babini, E. H. Van Den Boogerd, J. J. M. W. Van Den Heuvel, R. R. Frants, J. Haan, M. Pusch, A. M. J. M. Van Den Maagdenberg, M. D. Ferrari, and M. Dichgans, “Systematic analysis of three FHM genes in 39 sporadic patients with

hemiplegic migraine," *Neurology*, vol. 69, no. 23, pp. 2170–2176, 2007.

[47] M. De Fusco, R. Marconi, L. Silvestri, L. Atorino, L. Rampoldi, L. Morgante, A. Ballabio, P. Aridon, and G. Casari, "Haploinsufficiency of ATP1A2 encoding the Na+/K+ pump α2 subunit associated with familial hemiplegic migraine type 2," *Nat. Genet.*, vol. 33, no. 2, 2003.

[48] J. P. Morth, H. Poulsen, M. S. Toustrup-Jensen, V. R. Schack, J. Egebjerg, J. P. Andersen, B. Vilsen, and P. Nissen, "The structure of the Na+,K+-ATPase and mapping of isoform differences and disease-related mutations.," *Philos. Trans. R. Soc. Lond. B. Biol. Sci.*, vol. 364, no. 1514, pp. 217–227, Jan. 2009.

[49] T. J. Isaksen and K. Lykke-Hartmann, "Insights into the Pathology of the α 2 -Na + / K + -ATPase in Neurological Disorders ; Lessons from Animal Models," vol. 7, no. May, pp. 1–8, 2016.

[50] C. Fons, J. Campistol, E. Panagiotakaki, M. Giannotta, A. Arzimanoglou, G. Gobbi, B. Neville, F. Ebinger, S. Nevšímalová, L. Laan, P. Casaer, G. Spiel, M. Ninan, G. Sange, R. Artuch, T. Schyns, R. Vavassori, and D. Poncelin, "Alternating hemiplegia of childhood: Metabolic studies in the largest European series of patients," *Eur. J. Paediatr. Neurol.*, vol. 16, no. 1, pp. 10–14, 2012.

[51] M. A. Mikati, U. Kramer, M. L. Zupanc, and R. J. Shanahan, "Alternating hemiplegia of childhood: clinical manifestations and long-term outcome," *Pediatr. Neurol.*, vol. 23, no. 2, pp. 134–141, 2000.

[52] E. L. Heinzen, K. J. Swoboda, Y. Hitomi, F. Gurrieri, S. Nicole, B. de Vries, F. D. Tiziano, B. Fontaine, N. M. Walley, S. Heavin, E. Panagiotakaki, G. Neri, S. Koelewijn, J. Kamphorst, M. Geilenkirchen, N. Pelzer, L. Laan, J. Haan, M. D. Ferrari, A. van den Maagdenberg, C. Zucca, M. T. Bassi, F. Franchini, R. Vavassori, M. Giannotta, G. Gobbi, T. Granata, N. Nardocci, E. De Grandis, E. Veneselli, M. Stagnaro, F. Vigevano, C. Oechsler, A. Arzimanoglou, M. Ninan, B. Neville, F. Ebinger, C. Fons, J. Campistol, D. Kemlink, S. Nevšímalová, C. Peeters-Scholte, P. Casaer, G. Casari, G. Sange, G. Spiel, F. M. Boneschi, T. Schyns, F. Crawley, D. Poncelin, S. Fiori, E. Abiusi, L. Di Pietro, M. T. Sweney, T. M. Newcomb, L. Viollet, C. Huff, L. B. Jorde, S. P. Reyna, K. J. Murphy, K. V Shianna, C. E. Gumbs, L. Little, K. Silver, L. J. Ptáček, A. M. Bye, G. K. Herkes, C. M. Whitelaw, D. Webb, B. J.

Lynch, P. Uldall, M. D. King, I. E. Scheffer, A. M. J. M. van den Maagdenberg, S. M. Sisodiya, M. A. Mikati, and D. B. Goldstein, “De novo mutations in ATP1A3 cause alternating hemiplegia of childhood,” *Nat. Genet.*, vol. 44, no. 9, pp. 1030–1034, 2012.

[53] H. Rosewich, H. Thiele, A. Ohlenbusch, U. Maschke, J. Altmüller, P. Frommolt, B. Zirn, F. Ebinger, H. Siemes, P. Nürnberg, K. Brockmann, and J. Gärtner, “Heterozygous de-novo mutations in ATP1A3 in patients with alternating hemiplegia of childhood: a whole-exome sequencing gene-identification study.,” *Lancet. Neurol.*, vol. 11, no. 9, pp. 764–73, Sep. 2012.

[54] P. De Carvalho Aguiar, K. J. Sweadner, J. T. Penniston, J. Zaremba, L. Liu, M. Caton, G. Linazasoro, M. Borg, M. A. J. Tijssen, S. B. Bressman, W. B. Dobyns, A. Brashear, and L. J. Ozelius, “Mutations in the Na+/K+-ATPase α3 gene ATP1A3 are associated with rapid-onset dystonia parkinsonism,” *Neuron*, vol. 43, no. 2, pp. 169–175, 2004.

[55] M. P. DeAndrade, F. Yokoi, T. van Groen, J. B. Lingrel, and Y. Li, “Characterization of Atp1a3 mutant mice as a model of rapid-onset dystonia with parkinsonism,” *Behav. Brain Res.*, vol. 216, no. 2, pp. 659–665, 2011.

[56] A. Brashear, D. DeLeon, S. B. Bressman, D. Thyagarajan, M. R. Farlow, and W. B. Dobyns, “Rapid-onset dystonia-parkinsonism in a second family,” *Neurol.* , vol. 48, no. 4, pp. 1066–1069, Apr. 1997.

[57] G. Linazasoro, B. Indakoetxea, J. Ruiz, N. Van Blercom, and A. Lasa, “Possible sporadic rapid-onset dystonia-parkinsonism,” *Mov. Disord.*, vol. 17, no. 3, pp. 608–609, May 2002.

[58] J. Zaremba, H. Mierzewska, Z. Lysiak, P. Kramer, L. J. Ozelius, and A. Brashear, “Rapid-onset dystonia-parkinsonism: A fourth family consistent with linkage to chromosome 19q13,” *Mov. Disord.*, vol. 19, no. 12, pp. 1506–1510, Dec. 2004.

[59] W. B. Dobyns, L. J. Ozelius, P. L. Kramer, A. Brashear, M. R. Farlow, T. R. Perry, L. E. Walsh, E. J. Kasarskis, I. J. Butler, and X. O. Breakefield, “Rapid-onset dystonia-parkinsonism,” *Neurol.* , vol. 43, no. 12, p. 2596, Dec. 1993.

[60] P. Nicolaides, R. E. Appleton, and a Fryer, “Cerebellar ataxia, areflexia, pes cavus, optic atrophy, and sensorineural hearing loss (CAPOS): a new syndrome,” *J Med Genet*, vol. 33, no. 5, pp. 419–421, 1996.

[61] M. K. Demos, C. D. van Karnebeek, C. J. Ross, S. Adam, Y. Shen, S. H. Zhan, C. Shyr, G. Horvath, M. Suri, A. Fryer, S. J. Jones, and J. M. Friedman, "A novel recurrent mutation in ATP1A3 causes CAPOS syndrome.," *Orphanet J. Rare Dis.*, vol. 9, p. 15, 2014.

[62] T. H. Holm and K. Lykke-Hartmann, "Insights into the pathology of the α3 Na+/K+-ATPase ion pump in neurological disorders; lessons from animal models," *Frontiers in Physiology*, vol. 7, no. JUN. 2016.

[63] S. T. Yano, K. Silver, R. Young, S. D. DeBrosse, R. S. Ebel, K. J. Swoboda, and G. Acsadi, "Fever-induced paroxysmal weakness and encephalopathy, a new phenotype of ATP1A3 mutation," *Pediatr. Neurol.*, 2017.

[64] H. Rosewich, M. Baethmann, A. Ohlenbusch, J. Gärtner, and K. Brockmann, "A novel ATP1A3 mutation with unique clinical presentation," *J. Neurol. Sci.*, vol. 341, no. 1–2, pp. 133–135, 2014.

[65] A. R. Paciorkowski, S. S. McDaniel, L. A. Jansen, H. Tully, E. Tuttle, D. H. Ghoneim, S. Tupal, S. A. Gunter, V. Vasta, Q. Zhang, T. Tran, Y. B. Liu, L. J. Ozelius, A. Brashear, K. J. Sweadner, W. B. Dobyns, and S. Hahn, "Novel mutations in ATP1A3 associated with catastrophic early life epilepsy, episodic prolonged apnea, and postnatal microcephaly," *Epilepsia*, vol. 56, no. 3, pp. 422–430, 2015.

[66] R. Dard, C. Mignot, A. Durr, G. Lesca, D. Sanlaville, E. Roze, and F. Mochel, "Relapsing encephalopathy with cerebellar ataxia related to an ATP1A3 mutation," *Dev. Med. Child Neurol.*, vol. 57, no. 12, pp. 1183–1186, 2015.

[67] A. L. Woo, P. F. James, and J. B. Lingrel, "Characterization of the Fourth alpha Isoform of the Na, K-ATPase," *J. Membr. Biol.*, vol. 169, pp. 39–44, 1999.

[68] M. J. V. Clausen, P. Nissen, and H. Poulsen, "The α4 isoform of the Na+,K+-ATPase is tuned for changing extracellular environments," *FEBS J.*, vol. 283, no. 2, pp. 282–293, 2016.

[69] K. Geering, "The functional role of beta subunits in oligomeric P-type ATPases.," *J. Bioenerg. Biomembr.*, vol. 33, no. 5, pp. 425–38, Oct. 2001.

[70] D. C. Chow and J. G. Forte, "Functional significance of the β-subunit for heterodimeric

P-type ATPases," *J. Exp. Biol.*, vol. 198, pp. 1–17, 1995.

[71] K. Geering, "Functional roles of Na,K-ATPase subunits.," *Curr. Opin. Nephrol. Hypertens.*, vol. 17, no. 5, pp. 526–532, Sep. 2008.

[72] R. E. Dempski, K. Hartung, T. Friedrich, and E. Bamberg, "Fluorometric measurements of intermolecular distances between the alpha- and beta-subunits of the Na+/K+-ATPase.," *J. Biol. Chem.*, vol. 281, no. 47, pp. 36338–46, Nov. 2006.

[73] J. A. Lobato-Álvarez, M. L. Roldán, T. del C. López-Murillo, R. González-Ramírez, J. Bonilla-Delgado, and L. Shoshani, "The apical localization of Na+, K+-ATPase in cultured human retinal pigment epithelial cells depends on expression of the β2 subunit," *Front. Physiol.*, vol. 7, no. OCT, pp. 1–17, 2016.

[74] N. B. Pestov, G. Adams, M. I. Shakhparonov, and N. N. Modyanov, "Identification of a novel gene of the X,K-ATPase β-subunit family that is predominantly expressed in skeletal and heart muscles 1," *FEBS Lett.*, vol. 456, no. 2, pp. 243–248, Aug. 1999.

[75] N. B. Pestov, N. Ahmad, T. V Korneenko, H. Zhao, R. Radkov, D. Schaer, S. Roy, S. Bibert, K. Geering, and N. N. Modyanov, "Evolution of Na,K-ATPase beta m-subunit into a coregulator of transcription in placental mammals.," *Proc. Natl. Acad. Sci. U. S. A.*, vol. 104, pp. 11215–11220, 2007.

[76] E. Tokhtaeva, R. J. Clifford, J. H. Kaplan, G. Sachs, and O. Vagin, "Subunit isoform selectivity in assembly of Na,K-ATPase α-β heterodimers," *J. Biol. Chem.*, vol. 287, no. 31, pp. 26115–26125, 2012.

[77] L. Zhang, K. J. Morris, and Y.-C. Ng, "Fiber type-specific immunostaining of the Na+,K+-ATPase subunit isoforms in skeletal muscle: Age-associated differential changes," *Biochim. Biophys. Acta - Mol. Basis Dis.*, vol. 1762, no. 9, pp. 783–793, 2006.

[78] B. R. Larsen, A. Stoica, and N. MacAulay, "Managing brain extracellular K+ during neuronal activity: The physiological role of the Na+/K+-ATPase subunit isoforms," *Front. Physiol.*, vol. 7, no. APR, pp. 1–10, 2016.

[79] M. DiFranco, H. Hakimjavadi, J. B. Lingrel, and J. A. Heiny, "Na,K-ATPase alpha2 activity in mammalian skeletal muscle T-tubules is acutely stimulated by extracellular

K+," *J. Gen. Physiol.*, vol. 146, no. 4, pp. 281–94, 2015.

[80] H. Garty and S. J. D. Karlish, "Role of Fxyd Proteins in Ion Transport," *Annu. Rev. Physiol.*, vol. 68, no. 1, pp. 431–459, 2006.

[81] K. Geering, "FXYD proteins: new regulators of Na-K-ATPase.," *Am. J. Physiol. Renal Physiol.*, vol. 290, no. 2, pp. F241–F250, Feb. 2006.

[82] H. M. Berman, J. Westbrook, Z. Feng, G. Gilliland, T. N. Bhat, H. Weissig, I. N. Shindyalov, and P. E. Bourne, "The protein data bank.," *Nucleic Acids Res.*, vol. 28, no. 1, pp. 235–242, 2000.

[83] K. O. Håkansson, "The Crystallographic Structure of Na,K-ATPase N-domain at 2.6Å Resolution," *J. Mol. Biol.*, vol. 332, no. 5, pp. 1175–1182, 2003.

[84] J. P. Morth, B. P. Pedersen, M. S. Toustrup-Jensen, T. L.-M. Sørensen, J. Petersen, J. P. Andersen, B. Vilsen, and P. Nissen, "Crystal structure of the sodium-potassium pump.," *Nature*, vol. 450, no. 7172, pp. 1043–1049, Dec. 2007.

[85] T. Shinoda, H. Ogawa, F. Cornelius, and C. Toyoshima, "Crystal structure of the sodium-potassium pump at 2.4 A resolution.," *Nature*, vol. 459, no. 7245, pp. 446–450, May 2009.

[86] H. Ogawa, T. Shinoda, F. Cornelius, and C. Toyoshima, "Crystal structure of the sodium-potassium pump (Na+,K+-ATPase) with bound potassium and ouabain.," *Proc. Natl. Acad. Sci. U. S. A.*, vol. 106, no. 33, pp. 13742–13747, Aug. 2009.

[87] H. Ogawa, F. Cornelius, A. Hirata, and C. Toyoshima, "Sequential substitution of K+ bound to Na+,K+-ATPase visualized by X-ray crystallography," *Nat. Commun.*, vol. 6, p. 8004, 2015.

[88] L. Yatime, M. Laursen, J. P. Morth, M. Esmann, P. Nissen, and N. U. Fedosova, "Structural insights into the high affinity binding of cardiotonic steroids to the Na+,K+-ATPase.," *J. Struct. Biol.*, vol. 174, no. 2, pp. 296–306, May 2011.

[89] M. Laursen, J. L. Gregersen, L. Yatime, P. Nissen, and N. U. Fedosova, "Structures and characterization of digoxin- and bufalin-bound Na+,K+-ATPase compared with the ouabain-bound complex.," *Proc. Natl. Acad. Sci. U. S. A.*, vol. 112, no. 6, pp. 1755–60, Feb. 2015.

[90] M. Laursen, L. Yatime, P. Nissen, and N. U. Fedosova, “Crystal structure of the high-affinity Na+,K+-ATPase-ouabain complex with Mg2+ bound in the cation binding site.,” *Proc. Natl. Acad. Sci. U. S. A.*, vol. 110, no. 27, pp. 10958–63, Jul. 2013.

[91] J. L. Gregersen, D. Mattle, N. U. Fedosova, P. Nissen, and L. Reinhard, “Isolation, crystallization and crystal structure determination of bovine kidney Na^{+},K^{+}-ATPase,” *Acta Crystallogr. Sect. F Struct. Biol. Commun.*, vol. 72, no. 4, pp. 282–287, 2016.

[92] K. P. Wheeler and R. Whittam, “The Involvement of Phosphatidylserine in Adenosine Triphosphatase Activity of the Sodium Pump,” *J. Physiol.*, vol. 207, pp. 303–328, 1970.

[93] R. L. Post, A. K. Sen, and R. A. S., “A Phosphorylated dependent Intermediate in Adenosine Sodium and Potassium Transport across Kidney Membranes,” *J. Biol. Chem.*, vol. 240, no. 3, pp. 1437–1445, 1965.

[94] R. W. Albers, “Biochemical Aspects of Active Transport,” *Annu. Rev. Biochem.*, vol. 36, pp. 727–756, 1967.

[95] R. L. Post and C. Hegyvary, “Activation by Adenosine Triphosphate in the Phosphorylation Kinetics of Sodium and Potassium Ion Transport Adenosine Triphosphatase Activation Kinetics Transport by Adenosine Triphosphate in the Phosphorylation of Sodium and Potassium Ion Adenos,” 1972.

[96] S. Heyse, I. Wuddel, H. J. Apell, and W. Stürmer, “Partial reactions of the Na, K-ATPase: determination of rate constants.,” *J. Gen. Physiol.*, vol. 104, no. August, pp. 197–240, 1994.

[97] D. C. Gadsby, F. Bezanilla, R. F. Rakowski, P. De Weer, and M. Holmgren, “The dynamic relationships between the three events that release individual Na+ ions from the Na+/K+-ATPase,” *Nat. Commun.*, vol. 3, no. February 2008, p. 669, 2012.

[98] M. Holmgren, J. Wagg, F. Bezanilla, R. F. Rakowski, P. De Weer, and D. C. Gadsby, “Three distinct and sequential steps in the release of sodium ions by the Na+/K+-ATPase,” *Nature*, vol. 403, no. 6772, pp. 898–901, Feb. 2000.

[99] S. Yaragatupalli, J. F. Olivera, C. Gatto, and P. Artigas, “Altered Na+ transport after an

intracellular alpha-subunit deletion reveals strict external sequential release of Na+ from the Na/K pump.," *Proc. Natl. Acad. Sci. U. S. A.*, vol. 106, no. 36, pp. 15507–12, Sep. 2009.

[100] L. Grycova, P. Sklenovsky, Z. Lansky, M. Janovska, M. Otyepka, E. Amler, J. Teisinger, and M. Kubala, "ATP and magnesium drive conformational changes of the Na+/K+-ATPase cytoplasmic headpiece.," *Biochim. Biophys. Acta*, vol. 1788, no. 5, pp. 1081–1091, May 2009.

[101] A. Pilotelle-Bunner, F. Cornelius, P. Sebban, P. W. Kuchel, and R. J. Clarke, "Mechanism of Mg2+ binding in the Na+,K+-ATPase.," *Biophys. J.*, vol. 96, no. 9, pp. 3753–61, May 2009.

[102] M. Campos and L. Beaugé, "ATP-ADP exchange reaction catalyzed by Na+,K+-ATpase: Dephosphorylation by ADP of the E1P enzyme form," *Biochemistry*, vol. 36, no. 46, pp. 14228–14237, 1997.

[103] J.-D. Horisberger, "Recent Insights into the Structure and Mechanism of the Sodium Pump," *Physiology*, vol. 19, no. 6, pp. 377–387, 2004.

[104] L. A. Vasilets, "Structure-function relationships of cation binding in the Na+/K+-ATPase," *Biochim. Biophys. Acta*, vol. 1154, pp. 201–222, 1993.

[105] J. Wagg, J. B. Chapman, and S. a Wood, "A flux ratio analysis of the Post-Albers mechanism of the sodium pump.," *J. Theor. Biol.*, vol. 174, no. 1, pp. 73–85, May 1995.

[106] V. R. Schack, J. P. Morth, M. S. Toustrup-Jensen, A. N. Anthonisen, P. Nissen, J. P. Andersen, and B. Vilsen, "Identification and function of a cytoplasmic K+ site of the Na+, K+ -ATPase.," *J. Biol. Chem.*, vol. 283, no. 41, pp. 27982–90, Oct. 2008.

[107] D. C. Gadsby, A. Takeuchi, P. Artigas, and N. Reyes, "Review. Peering into an ATPase ion pump with single-channel recordings.," *Philos. Trans. R. Soc. Lond. B. Biol. Sci.*, vol. 364, no. 1514, pp. 229–38, Jan. 2009.

[108] N. Vedovato and D. C. Gadsby, "The two C-terminal tyrosines stabilize occluded Na/K pump conformations containing Na or K ions.," *J. Gen. Physiol.*, vol. 136, no. 1, pp. 63–82, Jul. 2010.

[109] K. O. Grishanin, V. Y. Tashkin, A. A. Lenz, H.-J. J. Apell, and V. S. Sokolov, "Involvement of protons in the ion transport cycle of Na+,K+-ATPase," *Biochem. Suppl. Ser. A Membr. Cell Biol.*, vol. 4, no. 4, pp. 397–402, 2010.

[110] H.-J. Apell, "Mechanistic principles of ion transport in the Na,K-ATPase," *Russ. J. Electrochem.*, vol. 53, no. 3, pp. 237–247, 2017.

[111] W. Withering, *An Account of the Foxglove and some of its Medical Uses With Practical Remarks on Dropsy and Other Diseases*. London: G. G. J. and J. Robinson, 1785.

[112] R. J. Y. Chen, T. Chung, F. Li, W. Yang, T. Jinn, and J. T. C. Tzen, "Steroid-like compounds in Chinese medicines promote blood circulation via inhibition of Na+/K+ -ATPase.," *Acta Pharmacol. Sin.*, vol. 31, no. 6, pp. 696–702, 2010.

[113] R. a Newman, P. Yang, a D. Pawlus, and K. I. Block, "Cardiac glycosides as novel cancer therapeutic agents," *Mol.Interv.*, vol. 8, pp. 36–49, 2008.

[114] L. K. Thakur and K. K. Jha, "Palytoxin-induced acute respiratory failure," *Respir. Med. Case Reports*, vol. 20, pp. 4–6, 2017.

[115] G. Philippe and L. Angenot, "Recent developments in the field of arrow and dart poisons," *J. Ethnopharmacol.*, vol. 100, no. 1–2, pp. 85–91, 2005.

[116] M. Huličiak, J. Vacek, M. Šebela, E. Orolinová, J. Znaleziona, M. Havlíková, and M. Kubala, "Covalent binding of cisplatin impairs the function of Na +/K +-ATPase by binding to its cytoplasmic part," *Biochem. Pharmacol.*, vol. 83, no. 11, pp. 1507–1513, 2012.

[117] M. Vosahlikova, H. Ujcikova, O. Chernyavskiy, J. Brejchova, L. Roubalova, M. Alda, and P. Svoboda, "Effect of therapeutic concentration of lithium on live HEK293 cells; increase of Na+/K+-ATPase, change of overall protein composition and alteration of surface layer of plasma membrane," *Biochim. Biophys. Acta - Gen. Subj.*, vol. 1861, no. 5, pp. 1099–1112, 2017.

[118] A. Aperia, "New roles for an old enzyme: Na,K-ATPase emerges as an interesting drug target.," *J. Intern. Med.*, vol. 261, no. 1, pp. 44–52, Jan. 2007.

[119] Z. Zhang, Z. Li, J. Tian, W. Jiang, Y. Wang, X. Zhang, Z. Li, Q. You, J. I. Shapiro, S.

Si, and Z. Xie, “Identification of Hydroxyxanthones as Na / K-ATPase Ligands,” vol. 77, no. 6, pp. 961–967, 2010.

[120] L. Yatime, M. J. Buch-Pedersen, M. Musgaard, J. P. Morth, A.-M. L. Winther, B. P. Pedersen, C. Olesen, J. P. Andersen, B. Vilsen, and B. Schiøtt, “P-type ATPases as drug targets: Tools for medicine and science,” *Biochim. Biophys. Acta - Bioenerg.*, vol. 1787, no. 4, pp. 207–220, Apr. 2009.

[121] R. J. Y. Chen, T. Jinn, Y. Chen, T. Chung, W. Yang, and J. T. C. Tzen, “Active ingredients in Chinese medicines promoting blood circulation as Na+/K+ -ATPase inhibitors.,” *Acta Pharmacol. Sin.*, vol. 32, no. 2, pp. 141–151, 2011.

[122] R. J. Bick, B. J. Poindexter, R. R. Sweney, and A. Dasgupta, “Effects of Chan Su, a traditional Chinese medicine, on the calcium transients of isolated cardiomyocytes: Cardiotoxicity due to more than Na, K-ATPase blocking,” *Life Sci.*, vol. 72, no. 6, pp. 699–709, Dec. 2002.

[123] A. Karadeniz, I. Aytekin, and Y. Akgul, “Effects of acute and subacute digoxin intoxication on haematological parameters and serum CK and LDH activities in dogs,” *Rev. Med. Vet. (Toulouse).*, vol. 159, no. 2, pp. 96–100, 2008.

[124] M. P. Blaustein, “Why isn’t endogenous ouabain more widely accepted?,” *AJP Hear. Circ. Physiol.*, vol. 307, no. 5, pp. H635–H639, 2014.

[125] R. J. Y. Chen, T. Chung, F. Li, N. Lin, and J. T. C. Tzen, “Effect of sugar positions in ginsenosides and their inhibitory potency on Na+/K+-ATPase activity.,” *Acta Pharmacol. Sin.*, vol. 30, no. 1, pp. 61–69, 2009.

[126] L. Q. de Sousa, K. da C. Machado, S. F. de C. Oliveira, L. da S. Araújo, E. dos S. Monção-Filho, A. A. de C. Melo-Cavalcante, G. M. Vieira-Júnior, and P. M. P. Ferreira, “Bufadienolides from amphibians: A promising source of anticancer prototypes for radical innovation, apoptosis triggering and Na+/K+-ATPase inhibition,” *Toxicon*, vol. 127, pp. 63–76, 2017.

[127] D. T. Stanton, J. Ankenbauer, D. Rothgeb, M. Draper, and S. Paula, “Identification and characterization of novel sodium/potassium-ATPase inhibitors by virtual screening of a compound database,” *Bioorganic Med. Chem.*, vol. 15, no. 18, pp. 6062–6070, 2007.

[128] D. K. Sharma, “Pharmacological properties of flavonoids including flavonolignans - Integration of petrocrops with drug development from plants,” *J. Sci. Ind. Res. (India).*, vol. 65, no. 6, pp. 477–484, 2006.

[129] D. Biedermann, E. Vavříková, L. Cvak, and V. Křen, “Chemistry of silybin,” *Nat. Prod. Rep.*, vol. 31, no. 9, p. 1138, 2014.

[130] M. S. A. Afifi, M. M. Ahmed, J. Pezzuto, and A. D. Kinghorn, “Cytotoxic flavonolignans and flavones from Verbascum sinaiticum leaves,” *Phytochemistry*, vol. 34, no. 3, pp. 839–841, 1993.

[131] M. Bouaziz, N. C. Veitch, R. J. Grayer, M. S. J. Simmonds, and M. Damak, “Flavonolignans from Hyparrhenia hirta,” *Phytochemistry*, vol. 60, no. 5, pp. 515–520, 2002.

[132] C. S. Chambers, V. Holečková, L. Petrásková, D. Biedermann, K. Valentová, M. Buchta, and V. Křen, “The silymarin composition… and why does it matter?,” *Food Res. Int.*, p. , 2017.

[133] V. Kren and D. Walterova, “Silybin and silymarin - new effects and applications,” *Biomed. Pap.*, vol. 149, no. 1, pp. 29–41, 2005.

[134] R. Gažák, D. Walterová, and V. Křen, “Silybin and silymarin--new and emerging applications in medicine.,” *Curr. Med. Chem.*, vol. 14, no. 3, pp. 315–338, 2007.

[135] D. R. de Oliveira, L. F. Schaffer, A. Busanello, C. P. Barbosa, L. R. Peroza, C. M. de Freitas, B. N. Krum, G. N. Bressan, A. A. Boligon, M. L. Athayde, I. R. A. de Menezes, and R. Fachinetto, “Silymarin has antioxidant potential and changes the activity of Na+/K+-ATPase and monoamine oxidase in vitro,” *Ind. Crops Prod.*, vol. 70, pp. 347–355, 2015.

[136] Y.-Q. Hu, C. Gao, S. Zhang, L. Xu, Z. Xu, L.-S. Feng, X. Wu, and F. Zhao, “Quinoline hybrids and their antiplasmodial and antimalarial activities,” *Eur. J. Med. Chem.*, vol. 139, pp. 22–47, 2017.

[137] a Y. Shen, S. N. Wu, and C. T. Chiu, “Synthesis and cytotoxicity evaluation of some 8-hydroxyquinoline derivatives.,” *J. Pharm. Pharmacol.*, vol. 51, no. 5, pp. 543–548, 1999.

[138] J. Kadrić, K. Motyka, P. Džubák, M. Hajdúch, and M. Soural, “Synthesis, cytotoxic activity, and fluorescence properties of a set of novel 3-hydroxyquinolin-4(1H)-ones,” *Tetrahedron Lett.*, vol. 55, no. 26, pp. 3592–3595, 2014.

[139] R. Krikavova, J. Vanco, Z. Travnicek, R. Buchtik, and Z. Dvorak, “Copper(ii) quinolinonato-7-carboxamido complexes as potent antitumor agents with broad spectra and selective effects,” *RSC Adv.*, vol. 6, no. 5, pp. 3899–3909, 2016.

[140] M. G. Neuman, L. B. Cohen, and R. M. Nanau, “Quinolones-induced hypersensitivity reactions,” *Clin. Biochem.*, vol. 48, no. 10–11, pp. 716–739, 2015.

[141] P. Hradil, P. Krejci, J. Hlavac, I. Wiedermannova, A. Lycka, and V. Bertolasi, “Synthesis, NMR spectra and X-ray data of chloro and dichloro derivatives of 3-hydroxy-2-phenylquinolin-4(1H)-ones and their cytostatic activity.,” *J. Heterocycl. Chem.*, vol. 41, no. 3, pp. 375–379, 2004.

[142] E. C. Pesci, J. B. J. Milbank, J. P. Pearson, S. McKnight, A. S. Kende, E. P. Greenberg, and B. H. Iglewski, “Quinolone signaling in the cell-to-cell communication system of Pseudomonas aeruginosa,” *Proc. Natl. Acad. Sci.*, vol. 96, no. 20, pp. 11229–11234, 1999.

[143] M. Grepl, J. Roithová, P. Hradil, and K. Lemr, “Ionization and fragmentation of monochloro-isomers of 3-hydroxy-2-phenyl-4(1 *H*)-quinolinone,” *Rapid Commun. Mass Spectrom.*, vol. 22, no. 18, pp. 2905–2914, Sep. 2008.

[144] J. G. Almeida, A. J. Preto, P. I. Koukos, A. M. J. J. Bonvin, and I. S. Moreira, “MEMBRANE PROTEINS STRUCTURES: A review on computational modeling tools,” *Biochim. Biophys. Acta - Biomembr.*, vol. 1859, no. 10, pp. 2021–2039, 2017.

[145] R. Rodriguez, G. Chinea, N. Lopez, T. Pons, and G. Vriend, “Homology modeling, model and software evaluation: three related resources.,” *Bioinformatics*, vol. 14, no. 6, pp. 523–528, 1998.

[146] E. Krieger, K. Joo, J. Lee, J. Lee, S. Raman, J. Thompson, M. Tyka, D. Baker, and K. Karplus, “Improving physical realism, stereochemistry, and side-chain accuracy in homology modeling: Four approaches that performed well in CASP8,” *Proteins Struct. Funct. Bioinforma.*, vol. 77, no. SUPPL. 9, pp. 114–122, 2009.

[147] A. Meier and J. Söding, “Automatic Prediction of Protein 3D Structures by Probabilistic Multi-template Homology Modeling,” *PLoS Comput. Biol.*, vol. 11, no. 10, pp. 1–20, 2015.

[148] L. Mollica, L. M. Bessa, X. Hanoulle, M. R. Jensen, M. Blackledge, and R. Schneider, “Binding Mechanisms of Intrinsically Disordered Proteins: Theory, Simulation, and Experiment,” *Front. Mol. Biosci.*, vol. 3, no. September, pp. 1–18, 2016.

[149] L. Pol-Fachin, V. H. Rusu, H. Verli, and R. D. Lins, “Gromos 53a6 an Improved GROMOS Force Field for Hexopyranose-Based Carbohydrates,” *J. Chem. Theory Comput.*, 2012.

[150] J. A. Maier, C. Martinez, K. Kasavajhala, L. Wickstrom, K. E. Hauser, and C. Simmerling, “ff14SB: Improving the Accuracy of Protein Side Chain and Backbone Parameters from ff99SB,” *J. Chem. Theory Comput.*, vol. 11, no. 8, pp. 3696–3713, 2015.

[151] M. J. Robertson, J. Tirado-Rives, and W. L. Jorgensen, “Improved Peptide and Protein Torsional Energetics with the OPLS-AA Force Field,” *J. Chem. Theory Comput.*, vol. 11, no. 7, pp. 3499–3509, 2015.

[152] F. J. Van Eerden, M. N. Melo, P. W. J. M. Frederix, X. Periole, and S. J. Marrink, “Exchange pathways of plastoquinone and plastoquinol in the photosystem II complex,” *Nat. Commun.*, vol. 8, no. May, p. 15214, 2017.

[153] V. Maingi, J. R. Burns, J. J. Uusitalo, S. Howorka, S. J. Marrink, and M. S. P. Sansom, “Stability and dynamics of membrane-spanning DNA nanopores,” *Nat. Commun.*, vol. 8, p. 14784, 2017.

[154] L. G. Trabuco, E. Villa, E. Schreiner, C. B. Harrison, and K. Schulten, “Molecular dynamics flexible fitting: A practical guide to combine cryo-electron microscopy and X-ray crystallography,” *Methods*, vol. 49, no. 2, pp. 174–180, Oct. 2009.

[155] G. Zhao, J. R. Perilla, E. L. Yufenyuy, X. Meng, B. Chen, J. Ning, J. Ahn, A. M. Gronenborn, K. Schulten, C. Aiken, and P. Zhang, “Mature HIV-1 capsid structure by cryo-electron microscopy and all-atom molecular dynamics,” *Nature*, vol. 497, no. 7451, pp. 643–646, 2013.

[156] H. Yu and K. Schulten, “Membrane Sculpting by F-BAR Domains Studied by Molecular Dynamics Simulations,” *PLoS Comput. Biol.*, vol. 9, no. 1, pp. 1–15, 2013.

[157] D. Aguayo, F. D. Gonza, and C. Chipot, “Insight into the Properties of Cardiolipin Containing Bilayers from Molecular Dynamics Simulations , Using a Hybrid All-Atom / United- Atom Force Field,” *J. Chem. Theory Comput.*, vol. 8, pp. 1765–1773, 2012.

[158] W. Zheng and F. Qin, “A combined coarse-grained and all-atom simulation of TRPV1 channel gating and heat activation,” *J. Gen. Physiol.*, vol. 145, no. 5, pp. 443–456, 2015.

[159] N. Goga, M. N. Melo, A. J. Rzepiela, A. H. De Vries, A. Hadar, S. J. Marrink, and H. J. C. Berendsen, “Benchmark of schemes for multiscale molecular dynamics simulations,” *J. Chem. Theory Comput.*, vol. 11, no. 4, pp. 1389–1398, 2015.

[160] H. J. C. Berendsen, J. P. M. Postma, W. F. Van Gunsteren, A. Dinola, and J. R. Haak, “Molecular dynamics with coupling to an external bath,” vol. 81, no. 8, pp. 3684–3691, 1984.

[161] I. Halperin, B. Ma, H. Wolfson, and R. Nussinov, “Principles of docking: An overview of search algorithms and a guide to scoring functions,” *Proteins Struct. Funct. Genet.*, vol. 47, no. 4, pp. 409–443, 2002.

[162] G. M. Morris, D. S. Goodsell, R. S. Halliday, R. Huey, W. E. Hart, R. K. Belew, and A. J. Olson, “Automated docking using a Lamarckian genetic algorithm and an empirical binding free energy function,” *J. Comput. Chem.*, vol. 19, no. 14, pp. 1639–1662, 1998.

[163] S. Kirkpatrick, C. D. Gelatt, and M. P. Vecch, “Optimization by Simulated Annealing,” *Science (80-.).*, vol. 220, no. 4598, pp. 671–680, 1983.

[164] O. Trott and A. J. Olson, “AutoDock Vina: Improving the speed and accuracy of docking with a new scoring function, efficient optimization, and multithreading,” *J. Comput. Chem.*, vol. 31, no. 2, pp. 455–61, 2010.

[165] R. D. Head, M. L. Smythe, T. I. Oprea, C. L. Waller, S. M. Green, and G. R. Marshall, “VALIDATE: A new method for the receptor-based prediction of binding affinities of novel ligands,” *J. Am. Chem. Soc.*, vol. 118, no. 16, pp. 3959–3969, 1996.

[166] L. Verlet, “Computer ‘Experiments’ on Classical Fluids. I. Thermodynamical Properties of Lennard-Jones Molecules,” vol. i, no. 5, pp. 98–103, 1967.

[167] J. W. Ponder and D. A. Case, “Force fields for protein simulations,” *Adv. Protein Chem.*, vol. 66, pp. 27–85, 2003.

[168] F. A. Momany, R. F. McGuire, A. W. Burgess, and H. A. Scheraga, “Energy parameters in polypeptides. 7. Geometric parameters, partial atomic charges, nonbonded interactions, hydrogen-bond interactions, and intrinsic,” *J. Phys. Chem.*, vol. 79, no. 22, pp. 2361–2381, 1975.

[169] A. Kryshtafovych, B. Monastyrskyy, and K. Fidelis, “CASP11 statistics and the prediction center evaluation system,” *Proteins Struct. Funct. Bioinforma.*, no. November 2015, pp. 15–19, 2016.

[170] M. J. Hartshorn, M. L. Verdonk, G. Chessari, S. C. Brewerton, W. T. M. Mooij, P. N. Mortenson, and C. W. Murray, “Diverse, high-quality test set for the validation of protein-ligand docking performance,” *J. Med. Chem.*, vol. 50, no. 4, pp. 726–741, 2007.

[171] N. Huang, B. K. Shoichet, and J. J. Irwin, “Benchmarking Sets for Molecular Docking,” vol. 49, no. 23, pp. 6789–6801, 2006.

[172] A. Glättli, X. Daura, D. Seebach, and W. F. Van Gunsteren, “Can one derive the conformational preference of a β-peptide from its CD spectrum?,” *J. Am. Chem. Soc.*, vol. 124, no. 44, pp. 12972–12978, 2002.

[173] C. Toyoshima and F. Cornelius, “New crystal structures of PII-type ATPases: excitement continues.,” *Curr. Opin. Struct. Biol.*, vol. 23, no. 4, pp. 507–14, Aug. 2013.

[174] Y. Norimatsu, K. Hasegawa, N. Shimizu, and C. Toyoshima, “Protein–phospholipid interplay revealed with crystals of a calcium pump,” *Nature*, vol. 545, no. 7653, pp. 193–198, 2017.

[175] C. Toyoshima, M. Nakasako, H. Nomura, and H. Ogawa, “Crystal structure of the calcium pump of sarcoplasmic reticulum at 2.6 [angst] resolution,” *Nature*, vol. 405, no. 6787, pp. 647–655, Jun. 2000.

[176] R. Ettrich, M. Melichercik, J. Teisinger, O. Ettrichová, R. Krumscheid, K. Hofbauerová, P. Kvasnicka, W. Schoner, and E. Amler, "Three-dimensional structure of the large cytoplasmic H4 – H5 loop of Na+/K+-ATPase deduced by restraint-based comparative modeling shows only one ATP binding site," *J. Mol. Model.*, vol. 7, no. 7, pp. 184–192, 2001.

[177] K. Hofbauerová, V. Kopecký, R. Ettrich, O. Ettrichová, and E. Amler, "Secondary and tertiary structure of nucleotide-binding domain of αsubunit of Na+/K+-ATPase," *Biopolymers*, vol. 67, no. 4–5, pp. 242–246, 2002.

[178] K. Hofbauerová, V. Kopecký Jr., R. Ettrich, M. Kubala, J. Teisinger, and E. Amler, "ATP-binding is stabilized by a stacking interaction within the binding site of Na+/K+-ATPase," *Biochem. Biophys. Res. Commun.*, vol. 306, no. 2, pp. 416–420, 2003.

[179] M. Kubala, L. Grycova, Z. Lansky, P. Sklenovsky, M. Janovska, M. Otyepka, and J. Teisinger, "Changes in electrostatic surface potential of Na+/K+-ATPase cytoplasmic headpiece induced by cytoplasmic ligand(s) binding.," *Biophys. J.*, vol. 97, no. 6, pp. 1756–1764, Sep. 2009.

[180] H. Ogawa and C. Toyoshima, "Homology modeling of the cation binding sites of Na+K+-ATPase.," *Proc. Natl. Acad. Sci. U. S. A.*, vol. 99, no. 25, pp. 15977–15982, 2002.

[181] R. F. Rakowski and S. Sagar, "Found : Na + and K + Binding Sites of the Sodium Pump," *News Physiol. Sci.*, vol. 18, pp. 164–168, 2003.

[182] K. O. Hakansson and P. L. Jorgensen, "Homology modeling of NKA A putative third sodium binding site...," *Ann. N. Y. Acad. Sci.*, vol. 16, no. 986, pp. 163–167, 2003.

[183] N. Reyes and D. C. Gadsby, "Ion permeation through the Na+,K+-ATPase.," *Nature*, vol. 443, no. 7110, pp. 470–4, Sep. 2006.

[184] M. Havlíková, M. Huličiak, V. Bazgier, K. Berka, and M. Kubala, "Fluorone dyes have binding sites on both cytoplasmic and extracellular domains of Na,K-ATPase," *Biochim. Biophys. Acta - Biomembr.*, vol. 1828, no. 2, pp. 568–576, 2013.

[185] H. Poulsen, P. Nissen, O. G. Mouritsen, and H. Khandelia, "Protein kinase A (PKA) phosphorylation of Na+/K+-ATPase opens intracellular C-terminal water pathway

leading to third Na+-binding site in molecular dynamics simulations.," *J. Biol. Chem.*, vol. 287, no. 19, pp. 15959–15965, May 2012.

[186] W. Kopec, B. Loubet, H. Poulsen, and H. Khandelia, "Molecular mechanism of Na(+),K(+)-ATPase malfunction in mutations characteristic of adrenal hypertension.," *Biochemistry*, vol. 53, no. 4, pp. 746–754, Feb. 2014.

[187] Y. A. Mahmmoud, W. Kopec, and H. Khandelia, "K+ Congeners That Do Not Compromise Na+ Activation of the Na+,K+-ATPase Hydration of the ion binding cavity likely controls ion selectivity," *J. Biol. Chem.*, vol. 290, no. 6, pp. 3720–3731, 2015.

[188] F. Hilbers, W. Kopec, T. J. Isaksen, T. H. H. Holm, K. Lykke-Hartmann, P. Nissen, H. Khandelia, and H. Poulsen, "Tuning of the Na,K-ATPase by the beta subunit," *Nat. Publ. Gr.*, vol. 6, no. October 2015, p. 20442, Feb. 2016.

[189] B. Webb and A. Sali, "Comparative Protein Structure Modeling Using MODELLER," *Curr. Protoc. Bioinforma.*, p. 47:5.6:5.6.1–5.6.32., 2014.

[190] M. Magrane and U. P. Consortium, "UniProt Knowledgebase: A hub of integrated protein data," *Database*, vol. 2011, pp. 1–13, 2011.

[191] S. Pronk, S. Páll, R. Schulz, P. Larsson, P. Bjelkmar, R. Apostolov, M. R. Shirts, J. C. Smith, P. M. Kasson, D. van der Spoel, B. Hess, and E. Lindahl, "GROMACS 4.5: a high-throughput and highly parallel open source molecular simulation toolkit.," *Bioinformatics*, vol. 29, no. 7, pp. 845–854, Apr. 2013.

[192] M. J. Abraham, T. Murtola, R. Schulz, S. Páll, J. C. Smith, B. Hess, and E. Lindah, "Gromacs: High performance molecular simulations through multi-level parallelism from laptops to supercomputers," *SoftwareX*, vol. 1–2, pp. 19–25, 2015.

[193] L. Schrödinger, "The PyMOL Molecular Graphics System, Version 1.6.0," 2010.

[194] W. Humphrey, A. Dalke, and K. Schulten, "VMD: Visual molecular dynamics," *J. Mol. Graph.*, no. 14, pp. 33–38, 1996.

[195] D. Sehnal, R. Svobodová Vařeková, K. Berka, L. Pravda, V. Navrátilová, P. Banáš, C.-M. Ionescu, M. Otyepka, and J. Koča, "MOLE 2.0: advanced approach for analysis of biomacromolecular channels.," *J. Cheminform.*, vol. 5, no. 1, p. 39, Jan. 2013.

[196] “Maestro Schrödinger.” Maestro, Schrödinger, LLC, New York, 2017.

[197] S. Salentin, S. Schreiber, V. J. Haupt, M. F. Adasme, and M. Schroeder, “PLIP: Fully automated protein-ligand interaction profiler,” *Nucleic Acids Res.*, vol. 43, no. W1, pp. W443–W447, 2015.

[198] M. G. Wolf, M. Hoefling, C. Aponte-Santamaria, H. Grubmuller, and G. Groenhof, “g_membed: Efficient insertion of a membrane protein into an equilibrated lipid bilayer with minimal perturbation,” *J. Comput. Chem.*, no. 31, p. 2169−2174, 2010.

[199] C. Oostenbrink, A. Villa, A. E. Mark, and W. F. Van Gunsteren, “A biomolecular force field based on the free enthalpy of hydration and solvation: The GROMOS force-field parameter sets 53A5 and 53A6,” *J. Comput. Chem.*, vol. 25, no. 13, pp. 1656–1676, 2004.

[200] O. Berger, O. Edholm, and F. Jähnig, “Molecular dynamics simulations of a fluid bilayer of dipalmitoylphosphatidylcholine at full hydration, constant pressure, and constant temperature.,” *Biophys. J.*, vol. 72, no. 5, pp. 2002–2013, May 1997.

[201] D. van der Spoel, K. A. Feenstra, M. A. Hemminga, and H. J. C. Berendsen, “Molecular modeling of the RNA binding N-terminal part of cowpea chlorotic mottle virus coat protein in solution with phosphate ions,” *Biophys. J.*, no. 71, pp. 2920–2932, 1996.

[202] C. Margreitter, D. Petrov, and B. Zagrovic, “Vienna-PTM web server: a toolkit for MD simulations of protein post-translational modifications.,” *Nucleic Acids Res.*, vol. 41, no. Web Server issue, pp. W422–W426, 2013.

[203] G. Bussi, D. Donadio, and M. Parrinello, “Canonical sampling through velocity rescaling.,” *J. Chem. Phys.*, vol. 126, no. 1, p. 14101, Jan. 2007.

[204] J. M. S. May, “The Verlet Algorithm for Molecular Dynamics Simulations,” no. May, pp. 1–9, 2013.

[205] M. Parrinello and A. Rahman, “Polymorphic transitions in single crystals: A new molecular dynamics method,” *J. Appl. Phys.*, vol. 52, no. 12, pp. 7182–7190, 1981.

[206] G. Morris and R. Huey, “AutoDock4 and AutoDockTools4: Automated docking with selective receptor flexibility,” *J. ...*, vol. 30, no. 16, pp. 2785–2791, 2009.

[207] M. R. Koebel, G. Schmadeke, R. G. Posner, and S. Sirimulla, “AutoDock VinaXB: Implementation of XBSF, new empirical halogen bond scoring function, into AutoDock Vina,” *J. Cheminform.*, vol. 8, no. 1, pp. 1–8, 2016.

[208] G. van Meer, D. R. Voelker, and G. W. Feigenson, “Membrane lipids: where they are and how they behave.,” *Nat. Rev. Mol. Cell Biol.*, vol. 9, no. 2, pp. 112–24, Feb. 2008.

[209] H. Bouvrais, F. Cornelius, J. H. Ipsen, and O. G. Mouritsen, “Intrinsic reaction-cycle time scale of Na+,K+-ATPase manifests itself in the lipid-protein interactions of nonequilibrium membranes.,” *Proc. Natl. Acad. Sci. U. S. A.*, vol. 109, no. 45, pp. 18442–6, 2012.

[210] P. Čechová, K. Berka, and M. Kubala, “Ion Pathways in the Na + /K + -ATPase,” *J. Chem. Inf. Model.*, vol. 56, no. 12, pp. 2434–2444, 2016.

[211] B. Vilsen, “Leucine 332 at the Boundary Between the Fourth Transmembrane Segment and the Cytoplasmic Domain of Na + , K + -ATPase Plays a Pivotal Role in the Ion Tanslocating Conformational Changes,” vol. 2960, no. 97, pp. 13312–13324, 1997.

[212] M. S. Toustrup-Jensen, M. Hauge, and B. Vilsen, “Mutational Effects on Conformational Changes of the Dephospho- and Phospho-forms of the Na+,K+-ATPase,” vol. 40, pp. 5521–5532, 2001.

[213] A. P. Einholm, M. S. Toustrup-Jensen, J. P. Andersen, and B. Vilsen, “Mutation of Gly-94 in transmembrane segment M1 of Na+ , K+-ATPase interferes with Na+ and K+□ binding in E2P conformation,” vol. 102, no. 32, pp. 11254–11259, 2005.

[214] A. P. Einholm, J. P. Andersen, and B. Vilsen, “Importance of Leu99 in Transmembrane Segment M1 of the Na+,K+-ATPase in the Binding and Occlusion of K+,” *J. Biol. Chem.*, vol. 282, no. 33, pp. 23854–23866, Jun. 2007.

[215] H. G. Shi, L. Mikhaylova, and A. E. Zichittella, “Functional role of cysteine residues in the (Na , K) -ATPase alpha subunit,” *Biochim. Biophys. Acta*, vol. 1464, pp. 177–187, 2000.

[216] J. M. Argüello, J. Whitis, M. C. Cheung, and J. B. Lingrel, “Functional Role of Oxygen-Containing Residues in the Fifth Transmembrane Segment of the Na,K-ATPase α Subunit,” *Arch. Biochem. Biophys.*, vol. 364, no. 2, pp. 254–263, Apr. 1999.

[217] M. Kubala, P. Čechová, J. Geletičová, M. Biler, T. Štenclová, P. Trouillas, and D. Biedermann, "Flavonolignans as a Novel Class of Sodium Pump Inhibitors," *Front. Physiol.*, vol. 7, no. March, pp. 1–10, 2016.

[218] M. S. Toustrup-Jensen, "Functional Consequences of Alterations to Ile279, Ile283, Glu284, His285, Phe286, and His288 in the NH2-terminal Part of Transmembrane Helix M3 of the Na+,K+-ATPase," *J. Biol. Chem.*, vol. 278, no. 40, pp. 38653–38664, 2003.

[219] T. A. Kuntzweiler, E. T. Wallick, C. L. Johnson, and J. B. Lingrel, "Amino Acid Replacement of Asp 369 in the Sheep alpha 1 Isoform Eliminates ATP and Phosphate Stimulation of [3H]Ouabain Binding Properties of the Enzyme," *J. Biol. Chem.*, vol. 270, no. 27, pp. 16206–16212, 1995.

[220] T. Imagawa, T. Yamamoto, S. Kaya, K. Sakaguchi, and K. Taniguchi, "Thr-774 (transmembrane segment M5), Val-920 (M8), and Glu-954 (M9) are involved in Na+ transport, and Gln-923 (M8) is essential for Na,K-ATPase activity.," *J. Biol. Chem.*, vol. 280, no. 19, pp. 18736–18744, May 2005.

[221] S. Teramachi, T. Imagawa, S. Kaya, and K. Taniguchi, "Replacement of several single amino acid side chains exposed to the inside of the ATP-binding pocket induces different extents of affinity change in the high and low affinity ATP-binding sites of rat Na/K-ATPase," *J. Biol. Chem.*, vol. 277, no. 40, pp. 37394–37400, 2002.

[222] H. R. Hinz and T. L. Kirley, "Lysine 480 is an essential residue in the putative ATP Site of lamb kidney (Na,K)-ATPase: Identification of the pyridoxal 5'-diphospho-5'-adenosine and pyridoxal phosphate reactive residue," *J. Biol. Chem.*, vol. 265, no. 18, pp. 10260–10265, 1990.

[223] J. V. Moler, B. Juul, and M. le Maire, "Structural organization, ion transport, and energy transduction of P-type ATPases," *Biochim. Biophys. Acta*, vol. 1286, pp. 1–51, 1996.

[224] D. Thoenges, "Tight Binding of Bulky Fluorescent Derivatives of Adenosine to the Low Affinity E2ATP Site Leads to Inhibition of Na+/K+-ATPase.," *J. Biol. Chem.*, vol. 274, no. 4, pp. 1971–1978, Jan. 1999.

[225] J. Šeflová, P. Čechová, M. Biler, P. Hradil, and M. Kubala, "Inhibition of Na+/K+-

ATPase by 5,6,7,8-tetrafluoro-3-hydroxy-2-phenylquinolin-4(1H)-one," *Biochimie*, vol. 138, pp. 56–61, 2017.

Appendix A – Post Albers diagrams

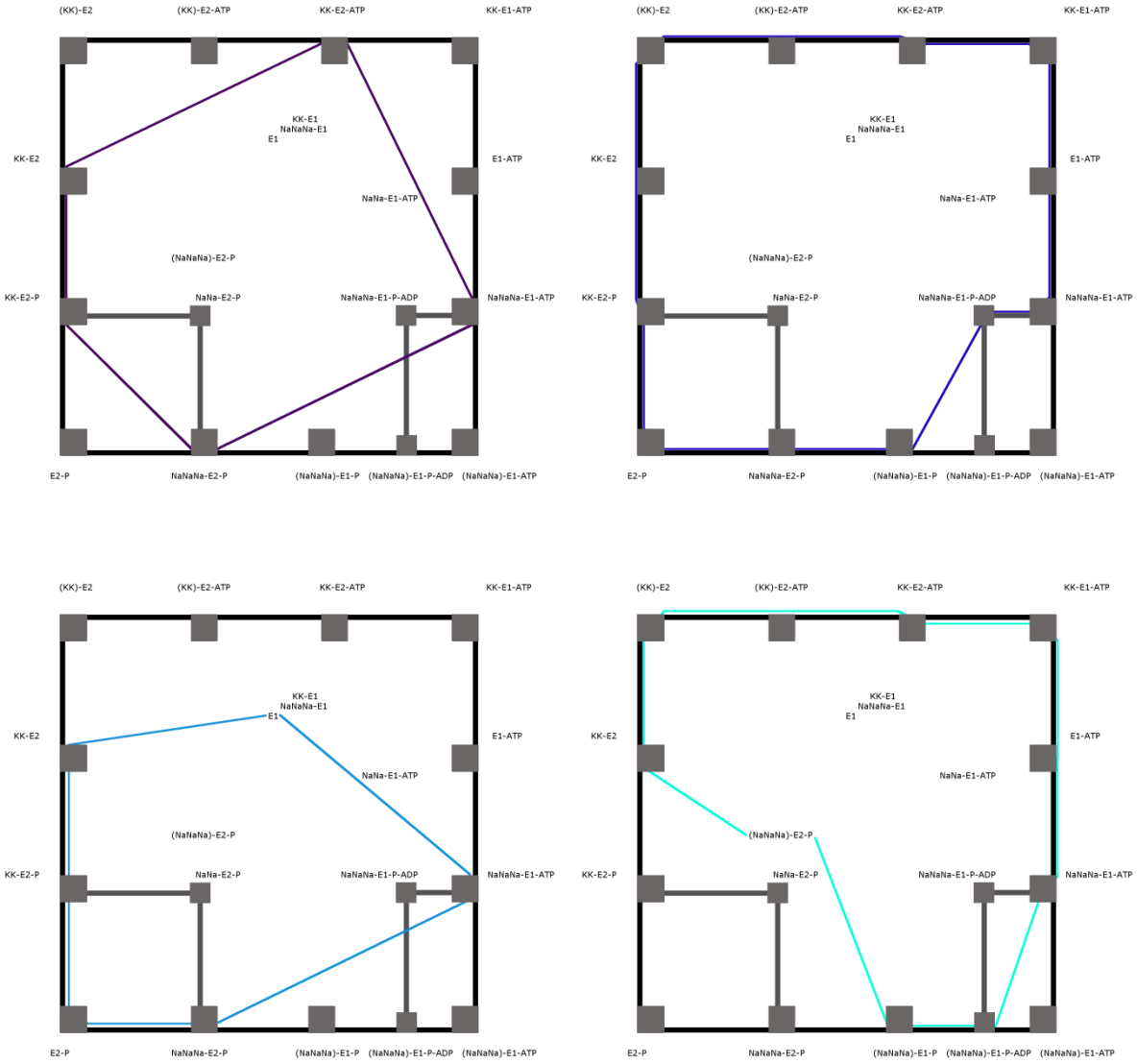

The different versions of the Post-Albers diagram. The colours depict the diagram as used by by Post [95] (purple, 1972), Vasilets [104] (dark blue, 1993), Rose [5] (light blue, 1994), Wagg [105] (cyan, 1995), The lines go inside of the rectangle in cases where the states go through all depicted step and outside when skipping a step.

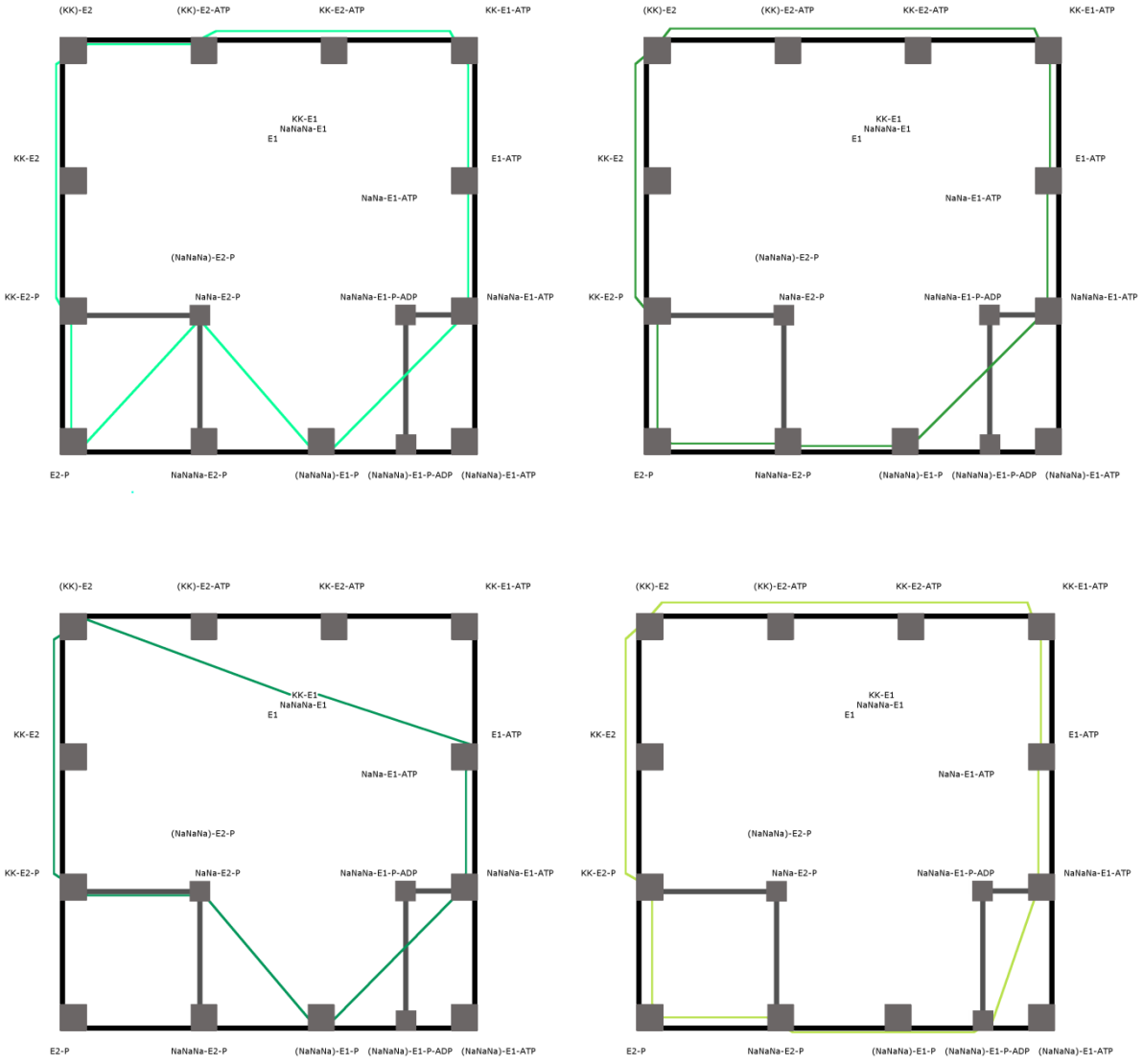

The different versions of the Post-Albers diagram. The colours depict the diagram as used by by Kaplan [8] (light green, 2002), Jorgensen [17] (forest green, 2003), Martin [14] (dark green, 2005), Dempski [72] (yellow-green, 2006). The lines go inside of the rectangle in cases where the states go through all depicted step and outside when skipping a step.

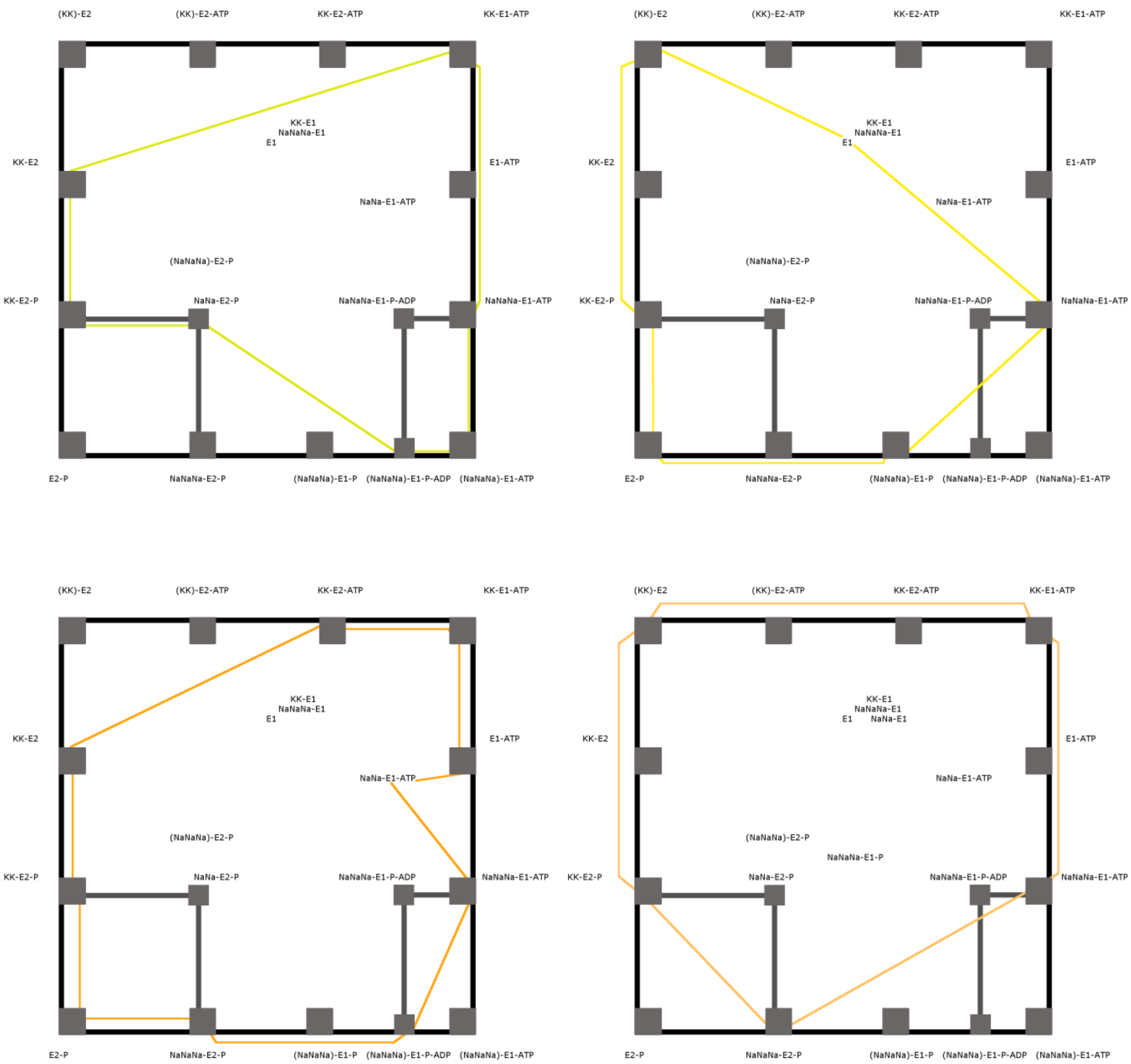

The different versions of the Post-Albers diagram. The colours depict the diagram as used by by Morth [84] (green-yellow, 2007), Schack [106] (yellow, 2008), Grycová [100] (orange, 2009), Gadsby [107] (light orange, 2009). The lines go inside of the rectangle in cases where the states go through all depicted step and outside when skipping a step.

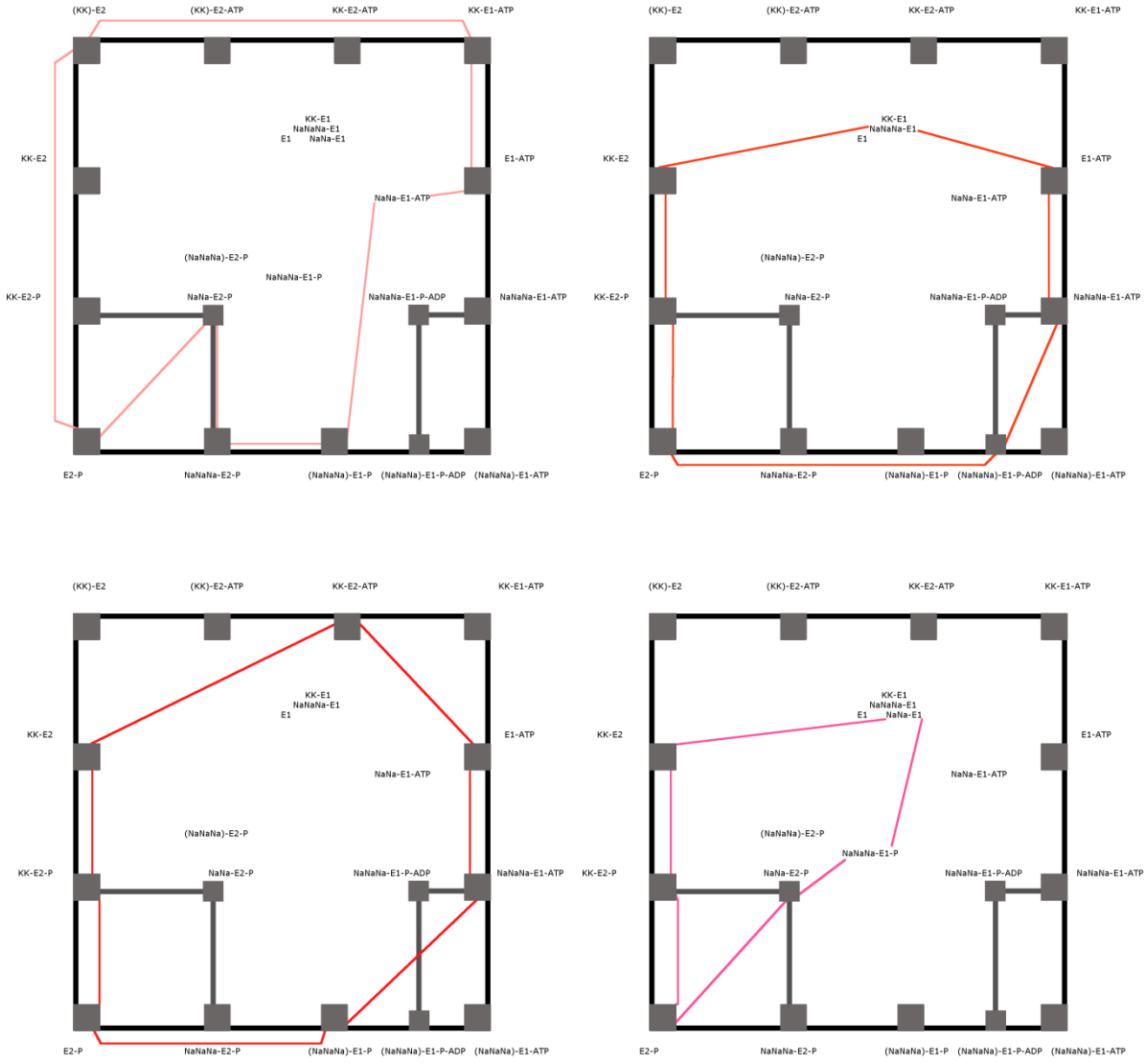

The different versions of the Post-Albers diagram. The colours depict the diagram as used by by Bublitz [11] (orange-red, 2010), Vedovato [108] (salmon, 2010), Toyoshima [15] (red, 2010), Grichanin [109] (pink, 2010). The lines go inside of the rectangle in cases where the states go through all depicted step and outside when skipping a step.

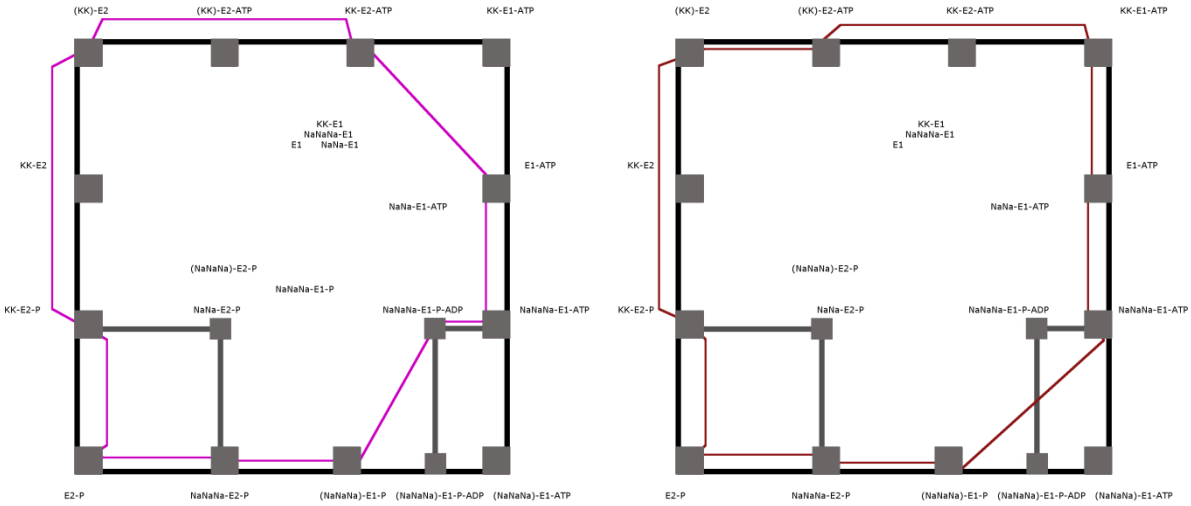

The different versions of the Post-Albers diagram. The colours depict the diagram as used by by Ogawa [87] (fuchsia, 2015), Appel [110] (dark red, 2017). The lines go inside of the rectangle in cases where the states go through all depicted step and outside when skipping a step.

Appendix B – Full Text Publications

JOURNAL OF CHEMICAL INFORMATION AND MODELING

Article

pubs.acs.org/jcim

Ion Pathways in the Na^+/K^+-ATPase

Petra Čechová,[†] Karel Berka,[‡] and Martin Kubala*[,†]

[†]Department of Biophysics, Centre of the Region Hana for Biotechnological and Agricultural Research, Faculty of Science, Palacký University, Šlechtitelů 27, 783 71, Olomouc, Czech Republic

[‡]Department of Physical Chemistry, Regional Centre of Advanced Technologies and Materials, Faculty of Science, Palacký University, 17. listopadu 12, 77146 Olomouc, Czech Republic

Supporting Information

ABSTRACT: Na^+/K^+-ATPase (NKA) is an essential cation pump protein responsible for the maintenance of the sodium and potassium gradients across the plasma membrane. Recently published high-resolution structures revealed amino acids forming the cation binding sites (CBS) in the transmembrane domain and variable position of the domains in the cytoplasmic headpiece. Here we report molecular dynamic simulations of the human NKA $\alpha1\beta1$ isoform embedded into DOPC bilayer. We have analyzed the NKA conformational changes in the presence of Na^+- or K^+-cations in the CBS, for various combinations of the cytoplasmic ligands, and the two major enzyme conformations in the 100 ns runs (more than 2.5 μs of simulations in total). We identified two novel cytoplasmic pathways along the pairs of transmembrane helices TM3/TM7 or TM6/TM9 that allow hydration of the CBS or transport of cations from/to the bulk. These findings can provide a structural explanation for previous mutagenesis studies, where mutation of residues that are distal from the CBS resulted in the alteration of the enzyme affinity to the transported cations or change in the enzyme activity.

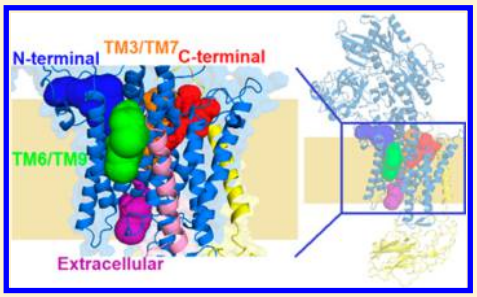

INTRODUCTION

Sodium−potassium pump (Na^+/K^+-ATPase, NKA) is an essential membrane protein important for the maintenance of sodium homeostasis and plasma membrane potential. It is present in all animal cells. During one catalytic cycle, NKA pumps 3 Na^+ ions and 2 K^+ ions in opposite directions across the plasma membrane in the presence of ATP and magnesium. The resulting Na^+ gradient is also essential for the function of numerous secondary active transporters.[1] Therefore, NKA is one of the most important enzymes in the animal metabolism (it accounts for nearly one-third of whole body ATP consumption[2]) and its inhibition or malfunction is related to severe diseases.[3,4]

NKA belongs to the superfamily of cation translocating P-type ATPases (subgroup 2C). Their main catalytic α-subunit is characterized by 10 transmembrane (TM) helices, and three cytoplasmic domains denoted as A (actuator), N (nucleotide-binding) and P (phosphorylation).[5] The subgroup 2C pumps (NKA and H^+/K^+-ATPase) have also the β-subunit, with a single TM helix and a large domain on the extracellular side. Despite the general agreement that the (α+β)-complex is the minimal functional unit, the membrane-purified proteins frequently contain also a small (6−8 kDa) tissue-specific protein from the FXYD family (sometimes denoted as a γ-subunit), that serves probably as a pump regulator.[6]

The catalytic cycle has been schematically described by the Post-Albers cycle that has been proposed already during 1960−70s, and later refined.[7,8] It postulates that the enzyme adopts two major conformations, denoted as E1 and E2. In E1, the cation-binding sites (CBS) are accessible from the cytoplasm, and NKA has high affinity to sodium and ATP. In E2, the CBS are open toward extracellular space, and NKA has high affinity to potassium, low affinity to ATP, and it is this form that is transiently autophosphorylated on the conserved aspartate residue after ATP hydrolysis. The Mg^{2+} cation is required as a cofactor for an efficient ATP hydrolysis. Its role has been studied relatively little, and although some authors assume that it is bound to the enzyme together with nucleotide as a MgATP complex, recent experiments revealed the it has good structural sense to consider the Mg^{2+}- and ATP-binding as two distinct events.[9,10]

In the past decade, X-ray crystallography provided information about the enzyme high-resolution structure. Because of difficulties in obtaining NKA in sufficient purity and amounts for crystallization experiments, only a few crystal structures in different points of the reaction cycle are available. Moreover, the crystals are obtained in the presence of non-natural ligands or inhibitors as listed in Table 1.

The main difference between the enzyme conformations in crystals is the position of the intracellular domains, which can be characterized as open or closed (Figure 1). In the open conformation, the A and N domains stand away from each other, with a visible gap between them. In the closed conformation, the domains rotate and move to each other, creating a more compact assembly. A different position of A domain in the open conformation leads to unwinding of the transmembrane helix 2 (TM2) at its intracellular end. The CBS

Received: June 15, 2016
Published: November 29, 2016

DOI: 10.1021/acs.jcim.6b00353
J. Chem. Inf. Model. XXXX, XXX, XXX−XXX

Table 1. Available High-Resolution Structures of NKA

PDB code	ions in CBS[a]	other ligands[b]	position of cytoplasmic domains	assigned state[c]	notes	ref
2ZXE	2 K^+	Mg^{2+}, MgF_4^{2-}, CHOL, NAG, NDG	open	E2-Pi		11
3A3Y	2 K^+	Mg^{2+}, MgF_4^{2-}, CHOL, ouabain, NAG	open	E2-Pi		12
3B8E	2 Rb^+	Mg^{2+}, MgF_4^{2-}, PC	open	E2-Pi	missing β subunit	13
3KDP	2 Rb^+	Mg^{2+}, MgF_4^{2-}, CHOL,	open	E2-Pi		13
3N23		Mg^{2+}, ouabain	open	E2P		14
4HYT	1 Mg^{2+}	Mg^{2+}, ouabain, CHOL, DOPS, $C_{12}E_8$, DTFA, FFDG	open	E2P		15
4RES	2 K^+	Mg^{2+}, bufalin, CHOL, DOPS, NAG, sucrose	open	E2P		16
3N2F	2 K^+		open	E2P		14
4RET	1 Mg^{2+}	Mg^{2+}, digoxin, CHOL, DOPS, NAG, sucrose	open	E2P		16
4HQJ	3 Na^+	Mg^{2+}, AlF_4^-, ADP, CHOL	closed	E1-Pi-ADP		17
3WGU	3 Na^+	$2Mg^{2+}$, AlF_4^-, ADP, CHOL, PC, NAG	closed	E1-Pi-ADP		18
3WGV	3 Na^+	$2Mg^{2+}$, AlF_4^-, ADP oligomycin A, CHOL, PC, NAG	closed	E1-Pi-ADP		18
5AVQ−5AW9	K^+/Rb^+/Tl^+	Mg^{2+}, MgF_4^{2-}, NAG	open	E2-Pi	ion exchange snapshots	19
4XE5	Mg^{2+}	Mg^{2+}, ouabain, CHOL	open	E2P		20

[a] Rb^+ and Tl^+ are K^+-analogs. [b] MgF_4^{2-} and AlF_4^- are phosphate analogues; ouabain, bufalin, digoxin, and oligomycin A are NKA inhibitors; cholesterol (CHOL), 1,2-dioleoyl-*sn*-glycero-3-phospho-L-serine (DOPC) and 3-*sn*-phosphatidylcholine (PC) are the membrane lipids; *N*-acetyl-D-glucosamine (NAG), 2-(acetylamino)-2-deoxy-α-D-glucopyranose (NDG), *o*-dodecanyl octaethylene glycol ($C_{12}E_8$), 1-*O*-decanoyl-β-D-tagatofuranosyl β-D-allopyranoside (DTFA), β-D-fructofuranosyl 6-*O*-decanoyl-α-D-glucopyranoside (FFDG) and sucrose are compounds of the crystallization buffers. [c] E2P denotes the phosphorylated enzyme, while E2-Pi and E1-Pi denote the enzyme with noncovalently bound phosphate.

are located in the transmembrane region between TM4, TM5, TM6, and TM8. The CBS for both K^+ ions and two of the Na^+ ions contain similar amino acids in binding site I (A330, E786, T779, S782, D811, D815, human α1 NKA subunit numbering) and binding site II (V329, V332, P333, E334, L808, D811), whereas the third Na^+ ion is bound in the binding site III (T781, Y778, Q930, D933).[11,17] The bound potassium ions in the open structures require more space, so helices TM5 and TM6 unwind to allow that. Sodium ions in the closed crystal structure are smaller and therefore both TM5 and TM6 are unperturbed in the whole length of the helix.

The precise mechanism of cations passage through the enzyme is still a matter of ongoing debates; also the interplay between ligand with binding sites on cytoplasmic domains and CBS has been little explored. In this study, we examined these problems using molecular dynamics (MD) simulations with membrane-embedded NKA (Figure 2). On the basis of the crystal structures, a set of simulations with different combinations of (a) ions in the CBS, (b) protonation state of carboxyls in the CBS, (c) in the presence or absence of magnesium in its intracellular binding site, (d) in the presence or absence of ATP or phosphate, and (e) open or closed conformation of the intracellular head domains of the α-subunit, was created to mimic the protein in different parts of the reaction cycle. We focused on monitoring the cation movements through the enzyme, and analyzed the influence of cytoplasmic ligands on the opening and closing of the pathways to CBS.

METHODS

The crystal structures 2ZXE (open)[11] and 4HQJ (closed)[17] were used as a template for homology modeling to obtain the sequence of human $\alpha_1\beta_1$FXYD2 isomer (UniProt IDs P05023, P05026, and P54710, respectively) using MODELLER 9.9 package.[21] The protein was then inserted into a dioleoylphosphatidylcholine (DOPC) bilayer in a fully hydrated 15 × 15 × 18 nm box with NaCl solution to mimic physiological conditions in water (154 mmol/L), see Figure 2. MD simulations were performed using GROMACS 4.5.4,[22] with Berger parameters for phospholipids[23] and Gromos 53a6 for protein, ions and ATP.[24] Phosphate anion (Pi) was parametrized as described in ref.[25] Periodic boundary conditions were applied in all directions. The protein was inserted into the membrane using the g_membed program.[26] No restraint influencing the bilayer was used. The individual simulations are denoted by the acronym describing the "conformation of cytoplasmic domains_cations in CBS_cytoplasmic ligands", e.g., C_2K_Pi or O_3Na_MgATP, where letters C and O stand for the closed or open conformation, respectively (see the complete list of acronyms in Supporting Information). The ATP molecule in the open simulations was placed near F482 as argued in ref 27. By default, all the carboxyl groups were kept deprotonated. However, it was suggested recently, that protonation state of amino acids forming the CBS can vary during the catalytic cycle.[28,29] In order to see, whether this factor can change outcomes of our simulations, we repeated all simulations with protonated E334, E386 and E961 in CBS, as suggested in refs.[30,31] These simulations are denoted by the prefix "h" (e.g., hC_2K_Pi).

The 100 ns-long simulation run was preceded by a 10 ns-long relaxation with position restrains applied to the protein. The integration step was 2 fs. The thermal coupling was performed by V-rescaled thermostat set to 310 K separately for the protein and the rest of the system.[32] The pressure coupling to 1 bar was performed using anisotropic Berendsen barostat[33] for the prerun and Parrinello−Rahman barostat[34] for the main run.

The results were processed using GROMACS built-in and homemade scripts; tunnel analysis was performed by the MOLE 2.0 software[35] and by visual observation of water movements through the protein. Only amino acids in the vicinity of water molecules in at least two simulations were taken into consideration for the tunnel description with notable exception of the extracellular pathway. VMD[36] and PyMol[37] programs were used for visualization.

DOI: 10.1021/acs.jcim.6b00353
J. Chem. Inf. Model. XXXX, XXX, XXX−XXX

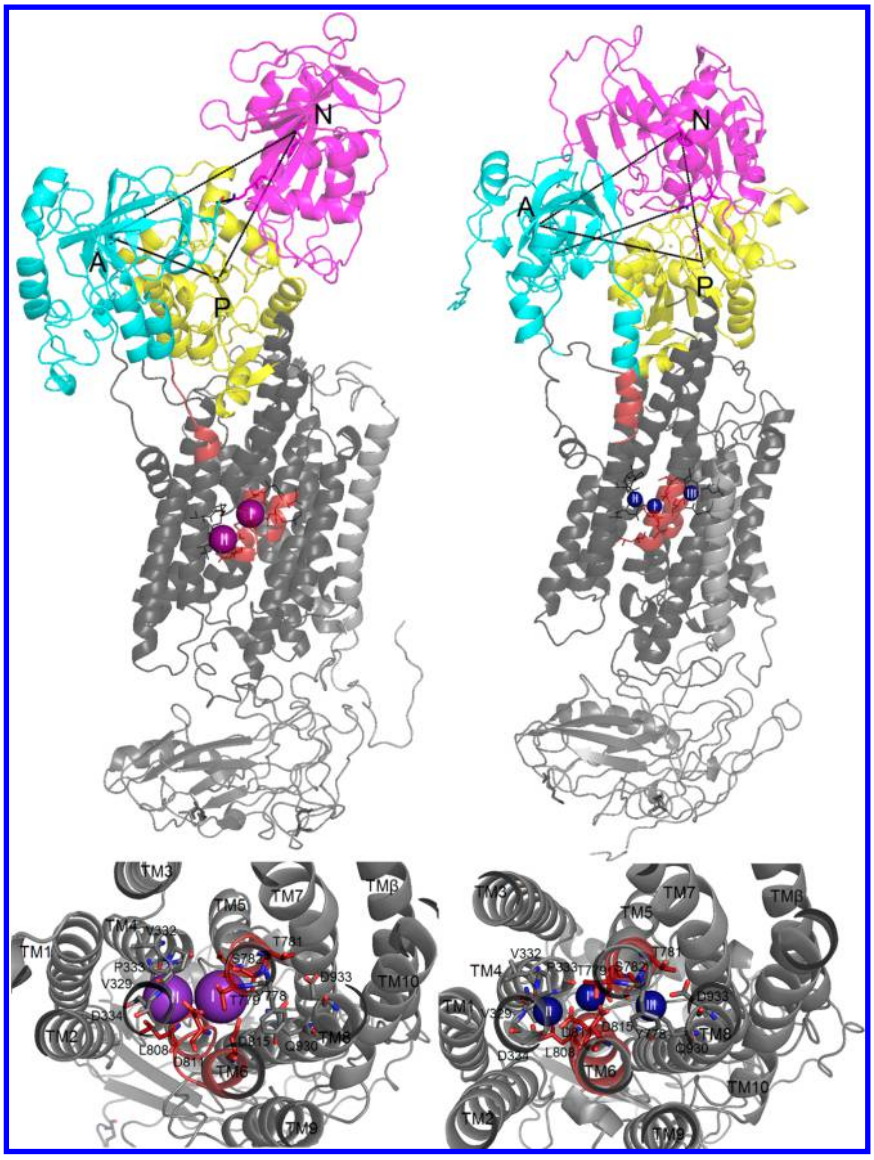

Figure 1. Comparison of the transmembrane regions of the open (left, with bound potassium) and closed (right, with bound sodium) conformations. Residues close to the ions (within 5 Å) are shown in stick. The images are human sequence homology models based on crystal structures 2ZXE for the open structure and 4HQJ for the closed one. The A domain (cyan) consists of residues 1 to 80 and 157 to 276, the N domain (magenta) consists of residues 383 to 595 and the P domain (yellow) consists of residues 356 to 383 and 595 to 750. The β subunit and the FXYD protein are in light gray. Regions of the biggest differences in helix structure are highlighted in red. Black lines denote residue distances analyzed in Figure 3. Lower panels show CBS from the intercellular side of the protein, with residues involved in Na^+ and K^+ binding (blue and purple, respectively); currently nonbinding residues are in black or red, depending on their position. Roman numbers denote binding sites.

RESULTS AND DISCUSSION

Molecular modeling has become a versatile tool in protein structural biology that complements the traditional experimental methods in vitro. It allows visualization of all atoms in large molecules, and in the case of NKA, it was previously used to predict the enzyme structure,[38] the cation-binding sites,[39] or to analyze the conformational changes induced by cytoplasmic ligand binding.[9] Recent publication of the experimentally determined high-resolution structures provides a good background for the use of more advanced computational methods, like molecular dynamics (MD) simulations. MD simulation displays not only the static picture, but allows observation of dynamic events during the enzyme work, thus in some respect, surpassing the possibilities of currently available high-resolution experimental methods. Moreover, it can more closely mimic the physiological conditions (compared, for example, to the crystal-growth conditions) and avoid the use of inhibitors, which fix the enzyme structure in a nonfunctional state. It has been recently used to evaluate protonation state of charged amino acids in CBS,[29] to analyze the effect of mutations occurring in hereditary diseases[40] or binding of cation analogs.[41]

However, the computational demands for simulation of multisubunit membrane enzymes are still enormous (e.g., data presented here represent approximately two-years work), and observation of the whole catalytic cycle for NKA (~10 ms) is far beyond the currently available time-scales. Therefore, we have analyzed a set of partial reactions that are expected during the catalytic cycle.

Model Stability. All simulations relaxed from the crystal structures during the first 20 ns and reached a stable state (RMSD < 5 Å from the final frame) after 50 ns. During the

DOI: 10.1021/acs.jcim.6b00353
J. Chem. Inf. Model. XXXX, XXX, XXX−XXX

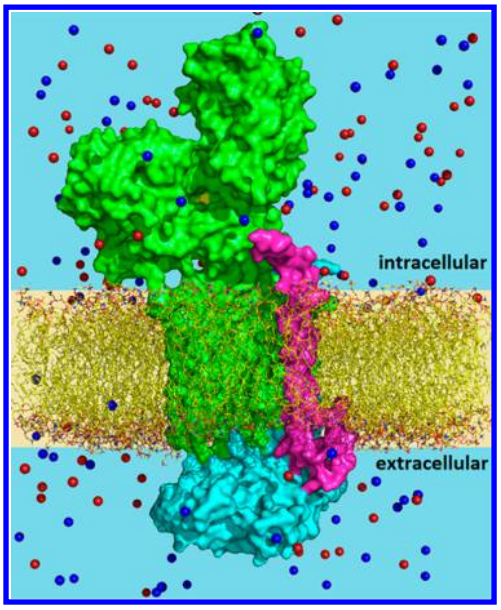

Figure 2. Simulation setup. The protein is in green (α subunit), cyan (β subunit), and magenta (the FXYD protein), a magnesium atom in yellow, sodium atoms in blue, chlorine in red.

simulation, the cytoplasmic domains are more mobile in the open structures than in the closed ones, and they move to one another and often make closing contact, even though none of the simulations reach a "properly closed" conformation resembling the closed crystal structures. The enzyme structure in closed conformation is relatively stable in all simulations.

The difference between the open and closed structures can be described by three main characteristics (Figure 3). The distance between residues F555 and M615, which roughly represent the centers of mass of N- and P-domains, respectively, is significantly shorter in all simulations with the closed conformation compared to the simulations with open conformation, except for simulation C_2K_Mg, where the N−P distance at the end of the simulation is more similar to the values estimated in simulations with the enzyme in the open conformation. In turn, the A−P distance of M615 to L203 (representing the center of mass of A-domain) is shorter in the open conformation. Here, the A−P distance for the enzyme in the open conformation approached the values for closed conformation only in simulations hO_2K_ATP, hO_3Na_ATP, and O_3Na_ATP. The A−P distance is closely related to the most apparent difference in the cytoplasmic headpiece, which is the rotation of the whole A-domain. This huge movement probably occurs on the time-scale that is beyond our simulation time, and therefore, we could not observe the

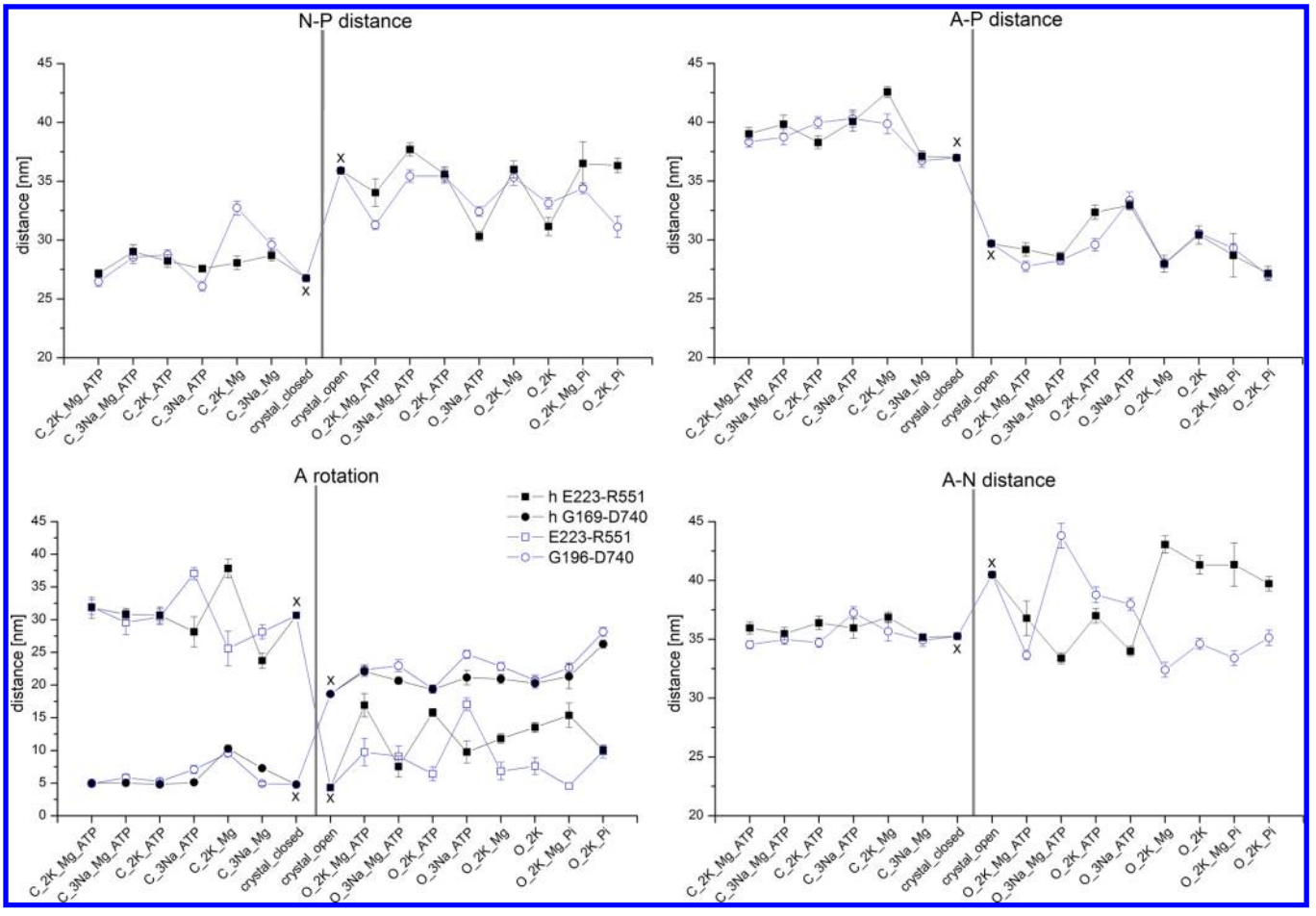

Figure 3. Approximate distances between the centers of the domains (measured as distance between the α carbon atoms of L203 in A domain, F555 in the N domain, and M615 in the P domain) in the last 10 ns of the simulation or in the first frame of the structures corresponding to closed and open crystal structures respectively (denoted by X). The distances between E223 and R551 or G196 and D740 illustrate the relative rotation of the A domain. Open symbols represent data from simulations with deprotonated CBS, solid symbols represent simulations with protonated CBS.

DOI: 10.1021/acs.jcim.6b00353
J. Chem. Inf. Model. XXXX, XXX, XXX−XXX

complete E1 ↔ E2 transition in any of our simulation setups. It should be noted that protonation of residues in CBS had large effect on distance E223−R551 in most of the simulations, while the distance G196-D940 was sensitive only a little.

Another apparent difference in the crystal structures is the larger distance between the A- and N-domains in the open conformation. However, it was the most fluctuating parameter in our simulations and numerous simulations with the open conformation finished with the A−N distance smaller than was the one estimated from the crystals with closed conformation. Again, the A−N distance was very sensitive to the protonation state of CBS, particularly, in the open conformation. It is possible that the long A−N distance in the crystals with open conformation reflects some transient position or it is an artifact due to intermolecular contacts in the head to head oriented molecules in the crystal (Figure 4).

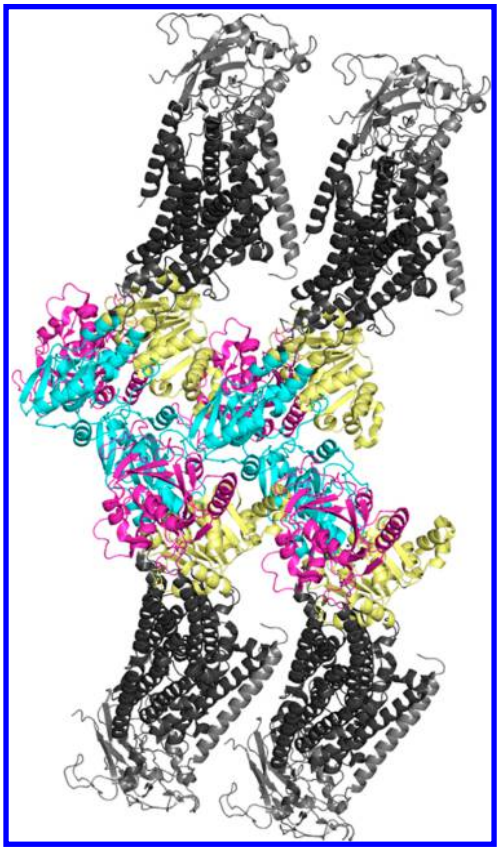

Figure 4. Contacts between cytoplasmic domains in the 2ZXE crystal structure and its symmetry mates. Light blue, magenta, and yellow highlight A, N, and P domains, respectively.

The nature of cations in CBS has also influence on the position of cytoplasmic domains. The most apparent difference between binding of sodium or potassium to CBS was observed for the open conformation in the presence of MgATP, and we could detect significant differences in A−N and N−P distances, as well as in the A-domain rotation. The same holds true to lesser extent also for the enzyme with only ATP bound in both open and closed conformations.

TM5 is a helix in close proximity of both P domain and CBS and, therefore, it can play a role in transferring the ligand-induced conformation changes across the protein. In the transmembrane region, TM5 stays regular (Figure 5, state A) in the simulation with the closed conformation, but it unwinds to some degree between L780 and P785 in the open conformation (state B). The unwinding is more pronounced in the potassium bound structures than in the sodium bound ones, with the exceptions of O_2K and O_2K_Mg_Pi. Notably, state B has not been observed in any of the simulations with protonated CBS. An unwinding at the cytoplasmic side of TM5 (between T760 and I768, state C) was observed in simulations with bound potassium and ATP in the closed conformation, with both deprotonated and protonated CBS (C_2K_ATP and hC_2K_ATP) as well as in hC_3Na_Mg. In two of the simulation in the open conformation, namely O_2K_ATP and hO_3Na_MgATP, the helix unwinds in both the mentioned segments (state D). The TM5 state is reflected in the positions of cytoplasmic domains (Figure 5). We can observe that if the TM5 is in state B or D, then the A-P distance and E223-R551 distance (which is used for the characterization of the A-domain rotation) are shorter, and distances N−P and G196-D740 (A-domain rotation) are longer compared to the state C. For the A-N distance, as well as the structures with TM5 in the state A, we can see no clear correlation.

Cation Binding Sites. In addition to the ions that freely move in the bulk solution, there are few ions that were bound to the protein already at the beginning of the simulation. The magnesium ion present in some simulations always stays in the vicinity of D376 for the whole simulation time (100 ns).

The ions that are in the CBS at the beginning of the simulation do not leave, although they move in the cavity delimited by the amino acid residues, which contains up to 19 additional water molecules in various simulations. Apart from the amino acids already identified in the crystal structures (A330, E786, T779, S782, D815 as binding site I, V329, V332, P333, E334, L808, D811 as binding site II and T781, S782, Y778, Q930, D933 as binding site III), some other amino acids take part in formation of the cavity. The most prominent ones are N331 (mostly in the closed conformation, in 15 out of 28 simulations) and N783 (mostly in the open conformation of the deprotonated simulations, evenly distributed in the protonated ones, in 7 out of 14 simulations without protonation and in all of the protonated ones) and I810, the backbone of which takes part in ion binding in 17 out of 28, evenly distributed in the deprotonated simulations, mostly in open protonated simulations. The transmembrane helix TM6 "breaks" at the CBS in the closed conformation (to extent depending on the bound ions) and completely unwinds in 5 out of 8 of the deprotonated open structures (the exceptions being both of the simulations with ATP and no magnesium and the simulation with bound magnesium and phosphate). TM5 stays unwound at the CBS in the deprotonated open structures and regular in the closed and protonated ones.

The crystals contain either 2 K^+ ions in the CBS for enzyme in open conformation or 3 Na^+ ions in the closed conformation. We tried to reverse the cations in CBS to see whether this change can influence the enzyme structure. It should be noted that in the simulations in the closed conformation, where 3 Na^+ were replaced only by 2 K^+, another sodium ion entered the CBS from the cytoplasmic bulk. It was not bound to the Site III, instead, it adopted another position in the proximity of Sites I and II, thus, influencing the positions of the two potassium cations (Figure 6). In C_2K_Mg_ATP, a cytoplasmic sodium ion moves briefly between the potassium ions in CBS (at D811), but then it spends the rest of the simulation on the other side of the TM6 chain at the backbone part of L812, G813, and T814. In

DOI: 10.1021/acs.jcim.6b00353
J. Chem. Inf. Model. XXXX, XXX, XXX−XXX

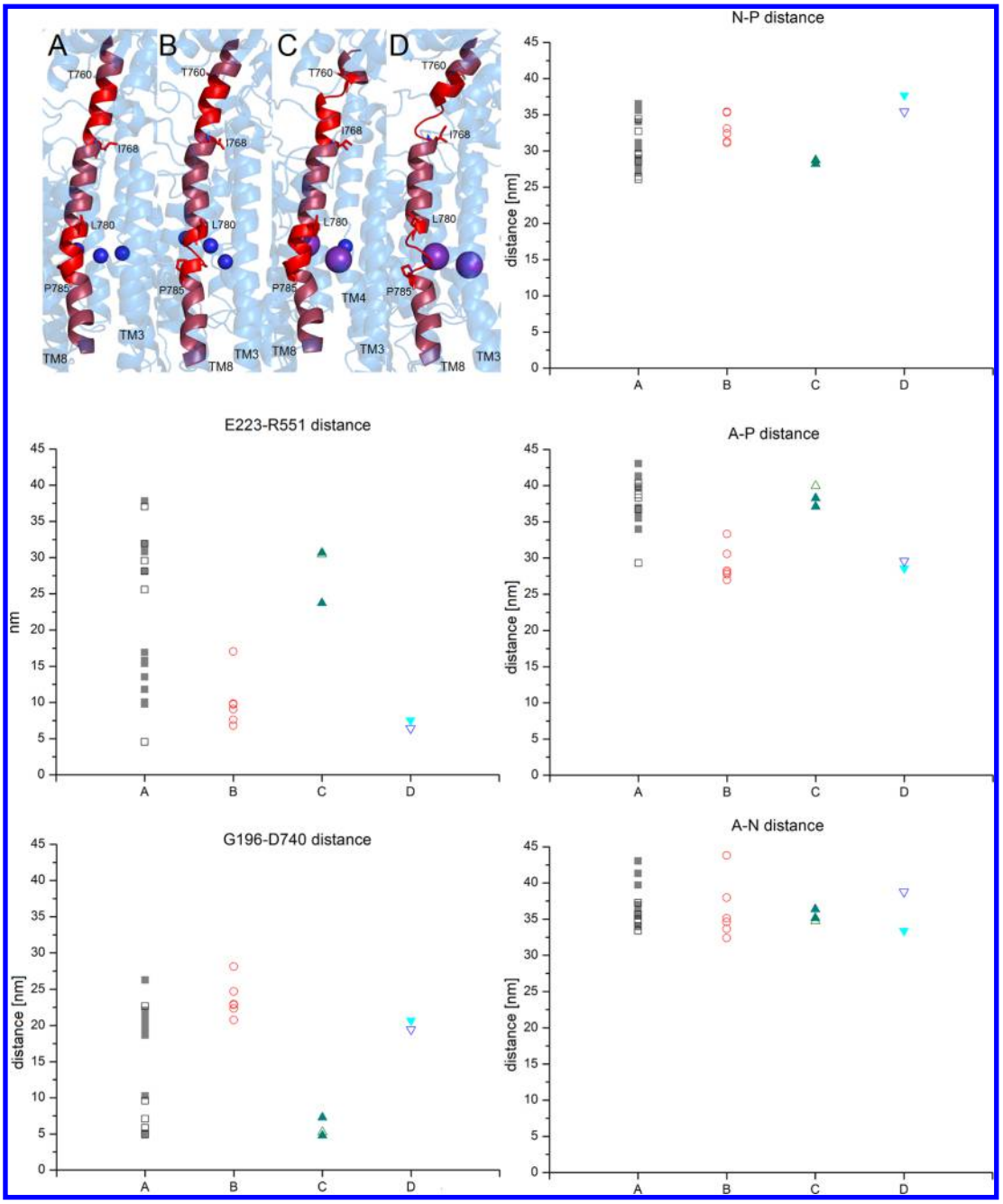

Figure 5. Upper left panel depicts the state of the TM5 helix in the last frame of the respective simulation: (A) regular helix (C_3Na_ATP), (B) helix unwound at the CBS (O_3Na_ATP), (C) helix unwound at the intracellular side (C_2K_ATP), and (D) helix unwound at both sites (O_2K_ATP). Unwinding regions are highlighted in a brighter red. The other panels describe attribution of the TM5 helix states to the state of cytoplasmic domains (cf. Figure 3). Open symbols represent data from simulations with deprotonated CBS, solid symbols represent simulations with protonated CBS.

C_2K_ATP, however, the sodium ion stays inside CBS, where it replaces one of the potassium atoms in its position between D811, D815, and E334 in binding site II, which causes the potassium ions to move to binding sites I and III between Y778, T814, and Q930. Interestingly, a similar movement of potassium cation to the binding site III happens also in hC_2K_Mg_ATP and hC_2K_ATP, even though no bulk sodium ion enters the CBS in these cases. In the simulation with only Mg^{2+} (C_2K_Mg), the sodium ion enters CBS through the N-terminal pathway and positions itself between D811, N331, E786 and the backbone of A330, which causes a potassium to move from this position to the other side of E786, T814, S782, Q930 and the backbone of D811.

In the only open simulation, where a sodium ion moves from the bulk into the CBS, O_2K_Mg, the ion comes through the TM3/TM7 channel (described in the next section) into the site II and then stays in a water pocket between E334, G335, N783 and E786.

Pathways. We have identified five pathways that allow water molecules or ions from the bulk solution to enter the CBS during the simulation run. In all of the simulations with the deprotonated CBS, there was at least one open pathway for some time, even though it might have closed later. The

DOI: 10.1021/acs.jcim.6b00353
J. Chem. Inf. Model. XXXX, XXX, XXX−XXX

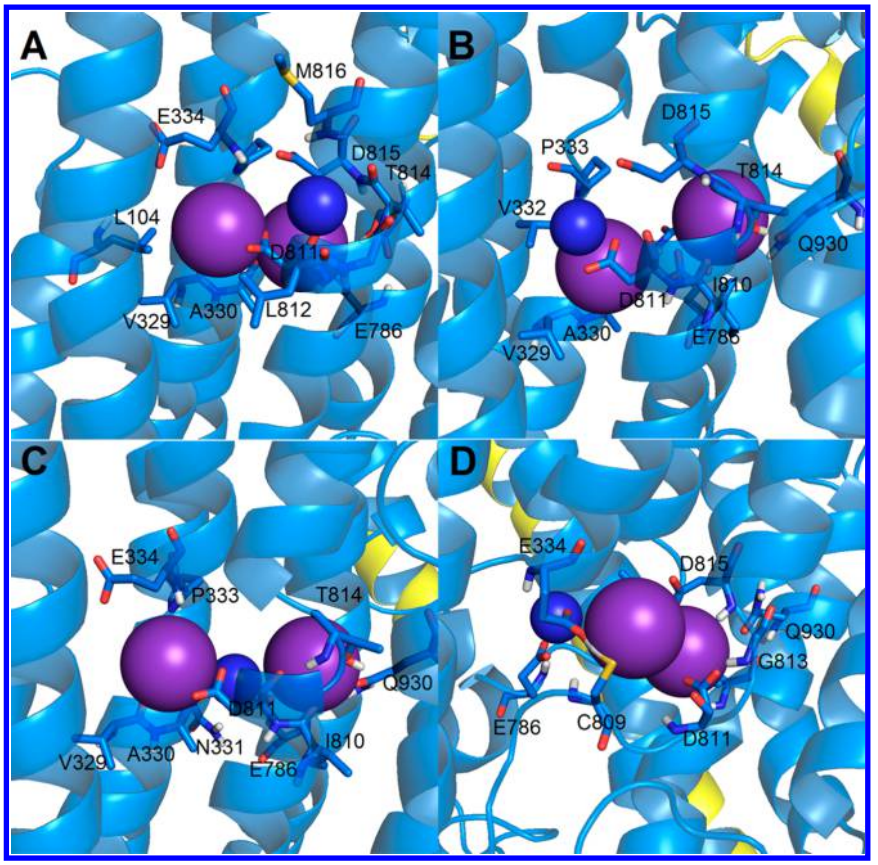

Figure 6. Position of the ions on the reaction site in the last frame of the respective simulation. C_2K_Mg_ATP (A), C_2K_ATP (B), C_2K_Mg (C), and O_2K_Mg (D). The protein is in light blue (α subunit) and yellow (β subunit), sodium atoms in blue, potassium ions in purple, water molecules are not shown.

pathways can be classified according to the intensity of transport (Table 2). In four cases, we observed the sodium ion from the bulk to enter CBS, and in another four cases, the channels were widely open for water molecules, but no cation movement was observed through the given pathway during the simulation time. In some cases, we observed narrow wires of water molecules connecting the bulk and CBS that allow hydration or protonation of the CBS, but that are unlikely to let the cations through. The protein is a very dynamic system, and frequently, we observed that some pathway was open either only at the beginning of the simulation or only on its end, in four cases, we observed repeated opening and closing of some pathway during the simulation time. In some cases, the pathway was blocked to such extent that it allowed passage of only less than five water molecules during the simulation time.

Three of the observed pathways have been mentioned previously in literature: the extracellular pathway,[42,43] N-terminal pathway[18] and C-terminal pathway.[28,44] During our simulations, we observed another two pathways along the pairs of transmembrane helices TM3/TM7 or TM6/TM9. In the next section, we will discuss them according to their occurrence during simulations.

The ***TM3/TM7 pathway*** is the most frequent one, present in 16 out of the 28 simulations. It lies between TM3 (H290, F291, I294, I295, V298) and TM7 (N783, E786, I787, V845, E847, I850, S851, Y854, G855) with a small contribution of TM4 (A330, N331, P333) and the β subunit (K21, E24, F27, R28, W32). It often serves as a way for water molecules to perform the initial hydration of CBS and then closes during the simulation. Only in C_2K_Mg_ATP, the TM3/TM7 pathway stays open during the whole simulation. Moreover, in O_2K_Mg this pathway serves as an entry for a sodium cation from the bulk solution to the cation binding site. After the sodium cation reached the CBS in a water pocket between E334, G335, N783 and E786, this pathway closes. Previous experiments revealed that mutagenesis of H290 or F291 increased the enzyme affinity to potassium and decreased the affinity to ATP[45] and cells with H290A mutation do not survive.[45] In turn, mutation E786A decreased affinity to both sodium and potassium ions and increased the affinity to ATP.[46] Residues H290 and F291 are located at the membrane level of the TM3/TM7 pathway, which is generally more open in the simulation with the closed conformation of the protein than in the ones with the open protein conformation (even more so in the CBS protonated cases). Therefore, these residues can play a role in closing the TM3/TM7 pathway during the conformation changes corresponding to the closed-to-open transition.

The ***C-terminal pathway*** is the second most frequent one (found in 13 out of 28 simulations), however, no ions move through it in any of the simulations and only in one of them (O_3Na_ATP) the pathway stays widely open the whole time. This pathway connects to CBS at the binding site III, regardless of the presence or absence of a sodium ion there, and then it continues out between TM5 (K774, A777, Y778, T781, N783), TM6 (D815), TM7 (E847, M852, A853, Q856, I857, Q861), TM9 (Q930, W931, D933, V935, I936, C937, K938, R940), and TM10 (I998, Y1001, D1002, R1005, I1009, Y1022,

DOI: 10.1021/acs.jcim.6b00353
J. Chem. Inf. Model. XXXX, XXX, XXX−XXX

Table 2. Simulated Ion or Water Pathways[a]

enzyme	CBS	ligand	pathways				
O/C	Na/K	ATP/ Mg/Pi	intra. N-terminal	TM3/TM7	TM6/TM9	intra. C-terminal	extracellular
C	2 K	Mg, ATP	open for water	open for water	**Na ion enters CBS**		
C	3 Na	Mg, ATP	alternatively open and closed	*closes rapidly*	<5W	opens during the simulation	
C	2 K	ATP	narrow water channel	alternatively open and closed	**Na ion enters CBS**	alternatively open and closed	
C	3 Na	ATP	open for water	*closes rapidly*		<5W	
C	2 K	Mg	**Na ion enters CBS**	closes during the simulation		narrow water channel	
C	3 Na	Mg	open for water	*closes rapidly*	<5W	<5W	<5W
O	2 K	Mg, ATP		closes during the simulation		alternatively open and closed	<5W
O	3 Na	Mg, ATP	opens and then closes	*closes rapidly*		closes during the simulation	<5W
O	2 K	ATP		*closes rapidly*		<5W	
O	3 Na	ATP			*closes rapidly*	open for water	
O	2 K	Mg		**Na ion enters CBS, and then closes**	*closes rapidly*		<5W
O	2 K	none		closes during the simulation		opens during the simulation	narrow water channel
O	2 K	Mg, Pi	<5 W	<5 W	narrow water channel	<5W	
O	2 K	Pi		closes during the simulation	<5W		

[a]Unless stated otherwise, the mentioned pathway stays open for the rest of the simulation. The pathways, where an ion from the bulk solution moved to the proximity of the CBS, are highlighted in bold. Description "open for water" signifies pathways that are wide enough for water molecules to move freely and that stay open during the whole simulation, "narrow water channel" denotes narrow wires of water molecules connecting the bulk and CBS, symbol " <5W" means that less than five water molecules passed through this pathway during the whole simulation. Some pathways stay open only for the part of the simulation, either in the first half ("closes during simulation"), in the second half ("opens during simulation") or in the middle ("opens and then closes"), in few cases, we observed more than one opening and closing event during the simulation ("alternatively open and closed"). The description "closes rapidly" denotes the pathways that are open on the beginning of the simulation, but close during the relaxation within the first 10 ns of simulation, typically, after hydration of CBS.

Y1023). In most cases, this channel is narrow and allows water molecules to move only in "one after another" fashion, or closes during the simulation. Mutations of C937[47] or N783[48] reduced the enzyme activity to ca. 20%, in the latter case, also a reduced affinity to sodium was observed. It was proposed previously that this pathway takes part in the CBS protonation.[28]

The ***N-terminal pathway*** is situated between TM1 (R94, Q95, G99, F100, S101, L104), TM2 (V39, T143, S147, Q150, E151), TM3 (A285, E289), TM4 (V332, E334, L337, V340, T341) with contribution of TM6 (M816) and it is open in most simulations with the closed conformation (11 out of 28 in total). An ion from the bulk solution moves through this pathway into the binding site II in C_2K_Mg. This channel is narrowly open in only two of the simulations with the enzyme in the open conformation. All the residues of TM1 and L337 of TM4 were previously subject to mutagenesis experiments.[49,50] Only mutations L104A and L104F decreased the enzyme activity to ∼40%. Some mutations of the amino acids on TM1 and TM3[49−52] decrease the sodium affinity when mutated (R94, Q95, and G99), while others (F100, L104, or L337) influence the potassium affinity and increase its deocclusion. Mutations of Q95, F100, L104, or L337 also increased the affinity to ATP. The sodium influencing amino acids are located on the outer part of the N-terminal pathway, whereas the residues influencing the potassium affinity (and occlusion) are closer to the CBS.

The ***TM6/TM9 pathway*** is situated between TM6 (L812, T814, D815, M816, V817, S821, Y824) and TM9 (L934, I953, F956, E960, E961) with contribution of TM2 (F146), TM5 (Y778) and the FXYD protein (R48, R51). It is present only in three of the simulations with the enzyme in the open conformation, and in two of them it closes after the CBS hydration. In two simulations with the enzyme in a closed conformation, potassium and ATP or MgATP bound, a sodium ion from the bulk solution passes through this channel to CBS into the binding site I. It is also to a degree open in hC_3Na_Mg and in hC_2K_Mg_ATP a sodium ion from the bulk solution enters the pathway, which however does not open all the way through and the ion stays within the membrane in the vicinity of E960 and F956. Residues in this pathway escaped an attention of experimentalists so far, and to our knowledge, only E960 and E961 were analyzed in mutagenesis studies.[53] While mutations of E960 and E961 to alanine did not show a great change in the affinities, mutations to lysine result in nonviable cell lines,[53] showing the significance of charge of these residues. The acid part of the residues is turned inward in the case of E960 and outward in E961 (with respect to the surface of the protein), so a charge switch would disrupt the interaction of residues near the CBS III position in case of E960, and in the case of E961, it would block the TM6/TM9 pathway for positively charged ions (and possibly water). Additionally, position near E960 is a stable point for ions moving through TM6/TM9 pathway. The ions tend to spend some time in the vicinity of E960 while moving toward the CBS.

The ***extracellular pathway*** is the only channel open to CBS from the extracellular side of NKA. It is worth to notice that this pathway can be blocked by ouabain.[12,15] This pathway is situated between TM2 (N129, Y131), TM6 (T804, T806, I807, L808, C809), TM8 (F916), and L9/10 (A977, R979); and it is

DOI: 10.1021/acs.jcim.6b00353
J. Chem. Inf. Model. XXXX, XXX, XXX−XXX

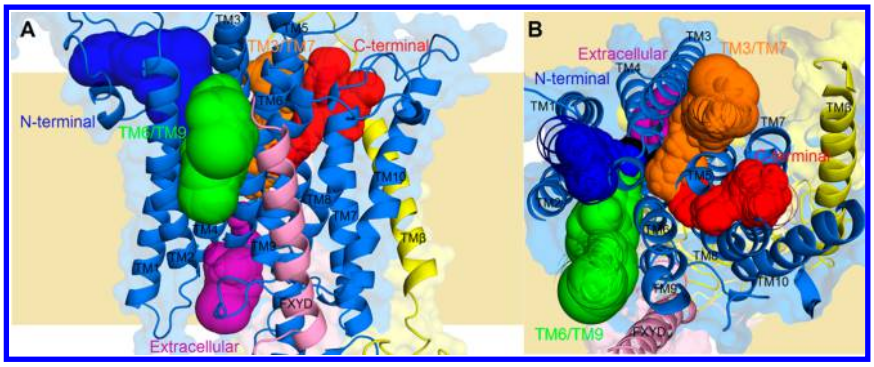

Figure 7. Ion or water pathways depicted as spheres showing the largest radii of a given pathway calculated with MOLE 2.0 on a grid over aligned NKA 10 snapshots from the last 10 ns of simulation (C_2K_Mg_ATP) parallel to the membrane (A) and from the cytoplasmic side (B).

present only in the O_2K simulation, which is quite understandable as we have excess of sodium in our simulations, hence NKA is open toward cytosolic side.

All the pathways are summarized in Figure 7.

Obviously, the protonation is strongly reflected in the close proximity of CBS, in general, negatively influencing the permeability of all pathways, except for the C-terminal one. All the simulations with enzyme in the open structure ended in the fully occluded state (except for the hO_Na_ATP, where the C-terminal pathway stays open for water). The C-terminal pathway is present in nearly all the closed or Na^+ bound simulations with the exception of hC_2K_Mg and hO_3Na_Mg_ATP. The N- terminal and the TM3/TM7 pathways are those directly influenced by the protonation of selected residues, given that E334 and E786 are at the end point of these two pathways. TM3/TM7 usually closes completely in the protonated simulations, while the N-terminal pathway stays open to a degree, but closes at the CBS of hC_3Na_Mg_ATP and hC_2K_Mg. In hC_2K_Mg_ATP, an ion from the bulk solution moves toward the CBS, but the pathway does not open all the way through and the ion stays within the membrane in the vicinity of E960 and F956. The extracellular pathway is closed in all the protonated simulations. We can conclude that protonation state of CBS also influences the conformation of the cytoplasmic headpiece. However, it should be stressed that MD represents very coarse approximation with respect to the issue of protonation. MD is based on the classical Newtonian equations, and hence, it cannot adequately describe the fast dynamic processes, such as proton dissociation or Grotthus mechanism of proton transfer. Therefore, the simulations should be interpreted rather cautiously.

Upon further analysis, amino acids lining all these pathways are underrepresented between natural variant mutations of NKA. We have compared these amino acid to those detected in genome-wide association studies (GWAS) present in UNIPROT repository within new Protein Feature Viewer application.[54] There is 329 known SNPs associated with ATP1A1 gene (dbSNP on Pubmed),[55] while NKA α1 subunit has 1,023 amino acids, meaning that on average every third amino acid shows natural variation in NKA α1 subunit. Among amino acids lining individual pathways we detect only a handful variants - K21E, R94Q, M816V, M859T, V935F in α1 subunit and R48K and R51H in FXYD2 protein, which are all considered benign. The only damaging variants are T341M and Y131C within N-terminal and extracellular pathways, respectively. As can be seen, the majority of the amino acids lining detected pathways are well conserved between human individuals.

Cation Exchange. While there is a general agreement, that the ion exchange Na_{out}−K_{in} accompanies the ATP-hydrolysis reaction in the cytoplasm, it is not that clear, which cytoplasmic event is related to the K_{out}−Na_{in} exchange. It could be dephosphorylation, Mg^{2+}-, ATP-, or MgATP-binding, moreover, the process may be accompanied by a change in CBS protonation. One of our original goals was to see this event (and it was the reason, why we performed the calculations for so many setups), however, we failed to give a clear answer, and there are several possibilities why. First, it is possible that this would require a conformational change of the protein that is beyond the time scale of our simulation. Alternatively, a dynamic protonation and/or deprotonation of the CBS residues might facilitate the change of ion affinity, leading to the ions moving toward an exit pathway. However, it is a serious limitation of classical MD that it is impossible to change the protonation state during one simulation, whereas the constant-pH MD is much more demanding. Also, it is possible that potassium release requires consecutive sequence of two events.

Another interesting observation is that in some of the simulations, a sodium ion enters the CBS in the presence of potassium. This sequence of events is incompatible with the traditional model assuming one cytoplasmic and one extracellular pathway, common for both sodium and potassium cations ("I-model", Figure 8). Existence of multiple cytoplasmic

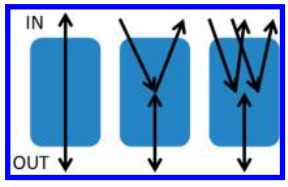

Figure 8. Schematic depiction of the I-, Y-, and W-models.

pathways supports rather the "Y-model" with one pathway for sodium entry and another pathway for potassium exit in the cytoplasmic side, or even the "W-model" with multiple different entry- and exit pathways on the cytoplasmic side.

CONCLUSIONS

Using molecular dynamic simulations, we have analyzed accessibility of the cation binding sites in NKA in the presence of various cytoplasmic ligands and for the different enzyme conformations, and we report more than 2.5 μs of simulation

DOI: 10.1021/acs.jcim.6b00353
J. Chem. Inf. Model. XXXX, XXX, XXX−XXX

time in total. It is evident that there is a mutual long-distance communication between the ligands bound to the cytoplasmic headpiece and the cation binding sites. We identified that local unwinding of the long TM5 helix plays an important role in this communication; however, it is obvious that it is not the only factor and that the intramolecular interactions are more complex, and they are influenced also by the protonation of cation binding sites. Since we have simulated NKA in the solution with excess of sodium cations, we were able to observe the flow of cations or water into the cation binding site. In addition to the three previously described pathways, we have identified two novel cytoplasmic pathways that allow hydration of the cation binding sites or transport of cations from/to the bulk. The amino acids lining these pathways mostly escaped attention of experimentalist up to now. They are all very well conserved in the human, which is a strong indication of their essentiality for the enzyme function.

■ ASSOCIATED CONTENT

Supporting Information

The Supporting Information is available free of charge on the ACS Publications website at DOI: 10.1021/acs.jcim.6b00353.

List of acronyms for MD simulations (PDF)

■ AUTHOR INFORMATION

Corresponding Author

*E-mail: martin.kubala@upol.cz.

ORCID

Karel Berka: 0000-0001-9472-2589

Martin Kubala: 0000-0002-3555-0016

Notes

The authors declare no competing financial interest.

■ ACKNOWLEDGMENTS

This work was supported by the grants LO1204 and LO1305 from the National Program of Sustainability I and IGA_PrF_2016_013 from Palacký University in Olomouc. This work was also supported by ELIXIR CZ research infrastructure project (MEYS Grant No: LM2015047). Access to computing and storage facilities owned by parties and projects contributing to the National Grid Infrastructure MetaCentrum, provided under the programme "Projects of Large Research, Development, and Innovations Infrastructures" (CESNET LM2015042), is greatly appreciated.

■ REFERENCES

(1) Clausen, M. J. V.; Poulsen, H. *Metallomics and the Cell*; Banci, L., Ed.; Springer: Dordrecht, the Netherlands, 2013; pp 41−67.

(2) Rolfe, D. F.; Brown, G. C. C. Cellular Energy Utilization and Molecular Origin of Standard Metabolic Rate in Mammals. *Physiol. Rev.* **1997**, *77*, 731−753.

(3) Rose, A. M.; Valdes, R. Understanding the Sodium Pump and Its Relevance to Disease. *Clin. Chem.* **1994**, *40*, 1674−1685.

(4) Heinzen, E. L.; Arzimanoglou, A.; Brashear, A.; Clapcote, S. J.; Gurrieri, F.; Goldstein, D. B.; Jóhannesson, S. H.; Mikati, M. A.; Neville, B.; Nicole, S.; Ozelius, L. J.; Poulsen, H.; Schyns, T.; Sweadner, K. J.; van den Maagdenberg, A.; Vilsen, B. Distinct Neurological Disorders with ATP1A3Mutations. *Lancet Neurol.* **2014**, *13*, 503−514.

(5) Martin, D. W. Structure-Function Relationships in the NA+,K+-Pump. *Semin. Nephrol.* **2005**, *25*, 282−291.

(6) Geering, K. FXYD Proteins: New Regulators of Na-K-ATPase. *Am. J. Physiol. Renal Physiol.* **2006**, *290*, F241−50.

(7) Rosenthal, A. S.; Post, R. L. A Phosphorylated Dependent Intermediate in Adenosine Sodium and Potassium Transport across Kidney Membranes. *J. Biol. Chem.* **1965**, *240*, 1437−1445.

(8) Albers, R. W. Biochemical Aspects of Active Transport. *Annu. Rev. Biochem.* **1967**, *36*, 727−756.

(9) Kubala, M.; Grycova, L.; Lansky, Z.; Sklenovsky, P.; Janovska, M.; Otyepka, M.; Teisinger, J. Changes in Electrostatic Surface Potential of Na+/K+-ATPase Cytoplasmic Headpiece Induced by Cytoplasmic Ligand(s) Binding. *Biophys. J.* **2009**, *97*, 1756−1764.

(10) Grycova, L.; Sklenovsky, P.; Lansky, Z.; Janovska, M.; Otyepka, M.; Amler, E.; Teisinger, J.; Kubala, M. ATP and Magnesium Drive Conformational Changes of the Na+/K+-ATPase Cytoplasmic Headpiece. *Biochim. Biophys. Acta, Biomembr.* **2009**, *1788*, 1081−1091.

(11) Shinoda, T.; Ogawa, H.; Cornelius, F.; Toyoshima, C. Crystal Structure of the Sodium-Potassium Pump at 2.4 A Resolution. *Nature* **2009**, *459*, 446−450.

(12) Ogawa, H.; Shinoda, T.; Cornelius, F.; Toyoshima, C. Crystal Structure of the Sodium-Potassium Pump (Na+,K+-ATPase) with Bound Potassium and Ouabain. *Proc. Natl. Acad. Sci. U. S. A.* **2009**, *106*, 13742−13747.

(13) Morth, J. P.; Pedersen, B. P.; Toustrup-Jensen, M. S.; Sørensen, T. L.-M.; Petersen, J.; Andersen, J. P.; Vilsen, B.; Nissen, P. Crystal Structure of the Sodium-Potassium Pump. *Nature* **2007**, *450*, 1043−1049.

(14) Yatime, L.; Laursen, M.; Morth, J. P.; Esmann, M.; Nissen, P.; Fedosova, N. U. Structural Insights into the High Affinity Binding of Cardiotonic Steroids to the Na+,K+-ATPase. *J. Struct. Biol.* **2011**, *174*, 296−306.

(15) Laursen, M.; Yatime, L.; Nissen, P.; Fedosova, N. U. Crystal Structure of the High-Affinity Na+,K+-ATPase-Ouabain Complex with Mg2+ Bound in the Cation Binding Site. *Proc. Natl. Acad. Sci. U. S. A.* **2013**, *110*, 10958−10963.

(16) Laursen, M.; Gregersen, J. L.; Yatime, L.; Nissen, P.; Fedosova, N. U. Structures and Characterization of Digoxin- and Bufalin-Bound Na+,K+-ATPase Compared with the Ouabain-Bound Complex. *Proc. Natl. Acad. Sci. U. S. A.* **2015**, *112*, 1755−1760.

(17) Nyblom, M.; Poulsen, H.; Gourdon, P.; Reinhard, L.; Andersson, M.; Lindahl, E.; Fedosova, N. U.; Nissen, P. Crystal Structure of Na+, K+-ATPase in the Na+-Bound State. *Science* **2013**, *342*, 123−127.

(18) Kanai, R.; Ogawa, H.; Vilsen, B.; Cornelius, F.; Toyoshima, C. SM: Crystal Structure of a Na+-Bound Na+,K+-ATPase Preceding the E1P State. *Nature* **2013**, *502*, 201−206.

(19) Ogawa, H.; Cornelius, F.; Hirata, A.; Toyoshima, C. Sequential Substitution of K+ Bound to Na+,K+-ATPase Visualized by X-Ray Crystallography. *Nat. Commun.* **2015**, *6*, 8004.

(20) Gregersen, J. L.; Mattle, D.; Fedosova, N. U.; Nissen, P.; Reinhard, L. Isolation, Crystallization and Crystal Structure Determination of Bovine Kidney Na^+, K^+-ATPase. *Acta Crystallogr., Sect. F: Struct. Biol. Commun.* **2016**, *72*, 282−287.

(21) Webb, B.; Sali, A. Comparative Protein Structure Modeling Using MODELLER. *Current Protocols in Bioinformatics* **2014**, *1137*, 5.6.1−5.6.32.

(22) Pronk, S.; Páll, S.; Schulz, R.; Larsson, P.; Bjelkmar, P.; Apostolov, R.; Shirts, M. R.; Smith, J. C.; Kasson, P. M.; van der Spoel, D.; Hess, B.; Lindahl, E. GROMACS 4.5: A High-Throughput and Highly Parallel Open Source Molecular Simulation Toolkit. *Bioinformatics* **2013**, *29*, 845−854.

(23) Berger, O.; Edholm, O.; Jähnig, F. Molecular Dynamics Simulations of a Fluid Bilayer of Dipalmitoylphosphatidylcholine at Full Hydration, Constant Pressure, and Constant Temperature. *Biophys. J.* **1997**, *72*, 2002−2013.

(24) Oostenbrink, C.; Villa, A.; Mark, A. E.; Van Gunsteren, W. F. A Biomolecular Force Field Based on the Free Enthalpy of Hydration and Solvation: The GROMOS Force-Field Parameter Sets 53A5 and 53A6. *J. Comput. Chem.* **2004**, *25*, 1656−1676.

(25) van der Spoel, D.; Feenstra, K. A.; Hemminga, M. A.; Berendsen, H. J. C. Molecular Modeling of the RNA Binding N-

DOI: 10.1021/acs.jcim.6b00353
J. Chem. Inf. Model. XXXX, XXX, XXX−XXX

Terminal Part of Cowpea Chlorotic Mottle Virus Coat Protein in Solution with Phosphate Ions. *Biophys. J.* **1996**, *71*, 2920−2932.
(26) Wolf, M. G.; Hoefling, M.; Aponte-Santamaria, C.; Grubmuller, H.; Groenhof, G. G_membed: Efficient Insertion of a Membrane Protein into an Equilibrated Lipid Bilayer with Minimal Perturbation. *J. Comput. Chem.* **2010**, *31*, 2169−2174.
(27) Kubala, M.; Krumscheid, R.; Schoner, W.; et al. Phe 475 and Glu 446 but Not Ser 445 Participate in ATP-Binding to the a -Subunit of Na+/K+-ATPase. *Biochem. Biophys. Res. Commun.* **2002**, *297*, 154−159.
(28) Poulsen, H.; Khandelia, H.; Morth, J. P.; Bublitz, M.; Mouritsen, O. G.; Egebjerg, J.; Nissen, P. Neurological Disease Mutations Compromise a C-Terminal Ion Pathway in the Na(+)/K(+)-ATPase. *Nature* **2010**, *467*, 99−102.
(29) Yu, H.; Ratheal, I. M.; Artigas, P.; Roux, B. Protonation of Key Acidic Residues Is Critical for the K+ -Selectivity of the Na/K Pump. *Nat. Struct. Mol. Biol.* **2011**, *18*, 1159−1163.
(30) Mahmmoud, Y. A.; Shattock, M.; Cornelius, F.; Pavlovic, D. Inhibition of K+ Transport through Na+, K + -ATPase by Capsazepine: Role of Membrane Span 10 of the Alpha-Subunit in the Modulation of Ion Gating. *PLoS One* **2014**, *9*, e96909.
(31) Hilbers, F.; Kopec, W.; Isaksen, T. J.; Holm, T. H. H.; Lykke-Hartmann, K.; Nissen, P.; Khandelia, H.; Poulsen, H. Tuning of the Na,K-ATPase by the Beta Subunit. *Sci. Rep.* **2016**, *6*, 20442.
(32) Bussi, G.; Donadio, D.; Parrinello, M. Canonical Sampling through Velocity Rescaling. *J. Chem. Phys.* **2007**, *126*, 014101.
(33) Berendsen, H. J. C.; Postma, J. P. M.; van Gunsteren, W. F.; Dinola, A.; Haak, J. R. *J. Chem. Phys.* **1984**, *81*, 3684−3691.
(34) Parrinello, M.; Rahman, A. Polymorphic Transitions in Single Crystals: A New Molecular Dynamics Method. *J. Appl. Phys.* **1981**, *52*, 7182−7190.
(35) Sehnal, D.; Svobodová Vařeková, R.; Berka, K.; Pravda, L.; Navrátilová, V.; Banáš, P.; Ionescu, C.-M.; Otyepka, M.; Koča, J. MOLE 2.0: Advanced Approach for Analysis of Biomacromolecular Channels. *J. Cheminf.* **2013**, *5*, 39.
(36) Humphrey, W.; Dalke, A.; Schulten, K. VMD: Visual Molecular Dynamics. *J. Mol. Graphics* **1996**, *14*, 33−38.
(37) Schrödinger, Inc., *The PyMOL Molecular Graphics System*, version 1.6.0, 2010.
(38) Ettrich, R.; Melichercik, M.; Teisinger, J.; Ettrichová, O.; Krumscheid, R.; Hofbauerová, K.; Kvasnicka, P.; Schoner, W.; Amler, E. Three-Dimensional Structure of the Large Cytoplasmic H4 − H5 Loop of Na+/K+-ATPase Deduced by Restraint-Based Comparative Modeling Shows Only One ATP Binding Site. *J. Mol. Model.* **2001**, *7*, 184−192.
(39) Rakowski, R. F.; Sagar, S. Found: Na + and K + Binding Sites of the Sodium Pump. *Physiology* **2003**, *18*, 164−168.
(40) Kopec, W.; Loubet, B.; Poulsen, H.; Khandelia, H. Molecular Mechanism of Na(+),K(+)-ATPase Malfunction in Mutations Characteristic of Adrenal Hypertension. *Biochemistry* **2014**, *53*, 746−754.
(41) Mahmmoud, Y. A.; Kopec, W.; Khandelia, H. K+ Congeners That Do Not Compromise Na+ Activation of the Na+,K+-ATPase Hydration of the Ion Binding Cavity Likely Controls Ion Selectivity. *J. Biol. Chem.* **2015**, *290*, 3720−3731.
(42) Takeuchi, A.; Reyes, N.; Artigas, P.; Gadsby, D. C. The Ion Pathway through the Opened Na(+),K(+)-ATPase Pump. *Nature* **2008**, *456*, 413−416.
(43) Takeuchi, A.; Artigas, P.; Gadsby, D. C.; et al. Visualizing the Mapped Ion Pathway through the Na, K-ATPase Pump. *Channels* **2009**, *3*, 383−386.
(44) Paulsen, P. A.; Jurkowski, W.; Apostolov, R.; Lindahl, E.; Nissen, P.; Poulsen, H. The C-Terminal Cavity of the Na,K-ATPase Analyzed by Docking and Electrophysiology. *Mol. Membr. Biol.* **2013**, *30*, 195−205.
(45) Toustrup-Jensen, M. S.; Vilsen, B. Functional Consequences of Alterations to Ile279, Ile283, Glu284, His285, Phe286, and His288 in the NH2-Terminal Part of Transmembrane Helix M3 of the Na+,K +-ATPase. *J. Biol. Chem.* **2003**, *278*, 38653−38664.
(46) Kuntzweiler, T. A.; Wallick, E. T.; Johnson, C. L.; Lingrel, J. B. Amino Acid Replacement of Asp 369 in the Sheep Alpha 1 Isoform Eliminates ATP and Phosphate Stimulation of [3H]Ouabain Binding Properties of the Enzyme. *J. Biol. Chem.* **1995**, *270*, 16206−16212.
(47) Shi, H. G.; Mikhaylova, L.; Zichittella, A. E.; et al. Functional Role of Cysteine Residues in the (Na, K) -ATPase Alpha Subunit. *Biochim. Biophys. Acta, Biomembr.* **2000**, *1464*, 177−187.
(48) Argüello, J. M.; Whitis, J.; Cheung, M. C.; Lingrel, J. B. Functional Role of Oxygen-Containing Residues in the Fifth Transmembrane Segment of the Na,K-ATPase α Subunit. *Arch. Biochem. Biophys.* **1999**, *364*, 254−263.
(49) Vilsen, B. Leucine 332 at the Boundary Between the Fourth Transmembrane Segment and the Cytoplasmic Domain of Na + , K + -ATPase Plays a Pivotal Role in the Ion Tanslocating Conformational Changes. *Biochemistry* **1997**, *36*, 13312−13324.
(50) Toustrup-Jensen, M. S.; Hauge, M.; Vilsen, B. *Biochemistry* **2001**, *40*, 5521−5532.
(51) Einholm, A. P.; Toustrup-Jensen, M. S.; Andersen, J. P.; Vilsen, B. *Proc. Natl. Acad. Sci. U. S. A.* **2005**, *102*, 11254−11259.
(52) Einholm, A. P.; Andersen, J. P.; Vilsen, B. Importance of Leu99 in Transmembrane Segment M1 of the Na+,K+-ATPase in the Binding and Occlusion of K+. *J. Biol. Chem.* **2007**, *282*, 23854−23866.
(53) Imagawa, T.; Yamamoto, T.; Kaya, S.; Sakaguchi, K.; Taniguchi, K. Thr-774 (Transmembrane Segment M5), Val-920 (M8), and Glu-954 (M9) Are Involved in Na+ Transport, and Gln-923 (M8) Is Essential for Na,K-ATPase Activity. *J. Biol. Chem.* **2005**, *280*, 18736−18744.
(54) Bateman, A.; Martin, M. J.; O'Donovan, C.; Magrane, M.; Apweiler, R.; Alpi, E.; Antunes, R.; Arganiska, J.; Bely, B.; Bingley, M.; Bonilla, C.; Britto, R.; Bursteinas, B.; Chavali, G.; Cibrian-Uhalte, E.; Da Silva, A.; De Giorgi, M.; Dogan, T.; Fazzini, F.; Gane, P.; Castro, L. G.; Garmiri, P.; Hatton-Ellis, E.; Hieta, R.; Huntley, R.; Legge, D.; Liu, W.; Luo, J.; Macdougall, A.; Mutowo, P.; Nightingale, A.; Orchard, S.; Pichler, K.; Poggioli, D.; Pundir, S.; Pureza, L.; Qi, G.; Rosanoff, S.; Saidi, R.; Sawford, T.; Shypitsyna, A.; Turner, E.; Volynkin, V.; Wardell, T.; Watkins, X.; Zellner, H.; Cowley, A.; Figueira, L.; Li, W.; McWilliam, H.; Lopez, R.; Xenarios, I.; Bougueleret, L.; Bridge, A.; Poux, S.; Redaschi, N.; Aimo, L.; Argoud-Puy, G.; Auchincloss, A.; Axelsen, K.; Bansal, P.; Baratin, D.; Blatter, M. C.; Boeckmann, B.; Bolleman, J.; Boutet, E.; Breuza, L.; Casal-Casas, C.; De Castro, E.; Coudert, E.; Cuche, B.; Doche, M.; Dornevil, D.; Duvaud, S.; Estreicher, A.; Famiglietti, L.; Feuermann, M.; Gasteiger, E.; Gehant, S.; Gerritsen, V.; Gos, A.; Gruaz-Gumowski, N.; Hinz, U.; Hulo, C.; Jungo, F.; Keller, G.; Lara, V.; Lemercier, P.; Lieberherr, D.; Lombardot, T.; Martin, X.; Masson, P.; Morgat, A.; Neto, T.; Nouspikel, N.; Paesano, S.; Pedruzzi, I.; Pilbout, S.; Pozzato, M.; Pruess, M.; Rivoire, C.; Roechert, B.; Schneider, M.; Sigrist, C.; Sonesson, K.; Staehli, S.; Stutz, A.; Sundaram, S.; Tognolli, M.; Verbregue, L.; Veuthey, A. L.; Wu, C. H.; Arighi, C. N.; Arminski, L.; Chen, C.; Chen, Y.; Garavelli, J. S.; Huang, H.; Laiho, K.; McGarvey, P.; Natale, D. A.; Suzek, B. E.; Vinayaka, C. R.; Wang, Q.; Wang, Y.; Yeh, L. S.; Yerramalla, M. S.; Zhang, J. UniProt: A Hub for Protein Information. *Nucleic Acids Res.* **2015**, *43*, D204−D212.
(55) Sherry, S. T.; Ward, M. H.; Kholodov, M.; Baker, J.; Phan, L.; Smigielski, E. M.; Sirotkin, K. dbSNP: The NCBI Database of Genetic Variation. *Nucleic Acids Res.* **2001**, *29*, 308−311.

DOI: 10.1021/acs.jcim.6b00353
J. Chem. Inf. Model. XXXX, XXX, XXX−XXX

Biochimie 138 (2017) 56–61

Contents lists available at ScienceDirect

Biochimie

journal homepage: www.elsevier.com/locate/biochi

Research paper

Inhibition of Na^+/K^+-ATPase by 5,6,7,8-tetrafluoro-3-hydroxy-2-phenylquinolin-4(1*H*)-one

Jaroslava Šeflová [a, **], Petra Čechová [a], Michal Biler [a, b], Pavel Hradil [c], Martin Kubala [a, *]

[a] Dept. of Biophysics, Centre of Region Haná for Biotechnological and Agricultural Research, Faculty of Science, Palacký University, Olomouc-Holice, Šlechtitelů 27, Czech Republic
[b] INSERM UMR 850, Univ. Limoges, School of Pharmacy, Limoges, France
[c] Dept. of Organic Chemistry, Faculty of Science, Palacký University, Olomouc, Czech Republic

ARTICLE INFO

Article history:
Received 2 February 2017
Accepted 18 April 2017
Available online 20 April 2017

Keywords:
Sodium pump
Na^+/K^+-ATPase
Quinolinones
Inhibition
Binding sites

ABSTRACT

Na^+/K^+-ATPase (NKA) is an enzyme of crucial importance for all animal cells. We examined the inhibitory effects of halogenated phenylquinolinones on NKA. The 5,6,7,8-tetrafluoro-3-hydroxy-2-phenylquinolin-4(1*H*)-one (TFHPQ) was identified as an efficient NKA inhibitor with IC_{50} near 10 μM. The inhibition by TFHPQ is particularly efficient at higher concentrations of K^+, where NKA adopts the E2 conformation. The experimental observations are in a good agreement with the outcomes from molecular docking. We identified an energetically favourable TFHPQ binding site for the K^+-bound NKA, which is located in the proximity of the cytoplasmic C-terminus.

1. Introduction

The sodium-potassium ATPase (E.C. 3.6.3.9, NKA) is a transmembrane protein that is essential for all animal cells. Its major role is the maintenance of the cytoplasmic concentrations of Na^+ and K^+, a part of the resting plasma membrane potential. Furthermore, it creates the gradient of Na^+, which is a driving force for numerous secondary active transporters, and thus, the NKA indirectly regulates concentrations of other solutes with physiological importance. It is not surprising that the dysfunction of NKA can result in a wide variety of pathological states.

On the other hand, NKA inhibitors have been used for treatment of cardiovascular diseases. Cardiac glycosides (or cardiotonic steroids, CTS) are a well-known group of compounds, which were historically used for congestive heart failure treatment due to their anti-arrhythmic effects. They are natural compounds, which can be extracted from plants (e.g. *Digitalis purpurea* L., *Nerium oleander* L., *Strophanthus gratus* L.) and animal secretions (*Bufo bufo*). Typical members of this group are digoxin, digitoxin, oleandrin, bufalin and a specific inhibitor of NKA, ouabain [1]. However, the use of cardiac glycosides is limited by their very narrow useful concentration range, which stimulates further search for other NKA inhibiting compounds.

Recently, we have identified flavonoids and their complexes with lignans as a novel class of NKA inhibitors, which have a different mode of action than CTS [2]. In this work, we present studies of phenylquinolone derivatives (Fig. 1), a group of molecules with three-member-ring skeleton, which is isosteric to flavonoids.

The group of 3-hydroxy-2-phenylquinolin-4(1*H*)-one derivatives exhibits cytostatic and antileukemic activity [3] and they can act as strong antiprotozoal agents due to their role in the cell-to-cell communication system [4,5]. Therapeutic properties of quinolones can be further altered by chemical modification of the quinolone scaffold, e.g. chloro- and dichloro- derivatives of 3-hydroxy-2-phenylquinolin-4(1*H*)-ones inhibited the growth of colon- and breast cancer cell lines [3,6].

The NKA consists of two subunits denoted as α and β, which are usually accompanied by a protein from the FXYD family (Fig. 2), which serves as a tissue-specific regulator. The α-subunit is the main catalytic one and it consists of ten transmembrane helices and three cytoplasmic domains (A, P and N) that move during the reaction cycle. The β-subunit is mostly extracellular, with one transmembrane helix. It functions as molecular chaperone and plays a role in K^+ selectivity [7]. The reaction cycle of the NKA is traditionally described by the Post-Albers scheme [8,9], which

* Corresponding author.
** Corresponding author.
E-mail addresses: seflova.jaroslava@gmail.com (J. Šeflová), martin.kubala@upol.cz (M. Kubala).

http://dx.doi.org/10.1016/j.biochi.2017.04.009
0300-9084/

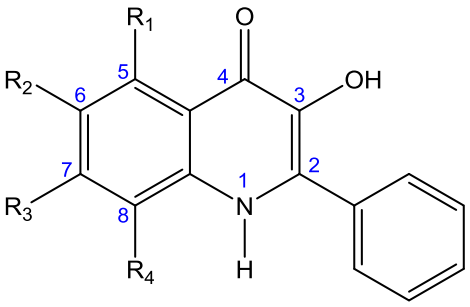

Acronym	R_1	R_2	R_3	R_4
TFHPQ	F	F	F	F
DFHPQ	H	F	F	H
8CHPQ	H	H	H	Cl
6CHPQ	H	Cl	H	H
DCHPQ	Cl	Cl	H	H

Fig. 1. Structure and acronyms of 3-hydroxy-2-phenylquinolin-4(1*H*)-one derivatives.

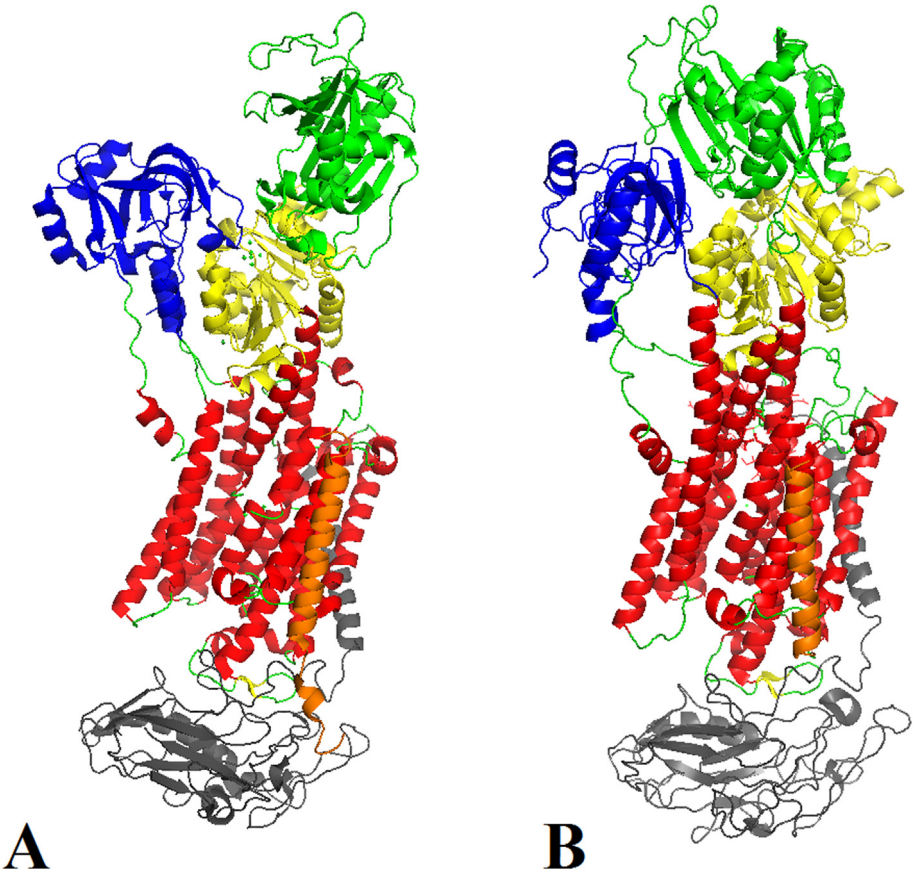

Fig. 2. Structure of NKA with the open (A) and closed (B) conformation of cytoplasmic domains. The transmembrane helices of the α-subunit are in red, the cytoplasmic A-domain in blue, N-domain in green and P-domain in yellow, the β-subunit is coloured grey, and the FXYD protein in orange.

postulates two major conformations, E1 and E2. The NKA in E1 state has a high affinity to sodium and ATP, whereas the enzyme in E2 state has a high affinity to potassium and a low affinity to ATP. In E2 state, the enzyme adopts a conformation with widely open cytoplasmic domains. On the contrary, the enzyme in E1 state assembles its cytoplasmic domains together, forming a closed conformation. High-resolution structures of the NKA in several distinguishable states were obtained using X-ray crystallography, and they revealed binding sites for transported ions as well as binding sites for other small molecules, such as a specific NKA inhibitor - ouabain. The combination of high-resolution protein structures and techniques of molecular modelling provides basis for identification of the potential binding sites for 3-hydroxyquinolin-4(1*H*)-ones and a rationalization of the inhibitory mechanism.

2. Experimental section

2.1. Material and methods

2.1.1. Chemicals

All used chemicals were from Sigma-Aldrich Chemie (Steinheim, Germany) unless stated otherwise. All chemicals were of Assay grade, except for KH_2PO_4 (ACS grade), L-histidine and

ammonium molybdate (BioUltra grade), SDS (BioXtra grade) and ouabain (HPLC grade).

2.1.2. Quinolinones tested for the effect on NKA activity

Chloro- and dichloro- derivatives of 3-hydroxy-2-phenylquinolin-4-(1*H*)-ones were prepared as described previously [3,6,10]). Fluorinated 3-hydroxy-2-phenylquinolin-4(1*H*)-ones were prepared as described elsewhere [11]. The LC-MS analysis revealed purity >99.5% and confirmed the molar mass of the analysed species.

2.1.3. Isolation of Na^+/K^+-ATPase

NKA was prepared from porcine kidney outer medulla using the method of Jorgensen [12] and Fedosova [13] with some modifications. The purified enzyme was pipetted into small aliquots and stored at −80 °C in the buffer (250 mM sucrose, 0.9 mM EDTA, 20 mM L-histidine, pH 7.0) containing SDS detergent. Molar concentration of NKA was estimated using the Bradford method with consideration of MW(α+β) = 165 000 Da. The protein purity >90% was estimated from SDS-PAGE and verified by Western blotting.

2.1.4. Measurement of ATPase activity

The measurements of NKA activity were performed using the Baginsky assay [14] with some modifications [2]. The assay was performed in microwell plates with 4 replicates for each point and automated in the pipetting station Freedom EVO (Tecan, Switzerland).

The reaction proceeded in imidazole buffer, pH 7.2, which contained by default 140 mM NaCl, 20 mM KCl, 3 mM $MgCl_2$ and 3 mM ATP (the reaction was started by addition of ATP), and in the absence or presence of 12.5 μM inhibitor, which was incubated with the enzyme for 15 min. In the experiment aimed at Na^+-, K^+- or ATP-dependence of NKA activity, only concentration of the given component varied, the others were present in the concentrations given above.

The Baginsky method detects the inorganic phosphate, which interacts with ammonium molybdate. The reaction results in a colour change, which can be monitored as a change of absorbance at 710 nm, and was measured using microplate reader Synergy Mx (BioTek, USA). The calibration line was determined using of KH_2PO_4 solutions, in the 0–37.5 nM concentration range.

The specific Na^+/K^+-ATPase activity is standardly estimated using the treatment by ouabain, which serves as a specific inhibitor of NKA. The ATPase activity decreases to less than 10% in the presence of 10 mM ouabain. This residual activity in the presence of ouabain has been subtracted from the total estimated ATPase activity in ouabain-untreated samples, and all data are presented as the ouabain-sensitive ATPase activity.

2.1.5. Computation of structures and molecular docking

The geometry optimization of 5,6,7,8-tetrafluor-3-hydroxy-2-phenylquinolin-4(1*H*)-one was carried out within the density functional theory formalism at the B3P86/6-31+G(d,p) level at 298 K and 1 atm. Gibbs energies were computed and ground-state geometries were confirmed by the absence of any imaginary frequency. Quantum calculations were performed in the gas phase with the Gaussian09 software package [15]. Optimized structure was used for the molecular docking to the open and closed structures of NKA.

The compound was docked into the homology model with the human α1β1FXYD2 sequence (Uniprot IDs P05023, P05026 and P54710 respectively) and the structures based on the crystals 2ZXE (open conformation, corresponding to the E2 state) [16] and 4HQJ (closed conformation, corresponding to the E1 state) [17]. The docking was performed in two steps – a general screening with the grid covering the whole protein (exhaustiveness set to 400 and num_modes to 9999) and then redocking into the most favourable regions – the C-terminal region of the open structure and the transmembrane part of the closed structure. The software used was Autodock Tools [18], Autodock Vina [19] for docking with the XB extension [20] better describing halogen binding, and PyMol [21] for visualization.

3. Results

3.1. Effects on NKA activity

In the initial screening, the selected halogenated quinolones were tested as potential NKA inhibitors at 10 μM final concentration. The activities measured in the presence of DFHPQ, DCHPQ, 6CHPQ or 8CHPQ did not significantly differ from the untreated control (Fig. 3A). Only TFHPQ reduced the NKA activity to ca. 45% of the untreated control, and it was a subject of further analyses.

The TFHPQ decreased the NKA activity in the concentration dependent manner (Fig. 3B). However, limited TFHPQ solubility in aqueous environment seriously limited precise IC_{50} determination.

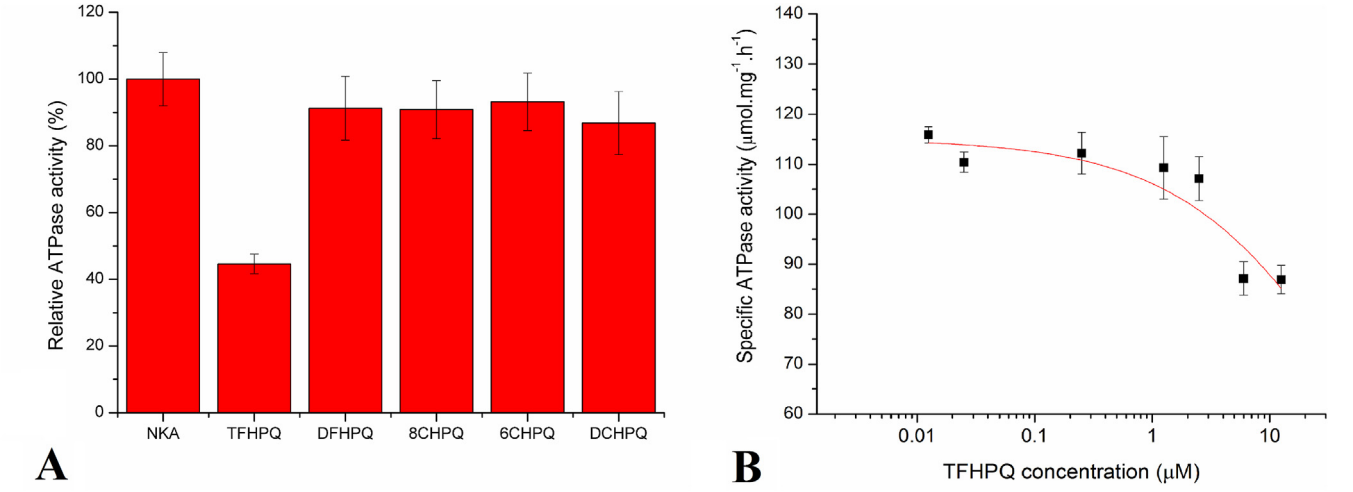

Fig. 3. (A) The changes of the relative ATPase activity caused by halogenated quinolinones (each at 10 μM final concentration). The relative ATPase activities were obtained by normalizing the ATPase activity of the quinolone-treated enzyme by the activity of the enzyme incubated without inhibitor. (B) Inhibition of NKA activity by increasing concentrations of TFHQP. Each data point represents average from four replicates.

Determination of the IC_{50} by fitting the data to the logistic function requires also estimation of the minimal activity at high inhibitor concentrations. Indeed, the increasing TFHPQ concentration progressively decreased the NKA activity, however, at concentrations higher than 15 μM, apparent aggregates of TFHPQ were visible. Consequently, we had only poor control of the real non-aggregated TFHPQ concentration in solution, and such data were useless for the quantitative analysis. Therefore, for the quantitative characteristic, we took advantage of the fortunate fact that the data point at 10 μM TFHPQ yielded 45% activity of the enzyme, which is very close to the 50%. Recalling that IC_{50} value is defined as the inhibitor concentration, at which the enzyme exhibits 50% activity, we can estimate that IC_{50} is near 10 μM. In order to better understand TFHPQ inhibition, we evaluated its effect on NKA activation by Na^+, K^+ or ATP (Fig. 4).

TFHPQ exhibited rather small effect on the Na^+ dependent NKA activation, altering the $K_{0.5}(Na^+)$ only from 14 mM to 9 mM. The activity at high NaCl concentration decreased only to 45% of maximal activity in the presence of THFPQ (Fig. 4A).

Similarly, the NKA activity was significantly decreased by TFHPQ at high K^+ concentrations, reaching only 45% of the control (Fig. 4B). Again, the $K_{0.5}(K^+)$ slightly decreased (from 0.8 mM to 0.6 mM), suggesting that the TFHPQ inhibition does not consist in the decrease of an enzyme affinity for transported cations.

The ATP-dependence of NKA activity follows the well-known bell-shaped curve [22]. The shape of the curve was not substantially affected by the presence of TFHPQ (Fig. 4C).

3.2. Molecular docking

Molecular docking was used for a prediction of a possible TFHPQ binding site. Computational analysis revealed that the molecule is not planar and the dihedral angle between the quinolone- and phenyl moieties is around 148° for free TFHPQ. Nevertheless, the phenyl group can freely rotate and the dihedral angle was kept flexible during the docking procedure.

Both major conformations of NKA (open with potassium bound, and closed with sodium bound) were used for examination of the ligand binding. The simulation revealed that the most preferred binding site in the open conformation of the enzyme (binding affinities −10.4 to −8.9 kcal/mol) was localized in a close proximity of the C-terminal part of the enzyme; TFHPQ was most frequently bound to Y1022 and βW12 (Fig. 5). In the closed conformation, the most frequently occupied pose was located within the transmembrane region of the enzyme in the proximity of Y970, W988 and F33 of FXYD protein, however, with substantially lower binding affinities (from −8.7 to −7.6 kcal/mol). Moreover, this site is normally occupied by a cholesterol molecule, which is absent in our model. Other binding poses on the closed conformation were spread within the enzyme cytoplasmic headpiece and near the extracellular part of the FXYD protein with lower frequency and binding affinity, and they were considered to be insignificant (not shown).

The other compounds could bind to the C-terminal binding site in the open structure, but with lower affinities than TFHPQ (by 1–3 kcal/mol). Moreover, they occupied also several other binding poses on the protein that were not available for TFHPQ. In the closed conformation, they bound to the similar poses as TFHPQ, but again, with lower affinities (−8.0 to −6.6 kcal/mol).

4. Discussion

Molecules isolated from plants used in a traditional medicine have a stable position in current research. They are either examined per se, or they serve as a base for further derivatization by the tools of organic chemistry. Recently, we have identified flavonolignans as a novel class of NKA inhibitors that have a different mode of action compared to the currently used cardiotonic steroids [2]. This study is focused on quinolones, which are structural analogues of natural

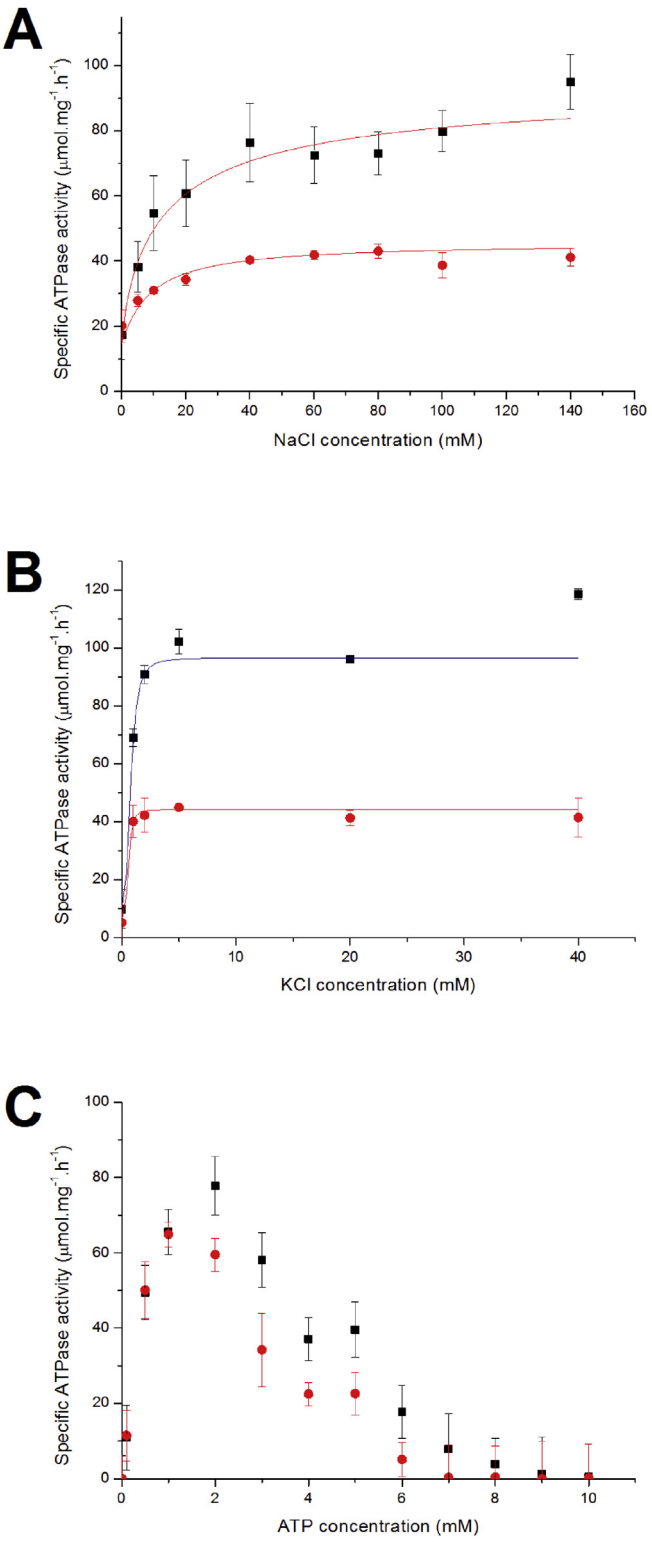

Fig. 4. The Na^+-dependence (A), K^+-dependence (B) and ATP-dependence (C) of NKA activity in the absence of any ligand (black squares) or in the presence of 12.5 μM TFHPQ (red circles).

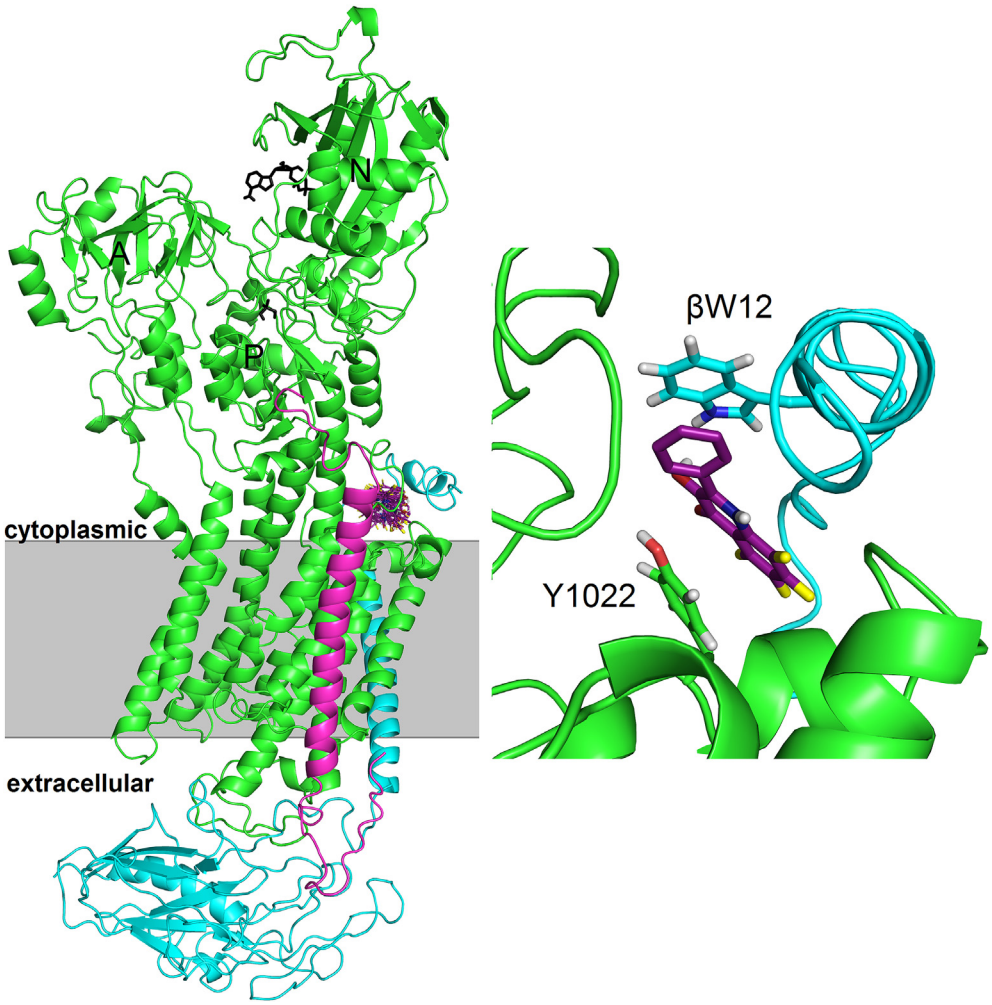

Fig. 5. Localization of TFHPQ binding site in the open conformation of the protein, and zoom (right). The docked compound is highlighted in purple, α-subunit is in green, β-subunit is in cyan and the FXYD protein is in magenta.

flavonoids. We examined changes in the activity of isolated porcine kidney NKA after the treatment with halogenated derivatives, which were previously shown to possess anticancer properties [3,23].

Of the five examined derivatives, only TFHPQ exhibited substantial inhibition of NKA. At 10 μM concentration, it decreased the NKA activity to approx. 45%, suggesting the estimate of IC_{50} to be slightly below 10 μM (unfortunately, this value could not have been determined more precisely due to the limited solubility of TFHPQ). This range is already interesting from the pharmaceutical point of view and this value is significantly lower than the one obtained for flavonolignans (~40 μM). The hydrophobicity and low solubility of quinolone-based drugs seem to be the major limitation for a potential use of these compounds. Nonetheless, it was shown recently that this limitation can be bypassed by using silica nanoparticles for the encapsulation of quinolone-like molecules [24].

The interaction is strongly dependent on the geometries of both the ligand and enzyme. The enzyme can reversibly change its conformation, reflecting binding of various ligands. Particularly, with the sodium ions bound, it prefers the closed conformation (traditionally denoted as E1), while in the presence of potassium, it adopts the open conformation (traditionally denoted as E2). In contrast to flavonolignans, where we have found several possible binding sites, we could identify a single binding site for TFHPQ that is energetically favourable over other possibilities. It is present only in the K^+-bound conformation of the protein and it is located in the proximity of the cytoplasmic C-terminus, corresponding to one of the binding sites that were proposed for flavonolignans [2]. It was suggested [25] that the release of sodium to the extracellular space is limited by a local disarrangement of the C-terminal part of the enzyme. A proton from the cytoplasm can be transferred through the C-terminal pathway, whereas two potassium ions interact with their binding sites. After occlusion, the pump releases potassium ions and proton into a cytoplasm enabling sodium binding. TFHPQ binding to the C-terminus can efficiently hinder this mechanism.

Molecular docking provided also a clue to the question, why only TFHPQ efficiently inhibited NKA, while the other analogues were rather inefficient. In fact, as all the examined molecules are structurally very similar, also the other analogues can bind to the THFPQ binding pose. However, their affinities were lower (by 1–3 kcal/mol), and in addition, they can bind with similar affinities also to several other sites on NKA, which are not available for TFHPQ. In practical experiment, binding of the molecules to these sites would effectively decrease the number of molecules that could bind to the inhibitory site. Hence, it seems that the superiority of TFHPQ over other analogues with respect to the potency to inhibit NKA activity is based on two factors – the best affinity, and the best specificity to the inhibitory site.

In conclusion, we have identified TFHPQ as a novel and efficient NKA inhibitor. Our data indicate that this molecule selectively binds to the potassium-bound state of NKA in the proximity of the C-terminus, thus, probably hindering the C-terminal pathway.

Authors and contributors

J.Š. prepared the manuscript, isolated NKA and performed the ATPase activity measurements,

P.Č. performed the molecular docking computations, contributed to the interpretation of data.

M.B. performed the conformational analysis and optimized the quinolinones structure for molecular docking.

P. H. prepared the tested quinolones.

M.K. designed the study and prepared the manuscript.

Funding

This work was supported by the grant LO1204 from the National Program of Sustainability I, by scholarship for M.B. from the French Embassy in the Czech Republic.

Acknowledgments

M.B. wishes to thank CALI (CAlcul en LImousin), where the calculations were performed. P.Č. would like to acknowledge that the computational resources were provided by the CESNET LM2015042 and the CERIT Scientific Cloud LM2015085, provided under the programme “Projects of Large Research, Development, and Innovations Infrastructures”.

References

[1] R.A. Newman, P. Yang, A.D. Pawlus, K.I. Block, Cardiac glycosides as novel cancer therapeutic agents, Mol. Interv. 8 (2008) 36–49, http://dx.doi.org/10.1124/mi.8.1.8.

[2] M. Kubala, P. Čechová, J. Geletičová, M. Biler, T. Štenclová, P. Trouillas, D. Biedermann, Flavonolignans as a novel class of sodium pump inhibitors, Front. Physiol. 7 (2016) 1–10, http://dx.doi.org/10.3389/fphys.2016.00115.

[3] P. Hradil, P. Krejci, J. Hlavac, I. Wiedermannova, A. Lycka, V. Bertolasi, Synthesis, NMR spectra and X-ray data of chloro and dichloro derivatives of 3-hydroxy-2-phenylquinolin-4(1H)-ones and their cytostatic activity, J. Heterocycl. Chem. 41 (2004) 375–379, http://dx.doi.org/10.1002/jhet.5570410311.

[4] E.C. Pesci, J.B.J. Milbank, J.P. Pearson, S. McKnight, A.S. Kende, E.P. Greenberg, B.H. Iglewski, Quinolone signaling in the cell-to-cell communication system of Pseudomonas aeruginosa, Proc. Natl. Acad. Sci. 96 (1999) 11229–11234, http://dx.doi.org/10.1073/pnas.96.20.11229.

[5] J. Kadrić, K. Motyka, P. Džubák, M. Hajdúch, M. Soural, Synthesis, cytotoxic activity, and fluorescence properties of a set of novel 3-hydroxyquinolin-4(1H)-ones, Tetrahedron Lett. 55 (2014) 3592–3595, http://dx.doi.org/10.1016/j.tetlet.2014.04.121.

[6] M. Grepl, J. Roithova, P. Hradil, K. Lemr, Ionisation and fragmentation of monochloro-isomers of 3-hydroxy-2-phenyl-4(1H)-quinolinone, Rapid Commun. Mass Spectrom. 22 (2008) 2905–2914.

[7] K. Geering, Functional roles of Na,K-ATPase subunits, Curr. Opin. Nephrol. Hypertens. 17 (2008) 526–532, http://dx.doi.org/10.1097/MNH.0b013e3283036cbf.

[8] R.L. Post, A phosphorylated dependent intermediate in adenosine sodium and potassium transport across kidney membranes, J. Biol. Chem. 240 (1965) 1437–1445.

[9] R.W. Albers, Biochemical Aspects of active transport, Annu. Rev. Biochem. (1967) 727–756.

[10] T.W.M. Spence, G. Tennant, The chemistry of nitro-compounds. Part I. Acid-catalysed ring-opening reactions of substitued o-nitriphenylethylene oxides involving participation by the nitro-group, J. Chem. Soc. Sect. C (1969) 3712–3719.

[11] J. Rehulka, P. Krejci, P. Dzubak, M. Hajduch, P. Hradil, J. Hlavac, Synthesis of Fluorinated Derivatives 2-phenyl-3-hydroxy-4(1H)-quinolinone and Study of Their Anticancer Activity, submitted.

[12] P.L. Jorgensen, Purification of Na^+,K^+-ATPase: enzyme sources, preparative problems, and preparation from mammalian kidney, Methods Enzymol. 156 (1988) 29–43.

[13] N. Fedosova, P-type ATPases: methods and protocols, in: M. Bublitz (Ed.), Springer Protoc. - Methods Mol. Biol. Purif. Na, K-ATPase from Pig Kidney, Springer, 2016, pp. 5–10, http://dx.doi.org/10.1007/978-1-4939-3179-8.

[14] E. Baginski, L.M. Weiner, B. Zak, The simple determination of nucleotide phosphorus, Clin. Chim. Acta 10 (1964) 378–379.

[15] M.J. Frisch, G.W. Trucks, l. H.B. Schlege, G.E. Scuseria, M.A. Robb, R.J. Cheeseman, E. Al, Gaussian 09, 2009, p. 2009.

[16] T. Shinoda, H. Ogawa, F. Cornelius, C. Toyoshima, Crystal structure of the sodium-potassium pump at 2.4 A resolution, Nature 459 (2009) 446–450, http://dx.doi.org/10.1038/nature07939.

[17] M. Nyblom, L. Reinhard, M. Andersson, E. Lindahl, N. Fedosova, P. Nissen, Crystal structure of Na^+,K^+-ATPase in the Na+-bound state, Science (80) 342 (2013) 123–127, http://dx.doi.org/10.1126/science.1243352.

[18] G.M. Morris, R. Huey, W. Lindstrom, M.F. Sanner, R.K. Belew, D.S. Goodsell, A.J. Olson, AutoDock4 and AutoDockTools4: automated docking with selective receptor flexibility, J. Comput. Chem. 31 (2010) 2967–2970, http://dx.doi.org/10.1002/jcc.

[19] O. Trott, A.J. Olson, AutoDock Vina: improving the speed and accuracy of docking with a new scoring function, efficient optimization and multithreading, J. Comput. Chem. 31 (2010) 455–461, http://dx.doi.org/10.1002/jcc.21334.AutoDock.

[20] M.R. Koebel, G. Schmadeke, R.G. Posner, S. Sirimulla, AutoDock VinaXB: implementation of XBSF, new empirical halogen bond scoring function, into AutoDock Vina, J. Cheminform 8 (2016) 1–8, http://dx.doi.org/10.1186/s13321-016-0139-1.

[21] The PyMOL Molecular Graphics System, 2013.

[22] J.C. Skou, Further investigations on a Mg^{++} + Na^+-activated adenosine-triphosphatase, possibly related to the active, linked transport of Na+ and K+ across the nerve membrane, Biochim. Biophys. Acta 42 (1960) 6–23.

[23] C.Y. Hong, S.H. Kim, Y.K. Kim, Novel 5-amino-6-methylquinolone antibacterials: a new class of non-6-fluoroquinolones, Bioorg. Med. Chem. Lett. 7 (1997) 1875–1878.

[24] K. Bürglová, J. Hlaváč, J.R. Bartlett, Synthesis of silica nanoparticles for encapsulation of oncology drugs with low water solubility: effect of processing parameters on structural evolution, J. Nanopart. Res. 17 (2015) 1–11, http://dx.doi.org/10.1007/s11051-015-3268-y.

[25] H. Poulsen, H. Khandelia, J.P. Morth, M. Bublitz, O.G. Mouritsen, J. Egebjerg, P. Nissen, Neurological disease mutations compromise a C-terminal ion pathway in the Na^+/K^+-ATPase, Nature 467 (2010) 99–102, http://dx.doi.org/10.1038/nature09309.

frontiers in Physiology

ORIGINAL RESEARCH
published: 30 March 2016
doi: 10.3389/fphys.2016.00115

Flavonolignans As a Novel Class of Sodium Pump Inhibitors

Martin Kubala[1], Petra Čechová[1], Jaroslava Geletičová[1], Michal Biler[1,2], Tereza Štenclová[1], Patrick Trouillas[2,3] and David Biedermann[4]*

[1] Department of Biophysics, Faculty of Science, Centre of Region Haná for Biotechnological and Agricultural Research, Palacký University, Olomouc, Czech Republic, [2] INSERM UMR 850, School of Pharmacy, University Limoges, Limoges, France, [3] Department of Physical Chemistry, Faculty of Science, Regional Centre of Advanced Technologies and Materials, Palacký University, Olomouc, Czech Republic, [4] Laboratory of Biotransformation, Institute of Microbiology, Czech Academy of Sciences, Prague, Czech Republic

We examined the inhibitory effects of three flavonolignans and their dehydro- derivatives, taxifolin and quercetin on the activity of the Na^+/K^+-ATPase (NKA). The flavonolignans silychristin, dehydrosilychristin and dehydrosilydianin inhibited NKA with IC_{50} of 110 ± 40 μM, 38 ± 8 μM, and 36 ± 14 μM, respectively. Using the methods of molecular modeling, we identified several possible binding sites for these species on NKA and proposed the possible mechanisms of inhibition. The binding to the extracellular- or cytoplasmic C-terminal sites can block the transport of cations through the plasma membrane, while the binding on the interface of cytoplasmic domains can inhibit the enzyme allosterically. Fluorescence spectroscopy experiments confirmed the interaction of these three species with the large cytoplasmic segment connecting transmembrane helices 4 and 5 (C45). The flavonolignans are distinct from the cardiac glycosides that are currently used in NKA treatment. Because their binding sites are different, the mechanism of inhibition is different as well as the range of active concentrations, one can expect that these new NKA inhibitors would exhibit also a different biomedical actions than cardiac glycosides.

Keywords: sodium pump, Na^+/K^+-ATPase, flavonolignans, inhibition, binding sites

OPEN ACCESS

Edited by:
Olga Vagin, University California, Los Angeles, USA

Reviewed by:
Pablo Martín-Vasallo, Universidad de La Laguna, Spain
Joseph Isaac Shapiro, Marshall University, USA

****Correspondence:***
Martin Kubala
martin.kubala@upol.cz

Specialty section:
This article was submitted to Membrane Physiology and Membrane Biophysics, a section of the journal Frontiers in Physiology

Received: *22 January 2016*
Accepted: *14 March 2016*
Published: *30 March 2016*

Citation:
Kubala M, Čechová P, Geletičová J, Biler M, Štenclová T, Trouillas P and Biedermann D (2016) Flavonolignans As a Novel Class of Sodium Pump Inhibitors. Front. Physiol. 7:115. doi: 10.3389/fphys.2016.00115

INTRODUCTION

Sodium pump (Na^+/K^+-ATPase, E.C. 3.6.3.9, NKA) is an enzyme of crucial importance for all animal cells. It is the major determinant of cytoplasmic Na^+ and K^+ concentrations and the resting plasma membrane potential. The steep Na^+ gradient on plasma membrane is essential for variety of secondary active transporters, e.g., Na^+/Ca^{2+}- and Na^+/H^+- exchanger or Na^+-dependent glucose transporter, and hence, NKA indirectly regulates also concentrations of other physiologically important solutes.

It is not surprising that an uncontrolled inhibition of NKA can result in severe diseases, e.g., renal failure, hypertension or diabetic neuropathies (Kaplan, 2002) or even death, and that the most specific NKA inhibitor cardiac glycoside ouabain was originally used as an arrow poison (Newman et al., 2008). Despite these risks, extracts containing cardiac glycosides were used to control heart tonics already in ancient medicine, and the extracts were prepared either from plants in Arabic medicine (Brewer, 2004) or secretions of frog *Bufo bufo* in Chinese medicine (Watabe et al., 1996). Compounds like digitalis or digoxin are still prescribed for control of congestive heart failure (Gheorghiade et al., 2004). However, the use of cardiac glycosides is limited by their very

narrow useful concentration range (Newman et al., 2008), which stimulates further search for other NKA inhibiting compounds.

Silymarin is an extract from the seeds of milk thistle (*Silybum marianum)*. It contains numerous polyphenolic compounds and it was shown to possess antioxidant (Vacek et al., 2013; Pyszková et al., 2015), hepatoprotective (Loguercio and Festi, 2011) or anticancer effects (Agarwal et al., 2006). In this study, we have tested effects on NKA activity for a flavonoid taxifolin (TAX) and three flavonolignans, namely silybin (SB), silychristin (SCH), and silydianin (SD), which are major silymarin compounds (Biedermann et al., 2014); their structures are shown in **Figure 1**. The corresponding 2,3-dehydro derivatives (DHSB, DHSCH, and DHSD, the 2,3-dehydrotaxifolin is termed quercetin, QUE) were also tested.

The NKA catalytic cycle is usually described by the Albers-Post cycle (Jorgensen et al., 2003). It postulates that during the catalytic cycle, the enzyme adopts two major conformations, denoted as E1 and E2. In E1, the enzyme has high affinity to sodium and ATP and the binding sites are open to the cytoplasm, while in E2, the enzyme has high affinity to potassium, low affinity to ATP and the cation-binding sites are open to the extracellular space. High-resolution structures of NKA were obtained in several conformational states thanks to recent progresses in X-ray crystallography of membrane proteins (Morth et al., 2007; Ogawa et al., 2009; Nyblom et al., 2013). They revealed the binding sites for transported cations within the transmembrane domain, or binding site for some ligands, including ouabain. Notably, in the crystals assigned to the enzyme in E1 conformation, the cytoplasmic domains are assembled together (further referred to as a closed conformation), while in the E2 conformation, the cytoplasmic headpiece is widely opened (opened conformation).

These different structures provided a solid basis to figure out molecular processes responsible for the mechanisms of enzyme inhibition. Moreover, based on these high-resolution structures, molecular modeling allows further identification of the binding sites of flavonolignans that inhibit NKA, and strongly support rationalization of mechanisms of inhibition.

MATERIALS AND METHODS

Chemicals

Unless stated otherwise, all used chemicals were from Sigma-Aldrich Chemie (Steinheim, Germany).

Species Tested for the Effect on NKA Activity

Silymarin was purchased from Liaoning Senrong Pharmaceutical Co., Ltd. (China), SB, SCH, and SD were isolated from the

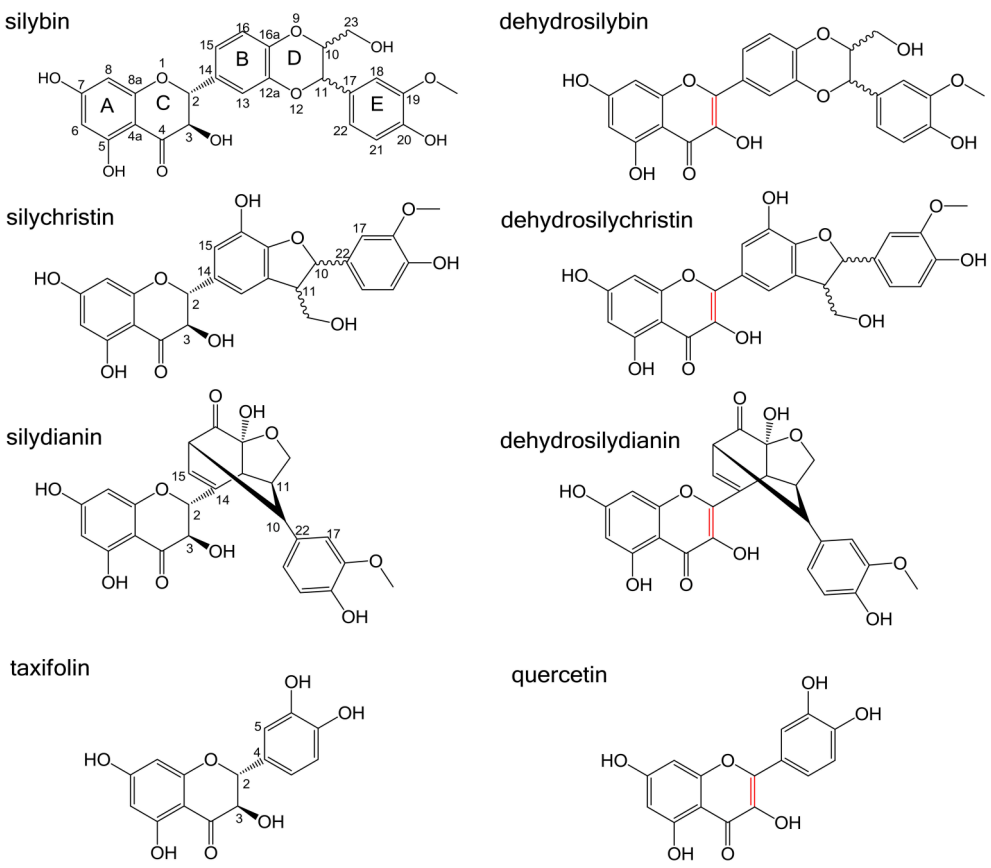

FIGURE 1 | Structures of silybin (SB), silychristin (SCH), silydianin (SD) and their dehydro-derivatives (DHSB, DHSCH, DHSD), taxifolin (TAX), and quercetin (QUE). The 2,3-double bond in dehydroderivatives is highlighted in red.

silymarin, and the dehydro- derivatives DHSB, DHSCH and DHSD were prepared as described previously (Džubák et al., 2006; Křenek et al., 2014; Pyszková et al., 2015). Silybin and silychristin were used as the natural diastereomeric mixture (ca. 1/1 and 95/5 respectively), silydianin is a single isomer. Dehydroderivatives were prepared from parent mixtures and are therefore enantiomeric mixtures (besides DHSD) (Pyszková et al., 2015). Taxifolin was purchased from Amagro (CZ). Quercetin was prepared by acidic hydrolysis of rutin with HCl/EtOH as described previously (Wang et al., 2011). Purity of all used compounds was over 95% (HPLC, PDA).

Isolation of Na^+/K^+-ATPase

The NKA was prepared from porcine kidney outer medulla using the method of Jorgensen and Klodos with some modifications (Jørgensen, 1988; Klodos et al., 2002; Kubala et al., 2014). An isolated enzyme was pipetted into small aliquots and stored at −20°C in ISE buffer (25 mM imidazole, 250 mM sucrose, 1 mM EDTA, pH 7.4) containing SDS detergent. The molar concentration of isolated NKA was estimated using the Bradford method with consideration of MW($\alpha + \beta$) = 165,000 Da. The protein purity >90% was estimated from SDS-PAGE (**Figure 2**).

Measurement of ATPase Activity

The measurements of NKA activity were performed using the Baginsky assay (Kubala et al., 2014). The assay was performed in microwell plates in 4 replicates for each point and automated in the pipetting station Freedom EVO (Tecan, Switzerland).

The reaction buffer was composed of 325 mM NaCl, 50 mM KCl, 7.5 mM $MgCl_2$, and 75 mM imidazole, pH 7.2. In the experiments where the K^+-dependence was estimated, the KCl concentration is ranging from 0 to 100 mM. The NKA (0.1 mg/mL) isolated from porcine kidney was mixed with reaction buffer without ATP. All inhibitors were solubilized in methanol immediately before the measurement and then premixed with the reaction buffer to the required concentration. Subsequently, 10 μL of inhibitor solution was added into 20 μL of enzyme solution and incubated for 2 min. In the control sample, only 10 μL of reaction buffer without inhibitor was added including corresponding amount of methanol. The reaction was started by the addition of ATP solution (20 μL, 7.5 mM in the stock, the final concentration in the reaction was 3 mM). The reaction proceeded for 6 min at room temperature and then was stopped by addition of 75 μL of staining solution, which was composed of 160 mM ascorbic acid, 3.7% (v/v) acetic acid, 3% (w/v) SDS, and 0.5% ammonium molybdate. The staining reaction was stopped after another 8 min by adding 125 μL of solution composed of 0.9% (w/v) bismuth citrate, 0.9% (w/v) sodium citrate and 3.7% HCl.

The Baginsky method detects a product of ATP hydrolysis, inorganic phosphate, which interacts with ammonium molybdate. The reaction results in a color change, which can be monitored as a change of absorbance at 710 nm, and was measured using microplate reader Synergy Mx (BioTek, USA). The calibration line was determined using KH_2PO_4 solutions, in 0–37.5 nM concentration range.

The specific NKA activity is standardly estimated using the treatment by ouabain, which serves as a specific inhibitor of NKA. The ATPase activity decreases to less than 10% in the presence of 10 mM ouabain. This residual activity in the presence of ouabain was subtracted from the total estimated ATPase activity in ouabain-untreated samples, and all data are presented as the ouabain-sensitive ATPase activity. The IC_{50} values were obtained from fitting the data to the logistic function.

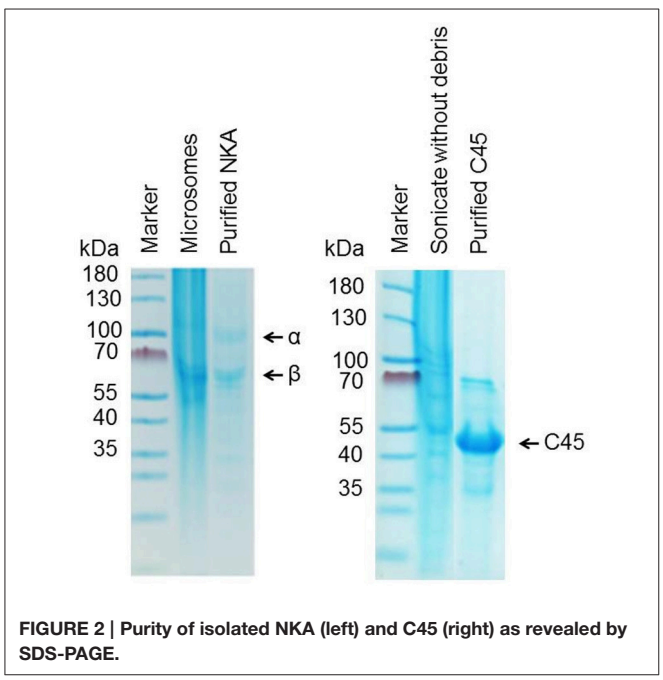

FIGURE 2 | Purity of isolated NKA (left) and C45 (right) as revealed by SDS-PAGE.

Expression and Purification of the Isolated Large Cytoplasmic Segment C45

The large cytoplasmic segment connecting the transmembrane helices 4 and 5 (C45 loop, residues L354-I777 of the mouse brain sequence) with a $(His)_6$-tag at the N-terminus was expressed in *E. coli* BL21 (Promega, USA) and purified using a Co^{2+}-based affinity resin (Clontech, USA) as described previously (Grycova et al., 2009). Immediately after elution, the protein was dialyzed into 20 mM Tris, 140 mM NaCl, pH 7.4 buffer and stored at −20°C.

Protein were analyzed by Coomassie blue stained SDS PAGE and concentration was determined using the Bradford assay (Bradford, 1976) using BSA as a standard.

Absorption and Fluorescence Spectroscopy

Spectroscopic experiments were performed in 20 mM Tris, 140 mM NaCl, pH 7.4 buffer. SCH, DHSCH and DHSD as well as protein C45 were diluted to 5 μM concentration.

Absorption spectra were measured on spectrometer Specord 250 Plus (Analytic Jena, Germany) in the range 300–600 nm, with the bandpass 2 nm, a step 1 nm and a scan-speed 2 nm/s. The reference spectrum was acquired using the cuvette with a pure buffer.

Fluorescence emission spectra were measured using Fluorolog-3 (Horiba Scientific, USA). The spectra were scanned with a step of 1 nm, both excitation- and emission bandpass 5 nm and integration time 1 s. For SCH, the excitation was 325 nm and emission was recorded in the 340–600 nm interval, for DHSCH and DHSD, the excitation wavelength was 380 nm and spectra were scanned in the 400–600 nm interval. Signal from pure buffer was subtracted as a background.

Computation of Structures for Molecular Docking

Geometry optimizations of all structures (**Figure 1**) was performed using the density functional theory (DFT) formalism with the software package Gaussian09 (Frisch et al., 2009). The hybrid functional B3P86 has been used because it has repeatedly succeeded in describing most of polyphenol properties (Trouillas et al., 2006, 2008). Gibbs energies (G) were computed at B3P86/6-31+G(d,p) level at 298 K, 1 atm. After a vibrational frequency analysis, ground-state geometries were confirmed by the absence of any imaginary frequency. Quantum calculations were performed in the gas phase.

The SB (stereoisomer A) and DHSB (stereoisomer A) initial structures were taken from Trouillas et al. (2008) and further re-optimized. Structure of the most stable isomers of SCH (stereoisomer A), DHSCH (stereoisomer A), SD and DHSD were already presented in Pyszková et al. (2015).

Molecular Docking

The compounds SCH, DHSCH, and DHSD were docked to the opened and closed structures of NKA (PDB, ID, 3KDP, and 4HQJ) using Autodock Tools (Morris et al., 2009) and Autodock Vina (Trott and Olson, 2010) with the grid covering the whole protein. The values of parameters exhaustiveness was set to 100 and num_modes to 9999 in order to reveal all possible docking modes. In the default setting, the bonds creating different conformers were freely rotable, to find optimal geometry of molecules interacting with the pump.

RESULTS

Conformational Analysis

Conformational analysis of both flavonoids TAX and its dehydro-analog QUE revealed two stable rotamers. In case of QUE, as reported previously (Trouillas et al., 2006), the planarity is observed, allowing π electron delocalization along the A, C and B rings, while for TAX, the planarity is lost due to the loss of the 2,3-double bond.

A conformation analysis of SB, DHSB, SCH, DHSCH, SD, and DHSD revealed 4 most stable representative conformers for all molecules within less than 1.6 kcal/mol difference in Gibbs energy (**Figure 3**). These conformers can be obtained by modification of the torsion angles Phi = C3–C2–C14–C15 and Psi = C11–C10–C22–C17 (Psi = C10–C11–C17–C22 for SB and DHSB) (**Table 1**), and the loss of the flavonoid moiety planarity is observed also for these molecules, when the 2,3-bond is hydrogenated (DHSB, DHSCH, and DHSD).

Effects on NKA Activity

Ouabain-sensitive ATPase activity was measured for increasing concentrations of all species (**Figure 4**). In the case of SB, DHSB, SD, and DHSD, the examined concentration range was

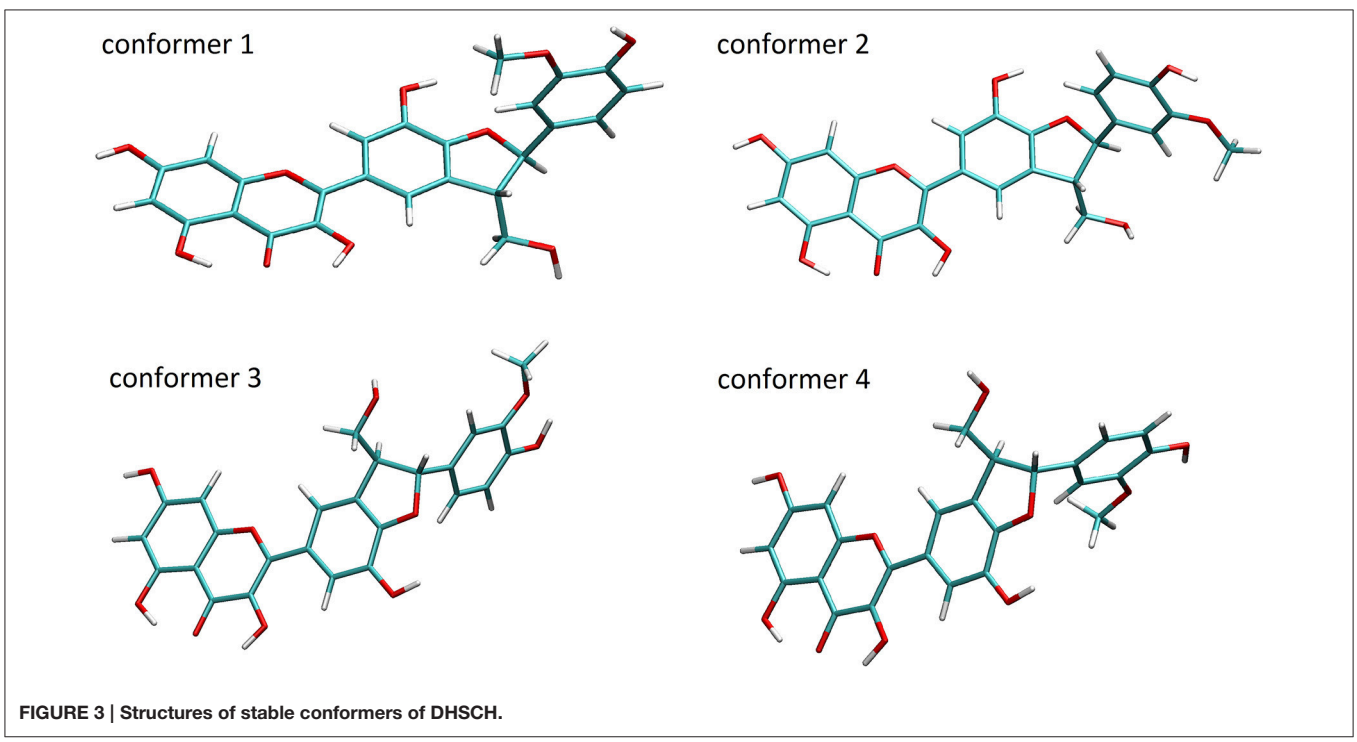

FIGURE 3 | Structures of stable conformers of DHSCH.

TABLE 1 | Structural parameters of the stable conformers.

Species	Conformer	Phi (°)	Psi (°)	Relative Gibbs energy (kcal/mol)
SB	1	77	−98	0
	2	83	81	0.4
	3	−96	−97	0.2
	4	−98	81	0.2
DHSB	1	3	−98	0
	2	−1	80	0.3
	3	−178	−98	0.1
	4	−176	83	0.5
SCH	1	81	−71	0
	2	82	98	0.9
	3	−105	52	0.1
	4	−97	−141	0.7
DHSCH	1	174	−52	0
	2	175	87	0.2
	3	9	97	0.1
	4	7	−55	1.6
SD	1	−3	−37	0
	2	−5	147	0.2
	3	−125	−42	0.5
	4	−123	142	0.4
DHSD	1	1	−45	0
	2	1	142	0.3
	3	166	−40	0.2
	4	166	145	0.8
TAX	1	−83		0
	2	80		0.1
QUE	1	180		0
	2	0		0.4

limited due to lower solubility of these species. Substantial inhibition was observed only for SCH, DHSCH and DHSD with IC_{50} 110 ± 40 μM, 38 ± 8 μM, and 36 ± 14 μM, respectively. In all these cases, we observed a Hill coefficient < 1, indicating the presence of multiple binding sites and negative cooperativity. The data are summarized in **Table 2**, and SCH, DHSCH, and DHSD were subject to further analyses.

We have tested influence of these three species on the ouabain inhibition and K^+-dependence of NKA activation. None of the species substantially influenced the IC_{50} for ouabain or the K^+/ouabain antagonism (**Figure 5**). The NKA activity is K^+-dependent and it increased with increasing concentration of potassium with $K_{0.5}(K^+) = 4.2 \pm 0.6$ mM. In contrast to ouabain, which raised the $K_{0.5}(K^+)$ to 14.8 ± 0.1 mM, none of the flavonolignans significantly altered the K^+-dependence of NKA activity (**Figure 6**).

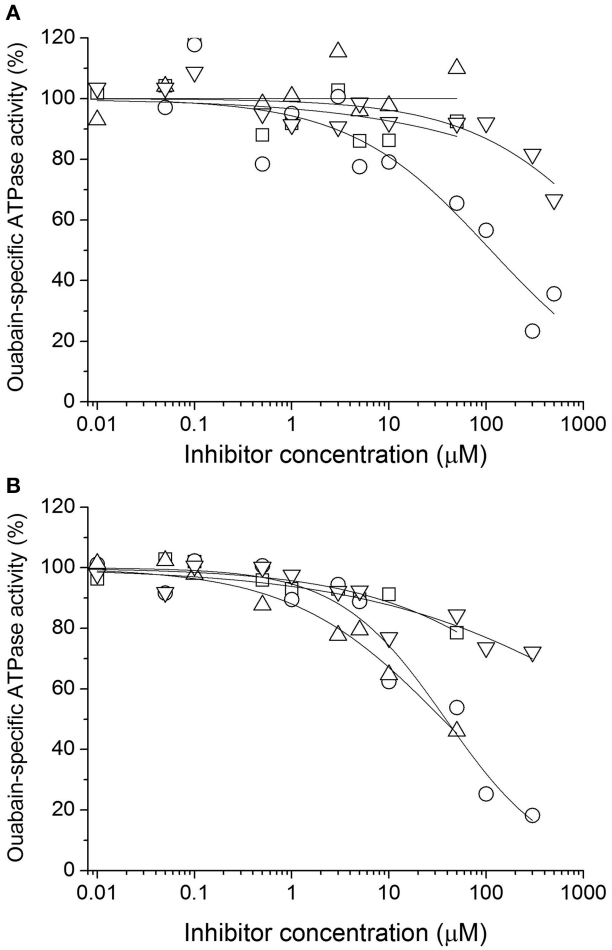

FIGURE 4 | Inhibition of NKA by (A) SB (squares), SCH (circles), SD (up triangles), TAX (down triangles) and (B) by the corresponding dehydro-derivatives DHSB, DHSCH, DHSD and QUE. The reference value (100%) represents ouabain-specific activity of untreated NKA.

Molecular Docking

Molecular docking enables prediction of the binding sites for small ligands on large biomolecules. Binding to NKA was examined for both major conformations of the enzyme. All SCH, DHSCH, and DHSD bound with a similar affinities (−11 to −9 kcal/mol) to all sites in both opened and closed conformations. We identified five major binding sites, three of them were common to both the opened and closed conformations (**Figure 7**), one binding pose was exclusively observed only for the opened conformation, and another one in turn only for closed conformation. All conformers bound to at least one binding site, nevertheless, their relative preferences for individual binding sites differed (**Table 3**).

In the closed conformation, by far the most favored site was near the phosphorylation site. All the conformers can occupy this site, except for conformer 4 of DHSCH. All compounds bound also to another pose between the A and N domains on the other side near R248 (**Figure 8**). However, this site only exists in the closed conformation. It is much more selective and

TABLE 2 | Values of IC_{50} for inhibition of the NKA activity, n, Hill coefficient, $K_{0.5}$(ouabain) indicates the value obtained in the presence of 5 mM KCl (in parentheses in 40 mM KCl) and 40 μM concentration of flavonolignan, $K_{0.5}(K^+)$ denotes the values for K^+-dependent activation of NKA obtained in the presence of 40 μM flavonolignan, n.d., not determined.

Species	IC_{50} (μM)	n	$K_{0.5}$(ouabain) (μM)	$K_{0.5}(K^+)$ (mM)
None			2.6 ± 1.3 (23 ± 3)	4.2 ± 0.6
SB	>1000	n.d.	n.d.	n.d.
DHSB	900 ± 800	0.5 ± 0.1	n.d.	n.d.
SCH	110 ± 40	0.6 ± 0.1	4.0 ± 1.7 (18 ± 2)	8 ± 5
DHSCH	38 ± 8	0.8 ± 0.1	1.5 ± 0.5 (24 ± 6)	4 ± 1
SD	>1000	n.d.	n.d.	n.d.
DHSD	36 ± 14	0.6 ± 0.1	3.3 ± 1.4 (19 ± 7)	3 ± 2
TAX	>1000	n.d.	n.d.	n.d.
QUE	>1000	n.d.	n.d.	n.d.

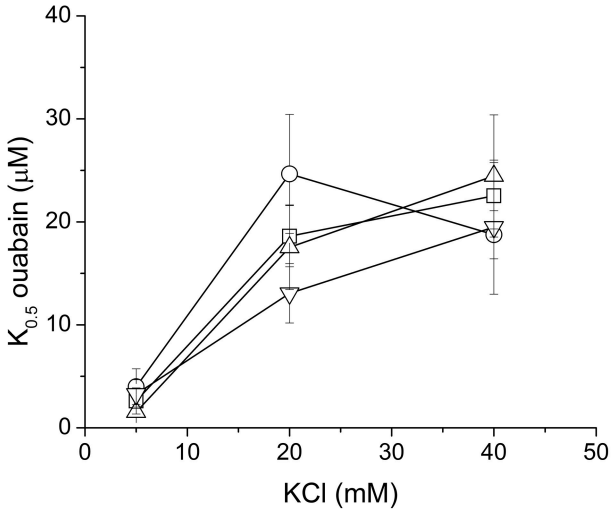

FIGURE 5 | The K^+/ouabain antagonism in the absence (squares) or in the presence of 40 μM SCH (circles), DHSCH (up triangles) or DHSD (down triangles).

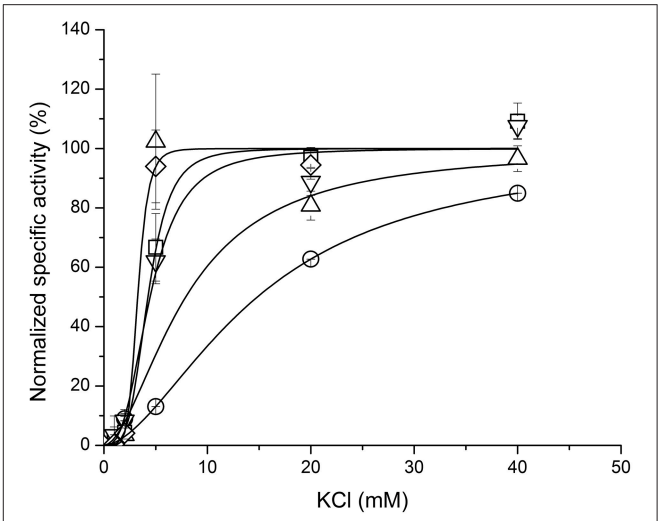

FIGURE 6 | The K^+-dependence of NKA activity in the absence of any ligand (squares) or in the presence of ouabain (circles), SCH (up triangles), DHSCH (down triangles) or DHSD (diamonds).

can be occupied only by conformer 3 of SCH, conformers 2 and 4 of DHSCH and conformer 1 of DHSD. Another possible binding location in the closed structure is on the extracellular side between E312 on TM4 and R886 (extracellular loop connecting TM7 and TM8), and it is the most favored site for conformer 4 of DHSCH. This site can serve as the entry for potassium ions during transport. Conformer 1 of SCH and conformers 1 and 4 of DHSCH are the only molecules that bind at the intracellular C-terminal site. Also this site was proposed to play a role in transport of cations through the plasma membrane (Toustrup-Jensen et al., 2009).

Also in the opened conformation, the binding to the groove between P and N cytoplasmic domains near the phosphorylation site was observed for all conformers, except for conformer 3 of DHSCH. It was the most preferred site for all SCH conformers and for conformers 1 of DHSCH and DHSD. The binding site specific only for the opened conformation is located under A domain, near the residues N353 and D740, where a regulatory potassium ion is bound (Schack et al., 2008). It is the most preferred site for conformers 2 and 4 of DHSCH and for conformer 2 of DHSD, but numerous other conformers can bind in this site as well. The site at the extracellular potassium entrance is the most preferred for the conformer 4 of DHSD. There is also a binding pose at the C-terminal of the protein, but it can be occupied only by DHSCH or DHSD, and for conformer 3 of both species it is the most preferred site.

Interaction with the Isolated Large Cytoplasmic Segment C45

Based on the prediction from molecular docking, we examined whether SCH, DHSCH, and DHSD could interact with the isolated large cytoplasmic segment C45 using absorption and fluorescence spectroscopy. Absorption spectra of SCH, DHSCH, and DHSD exhibited maxima at ca. 325, 385, and 375 nm, respectively, and the presence of C45 did not substantially alter the spectra (not shown), thus, providing no further clue about the interaction.

On the other hand, the interaction with C45 was clearly manifested in the fluorescence spectra for all three species. We observed no detectable fluorescence above background for the free SCH. The interaction with C45 protein turned out to be fluorogenic, and in the presence of C45, a bright SCH fluorescence appeared (quantum yield increased more than 1000 times compared to the free SCH) with a maximum at 394 nm (**Figure 9**). For the free DHSCH, we observed only very weak fluorescence with a maximum at 537 nm and an apparent shoulder at ca. 475 nm. In the presence of C45, the fluorescence intensity increased ca. 3-times, and two peaks at 466 and 527 nm could be resolved. Similarly for the free DHSD, there is only a weak fluorescence with a maximum at 472 nm. In the presence of C45, the three-fold intensity increase is accompanied by a shift of

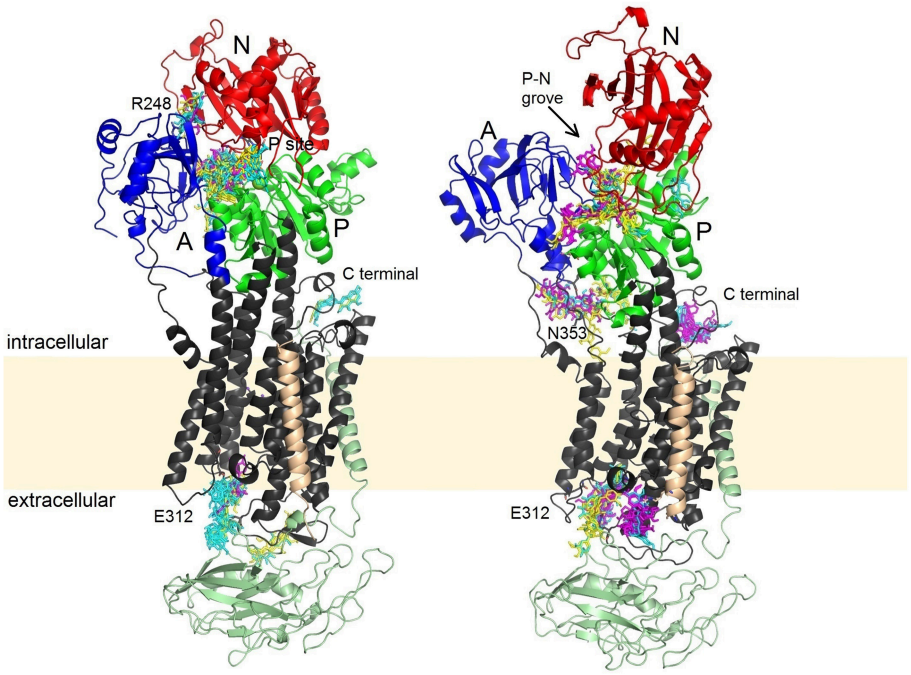

FIGURE 7 | Binding sites of SCH (yellow), DHSCH (cyan) and DHSD (magenta) on the opened and closed structure. Beta subunit is in light green, the FXYD protein light orange, A, domain blue; N, domain red; P, domain green.

the maximum to 459 nm, and there is also an apparent shoulder at 510 nm.

DISCUSSION

Recent pharmacology greatly benefits from the species isolated from the plants used in traditional medicine. In addition, these species also serve as precursors or inspiration for synthesis of new active derivatives, which can turn out to be even more effective in biochemical interactions. This study was focused on interactions of a series of phenolic compounds from silymarin (being or not hydrogenated on 2,3-bond of the flavonoid moiety) with one of the most important enzymes in the animal metabolism, the NKA.

Bioavailability of most polyphenolic compounds naturally found in silymarin is limited by their lower solubility in water, only SCH and SD exhibit substantially higher solubility in aqueous environment. In our experiments, we observed that only SCH inhibited the NKA with IC_{50} of 110 ± 40 μM, and similar concentrations can hardly be reached within the living organism. On the other hand, two of the 2,3-dehydroderivatives, DHSCH and DHSD, inhibited NKA substantially more efficiently with IC_{50} of 38 ± 8 μM and 36 ± 14 μM, respectively. Interestingly, none of the flavonolignans exhibited influence on the known K^+/ouabain antagonism (Müller-Ehmsen et al., 2001). Moreover, in contrast to ouabain, they did not alter the K^+-dependence of NKA activity, suggesting that the flavonolignans have different mode of inhibition than ouabain.

Interaction of small molecules with large biomolecules is one of the key issues in structural biology, and recently, it has gained benefits from the development in computational techniques. The classical key-and-lock concept assumes that small molecules can specifically interact with enzymes when their geometries fit each other. The induced-fit concept that was proposed later, has not that strict requirements on the geometries of the interaction partners, and it assumes that after the first contact, the enzyme can rearrange its conformation to fit the shape of the small ligand (Koshland, 1995).

Our calculations revealed that all flavonolignans (including the dehydro- derivatives) can adopt several stable conformations. Their stabilizing energies calculated in the gas phase appeared very similar, suggesting that they are all present in solution in roughly equimolar mixtures. Although differences between flavonolignans conformers may play no important role in, e.g., their redox properties, the precise geometry is crucial in the interaction with enzymes, and some conformers can be tightly bound to the enzyme, while the others can be inactive.

However, the situation is probably more complex in our case. The fitting of the inhibition curves revealed the Hill coefficient different from 1 for all SCH, DHSCH, and DHSD, indicating the presence of multiple binding sites. Indeed, molecular docking revealed one extracellular binding site and four other sites in the cytoplasmic segment of the protein, indicating multiple possibilities of how the flavonolignans could inhibit the enzyme. The main enzyme function is translocation of cations through the plasma membrane. The cations are transiently bound to their binding sites formed by residues TM4, TM5, TM6, and TM8 in the transmembrane domain (Morth et al., 2007), while the extracellular- and cytoplasmic pathways to these binding sites alternatively open and close. Binding of flavonolignans to the extracellular binding site or to the C-terminal binding site can

efficiently block these pathways, and thus, can stop the cation transport. The opening and closing of the extracellular- and cytoplasmic gates is accompanied by the change in the position of cytoplasmic domains, as a consequence of ATP-binding and hydrolysis (Kubala, 2006). Localization of the flavonolignan on the interfaces between N- and P- or N- and A-domains can hinder the interactions between cytoplasmic domains, and thus, inhibit the enzyme allosterically. All conformers of all SCH, DHSCH, and DHSD were able to bind to at least to one binding pose, but by far the most occupied site was the one at the interface of N- and P-domains near the phosphorylation site. It can be occupied by almost all conformers, it is present in both opened and closed enzyme conformations, and we experimentally verified binding of all SCH, DHSCH, and DHSD to the large cytoplasmic segment connecting TM4 and TM5 (C45) using fluorometry.

The C45 constitutes approx. 40% of the enzyme mass and forms the cytoplasmic domains N and P. It can be overexpressed without the rest of the enzyme in high quantities in *E. coli* (Grycova et al., 2009). So far, all the experiments indicate that it retains its structure, ability to bind ATP and TNP-ATP (Kubala et al., 2003a,b, 2004), and dynamic properties (Grycova et al., 2009; Kubala et al., 2009) as when it is a part of the entire enzyme. Its solubility greatly facilitates all subsequent

TABLE 3 | The fractions of conformers bound to the selected binding sites.

CLOSED	P site	R248	Extracellular	C terminal	Other
DHSD1	**0.23**	0.05	0.03	ND	ND
DHSD2	**0.15**	ND	ND	ND	ND
DHSD3	**0.25**	ND	0.03	ND	ND
DHSD4	**0.28**	ND	ND	ND	ND
DHSCH1	**0.28**	ND	ND	0.03	0.03
DHSCH2	**0.23**	0.03	0.08	ND	0.05
DHSCH3	**0.13**	ND	0.03	ND	ND
DHSCH4	ND	0.03	**0.05**	0.03	0.05
SCH1	**0.15**	ND	0.03	0.03	0.05
SCH2	**0.33**	ND	ND	ND	ND
SCH3	**0.18**	0.03	0.03	ND	0.03
SCH4	**0.15**	ND	0.03	ND	ND
OPENED	**P site**	**N353**	**Extracellular**	**C terminal**	**Other**
DHSD1	**0.05**	0.03	0.03	0.03	0.05
DHSD2	0.03	**0.05**	ND	0.03	ND
DHSD3	0.05	ND	0.03	**0.10**	0.05
DHSD4	0.08	0.08	**0.15**	ND	0.20
DHSCH1	**0.10**	0.03	0.05	0.03	0.10
DHSCH2	0.05	**0.13**	ND	0.03	0.20
DHSCH3	ND	ND	ND	**0.03**	0.05
DHSCH4	0.08	**0.08**	0.03	ND	0.05
SCH1	**0.10**	0.05	0.05	ND	0.15
SCH2	**0.10**	ND	ND	ND	0.10
SCH3	**0.08**	0.05	0.05	ND	0.03
SCH4	**0.13**	0.05	ND	ND	0.08

The most preferred binding site of each conformer in bold, "P site" stands for phosphorylation site. ND, binding to this site was not detected.

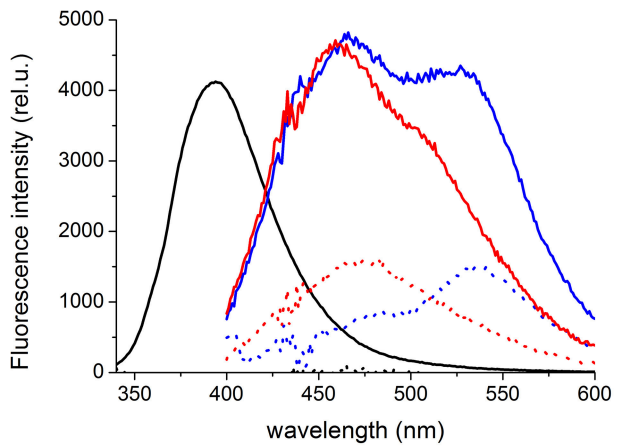

FIGURE 9 | Fluorescence emission spectra of 5 μM SCH (black), DHSCH (blue) and DHSD (red) in the presence (solid line) or absence (dotted line) of 5 μM C45. The fluorescence intensity in the spectrum of SCH in the C45 presence was divided by a factor of 20 to fit the graph.

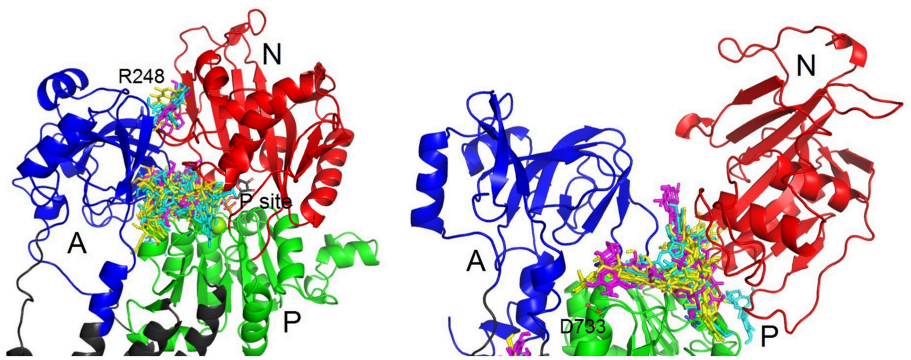

FIGURE 8 | Zoom on the binding sites of SCH (yellow), DHSCH (cyan) and DHSD (magenta) on cytoplasmic loops in the opened and closed structure. A, domain is blue; N, domain red; P, domain green.

experiments and this model system was successfully used for closer localization of binding sites of numerous other small molecules on the cytoplasmic part of NKA (Huličiak et al., 2012; Havlíková et al., 2013). Also in the case of SCH, DHSCH and DHSD, the spectroscopic experiments unambiguously confirmed that these molecules interact with C45. Moreover, in the case of DHSCH and DHSD, we could observe two peaks in the emission spectra of the protein-bound forms. It reveals that there are two binding modes of these species to the C45 and it is in line with predictions from molecular docking.

In conclusion, flavonolignans are proposed to be a novel class of NKA inhibitors, and particularly the 2,3-dehydroderivatives DHSCH and DHSD seem to be very promising agents. The flavonolignans are distinct from the cardiac glycosides that are currently used in NKA treatment. Because their binding sites are different, the mechanism of inhibition is different as well as the range of active concentrations, one can expect that these new NKA inhibitors would exhibit also a different biomedical actions than cardiac glycosides. Currently, the major problem seems to be the low specificity in interaction with biomolecules, which is probably partially related to significant number of stable flavonolignan conformers. Syntheses of more than 100 flavonolignan derivatives have been described (Biedermann et al., 2014), and further screening could identify a derivative that would be useful at lower concentrations and with higher specificity.

AUTHOR CONTRIBUTIONS

MK designed the study, prepared the manuscript, performed the absorption- and fluorescence spectroscopy experiments. PČ performed the molecular docking computations, contributed to the interpretation of data. JG isolated NKA and performed the ATPase activity measurements. MB performed the conformational analysis and prepared the flavonolignan molecules for docking. TŠ expressed and purified the C45 protein for spectroscopic analyses. PT participated to the conformational analysis and manuscript preparation. DB isolated, prepared, purified and supplied the compounds studied.

FUNDING

This work was supported by the grant LO1024 from the National Program of Sustainability I, by scholarship for MB from the French Embassy in the Czech Republic, and by grants 15-03037S and P208/12/G016 from the Czech Science Foundation.

ACKNOWLEDGMENTS

MB and PT wish to thank CALI (CAlcul en LImousin), where the calculations were performed. Prof. J. Ulrichová from the Dept. of Medical Chemistry and Biochemistry, Faculty of Medicine and Dentistry, Palacký University, is acknowledged for the logistic support and discusions.

REFERENCES

Agarwal, R., Agarwal, C., Ichikawa, H., Singh, R. P., and Aggarwal, B. B. (2006). Anticancer potential of silymarin: from bench to bed side. *Anticancer Res.* 26, 4457–4498.

Biedermann, D., Vavříková, E., Cvak, L., and Křen, V. (2014). Chemistry of silybin. *Nat. Prod. Rep.* 31, 1138–1157. doi: 10.1039/C3NP70122K

Bradford, M. M. (1976). A rapid and sensitive method for the quantitation of microgram quantities of protein utilizing the principle of protein-dye binding. *Anal. Biochem.* 72, 248–254.

Brewer, H. (2004). Historical perspectives on health: early Arabic medicine. *J. R. Soc. Promot. Health.* 124, 184–187. doi: 10.1177/146642400412400412

Džubák, P., Hajdúch, M., Gažák, R., Svobodová, A., Psotová, J., Walterová, D., et al. (2006). New derivatives of silybin and 2,3-dehydrosilybin and their cytotoxic and P-glycoprotein modulatory activity. *Bioorg. Med. Chem.* 14, 3793–3810. doi: 10.1016/j.bmc.2006.01.035

Frisch, M. J., Trucks, G. W., Schlegel, H. B., Scuseria, G. E., Robb, M. A., Cheeseman, J. R., et al. (2009). *Gaussian 09, version A02*. Wallingford, CT: Gaussian. Inc.

Gheorghiade, M., Adams, K. F. Jr., and Colucci, W. S. (2004). Digoxin in the management of cardiovascular disorders. *Circulation* 109, 2959–2964. doi: 10.1161/01.CIR.0000132482.95686.87

Grycova, L., Sklenovsky, P., Lansky, Z., Janovska, M., Otyepka, M., Amler, E., et al. (2009). ATP and magnesium drive conformational changes of the Na^+/K^+-ATPase cytoplasmic headpiece. *Biochim. Biophys. Acta* 1788, 1081–1091. doi: 10.1016/j.bbamem.2009.02.004

Havlíková, M., Huličiak, M., Bazgier, V., Berka, K., and Kubala, M. (2013). Fluorone dyes have binding sites on both cytoplasmic and extracellular domains of Na,K-ATPase. *Biochim. Biophys. Acta* 1828, 568–576. doi: 10.1016/j.bbamem.2012.10.029

Huličiak, M., Vacek, J., Šebela, M., Orolinová, E., Znaleziona, J., Havlíková, M., et al. (2012). Covalent binding of cisplatin impairs the function of Na^+/K^+-ATPase by binding to its cytoplasmic part. *Biochem. Pharmacol.* 83, 1507–1513. doi: 10.1016/j.bcp.2012.02.015

Jørgensen, P. L. (1988). Biomembranes Part P: ATP-driven pumps and related transport: the Na,K-Pump. *Methods Enzymol.* 156, 29–43.

Jorgensen, P. L., Håkansson, K. O., and Karlish, S. J. D. (2003). Structure and mechanism of Na,K-ATPase: functional sites and their interactions. *Annu. Rev. Physiol.* 65, 817–849. doi: 10.1146/annurev.physiol.65.092101.142558

Kaplan, J. H. (2002). Biochemistry of Na,K-ATPase. *Annu. Rev. Biochem.* 71, 511–535. doi: 10.1146/annurev.biochem.71.102201.141218

Klodos, I., Esmann, M., and Post, R. L. (2002). Large-scale preparation of sodium-potassium ATPase from kidney outer medulla. *Kidney Int.* 62, 2097–2100. doi: 10.1046/j.1523-1755.2002.00654.x

Koshland, D. E. (1995). the key–lock theory and the induced fit theory. *Angew. Chemie Int. Ed English.* 33, 2375–2378. doi: 10.1002/anie.199423751

Křenek, K., Marhol, P., Peikerová, Z., Křen, V., and Biedermann, D. (2014). Preparatory separation of the silymarin flavonolignans by Sephadex LH-20 gel. *Food Res. Int.* 65, 115–120. doi: 10.1016/j.foodres.2014.02.001

Kubala, M. (2006). ATP-binding to P-type ATPases as revealed by biochemical, spectroscopic, and crystallographic experiments. *Proteins* 64, 1–12. doi: 10.1002/prot.20969

Kubala, M., Geleticova, J., Huliciak, M., Zatloukalova, M., Vacek, J., and Sebela, M. (2014). Na^+/K^+-ATPase inhibition by cisplatin and consequences for cisplatin nephrotoxicity. *Biomed. Pap.* 158, 194–200. doi: 10.5507/bp.2014.018

Kubala, M., Grycova, L., Lansky, Z., Sklenovsky, P., Janovska, M., Otyepka, M., et al. (2009). Changes in electrostatic surface potential of Na^+/K^+-ATPase cytoplasmic headpiece induced by cytoplasmic ligand(s) binding. *Biophys. J.* 97, 1756–1764. doi: 10.1016/j.bpj.2009.07.002

Kubala, M., Plášek, J., and Amler, E. (2003b). Limitations in linearized analyses of binding equilibria: binding of TNP-ATP to the H4-H5 loop of Na/K-ATPase. *Eur. Biophys. J.* 32, 363–369. doi: 10.1007/s00249-003-0278-y

Kubala, M., Plášek, J., and Amler, E. (2004). Fluorescence competition assay for the assessment of ATP binding to an isolated domain of Na^+,K^+-ATPase. *Physiol. Res.* 53, 109–113. doi: 10.1021/bi010270

Kubala, M., Teisinger, J., Ettrich, R., Hofbauerová, K., Kopecký, V., Baumruk, V., et al. (2003a). Eight amino acids form the ATP recognition site of Na+/K^+-ATPase. *Biochemistry* 42, 6446–6452. doi: 10.1021/bi034162u

Loguercio, C., and Festi, D. (2011). Silybin and the liver: from basic research to clinical practice. *World J. Gastroenterol.* 17:2288. doi: 10.3748/wjg.v17.i18.2288

Morris, G. M., Huey, R., Lindstrom, W., Sanner, M. F., Belew, R. K., Goodsell, D. S., et al. (2009). AutoDock4 and AutoDockTools4: automated docking with selective receptor flexibility. *J. Comput. Chem.* 30, 2785–2791. doi: 10.1002/jcc.21256

Morth, J. P., Pedersen, B. P., Toustrup-Jensen, M. S., Sørensen, T. L.-M., Petersen, J., Andersen, J. P., et al. (2007). Crystal structure of the sodium–potassium pump. *Nature* 450, 1043–1049. doi: 10.1038/nature06419

Müller-Ehmsen, J., Juvvadi, P., Thompson, C. B., Tumyan, L., Croyle, M., Lingrel, J. B., et al. (2001). Ouabain and substrate affinities of human Na^+ -K^+ -ATPase α1β1, α2β1, and α3β1 when expressed separately in yeast cells. *Am. J. Physiol. Cell Physiol.* 281, 1355–1364.

Newman, R. A., Yang, P., Pawlus, A. D., and Block, K. I. (2008). Cardiac glycosides as novel cancer therapeutic agents. *Mol. Interv.* 8, 36–49. doi: 10.1124/mi.8.1.8

Nyblom, M., Poulsen, H., Gourdon, P., Andersson, M., Lindahl, E., and Fedosova, N. (2013). Crystal structure of Na^+, K^+-ATPase in the Na^+-bound state. *Science* 342, 123–127. doi: 10.1126/science.1243352

Ogawa, H., Shinoda, T., Cornelius, F., and Toyoshima, C. (2009). Crystal structure of the sodium-potassium pump (Na^+,K^+-ATPase) with bound potassium and ouabain. *Proc. Natl. Acad. Sci. U.S.A.* 106, 13742–13747. doi: 10.1073/pnas.0907054106

Pyszková, M., Biler, M., Biedermann, D., Valentová, K., Kuzma, M., Vrba, J., et al. (2015). Flavonolignan 2,3-dehydroderivatives: preparation, antiradical and cytoprotective activity. *Free Radic. Biol. Med.* 90, 114–125. doi: 10.1016/j.freeradbiomed.2015.11.014

Schack, V. R., Morth, J. P., Toustrup-Jensen, M. S., Anthonisen, A. N., Nissen, P., Andersen, J. P., et al. (2008). Identification and function of a cytoplasmic K^+ site of the Na^+,K^+-ATPase. *J. Biol. Chem.* 283, 27982–27990. doi: 10.1074/jbc.M803506200

Toustrup-Jensen, M. S., Holm, R., Einholm, A. P., Schack, V. R., Morth, J. P., Nissen, P., et al. (2009). The C terminus of Na^+,K^+-ATPase controls Na^+ affinity on both sides of the membrane through Arg935. *J. Biol. Chem.* 284, 18715–18725. doi: 10.1074/jbc.M109.015099

Trott, O., and Olson, A. J. (2010). AutoDock Vina: improving the speed and accuracy of docking with a new scoring function, efficient optimization, and multithreading. *J. Comput. Chem.* 31, 455–461. doi: 10.1002/jcc.21334

Trouillas, P., Marsal, P., Siri, D., Lazzaroni, R., and Duroux, J.-L. (2006). A DFT study of the reactivity of OH groups in quercetin and taxifolin antioxidants: the specificity of the 3-OH site. *Food Chem.* 97, 679–688. doi: 10.1016/j.foodchem.2005.05.042

Trouillas, P., Marsal, P., Svobodová, A., Vostálová, J., Gazák, R., Hrbác, J., et al. (2008). Mechanism of the antioxidant action of silybin and 2,3-dehydrosilybin flavonolignans: a joint experimental and theoretical study. *J. Phys. Chem. A.* 112, 1054–1063. doi: 10.1021/jp075814h

Vacek, J., Zatloukalová, M., Desmier, T., Nezhodová, V., Hrbáč, J., Kubala, M., et al. (2013). Antioxidant, metal-binding and DNA-damaging properties of flavonolignans: a joint experimental and computational highlight based on 7-O-galloylsilybin. *Chem. Biol. Interact.* 205, 173–180. doi: 10.1016/j.cbi.2013.07.006

Wang, J., Zhao, L., Sun, G., Liang, Y., Wu, F., Chen, Z., et al. (2011). A comparison of acidic and enzymatic hydrolysis of rutin. *J. Biotechnol.* 10, 1460–1466. doi: 10.5897/AJB10.2077

Watabe, M., Masuda, Y., Nakajo, S., Yoshida, T., Kuroiwa, Y., and Nakaya, K. (1996). The Cooperative interaction of two different signaling pathways in response to bufalin induces apoptosis in human leukemia U937 cells. *J. Biol. Chem.* 271, 14067–14073. doi: 10.1074/jbc.271.24.14067

Conflict of Interest Statement: The authors declare that the research was conducted in the absence of any commercial or financial relationships that could be construed as a potential conflict of interest.

Nucleotide Dynamics in the Na^+/K^+-ATPase

Petra Čechová[a], Karel Berka[b], Martin Kubala[a]*

[a] Department of Biophysics, Centre of the Region Hana for Biotechnological and Agricultural Research, Faculty of Science, Palacký University, Šlechtitelů 27, 783 71, Olomouc , Czech Republic

[b] Department of Physical Chemistry, Regional Centre of Advanced Technologies and Materials, Faculty of Science, Palacký University, 17. listopadu 12, 77146 Olomouc, Czech Republic

*corresponding author e-mail: martin.kubala@upol.cz

Abstract:

The Na^+/K^+-ATPase (NKA) is an essential cation pump responsible for the maintenance of the cell membrane potential. The creation of sodium and potassium gradients across the plasma membrane is energized by ATP hydrolysis. Here we report molecular dynamic simulations of the human NKA α1β1 isoform embedded into DOPC bilayer. We have analyzed the nucleotide behavior within its binding pocket, which is located on the cytoplasmic headpiece of the NKA, in a series of molecular dynamic simulations (ca. 2.5 μs of simulations in total). We found a large number of stable nucleotide positions, which can be influenced not only by the enzyme conformational changes, or the presence of cytoplasmic Mg^{2+} cation, and by the protonation state of residues in cation binding site (CBS), but not by the CBS-bound ions. Interestingly, we

observed that the binding of MgATP complex was substantially different when the sodium ions in the bulk solution were replaced by the potassium ones, which can be a part of a feedback loop for the pump functional regulation.

Introduction:

The sodium-potassium ATPase (NKA) is an essential membrane protein present in all animal cells. It uses the energy from ATP hydrolysis to transport Na^+ and K^+ ions across the plasma membrane, creating steep Na^+ ion gradient, which is a significant contribution to the plasma membrane potential and a driving force for numerous secondary active transporters[1].

The minimal functional unit of NKA consists of two main subunits denoted α and β. The main catalytic α-subunit is responsible for the cation transport as well as for ATP hydrolysis and contains the transient phosphorylation site at Asp376 (human α1 isoform sequence numbering). The β-subunit acts as a chaperone[2] and plays a role in K^+ ion selectivity[3]. It is anchored to the membrane by a single TM helix, but most of its mass forms the extracellular domain of NKA. Frequently, these two subunits are accompanied by a protein from the FXYD family, which is tissue-specific and probably serves as an enzyme modulator [4].

The catalytic α-subunit has 10 transmembrane (TM) helixes, and residues at TM4, TM5, TM6 and TM8 form the cation binding sites (CBS). In the cytoplasm, there are three functional domains, denoted as A (actuator), N (nucleotide binding) and P (phosphorylation site). The extended N-terminus and cytoplasmic loop between TM2 and TM3 (C23) form the A-domain, while the N- and P-domains are formed by cytoplasmic loop between TM4 and TM5 (C45).

While there are numerous groups exploring the cation binding sites (CBS) within the TM domain, the number of papers devoted to the analysis of nucleotide interaction with the enzyme is significantly lower. Particularly, the molecular mechanism explaining the coupling of the ATP

binding and hydrolysis, occurring in the cytoplasmic part, to the conformational changes observed in the TM domain, is still puzzling. Most of the reported experiments aimed at elucidation of structural details of ATP binding were based on use of ATP-analogues [5,6,7,8,9,10], site-directed mutagenesis[11,12,13] and variety of indirect spectroscopic and biochemical techniques. They, however, come from the period before the high-resolution structures were known, and their interpretation must be evaluated rather carefully. On the other hand, the recent X-ray crystallography determined structures (PDB entries 4HQJ,[14] 3WGU,[15] 3WGV [15]) contain of all the nucleotides only ADP or, in the case of relative P-type ATPase SERCA, TNP-ATP[16]. However, this analogue is known to serve as enzyme inhibitor[17], and its position within the binding pocket is probably slightly different from the natural ATP one[18]. Binding of the natural ATP has been displayed only in the case of isolated N-domain, by NMR (PDB entries 1MO7[19] 1MO8[19]). Substantial limitation of these NMR based structures is the absence of the P-domain containing the phosphorylation site. Despite none of the experiments being perfect (for critical review, see [20]), there is a general agreement about the localization of the nucleotide-binding pocket on the N-domain and the phosphorylation site on the P-domain.

To regulate the gating of the outward Na^+ and inward K^+ vectorial transport a sequence of enzyme conformational changes enabling an alternative opening of pathways to CBS from cytoplasm or extracellular milieu during the NKA pumping cycle is required. The conformational changes are driven by the binding of various ligands and transient autophosphorylation of the enzyme. The precise sequence of these complex interactions is a topic of ongoing debates. The X-ray crystallography determined structures revealed that with the sodium ions in the CBS, the cytoplasmic domains form a compact assembly (closed conformation[14]), while with potassium ions in CBS, they are well separated each from other

(open conformation[21]). Moreover, it was proposed that charged residues in CBS change their protonation state[22], influencing the enzyme conformation and affinity to cations. One also has to consider the Mg^{2+} ions that are not transported across the plasma membrane, but are known to be an essential NKA cofactor[23]. Although numerous authors assume that they are bound to the enzyme together with ATP as MgATP complex, recent experiments revealed that it makes good sense to consider Mg^{2+} and ATP binding as two different events in the catalytic cycle[24,25].

Molecular dynamics (MD) simulations are able to monitor movements of all atoms in the system and to assess even the distal effects of ligand binding. In our previous paper[26], we have created the human sequence NKA model embedded into a DOPC bilayer and analyzed the effects of various ligands on the opening of pathways for transported cations to CBS. We have performed further simulations, and this report is focused on the nucleotide interactions with the enzyme, monitoring the nucleotide binding protein residues and the nucleotide conformation. We ran MD simulations with various combinations of nucleotide bound to NKA in the form of ATP or ADP, in the presence or absence of Mg^{2+} ions, in two conformations of the protein (open/closed), with different ions in the cation binding site (Na^+/K^+), and with different ions in the bulk solution (NaCl/KCl).

Experimental Setup:

The protein is a homology model of human sequence (α1β1FYXD2, Uniprot IDs P05023, P05026 and P54710, respectively) based on the crystal structures with PDB ID 2ZXE[21] (open conformation) and 4HQJ[14] (closed conformation). It was inserted into a DOPC membrane using g_membed[27] and hydrated in a 15x15x20 nm box. Periodic boundary conditions were applied in all directions. To achieve more physiological environment, additional sodium, potassium and chlorine ions were added to the bulk solution in concentration 154 mM of NaCl or KCl,

respectively. The main 100 ns-long simulation run was preceded by a 10 ns run with restrains on the protein backbone movement. In the simulation with the closed protein conformation, nucleotide molecule was in the position corresponding to ADP + inhibitor in the crystal structure. In the open protein conformation, ATP was placed near F482 as argued in ref. [24] (unless otherwise stated, all residue numbers correspond to human α1 sequence).

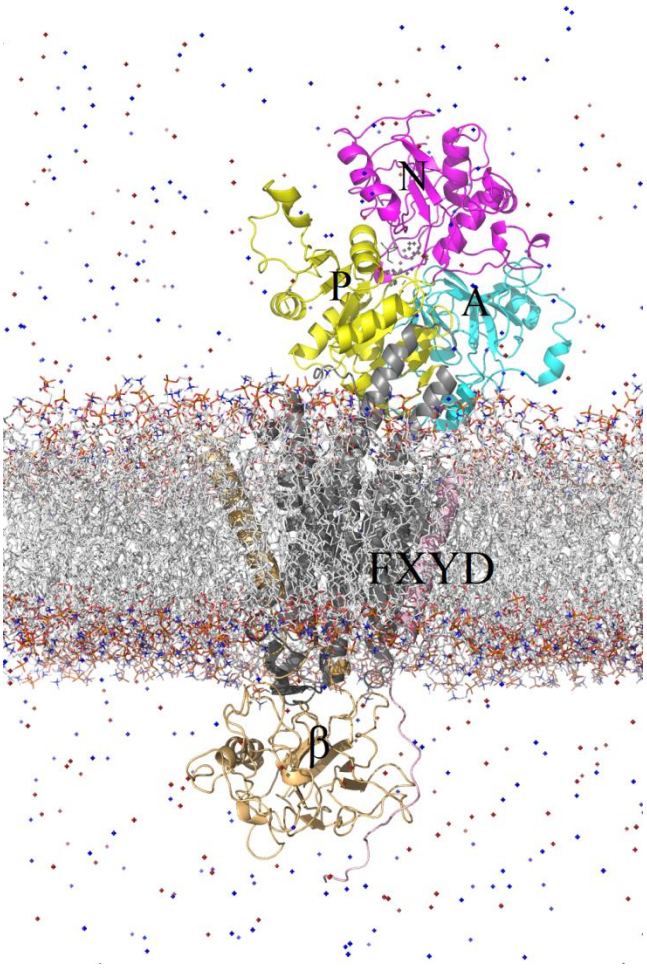

Figure 1: Simulation box – the transmembrane domain of the α-subunit is in grey, A-domain in cyan, N-domain in magenta, P-domain in yellow, β-subunit in pale orange, the FXYD protein in light grey, the membrane lipids in white, bulk ions in red (chlorine) and blue (sodium or potassium).

Force field used for the protein, ATP and ions was gromos53a6, the Berger force field[28] was used for lipids and parametrization according to ref. [29] was used for Pi and ref. [30] for ADP.

The simulation was performed and evaluated using GROMACS 5.1.2[31] and home-made scripts. PyMol and VMD were used for data visualization. Residues binding the nucleotide were found using PLIP with default settings[32] and Maestro ligand interaction tool[33] from the final frame of a simulation, without water molecules and by analyzing residue distances during the last 10 ns of the simulation using the GROMACS g_mindist program. Residues closer than 0.35 nm to the nucleotide in more than a half of the final frames were taken into account.

Each simulation is a different combination of either open or closed protein conformation (denoted as O or C in the simulation name), ions in the CBS (sodium or potassium), the presence or absence of one magnesium ion at D736, different molecules at the cytoplasmic domains (ATP, ADP, Pi) and with either sodium or potassium cations in the bulk solution (the latter denoted as KSOL). In the majority of the simulations, the CBS residues were deprotonated; in some of the simulations (denoted by prefix h), E344, E786 and E961 were protonated as argued in refs 34 and 22. The full list of acronyms for various simulation setups is in the Table S1 in Supplementary Information.

Results and Discussion

High Resolution Structures Nucleotide Binding

The first experimental information about the nucleotide binding site came from the NMR-determined structure of isolated N-domain in complex with ATP (1MO8[19]). The N-domain is composed of five alternating β-sheets and α-helices and the ATP was bound in the pocket formed by the ends of sheets β3 and β4 (F482, K487 and K508-E513), with the contribution of the lower

part of sheet β5, and hydrogen bonding between adenine moiety and Gln489 was observed (Fig. 2).

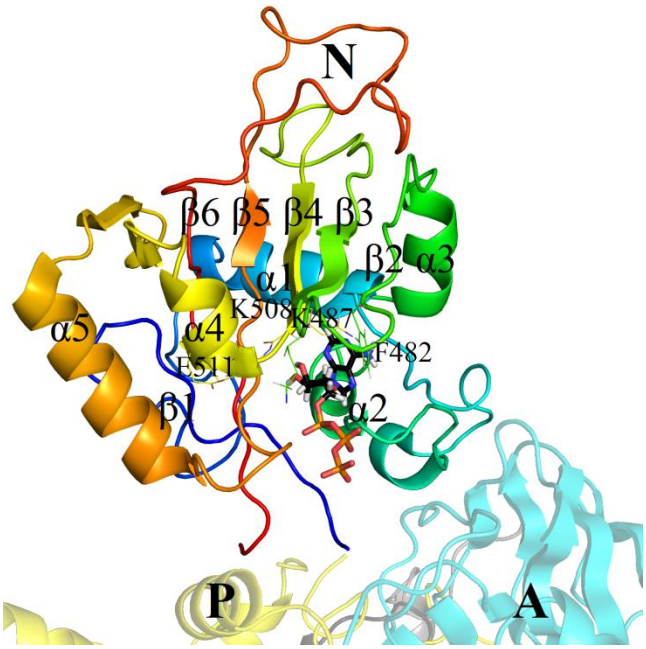

Figure 2: The N-domain structure 1MO8, colored according to the residue number blue to red, sheets and helices labeled according to [19], aligned to the open structure of NKA. ATP binding residues F482, K487 and K508-E513 are displayed in lines.

There are three NKA crystal structures with bound nucleotide (4HQJ[14], 3WGU[15] and 3WGV[15]). In all cases, they were obtained for a state with the enzyme in the closed conformation with three Na^+ ions bound in the CBS and the nucleotide in the form of ADP and AlF_4^- ion serving as a phosphate analogue. An Mg^{2+} ion is also present in the proximity of phosphate chain; moreover, two such ions were reported in 3WGU and 3WGV.

In the 4HQJ crystal, adenine is held by π-stacking interactions at F482 and by hydrogen bonds by D450 and S452. R551, R692 and H620 bind the ribose in the crystal (Fig. 3). T378 and N720 take part in the phosphate chain binding, D376 binds AlF_4. In 3WGU, adenine is bound by the same residues as in 4HQJ, with the addition of E453. V552 and R692 bind the ribose, K377,

T379, K487, S484, R551, D619 and N720 take part in the phosphate chain binding. In 3WGV, the ADP is bound similarly to 3WGU, only R551 doesn't bind the phosphate chain but the ribose, and K377 does not participate in binding.

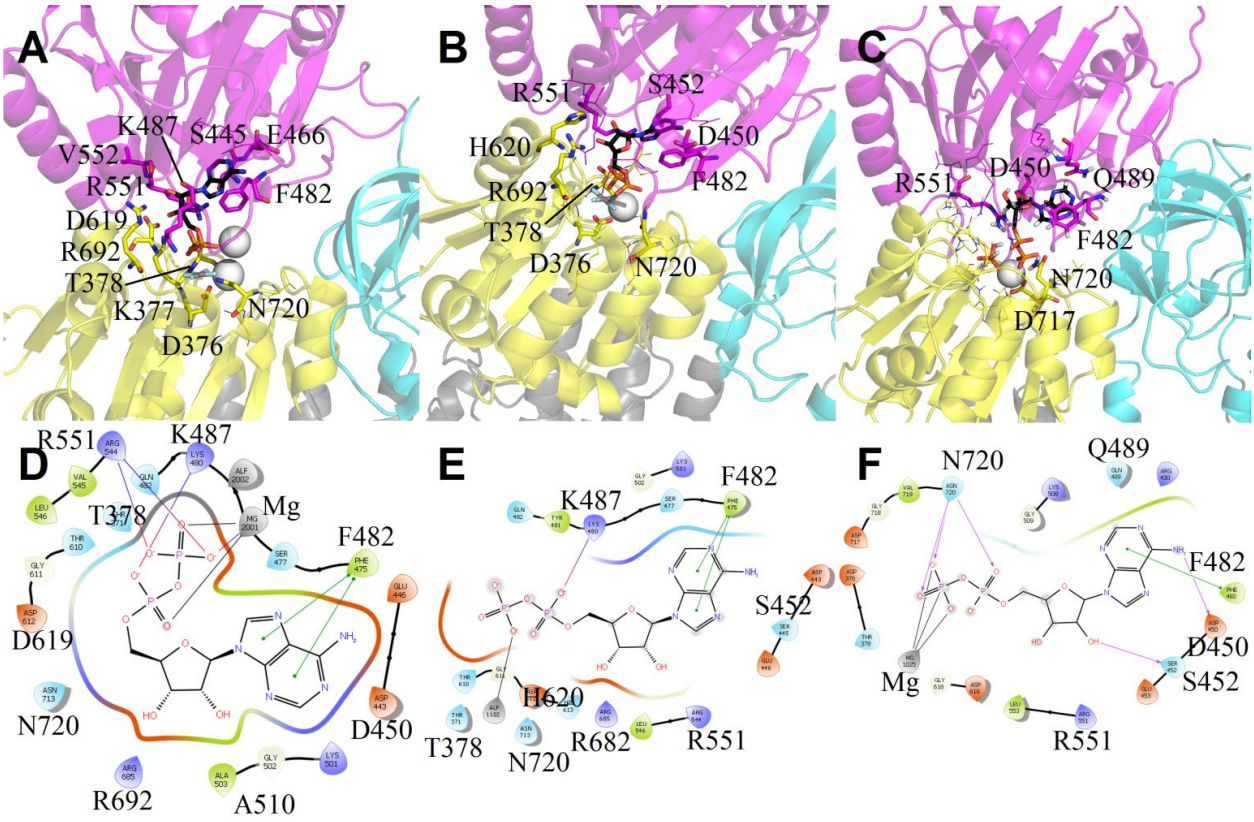

Figure 3: The nucleotide binding site in 3WGU (A), in 4HQJ (B) and the nucleotide position of hC_3Na_Mg_ADP_Pi in the first frame after the 10 ns prerun (C) as calculated by PLIP. A-domain is in cyan, P-domain in yellow, N-domain in magenta, Mg^{2+} ion in a ball representation white, Na^{+} ion blue. The corresponding ligand interaction diagrams are below as D, E, F, respectively. Charged negative residues are in red, charged positive in dark blue, polar in light blue, hydrophobic in green, glycine in white, metals in grey. Interactions are: π –π stacking green line, H-bond with sidechain purple to red, metal interactions in grey.

We compared also the crystal structures with the structures in the simulations under corresponding conditions. In line with experimental data previously published for SERCA[35], our simulations indicate that there may be differences between enzyme/ligand geometries observed in the crystals and geometries for the molecules that form the complex in the solution. In the hC_3Na_Mg_ADP_Pi structure after 10 ns prerun, the ADP is bound similarly to the 4HQJ crystal, but the adenine moves away from S452 towards Q489. In addition to N720, the phosphate chain is bound by D717 instead of H620 and R692. Unlike AlF_4^-, which stays near D376, the phosphate is bound not only by D377 and T378 but also moves towards the segment T617-D619 (Fig. 3).

The Nucleotide Binding Sites

The nucleotide adopts different positions depending on the presence of other ligands, enzyme conformation and nature of cations in the solvent. Based on the PLIP[32] analysis of direct nucleotide interactions with amino acids, we could sort the most frequently present residues into five major clusters (Fig. 4). Residues mentioned here are taking part in binding in at least five simulations; those present in more than ten simulations are in bold. These results are corroborated by both ligand interaction diagrams and the residue distance analysis from the last 10 ns of simulations.

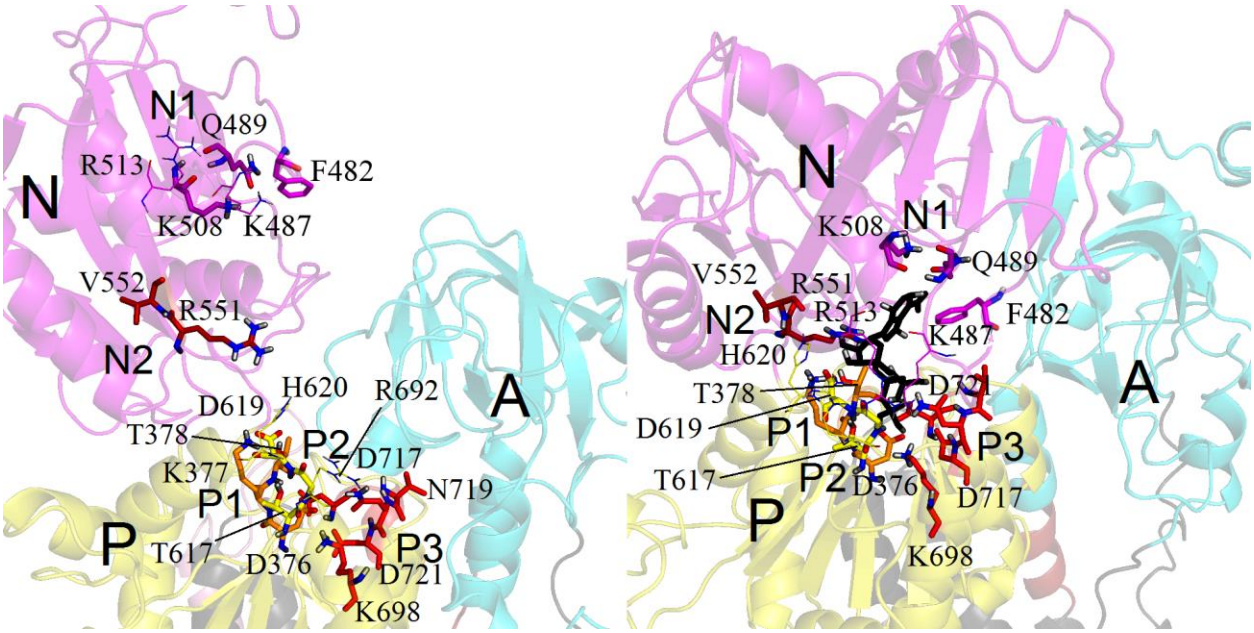

Figure 4: Nucleotide binding site in the open (left) and closed (right) conformation of the NKA. A-domain is in cyan, P-domain in yellow, N-domain in magenta. The residues in abovementioned sites are in stick representation. Site P1 in orange, P2 yellow, P3 and N2 different shades of red, N1 in purple. K487, R513, H620, and R692 are displayed in lines.

Phosphate sites are well located on the P domain. ***Site P1*** consists of the phosphorylated **D376** identified by mutagenesis studies[36] and neighboring **K377** and **T378**. These residues bind the terminal ATP/ADP phosphate and the Mg^{2+} or bulk ion, which is in a good agreement with finding that this segment is proximal to ATP, as revealed by iron-oxidative cleavage experiments (Fe^{2+} is Mg^{2+} analog)[37]. ***Site P2*** is made by residues **T617**, **G618**, **D619** and this site takes part in binding of the ATP/ADP phosphate chain and/or ribose. ***Site P3*** is located opposite to site P2 with respect to D376, and it is comprised of **K698**, and residues D717, V719, N720 and D721, which have been previously identified as Mg^{2+}-binding site[38], thus supporting our findings.

This site takes a direct part in the nucleotide binding less frequently than the previous ones, because the bound ion (especially in the simulations without magnesium present) is situated

between this site and the phosphate chain of the nucleotide. This effect is less pronounced for K698 as there is a hinge between the helix, where it is located, and the D717-D721 loop, which is also closer to the A-domain and can be influenced by its movements.

The binding sites on the N-domain binding sites are a less defined, but there are still residues that bind the nucleotide with high frequency. The N-domain is also rich in residues with long side-chains (e.g. arginine or lysine), which can reach relatively far into the space between the domains. ***Site N1*** ends at the hydrogen bond between the backbone of **Q489** and K508 on sheets β3 and β4, respectively, and it is lined by these two residues, which were identified previously to participate to the nucleotide binding[12,13,39,40]. In the last 10 ns analysis, G509 (identified in the 2-azido-ATP labeling experiments[6] and A510 also appear close to the nucleotide. The crucial ATP-coordinating residue **F482**[12] (on the loop connecting β2 and β3), where the ATP in the open structures was placed, is located in the vicinity of the binding site N1, but the π-stacking interaction between this residue and the nucleotide was not observed in the final frame analysis, possibly due to strict PLIP and ligand interaction binding criteria for π-stacking. However it is present in more than two thirds of the simulations in the analysis results from last 10 ns of simulation. ***Site N2*** consists of the main chain parts **R551** and **V552** at the start of the β5 strand. It binds the ribose or nucleotide of ATP/ADP, depending on the orientation of the molecule in the binding pocket, which is in agreement with previous mutagenesis experiments [41]. In the analysis from the last 10 ns of simulation, L553 is also in the vicinity to the nucleotide and, similarly to V552, can take part in its binding with its backbone.

K487 identified to contribute to the ATP binding by both labeling and mutagenesis experiments [5,41] was not included in any of the previous binding sites, even though it takes part in nucleotide binding in more than 80% of the simulations. It typically contributes to phosphate

chain binding with its sidechain, but it can also bind the adenine part with its main chain. This dual role is in line with conclusions based on experiments with analogs pyridoxal 5´-diphospho-5´-adenosine and pyridoxal phosphate[7].

Given the fact that ATP in the open simulations was placed near F482 on the N-domain, and the large distance between cytoplasmic domains, it is not surprising that the nucleotide binds to the P-sites only in the simulations with the closed conformation. H620 and R692 can, however, extend their sidechains out to the space and therefore reach far enough to capture the phosphate chain of the ATP even in the open conformation of the domains. In the closed conformation H620 faces outwards, where it binds the adenine in hC_2K_Mg_ATP, while R692 does not take part in nucleotide binding.

R513 is on the outer side of the N-domain α4 loop and takes part in binding the nucleotide outside the N-domain binding sites, in the simulations where ATP leaves the N-domain binding pocket.

Previous experiments revealed that the above mentioned amino acid in the clusters play important role in the interaction with the nucleotide. They are also part of the sequences 376DKTGTLT, 508KGAPE, 615MVTGD and 712VAVTGDGVNDS, which are conserved among P-type ATPases[42], indicating that they are essential for the enzyme function.

The Nucleotide Conformation

Large number of experiments has been performed with various ATP analogues. From the point of view of NKA function, some of them can serve as enzyme substrates, others as inhibitors. Previous experiments revealed that the ribose flexibility is preserved in the former group, while modification results in ribose fixation in C2´-endo or C3´-endo conformation in the latter[17].

Hence it seems that the nucleotide conformation plays an important role and it must vary during the catalytic cycle.

The nucleotide conformation can be described using different dihedral angles[43]. The ribose carbons dihedral angle C1'-C2'-C3'-C4' was evaluated to describe the conformational changes of the sugar moiety. C1'-C2'-C3'-C4'>180 corresponds to the C2'-endo conformation, while C1'-C2'-C3'-C4'<180 corresponds to the C3'-endo one. The relative position of the adenine with respect to the ribose is described by the O4'-C1'-N9-C4 dihedral angle (Fig. 5).

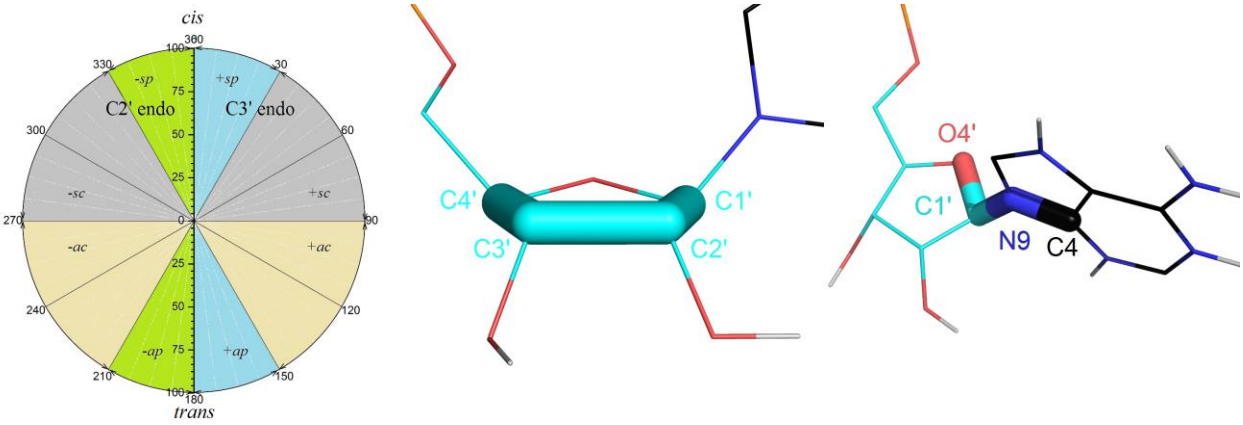

Figure 5: The angle circle and the dihedral angle between the ribose carbons and between the ribose and the adenine. The positive values are in the clockwise direction viewed from the first bond, letters correspond to the sp, synperiplanar; sc, synclinal, ap, antiperiplanar; ac, anticlinal positions respectively.

The angles measured during all the simulations show that there are two main conformations of the adenine moiety – one at about 50±20° (+sc), another one at about 250±35° (-ac). The adenine angle is, interestingly, more varied in the closed conformation, while in the open conformation there is a distinct trend of a time dependent angle change, with several simulations ending in the +sc area at the end of the simulation. The angles in the open conformation seem to be more evenly spread around the 60° value, while in the closed conformations, they are shifted towards

45°. Contrary, the angles in the closed simulations are more evenly spread across the –ac area, while the open ones are shifted towards 250°.

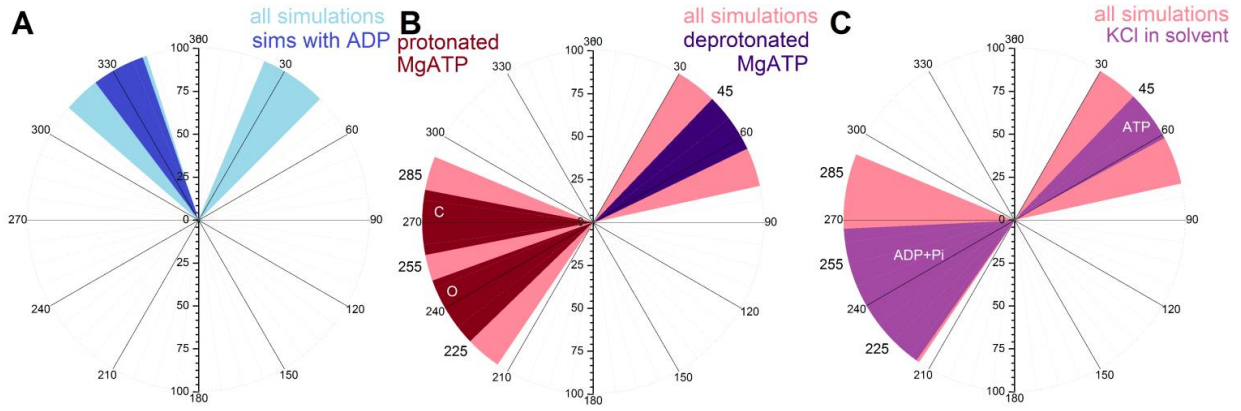

Figure 6: The area where most of the dihedral angle values are present for ribose (A) - light blue depicts the angle range where most of the values lie in all the simulations, and dark blue depicts the most frequent angle range for the simulations with bound ADP. The other images show the angle between ribose and adenine, with the pink area depicting the angle range where most of the values lie in all the simulations and in B) purple highlighted area shows the angle range for simulations with MgATP and deprotonated CBS, while crimson shows the angle range for simulations with MgATP and protonated CBS in open and closed conformations. In C, the violet highlighted area shows the ribose-adenine dihedral angle range for simulations with KCl in the bulk solutions for simulations with bound ATP or ADP+Pi, respectively.

The ribose angles in the C2'-endo conformation are spread more around 330° in the closed conformations and at 340° in the open ones and at about 35° in the C3'-endo conformation. The largely prevalent ribose conformation is the C2′-endo; the C3′-endo is present only in three simulations, C_3Na_Mg_ATP, C_2K_Mg_ATP, and C_2K_Mg_ATP_KSOL. As can be seen, the conformation of the protein changes also the preference of conformation of the ATP bound.

The Effect of Ligands

ATP vs. ADP+Pi

Our simulations revealed that ATP can be located at numerous binding sites and adopts variable conformations with respect to both adenine and ribose angle. Only in the simulations with ATP in the absence of magnesium ion (C_3Na_ATP, C_3Na_ATP_KSOL), the nucleotide stays in a position similar to the crystal one – with the adenine in the vicinity of the N1 site and the ribose at R551 (C_3Na_ATP) or with the ribose near the P2 site residues (C_3Na_ATP_KSOL, with R551 contributing to the phosphate chain binding). In C_3Na_Mg_ATP, the adenine is fully in the N2 site and the ribose O4' is held by R551 while O2' and O3' are turned towards the bulk solution (since 63 ns).

In the open structures, the nucleotide can in principle move more freely; nevertheless, it stays mostly in the vicinity of the binding sites N1 and N2. However, although the ATP molecule was originally placed in the vicinity of F482, the adenine usually moved away from the residue. In the simulations with ATP and magnesium and deprotonated CBS (O_2K_Mg_ATP, O_3Na_Mg_ATP), the nucleotide remains in a similar position to the one in the closed conformation, with the adenine in the N1 site and the ribose in the N2 site. In O_3Na_Mg_ATP, E453 of the α2 helix also takes part in nucleotide binding. In the simulations without magnesium, the nucleotide position is more variable – in O_3Na_ATP the ribose moves from the N2 site towards the α5 helix and the P-domain, while the adenine points into the bulk solution, while in O_2K_ATP the whole nucleotide is in the position between the N- and A- domains.

The ATP is hydrolyzed to ADP and inorganic phosphate during the catalytic cycle, and logically, it is expected that this reaction occurs when the cytoplasmic domains are in the closed conformation, where the γ-phosphate approaches the phosphorylation site. We tested this by replacing ATP by ADP+Pi and these simulations were run in two different setups. Either the

ADP+Pi were placed directly into the initial structures based on crystals (these are denoted ADP_Pi in the acronym) or after the end of selected simulations ATP molecule was replaced by ADP and phosphate (denoted as ATP2D). In general in the ADP-bound simulations, the conformation variability of the nucleotide is much lower compared to the ATP-bound ones; in particular, the ribose angle spread is very narrow around 325° in the simulations with ADP (Fig. 6). The free phosphate (Pi) is bound either in the P1 site (K377, T378) or in the P2 site (T617, G618).

In the simulations with ADP+Pi, starting from the crystal structure, the nucleotide moves away from the N domain binding sites, partially in C_3Na_Mg_ADP_Pi (the adenine is between K487 and R551) or completely in C_3Na_Mg_ADP_Pi_KSOL, where the nucleotide hangs between the N-domain's α4 helix and the P-domain (Fig. 7). If the ATP is replaced by ADP+Pi with Na^+ in the CBS (C_3Na_Mg_ATP2D), the nucleotide is held between the N2 site and K487, while both the O2' and O3' of the ribose are held by D450 of the α2 helix (since 90 ns). The simulation where ATP was exchanged for ADP+Pi with K^+ in CBS (C_2K_Mg_ATP2D) differs from the others. The phosphate leaves the binding site and moves freely in the bulk solution in this simulation, and the nucleotide turns so that the adenine is between the N2 site and the β4/α4 loop, and the ribose points towards K487.

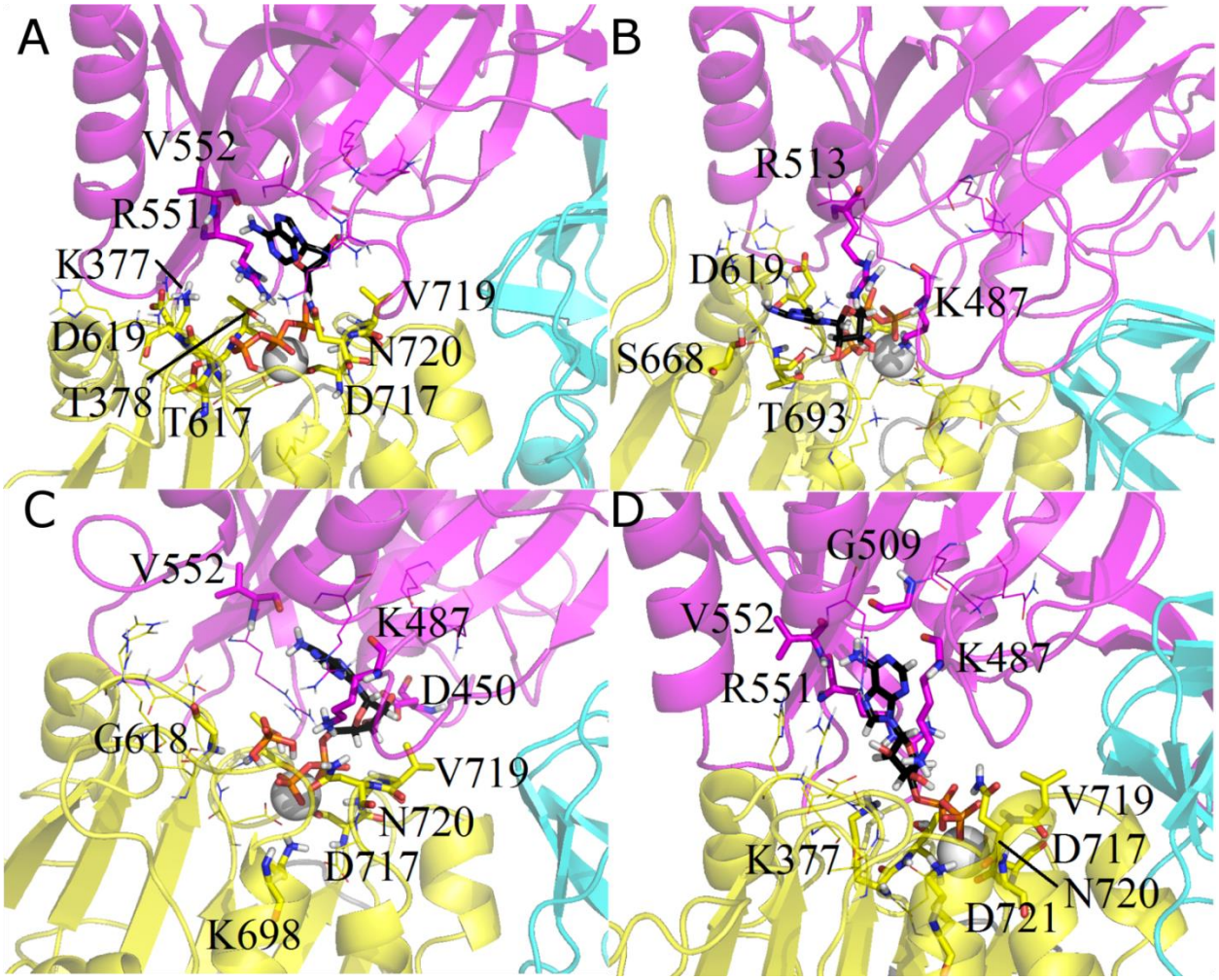

Figure 7: The final frames of simulations C_3Na_Mg_ATP (A), C_3Na_Mg_ADP_Pi_KSOL (B), C_3Na_Mg_ATP2D (C) and C_2K_Mg_ATP2D (D) A-domain in cyan, P-domain in yellow, N-domain in magenta, Mg^{2+} ion as a white sphere.

Effect of Mg^{2+} and protonation of CBS

In general, magnesium ions have stabilizing effect on the protein and on ligand-binding. In the simulation C_2K_ATP without magnesium ion, the nucleotide moves away from the N2 site completely and it is held only between the N1 site (adenine) and D619 of the P2 site (Fig. 8B). In the simulation with protonated CBS (hC_2K_ATP), the adenine is in the vicinity of the N1 site and the ribose is held only by the sidechain of R551. D430 of the loop between the α1 and α2 helices takes part on the phosphate chain binding. In hO_2K_ATP the nucleotide moves between

the N- and the P- domains. In hO_3Na_ATP the adenine moves to the N2 site and the ribose shifts towards the α4 helix.

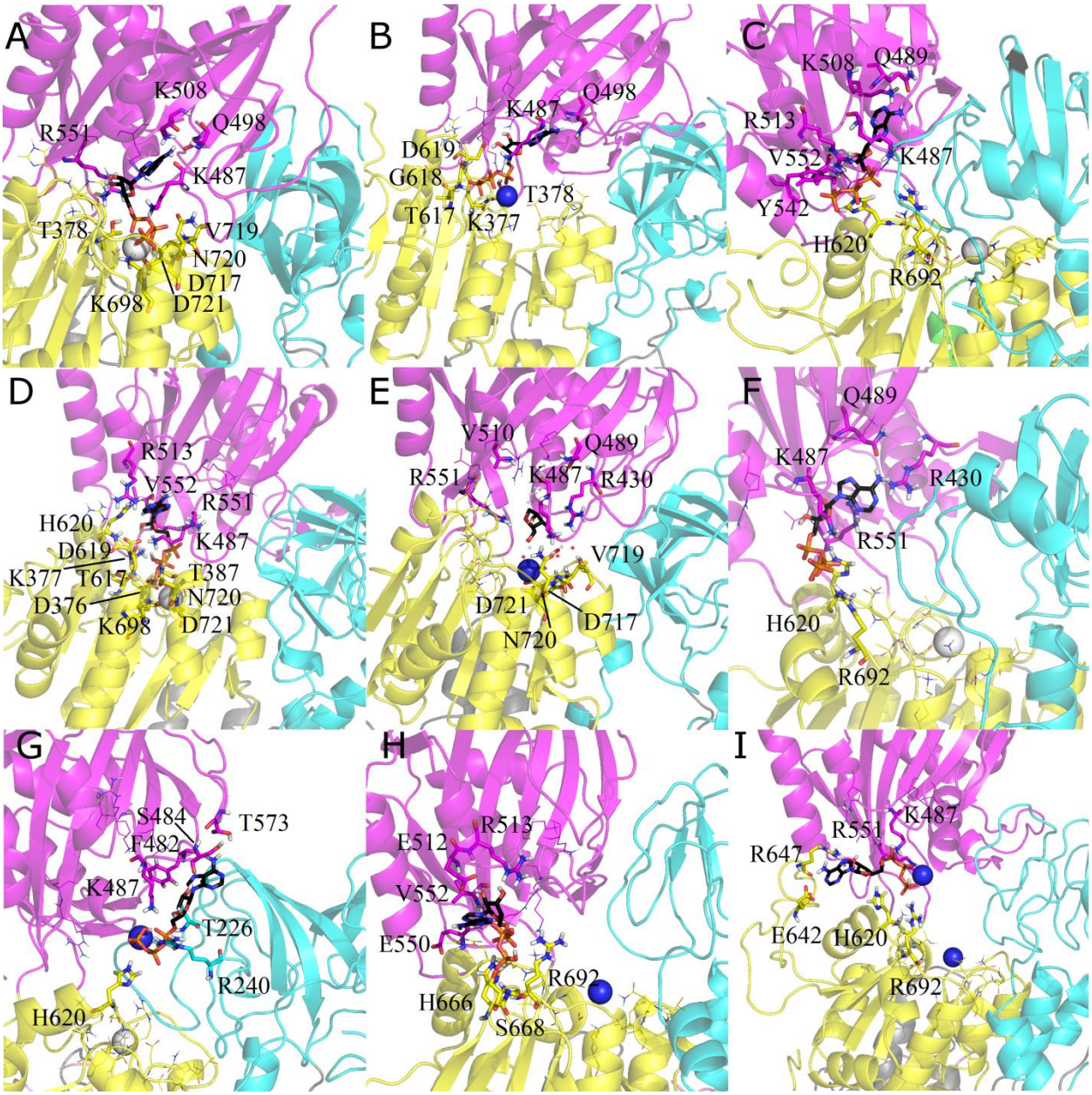

Figure 8: The final frames of C_2K_Mg_ATP (A), C_2K_ATP (B) and O_2K_Mg_ATP (C),hC_2K_Mg_ATP(D), hC_2K_ATP (E), hO_2K_Mg_ATP(F), hO_3Na_Mg_ATP(G), hO_3Na_ATP(H), hO_2K_ATP(I). A-domain is in cyan, P-domain in yellow, N-domain in magenta, Mg^{2+} ion as a white sphere, Na^{+} ions as blue spheres.

The influence of Mg^{2+} on nucleotide can be understood only when other factors are taken into account. The analysis revealed that if the enzyme has deprotonated residues in CBS, the adenine angle in the Mg^{2+} presence is restricted to 55°±10°, corresponding to +sc conformation. When the CBS are protonated, this angle is around 270° for the enzyme in closed conformation and around 240° (-ac) for the enzyme in the open conformation (Fig. 6).

In the simulations with closed conformation of the protein and protonated CBS, potassium in the CBS and magnesium at the phosphorylation site (hC_2K_Mg_ATP), the ribose is held between the N2 site and the P domain, while the adenine is out of the binding pocket and stays at R513 of the α4 helix. In the simulations with open conformation and protonated CBS, the nucleotide can also move considerably. It stays in the vicinity of Q489 and R430 in hO_2K_Mg_ATP, with the ribose in the N2 site, while it is between the N- and A- domains in hO_3Na_Mg_ATP.

Effect of the transported cations

In the traditional description, the pumping cycle is depicted by the Post-Albers scheme, in which the enzyme conformation switches between states E1 and E2 with high affinity to sodium or potassium ions, respectively. In the experiments, high concentration of sodium or potassium is used, in order to force the enzyme to adopt one of the abovementioned conformations and it has been known for a long time that the enzyme has high or low affinity to the nucleotide in these states, respectively [44].

The nature of cations in CBS seems to have rather little effect on the nucleotide binding interactions and most of the residues bind in a similar fashion regardless of the ions in the CBS.In contrast, the nature of cations in bulk solution can affect the nucleotide binding. Normally, the simulations were performed with sodium ions in the bulk solution, but in five

cases, they were substituted by potassium ions. Also here, residues from all binding sites can take part in the nucleotide binding, with the exception of site P3, where only D717 takes part and only in one simulation. In the simulations with KCl in the bulk solution, the adenine angles fall into narrower areas – around 50° for ATP around 240° for the ADP (Fig. 6). In C_3Na_Mg_ATP_KSOL simulation, the nucleotide adopts completely different position and it is located between the β4 and β5 sheets with the ribose held by D450 of the α2 helix (Fig. 9).

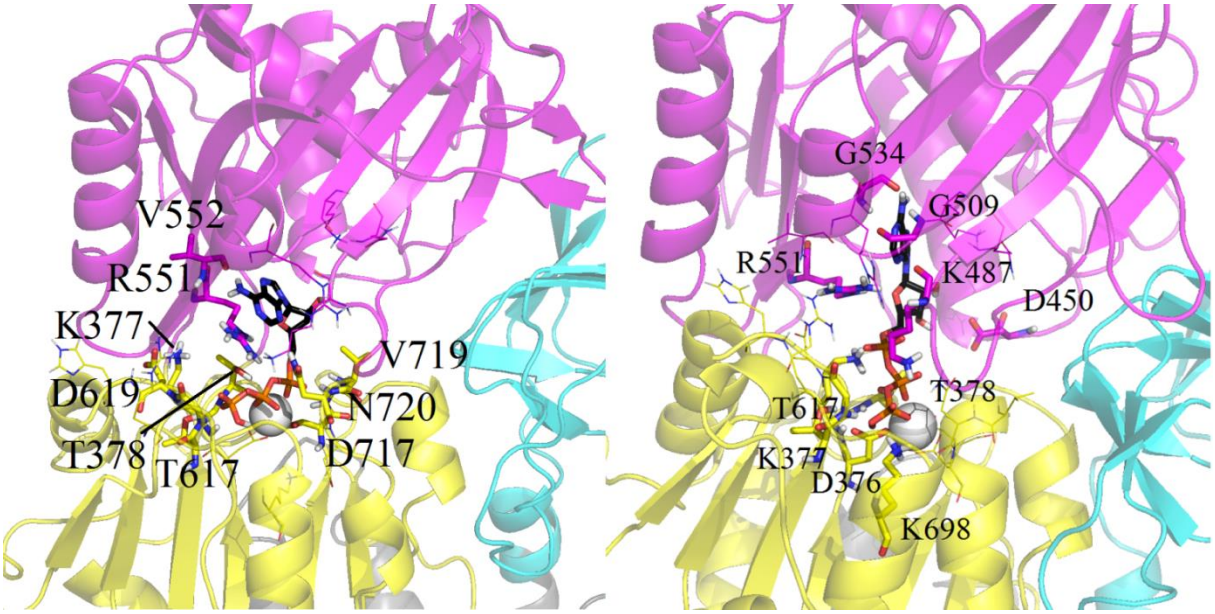

Figure 9: C_3Na_Mg_ATP (left) and C_3Na_Mg_ATP_KSOL (right). A-domain is in cyan, P-domain in yellow, N-domain in magenta, Mg^{2+} ion as a white sphere.

This observation can have interesting consequences for the enzyme function. The goal of the enzyme under normal physiological conditions is to expel sodium ions and bring potassium ions to the cytoplasm. Our observation suggests that this cation exchange can influence the enzyme affinity to the nucleotide, which can serve as a kind of feedback for the enzyme function.

Conclusions

The nucleotide interaction with NKA is one of the key events in the pumping cycle and the ATP hydrolysis provides energy for whole the cation transportation process. Our simulations revealed that the nucleotide interaction with NKA is a very dynamic event and that there is a large number of various stable nucleotide positions when it is bound to the enzyme. The position of the nucleotide is influenced not only by the conformational state of the enzyme, but also by the presence of other ligands, and interestingly, also by the nature of cations in the bulk solution. Consequently, it seems that nucleotide binding affinity is not constant during the catalytic cycle, and experimentally determined values are either valid only for the given state under given experimental conditions or averaged values for multiple substates.

Acknowledgements

This work was supported by grant No. LO1204 (Sustainable development of research in the Centre of the Region Haná) from the National Program of Sustainability I, MEYS. Computational resources were provided by the CESNET LM2015042 and the CERIT Scientific Cloud LM2015085, provided under the programme "Projects of Large Research, Development, and Innovations Infrastructures".

References

(1) Jorgensen, P. L., Hakansson, K. O., and Karlish, S. J. D. (2003) Structure and mechanism of Na,K-ATPase: functional sites and their interactions. *Annu. Rev. Physiol. 65*, 817–849.

(2) Geering, K. (2008) Functional roles of Na,K-ATPase subunits. *Curr. Opin. Nephrol. Hypertens. 17*, 526–532.

(3) Toyoshima, C., Kanai, R., and Cornelius, F. (2011) First crystal structures of Na+,K+-ATPase: new light on the oldest ion pump. *Structure 19*, 1732–1738.

(4) Geering, K. (2006) FXYD proteins: new regulators of Na-K-ATPase. *Am. J. Physiol. Renal Physiol. 290*, F241–F250.

(5) Tran, C., Scheiner-Bobis, G., Schoner, W., and Farley, R. (1994) Identification of an amino acid in the ATP binding site of Na(+)/K(+)-ATPase after photochemical labeling with 8-azido-ATP. *Biochemistry. 33*, 4140–4147.

(6) Tran, C., Huston, E., and Farley, R. (1994) Photochemical labeling and inhibition of Na,K-ATPase by 2-Azido-ATP. Identification of an amino acid located within the ATP binding site. *J. Biol. Chem. 269*, 6558–6565.

(7) Hinz, H. R., and Kirley, T. L. (1990) Lysine 480 is an essential residue in the putative ATP Site of lamb kidney (Na,K)-ATPase: Identification of the pyridoxal 5'-diphospho-5'-adenosine and pyridoxal phosphate reactive residue. *J. Biol. Chem. 265*, 10260–10265.

(8) Farley, R. A., Tran, C. M., Carilli, C. T., Hawke, D., and Shively, J. E. (1984) The amino acid sequence of a fluorescein-labeled peptide from the active site of (Na,K)-ATPase. *J. Biol. Chem. 259*, 9532–9535.

(9) Kubala, M., Plášek, J., and Amler, E. (2003) Limitations in linearized analyses of binding equilibria: Binding of TNP-ATP to the H4-H5 loop of Na/K-ATPase. *Eur. Biophys. J. 32*, 363–369.

(10) Kubala, M., Obšil, T., Obšilová, V., Lánský, Z., and Amler, E. (2004) Protein Modeling Combined with Spectroscopic Techniques: An Attractive Quick Alternative to Obtain Structural Information. *Physiol. Res. 53*, S187–S197.

(11) McIntosh, D. B., Woolley, D. G., Vilsen, B., and Andersen, J. P. (1996) Mutagenesis of Segment 487 Phe-Ser-Arg-Asp-Arg-Lys492 of Sarcoplasmic Reticulum Ca 2+ -ATPase Produces Pumps Defective in ATP Binding *271*, 25778–25789.

(12) Kubala, M., Krumscheid, R., and Schoner, W. (2002) Phe 475 and Glu 446 but not Ser 445 participate in ATP-binding to the a -subunit of Na+/K+-ATPase. *Biochem. Biophys. Res. Commun. 297*, 154–159.

(13) Kubala, M., Teisinger, J., Krumscheid, R., and Schoner, W. (2003) Eight Amino Acids Form the ATP Recognition Site of Na + /K + -ATPase. *Biochemistry* 6446–6452.

(14) Nyblom, M., Poulsen, H., Gourdon, P., Reinhard, L., Andersson, M., Lindahl, E., Fedosova, N. U., and Nissen, P. (2013) Crystal Structure of Na+, K+-ATPase in the Na+-Bound State. *Science 342*, 123–127.

(15) Kanai, R., Ogawa, H., Vilsen, B., Cornelius, F., and Toyoshima, C. (2013) Crystal structure of a Na + -bound Na +,K + -ATPase preceding the E1P state. *Nature 502*, 201–206.

(16) Toyoshima, C., Nakasako, M., Nomura, H., and Ogawa, H. (2000) Crystal structure of the calcium pump of sarcoplasmic reticulum at 2.6 [angst] resolution. *Nature 405*, 647–655.

(17) Thoenges, D. (1999) Tight Binding of Bulky Fluorescent Derivatives of Adenosine to the Low Affinity E2ATP Site Leads to Inhibition of Na+/K+-ATPase. *J. Biol. Chem. 274*, 1971–1978.

(18) Lánský, Z., Kubala, M., Ettrich, R., Kutý, M., Plášek, J., Teisinger, J., Schoner, W., and Amler, E. (2004) The Hydrogen Bonds between Arg 423 and Glu 472 and Other Key Residues , Asp 443 , Ser 477 , and Pro 489 , Are Responsible for the Formation and a Different Positioning of TNP-ATP and ATP within the Nucleotide-Binding Site of Na + / K + -ATPase. *Biochemistry 43*, 8303–8311.

(19) Hilge, M., Siegal, G., Vuister, G. W., Güntert, P., Gloor, S. M., and Abrahams, J. P. (2003) ATP-induced conformational changes of the nucleotide-binding domain of Na,K-ATPase. *Nat. Struct. Biol. 10*, 468–474.

(20) Kubala, M. (2006) ATP-Binding to P-Type ATPases as Revealed by Biochemical , Spectroscopic , and Crystallographic. *Proteins Struct. Funct. Bioinforma. 12*, 1–12.

(21) Shinoda, T., Ogawa, H., Cornelius, F., and Toyoshima, C. (2009) Crystal structure of the sodium-potassium pump at 2.4 A resolution. *Nature 459*, 446–450.

(22) Poulsen, H., Khandelia, H., Morth, J. P., Bublitz, M., Mouritsen, O. G., Egebjerg, J., and Nissen, P. (2010) Neurological disease mutations compromise a C-terminal ion pathway in the Na(+)/K(+)-ATPase. *Nature 467*, 99–102.

(23) Skou, J. C. (1960) Further investigations on a Mg++ + Na+-activated adenosintriphosphatase, possibly related to the active, linked transport of Na+ and K+ across the nerve membrane. *Biochim. Biophys. Acta 42*, 6–23.

(24) Kubala, M., Grycova, L., Lansky, Z., Sklenovsky, P., Janovska, M., Otyepka, M., and Teisinger, J. (2009) Changes in electrostatic surface potential of Na+/K+-ATPase cytoplasmic headpiece induced by cytoplasmic ligand(s) binding. *Biophys. J. 97*, 1756–1764.

(25) Grycova, L., Sklenovsky, P., Lansky, Z., Janovska, M., Otyepka, M., Amler, E., Teisinger, J., and Kubala, M. (2009) ATP and magnesium drive conformational changes of the Na+/K+-ATPase cytoplasmic headpiece. *Biochim. Biophys. Acta 1788*, 1081–1091.

(26) Čechová, P., Berka, K., and Kubala, M. (2016) Ion Pathways in the Na + /K + -ATPase. *J. Chem. Inf. Model. 56*, 2434–2444.

(27) Wolf, M. G., Hoefling, M., Aponte-Santamaria, C., Grubmuller, H., and Groenhof, G. (2010) g_membed: Efficient insertion of a membrane protein into an equilibrated lipid bilayer with minimal perturbation. *J. Comput. Chem.* 2169−2174.

(28) Berger, O., Edholm, O., and Jähnig, F. (1997) Molecular dynamics simulations of a fluid bilayer of dipalmitoylphosphatidylcholine at full hydration, constant pressure, and constant temperature. *Biophys. J. 72*, 2002–2013.

(29) Damjanovic, A., García-Moreno E., B., and Brooks, B. R. (2009) Self-guided Langevin dynamics study of regulatory interactions in NtrC. *Proteins Struct. Funct. Bioinforma. 76*, 1007–1019.

(30) Margreitter, C., Petrov, D., and Zagrovic, B. (2013) Vienna-PTM web server: a toolkit for MD simulations of protein post-translational modifications. *Nucleic Acids Res. 41*, W422–W426.

(31) Pronk, S., Páll, S., Schulz, R., Larsson, P., Bjelkmar, P., Apostolov, R., Shirts, M. R., Smith, J. C., Kasson, P. M., van der Spoel, D., Hess, B., and Lindahl, E. (2013) GROMACS 4.5: a high-throughput and highly parallel open source molecular simulation toolkit. *Bioinformatics 29*, 845–854.

(32) Salentin, S., Schreiber, S., Haupt, V. J., Adasme, M. F., and Schroeder, M. (2015) PLIP: Fully automated protein-ligand interaction profiler. *Nucleic Acids Res. 43*, W443–W447.

(33) (2017) Maestro Schrödinger. Maestro, Schrödinger, LLC, New York.

(34) Yu, H., Ratheal, I. M., Artigas, P., and Roux, B. (2011) Protonation of key acidic residues is critical for the K+ -selectivity of the Na/K pump. *Nat Struct Mol Biol 2*, 1159–1163.

(35) Picard, M., Toyoshima, C., and Champeil, P. (2005) The average conformation at micromolar [Ca2+] of Ca 2+-ATPase with bound nucleotide differs from that adopted with the transition state analog ADP·AlFx or with AMPPCP under crystallization conditions at millimolar [Ca2+]. *J. Biol. Chem. 280*, 18745–18754.

(36) Kuntzweiler, T. A., Wallick, E. T., Johnson, C. L., and Lingrel, J. B. (1995) Amino Acid Replacement of Asp 369 in the Sheep alpha 1 Isoform Eliminates ATP and Phosphate Stimulation of [3H]Ouabain Binding Properties of the Enzyme. *J. Biol. Chem. 270*, 16206–16212.

(37) Patchornik, G., Munson, K., Goldshleger, R., Shainskaya, A., Sachs, G., and Karlish, S. J. D. (2002) The ATP-Mg2+ binding site and cytoplasmic domain interactions of sodium, potassum-ATPase investigated with Fe2+-catalyzed oxidative cleavage and molecular modeling. *Biochemistry 41*, 11740–11749.

(38) Pedersen, P. A. (2000) Importance of Conserved alpha -Subunit Segment 709GDGVND for Mg2+ Binding, Phosphorylation, and Energy Transduction in Na,K-ATPase. *J. Biol. Chem. 275*, 37588–37595.

(39) Farley, R. A., Heart, E., Kabalin, M., Putnam, D., Wang, K., Kasho, V. N., and Faller, L. D. (1997) Site-Directed Mutagenesis of the Sodium Pump : Analysis of Mutations to Amino Acids in the Proposed Nucleotide Binding Site by Stable Oxygen Isotope *2960*, 941–951.

(40) Linnertz, H., Lanz, E., Gregor, M., Antolovic, R., Krumscheid, R., Obsil, T., Slavik, J., Kovarik, Z., Schoner, W., and Amler, E. (1999) Microenvironment of the high affinity ATP-binding site of Na+/K+-ATPase is slightly acidic. *Biochem. Biophys. Res. Commun. 254*, 215–221.

(41) Teramachi, S., Imagawa, T., Kaya, S., and Taniguchi, K. (2002) Replacement of several single amino acid side chains exposed to the inside of the ATP-binding pocket induces different extents of affinity change in the high and low affinity ATP-binding sites of rat Na/K-ATPase. *J. Biol. Chem. 277*, 37394–37400.

(42) Moler, J. V., Juul, B., and le Maire, M. (1996) Structural organization, ion transport, and energy transduction of P-type ATPases. *Biochim. Biophys. Acta 1286*, 1–51.

(43) Liébecq, C. (Ed.). (1992) Biochemical Nomenclature and Related Documents 2nd ed. Portland Press.

(44) Albers, R. W. (1967) Biochemical Aspects of Active Transport. *Annu. Rev. Biochem. 36*, 727–756.

PALACKÝ UNIVERSITY OLOMOUC
FACULTY OF SCIENCE
DEPARTMENT OF BIOPHYSICS

Petra Čechová

Computer Simulations of Na^+/K^+-ATPase its Interactions with Small Molecules

Disertační práce
Autoreferát

Doktorský studijní program: P1703 Biofyzika

Školitel doc. RNDr. Martin Kubala, Ph.D.

Olomouc 2018

Student DSP:

Mgr. Petra Čechová

Oponenti disertační práce:

……
……
……
……

Vedoucí práce:

doc. RNDr. Martin Kubala, Ph.D.

Katedra biofyziky

Přírodovědecká fakulta Univerzity Palackého v Olomouci

Šlechtitelů 27

783 71 Olomouc – Holice

Autoreferát rozeslán dne: ……

Obhajoba disertace se koná: ……

S disertační prací je možno se seznámit

SHRNUTÍ

Na^+/K^+-ATPasa (NKA) je esenciální membránový protein pumpující sodné a draselné ionty přes buněčnou membránu za spotřeby ATP. Tímto vytváří gradient sodných iontů, který je součástí membránového potenciálu. NKA se vyskytuje ve všech živočišných buňkách a poruchy její funkce vedou ke zdravotním problémům jako hypokalemie, šedý zákal, zvýšený krevní tlak a z toho vyplývající komplikace až po závažné poruchy nervové a svalové činnosti.

Pro stadium vlastností NKA byly využity dvě různé metody výpočetní biologie – molekulární dynamiku a dokování. Molekulární dynamika využívá soubor parametrů (silové pole) k popisu vlastností atomů a interakcí mezi nimi, na základě kterých je možné zjistit změnu polohy všech atomů daného systému a následné pohyby a konformační změny celé biomolekuly. Pomocí této metody byly popsány kanály pro pohyb vody a iontů transmembránovou částí NKA

Molekulární dokování na rozdíl od molekulární dynamiky považuje protein za rigidní molekulu, do které se pak snaží navázat mobilní molekulu inhibitoru a spočítat její afinitu k danému vazebnému místu. Tuto metodu jsme použili pro zkoumání vazby flavanolignanů a quinolinonů na otevřenou a zavřenou konformaci NKA.

SUMMARY

Na^+/K^+-ATPase (NKA) is a membrane protein present in great amounts within all cells, where it maintains sodium ion gradient. In the brain, it takes part in the rapid repolarization of neurons between neural impulses, or potassium clearance. In heart and muscles it facilitates ion exchange necessary for their function and in kidneys it handles sodium and fluid reabsorptions. Mutations in the genes encoding this protein can result in several neurological disorders, muscle dystonia or hyperkalaemia and hypertension.

This thesis focuses on studies of the Na^+/K^+-ATPase by the methods of computational biology. Molecular dynamics studies of the protein in different environments were performed to depict the movements in the transmembrane part (opening and closing of ion pathways) and cytoplasmic part (with respect to the binding of ATP and ADP).

Molecular docking studies were used to describe the interactions between the Na^+/K^+-ATPase with two groups of small organic compounds – flavonolignans (currently used as anti-inflammatory and liver-protection medicaments) and quinolinones (potential anti-cancer drugs).

PUBLICATION LIST

I. **Čechová, P.**, Berka, K., and Kubala, M. (2016) *Ion Pathways in the Na $^{+}$/K $^{+}$-ATPase,* Journal of Chemical Information and Modeling, Volume 56, Issue 12, 27 December 2016, Pages 2434-2444

II. Šeflová J., **Čechová P.**, Biler M., Kubala M. and Hradil P. (2017) *Inhibition of Na+K+-ATPase by tetrafluoro-3-hydroxyquinolin-4(1H)-one*, Biochimie, Volume 138, July 2017, Pages 56-61

III. Kubala, M., **Čechová, P.**, Geletičová, J., Biler, M., Štenclová, T., Trouillas, P., and Biedermann, D. (2016) *Flavonolignans as a Novel Class of Sodium Pump Inhibitors,* Frontiers in Physiology, Volume 7, Pages 1–10

IV. **Čechová, P.,** Berka, K., and Kubala, M. *Nucleotide Dynamics in the Na^{+}/K^{+}-ATPase,* submitted to Journal of Chemical Information and Modeling

TABLE OF CONTENTS

Introduction

Membrane proteins play a crucial role in regulating cellular environment and cell-to-cell communication. They also serve as targets or transporters for various medically active compounds. However, due to the fact they often contain a large hydrophobic part, or require to be inserted in a lipid environment, they remain a challenge for experimental studies.

Na^+/K^+-ATPase is a membrane protein present in great amounts within all cells, where it maintains sodium ion gradient. Mutations in the genes encoding this protein can result in several neurological disorders, muscle dystonia or hyperkalaemia and hypertension.

Computational biology uses the available information about protein sequence and structure to build a model, which can be further analysed in static or dynamic studies. Molecular dynamics simulates the time-depended evolution of the protein model. It captures large-scale movements and dynamic events that are beyond the reach of experimental methods. Moreover, it allows to observe the protein properties in a more physiological environment that the one necessary for obtaining crystal structures. Molecular docking treats the protein model as a receptor for a small organic molecule and calculates binding affinities of the protein-ligand complex. It is widely used as a tool of evaluating biologically active compounds and their potential use as pharmacological drugs

1. Theory

1.1. Subunits of Na^+/K^+-ATPase

The Na^+/K^+-ATPase (NKA) is an essential membrane protein that is present in all animal cells in a tissue specific manner. It transports three intracellular Na^+ and two extracellular K^+ ions across the plasma membrane to create a sodium ion gradient, which is a part of membrane potential. Moreover, sodium gradient is used as a driving force for several secondary transporters (such as glucose transporter, or Na^+/Ca^{2+} exchanger).

The smallest functional unit of NKA is a heterodimer of two subunits denoted α and β. NKA can also associate with a protein of the FXYD family, formerly denoted as subunit γ.

1.1.1. Subunit α

Subunit α is the main catalytic subunit of the NKA. It weights approximately 110 kDa and has ten transmembrane (TM) helices. The large cytoplasmic loops between helices TM2/TM3 (C23) and TM4/TM5 (C45) form cytoplasmic (A-, P- and N-) domains that bind ATP and undergo phosphorylation. The A-domain (*actuator*) consists of the N terminal part of the subunit and C23 loop. It rotates during the reaction cycle, the movement also influencing the cytoplasmic part of TM2. The P- (*phosporylation*) and N-(*nucleotide*) domains are located on the C45 loop. The N-domain is comprised of the middle of the loop, while the P-domain consists of two parts – before and after the N-domain. The ATP molecule required for ion pumping is stretched between the N- and P-domains.

We studied the nucleotide binding in different molecular dynamics simulation setups in publication IV.

The helices in the transmembrane part of NKA form the cation binding site (CBS) for the transported ions and several pathways for these ions (and water) to reach the CBS. There are three cation binding sites (CBS). The binding and potential transport of protons through the CBS has also been discussed. Recently it was suggested that the opening and closing of the pathways is controlled by CBS residue protonation.

We studied the influence of different ligands and protonation on the opening and closing of ion pathways leading to CBS in publication I.

1.1.2. Subunit β

The β subunit is located mostly in the extracellular environment, with one transmembrane helix (TMβ) at the N-terminus. The presence of β subunit in H^+/K^+-ATPase, but not in the sarcoplasmic Ca^+-ATPase (SERCA), suggests that β subunit is also necessary for potassium transport. β subunit also serves as a molecular chaperone which allows the protein to fold properly and plays a crucial role in the protein maturation.

1.1.3. The FXYD Family Proteins

The FXYD family proteins are a group of tissue specific NKA regulators, which consist mostly of one transmembrane helix. The FXYD helix is located next to α subunit TM9 and TMβ and connects with them on the extracellular side by the specific FXYD sequence One of the most frequently present FXYD proteins in the human body is FXYD2, which is present in kidneys and is also present in all the crystal structures.

1.2. Available Structures

There are several high resolution NKA structures in the Protein Data Bank (PDB) archive. All structures of the whole NKA were obtained by the X-ray crystallography with different resolutions. They can be divided into two groups according to the conformational state of the protein (*Figure 1*)

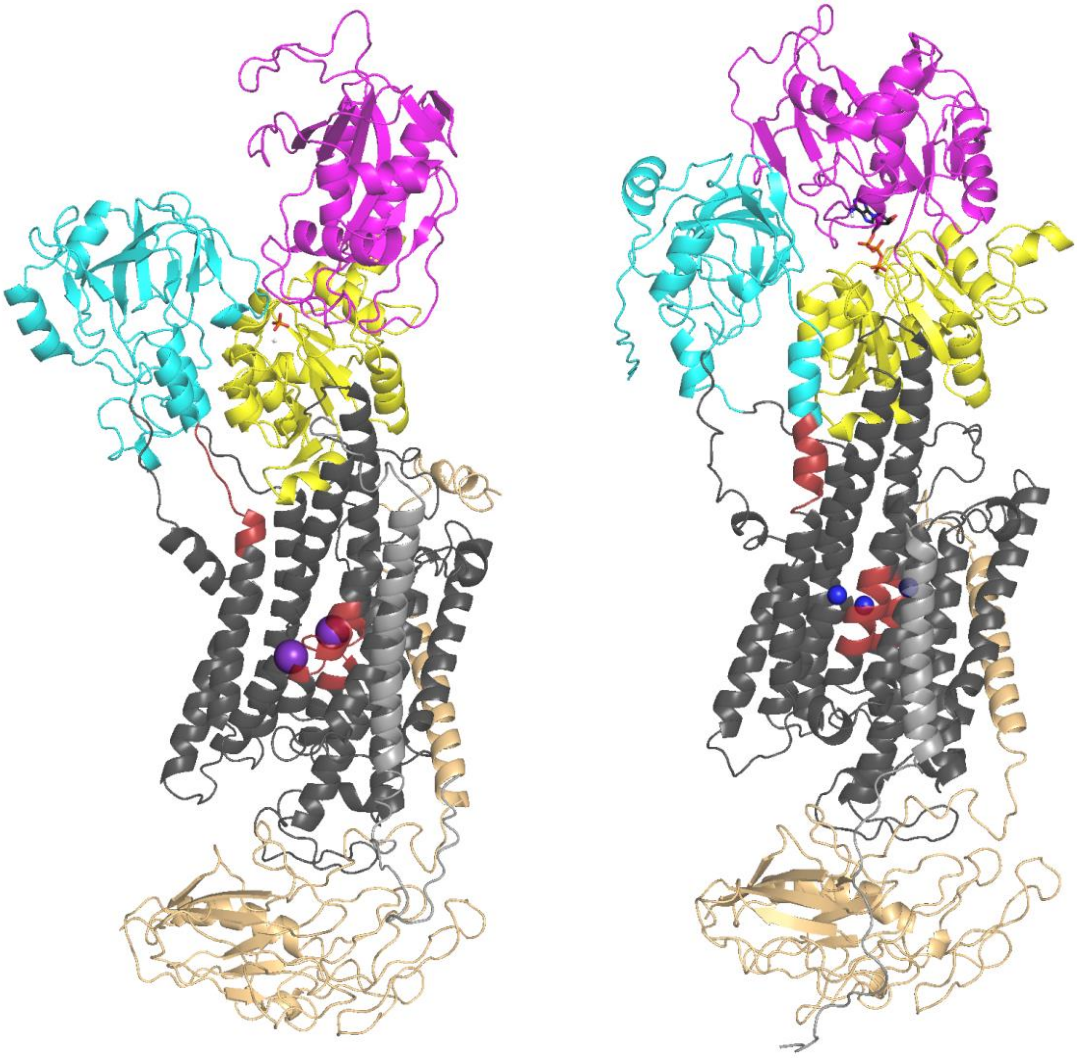

Figure 1: Open (left) and closed (right) crystal conformations. The transmembrane part of α subunit is in dark grey with cytoplasmic domains in cyan (A-domain), magenta (N-domain) and yellow (P-domain). The β subunit is in pale yellow, the FXYD family protein in light grey. CBS ions are in purple (potassium) or blue (sodium; between the domains there is phosphate in orange, ATP in black with orange phosphate chain. Red colour highlights the main structural differences of TM helixes between the open and closed conformation.

The most prominent feature of the open conformation of the NKA is the position of the A- and N- domains wide apart (about 3.5 nm). There are two main groups of the open crystal structures based on the phosphorylation state of the protein. Structures with bound MgF_4^{2-} as a free phosphate analogue (mimicking the E2·Pi state) and structures with phosphorylated D376 (or corresponding residue in porcine or bovine form, mimicking the E2-P state). The cytoplasmic domains of the closed structures are closely packed together, with an ADP molecule in the binding pocket between the N- and P-domains.

1.3. The Reaction Cycle

The basics of the NKA reaction cycle were already outlined in the 1960's by Post and Albers and later refined by other authors. The main feature of the Post-Albers diagram is dividing the protein conformations into E1 and E2 states. However, the definitions of the states are stated with respect to affinities to ions (E1 with high affinity to sodium and E2 with high affinity to potassium) or ATP (E1 with high ATP affinity and E2 with low ATP affinity). Currently, both the ion affinity and ATP affinity definitions of the states are in use.

The reaction cycle can be described as the sequence of following steps: ATP binding → intracellular sodium binding → protein phosphorylation → ADP release → extracellular sodium release → extracellular potassium binding → protein dephosphorylation → intracellular potassium release → ATP binding.

1.4. Compounds Interacting with Na^+/K^+-ATPase

Compounds influencing the NKA function have been long used in the treatment of heart problems, to promote blood circulation or, more recently, are in the clinical trials for cancer therapy. On the other hand, in higher doses, they can induce acute organ failure] and were used in poison arrows..

1.4.1. Cardiotonic Steroids

The largest group widely used group of NKA active compounds currently used in medicine are cardiotonic steroids (CTS). Even though ouabain and digoxin are used in the treatment of congestive heart failure and atrial arrhythmias; however, their toxicity requires only low doses to be administered.

1.4.2. Flavonolignans

Flavonoids are a group of compounds present in extracts from medical plants. They have been shown to possess antioxidant, antibacterial and anti-ageing properties. A standardised extract from the milk thistle seeds is called silymarin.

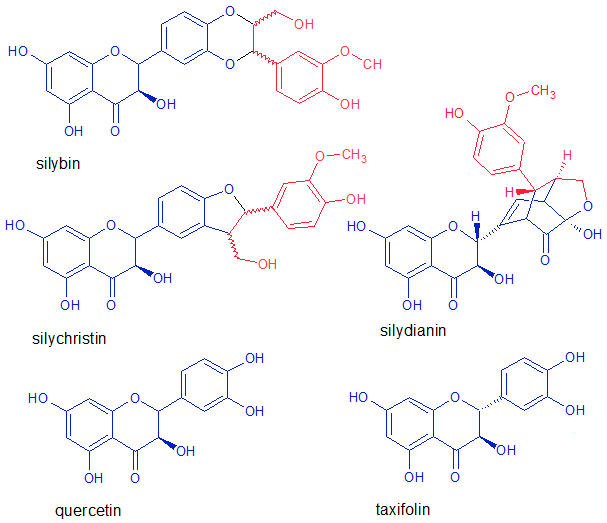

Figure 2: Compounds present in silymarin. Flavonoid part is in blue, lignan part in red.

In publication II we examined the inhibitory effect of different silymarin flavonolignans on NKA using both experimental and computational approach.

1.4.3. Quinolines

Quinoline and its derivatives are a diverse group of pharmacologically active compounds, exhibiting antibiotic, antitumor or anti-inflammatory activities. 4-hydroxyquinoline is a tautomer of 4-quinolone, a skeletal structure of a wide range of antibiotics .

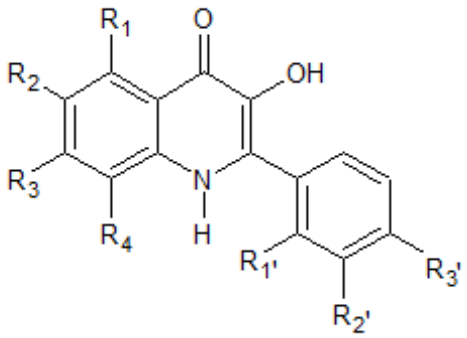

Figure 3: The structure of phenylquinolone and sites of chemical modifications.

In publication III, we studied the interactions of chloro- and floro-derivatives of 3-hydroxy-2-phenylquinolin-4(*1H*)-one with NKA using activity measurements and the methods of computational chemistry and biology.

1.5. Computational Methods in Biology

1.5.1. Homology Modelling

To build a reliable model, a homologous protein of a known structure is necessary, ideally with a high similarity of the sequence. Then the sequences are aligned and a template

structure is selected, either manually or as a part of the modelling software. The homology model sequence is then built as close to the template structure as possible, while taking into the account amino acid differences. The new structure is optimised to avoid steric clashes.

1.5.2. Molecular Mechanics

Molecular mechanics (MM) describes systems using classical mechanics to evaluate the energy of the system and it can be used for larger systems than quantum mechanics.

1.5.2.1. Force Fields

To simulate the properties of different atoms and interactions force fields are implemented. They consist of a series of equations describing bonded and non-bonded interactions and constants describing atoms which can be parametrised empirically .The total potential can then be described as:

$$V_{total}(r,s) = V_{bonded}(r,s) + V_{non-bonded}(r,s),$$

where *r* is the position of the atoms and *s* force field parameters.

1.5.3. Molecular Dynamics

Molecular dynamics (MD) is a computational method that allows the simulation of systems in an environment close to physiological and on a timescale of the biological processes. It is based on periodic calculations of potentials and velocities of the atoms in the system.

1.5.3.1. Molecular Dynamics Algorithm

The potential energies of the system are in a given steps are calculated using a MM force field. Then, in a certain time step (usually 2 fs for biological systems), the atomic forces in the system are computed using the second Newton's law. Moreover, we can to describe the change of the coordinates caused by this force. In practice, the MD algorithm can calculate both the velocities (*v*) and coordinate change (*x*) in the same time step or the velocities and coordinate change can be calculated in alternating half-steps as in the leap-frog algorithm.

1.5.4. Molecular Docking

Molecular docking is a method used in computational drug design to describe and evaluate the binding of small molecules to proteins. It consists of two main steps – a binding conformation search and the binding energy evaluation. In some cases, a structure of a drug within the target protein is known beforehand and can be used as a reference for the docking evaluation.

1.5.4.1. Conformation Search

Usually, the whole target protein (with the possible exception of a known binding site) is considered to be a rigid structure and does not move in the course of docking. Therefore, the

main objective of this step is to generate different conformations of the ligand (based on the number of rotable bonds) and to fit them into the target protein structure.

1.5.4.2. Energy Evaluation

To evaluate the binding energy of the ligand a free binding energy between the target protein and ligands can be used. It features similar contributions to molecular modelling potentials, but with more focus on evaluating different non-bonded interactions and ligand properties.

As in the case of the optimisation algorithms, the exact method of binding energy evaluation differs widely among docking programs, which can also use a combination of different approaches

1.6. Previous Simulations of Na^+/K^+-ATPase

1.6.1. Homology Models

Homology models NKA were used to support and explain experimental data in numerous cases. The main goal of static homology models of the whole α subunit of NKA was to discover and describe the cation binding sites, especially the location of sodium binding sites, ultimately, placed between TM5, TM7.

NKA has also been a target of molecular docking studies of compounds found in Chinese medicines. All studied compounds bound the extracellular pathway, similarly to ouabain, but differed by the depth of insertion Fluorone dyes were docked into a human-sequence homology model of the protein in the open conformation and into the closed C45 loop

1.6.2. Molecular Dynamics

Molecular dynamic studies of the whole NKA started to appear as the first NKA crystal structures were available, which together with the lowering cost of high-performance computational systems led to better achievability of whole protein computational studies.

A set of structures was created to examine the role of a mutation in the C-terminal region of the α subunit. The simulations showed a C-terminal water pathway leading to sodium-only binding site. The pathway was suggested to serve as a way for proton movement form the cytoplasmic side to CBS as a possible explanation of previous studies. A pKa analysis followed by simulations the open conformation, lead to the conclusion that the protonation leads to CBS selectivity for potassium and ensure the stability of CBS in the E2-P state.

2. Simulation Setup

2.1. Molecular Dynamics

The protein structure was based on the crystal structures with PDB IDs 2ZXE for the open conformation, and 4HQJ for the closed conformation. Homology models with the human $\alpha_1\beta_1$FXYD2 sequence were created using MODELLER 9.9 package and Uniprot IDs

P05023, P05026 and P54710 respectively. The simulations were performed and processed with GROMACS 4.5.4 .Tunnel analysis was performed by MOLE 2.0 and ligand binding analysis was performed by Maestro ligand interaction tool and by PLIP 1.2.

Several different combinations of protein conformation, CBS ions, CBS residue protonation, cytoplasmic domain ligands and bulk ions were created to simulate NKA in different points of the reaction cycle.

The protein was inserted into a dioleoylphosphatidylcholine (DOPC) bilayer in a 15×15×20 nm hydrated box. To simulate conditions closer to physiological, ions corresponding to 154 mM of NaCl or KCl were added to the system. The system was minimised and 10 ns prerun with fixed protein backbone was performed before each simulation. The main run was performed with time step 2 fs, for 100 ns, at 310K.

2.2. Molecular Docking

The protein models for molecular docking were crystal structures with PDB IDs 3KDP (open conformation) and 4HQJ (closed conformation) or human sequence homology model – the starting point of simulation C_3Na_Mg_ATP. The structures of organic compounds for docking were obtained by DFT calculations by M. Biler.

The structures were prepared for docking by Autodock Tools 1.5.6, with all single bonds remaining rotable. The docking was performed by Autodock Vina 1.1.2 with the grid covering the whole protein (exhaustiveness set to 400 and num_modes to 9999).

3. Results and Discussion

3.1. Simulation Properties

3.2. Ion Pathways

The main function of NKA is to transport sodium ions against concentration gradient out from the cell and potassium ions inside. To achieve that, ions must move into the CBS, where they are occluded, before they are released on the opposite side of the membrane. Therefore, the knowledge of molecular pathways and when in the reaction cycle they open and close, is an large important step towards better understanding the details of protein function and the way how a mutation impacts its function leading to a disease.

We identified five different ion and water pathways leading to the cation binding site from both intracellular and extracellular side of the membrane (*Figure 4*). Three of them – the N-terminal, the C-terminal and the extracellular pathway had been described before. The TM3/TM7 and TM6/TM9 pathways are novel.

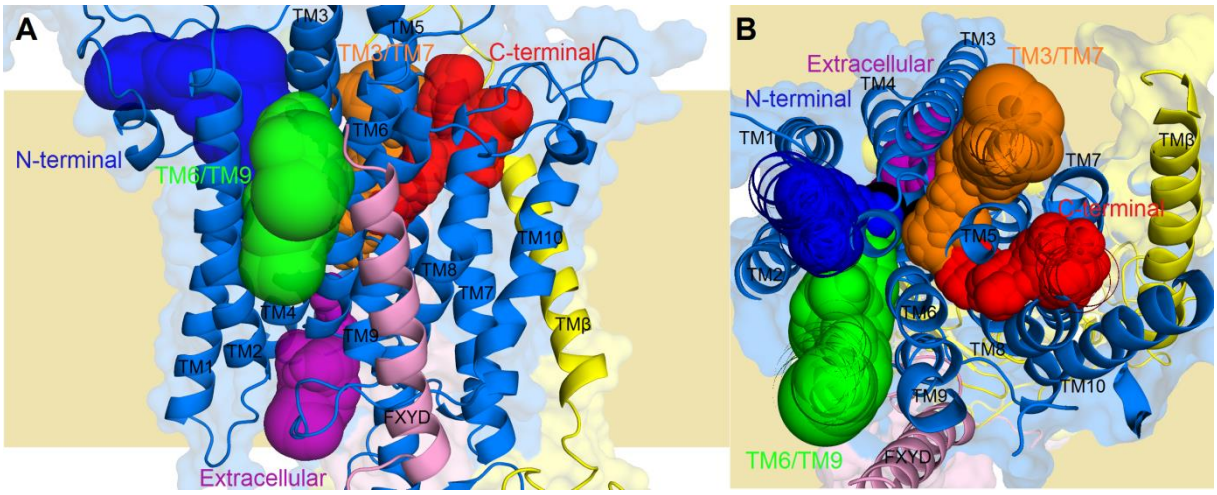

Figure 4: The pathways from the view parallel to the membrane (A) and from the intracellular side (B) .

Moreover, we observed various dynamic properties of the pathways, such as their opening, closing, or movement of water molecules and ions from the bulk solution to the CBS.

3.3. Nucleotide Binding

3.3.1. The Nucleotide Binding Modes

To describe the nucleotide binding, several simulations with bound ATP and ADP+Pi and different combinations of ions in CBS and the bulk solution were analysed. We used three different methods (PLIP, ligand interaction diagram, both for the last frame of the simulation, and analysis of residues closer than 3.5 Å from the nucleotide in the last 10 ns of the simulation) to depict the nucleotide binding. We identified five different binding sites on the P- and N-domain (*Figure 5*).

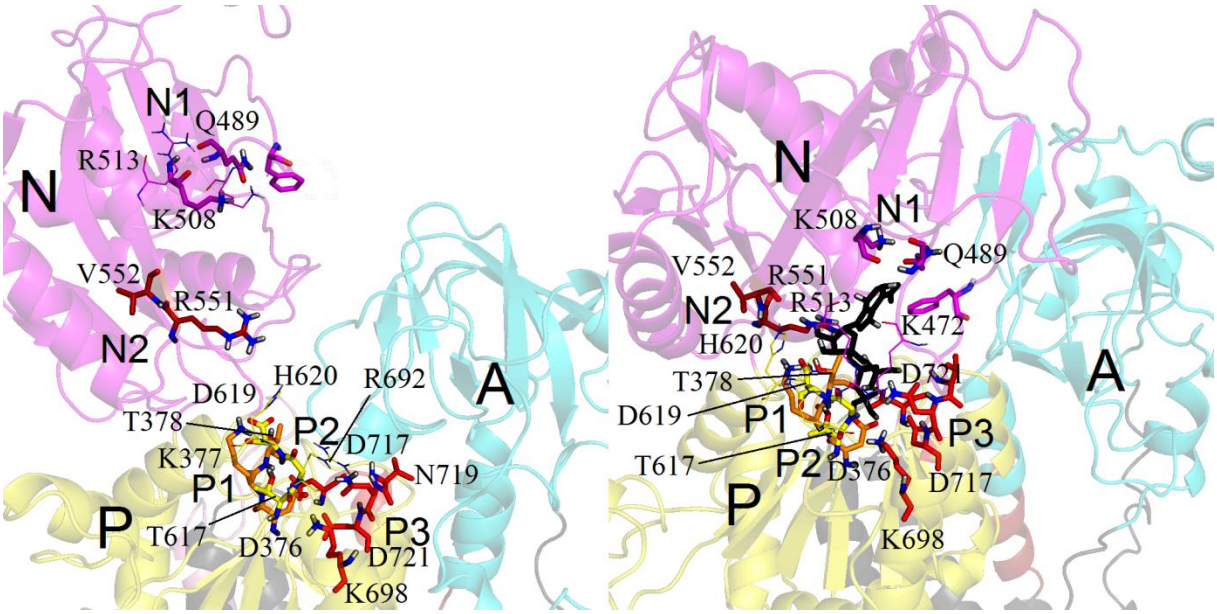

Figure 5: The nucleotide binding sites in the open (left) and closed (right) conformation of the protein. A-domain is in cyan, P-domain in yellow, N-domain in magenta, ATP in black. The residues taking part in nucleotide binding are in stick representation. Site P1 in orange, P2 yellow, P3 and N2 different shades of red, N1 in purple. K487, R513, H620, and R692 are displayed in lines.

The residues of the above mentioned nucleotide binding sites also take part in ADP binding in the available crystal structures. Our simulation results are also in good agreement with the fact that the N- and P-domain sequences 376DKTGTLT (site P1), 508KGAPE (site N1), 615MVTGD (site P2) and 712VAVTGDGVNDS (site P3) are conserved among the P-type ATPases.

3.3.2. The Nucleotide Binding Conformations

Apart from the position of the nucleotide on NKA, we also studied the different conformations of the nucleotide itself. To describe them, we defined two dihedral angles. The angle describing the conformation of ribose (because compounds with immobile ribose have been shown to be NKA inhibitors) as the ribose carbons dihedral angle C1'-C2'-C3'-C4' and the dihedral angle between ribose and adenine as O4'-C1'-N9-C4 (*Figure 6*). The C1'-C2'-C3'-C4' angle larger than 180° corresponds to the C2'-endo conformation while the angle smaller than 180° corresponds to the C3'-endo conformation of the ribose.

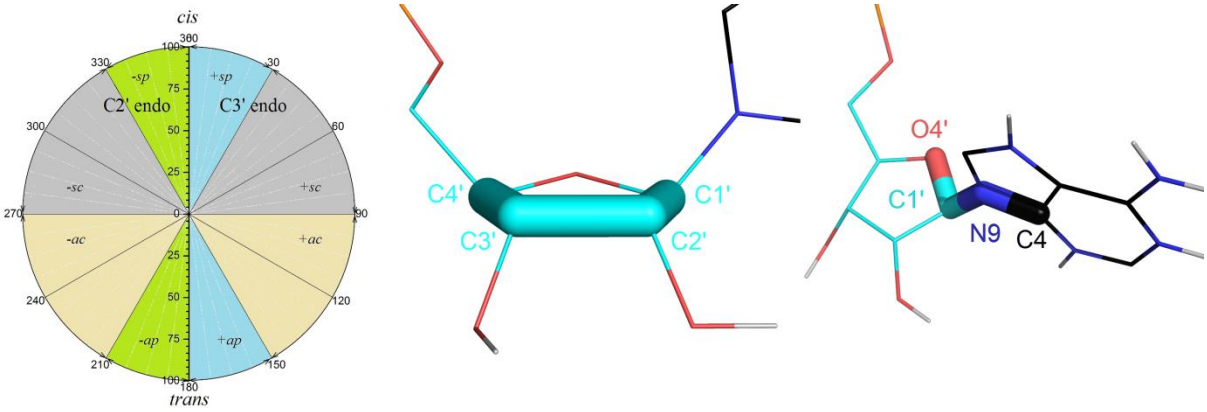

Figure 6: The circle of possible angles and depiction of the the dihedral angle between the ribose carbons and between the ribose and the adenine.

Collectively, the angles between different parts of the nucleotides show that there are several possible conformations of the nucleotide in the binding pocket on the protein, documenting the flexibility of the nucleotide necessary for NKA substrates. Interestingly, the ions in the bulk solution also influence the nucleotide binding, suggesting a possible feedback loop for NKA regulation.

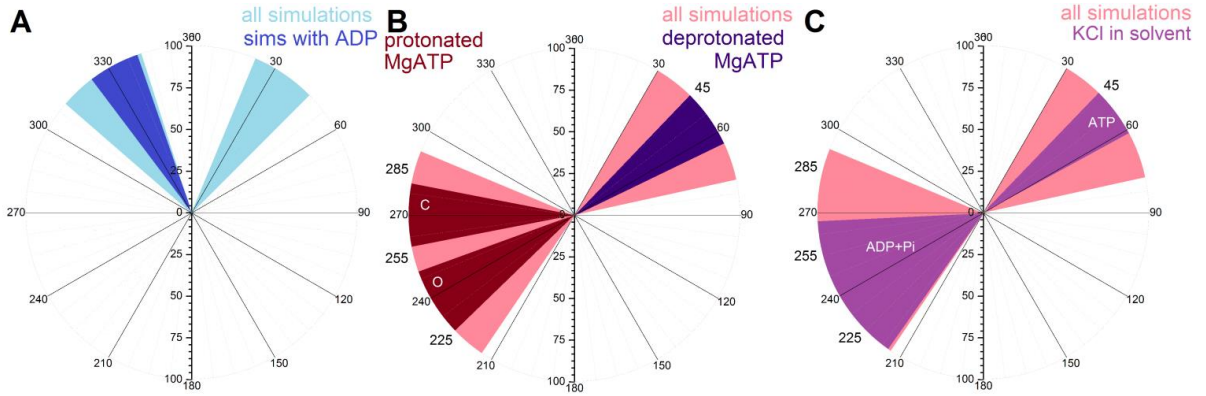

Figure 7: The area where most of the dihedral angle values are located for ribose (A) - light blue depicts the angle range where most of the values lie in all the simulations, and dark blue depicts the most frequent angle range for the simulations with bound ADP. B and C show the angle between ribose and adenine, with the pink area depicting the angle range where most of the values lie in all the simulation.

3.4. Molecular Docking of Potentially Therapeutic Compounds

3.4.1. Flavonolignans

A series of flavonolignans was obtained in the collaboration with laboratory of V.Křen from the Institute of Microbiology of the Czech Academy of Sciences. Based on the results of the initial screening of the effect of the compounds on NKA activity, silychristin (SCH), dehydrosilychristin (DHSCH), and dehydrosilydianin (DHSD) were selected for molecular docking (*Figure 8*).

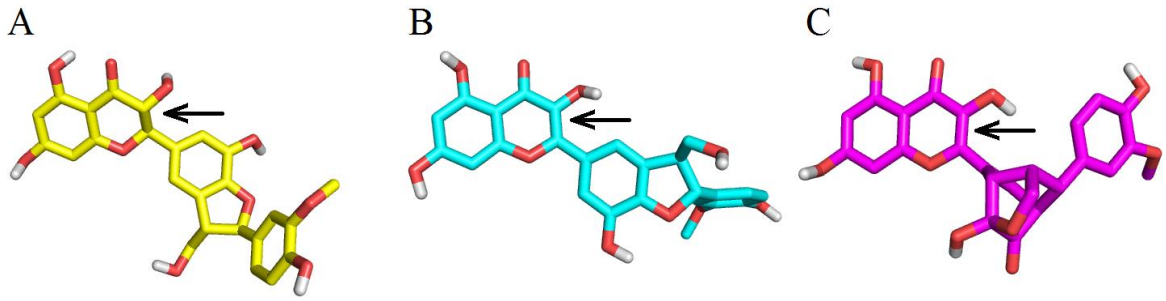

Figure 8: The structures of flavonolignans used in molecular docking. The carbons of silychristin (A) are in yellow, dehydrosilychristin (B) in cyan and dehydrosilydianin (C) in magenta, oxygens in red, hydrogens in white. The arrow denotes the dehydrated bond.

The flavonolignans bind to the pump in five different positions (*Figure 9*) – three at the entrances to pathways and two at the cytoplasmic domains. The pose specific for the open conformation is under the A-domain, near N353 (porcine numbering), while the closed-conformation specific one is near R248.

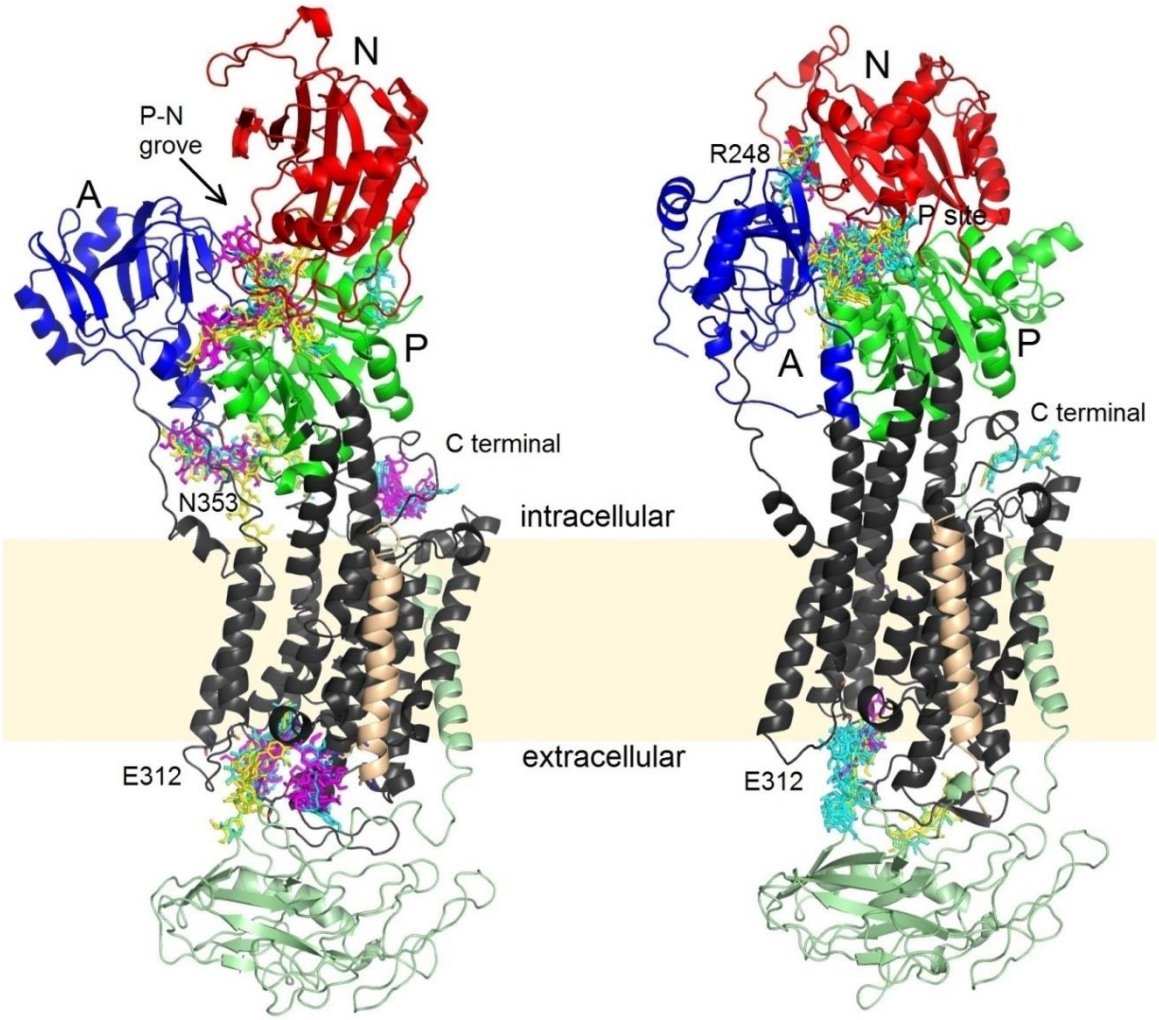

Figure 9: The open (left) and closed (right) conformations of NKA with the binding sites for flavonolignans. Silychristin is in yellow, dehydrosilychristin in cyan and dehydrosilydianin in magenta. Beta subunit is in light green, the FXYD protein light orange, A-domain blue, N-domain red and P-domain

Flavonolignan binding at the pathway exits can hinder the ion movement through the pathways or interfere with the opening and closing of these pathways.

3.4.2. Quinolinones

The main focus was aimed on 5,6,7,8-tetrafluor-3-hydroxy-2- phenylquinolin-4(1*H*)-one (TFHPQ), which exhibited the biggest NKA activity change in experimental measurements, while the other compounds were halogenated by only one or two chlorine or fluorine atoms see *Figure 10*.

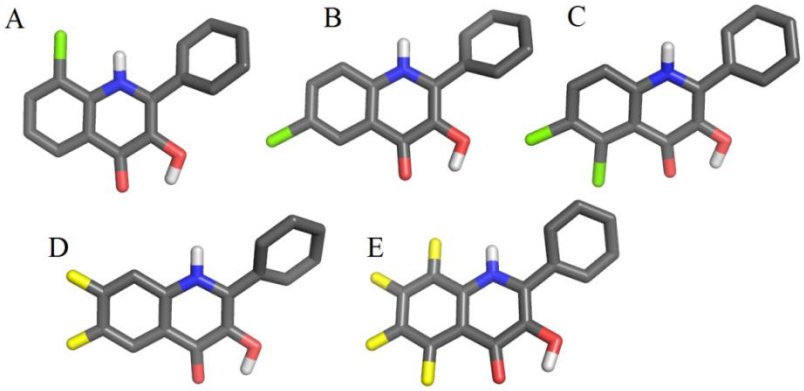

Figure 10: The quinolinones used for docking - 6CHPQ (A), 8CHPQ (B), DCHPQ (C), DFHPQ (D) and TFHPQ (E). The carbon atoms are in grey, oxygen in red, nitrogen in blue, chlorine in green, fluorine in yellow and hydrogen in white.

On the open conformation, TFHPQ binds exclusively to the C-terminal area of NKA, in the vicinity of Y1022 of α subunit and W12 of β subunit (*Figure 11*). Unlike TFHPQ, the other compounds bind not only to the C-terminal site, but also in different positions on the protein.

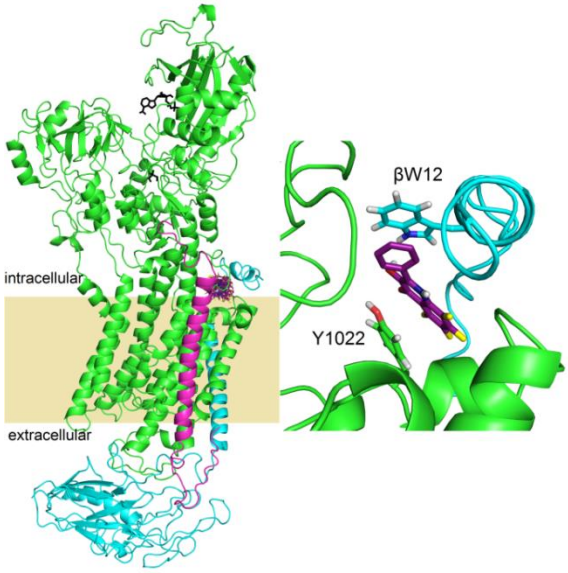

Figure 11: The binding site of TFHPQ on the open structure of NKA. TFHPQ is in purple,α subunit in green, β subunit in cyan, the FXYD protein in pink

When compared to the other quinolinones studied by molecular docking, TFHPQ binds with higher affinity on both open and closed conformation of NKA.

4. Conclusions

Na^+/K^+-ATPase is a membrane protein essential for its role in maintaining cell homeostasis and ion clearance. Its malfunction can lead to hyperkalaemia, hypertension or several disorders of the neural and muscular system. Computational biology serves as a powerful tool to corroborate and explain experimental findings by creating a model of a selected protein in a selected environment. Molecular dynamic simulates biomolecule movements with atomic resolution on the nanosecond timescale, while molecular docking describes the binding of small molecules to a selected protein target.

In two studies, we examined NKA using molecular dynamics – the transmembrane part, with focus on ion movements and the cytoplasmic part with respect to nucleotide binding. We revealed that water molecules and ions from the solution can move to the cation binding site through five different pathways, two of which had not been described before. Amino acids lining these pathways had been connected to diseases or protein affecting mutations. The nucleotide binding to the cytoplasmic domain is a dynamic process with several possible substates of the binding pocket. It is also influenced by the protonation of CBS residues and ions present in the bulk solution, suggesting a possible feedback loop for protein activity.

Using molecular docking, we studied two groups of active compounds – flavonolignans and quinolinones. Flavonolignans can bind to the transmembrane part of NKA, obstructing the entry to the C-terminal and extracellular ion pathways. In addition to that, they bound with great frequency on the cytoplasmic domains. Due to significant movements of these domains during the reaction cycle, flavonolignans can obstruct the proper domain movement and inhibit the protein allosterically. Quinolinones bind with the greatest frequency at the entrance to the C-terminal pathway. Experimentally the most active quinolinone, TFHPQ, binds with higher specificity and affinity than the other quinolinones. Therefore it can inhibit NKA more efficiently than the other compounds.

The findings of ion pathways and the nucleotide binding dynamics suggests that the NKA reaction cycle is on the molecular level more complex than what can be efficiently described by the currently used E1-E2 state notation. They also indicate a complex long-distance communication system between the transmembrane cation binding site and the cytoplasmic domains. Molecular docking helped to describe two groups of active compounds that have different mechanism of effect from currently medically used, but toxic, cardiotonic steroids, and can therefore serve as potential new drugs affecting the Na^+/K^+-ATPase.